

1-1-2003

## Demonstration project using railroad flatcars for low-volume road bridges

Justin Dale Doornink  
*Iowa State University*

Follow this and additional works at: <https://lib.dr.iastate.edu/rtd>

---

### Recommended Citation

Doornink, Justin Dale, "Demonstration project using railroad flatcars for low-volume road bridges" (2003).  
*Retrospective Theses and Dissertations*. 19950.  
<https://lib.dr.iastate.edu/rtd/19950>

This Thesis is brought to you for free and open access by the Iowa State University Capstones, Theses and Dissertations at Iowa State University Digital Repository. It has been accepted for inclusion in Retrospective Theses and Dissertations by an authorized administrator of Iowa State University Digital Repository. For more information, please contact [digirep@iastate.edu](mailto:digirep@iastate.edu).

**Demonstration project using railroad flatcars  
for low-volume road bridges**

by

**Justin Dale Doornink**

A thesis submitted to the graduate faculty  
in partial fulfillment of the requirements for the degree of  
**MASTER OF SCIENCE**

Major: Civil Engineering (Structural Engineering)

Program of Study Committee:  
F. Wayne Klaiber, Co-major Professor  
Terry J. Wipf, Co-major Professor  
Loren W. Zachary

Iowa State University

Ames, Iowa

2003

Graduate College  
Iowa State University

This is to certify that the master's thesis of

Justin Dale Doornink

has met the thesis requirements of Iowa State University

Signatures have been redacted for privacy

---

## TABLE OF CONTENTS

LIST OF FIGURES .....	vi
LIST OF TABLES .....	x
1. INTRODUCTION .....	1
1.1 Background.....	1
1.2 Objective and Scope of Demonstration Project .....	4
1.3 Selected RRFC Bridge Sites .....	4
1.3.1 Buchanan County Site .....	5
1.3.2 Winnebago County Site .....	6
2. RRFC INSPECTION AND SELECTION .....	9
2.1 Inspection of Alternative RRFCs .....	9
2.2 RRFC Selection Criteria .....	22
2.2.1 Structural Element Sizes, Load Distributing Capabilities, and Support Locations .....	22
2.2.2 Member Straightness/Damage .....	23
2.2.3 Structural Element Connections .....	23
2.2.4 Uniform, Matching Cambers .....	24
2.2.5 RRFC Availability.....	25
2.3 RRFC Selection for the Demonstration Bridges .....	25
2.3.1 Selection of RRFCs for the BCB.....	26
2.3.2 Selection of RRFCs for the WCB.....	26
2.4 RRFC Preparation and Delivery .....	28
3. CONSTRUCTION OF THE DEMONSTRATION BRIDGES .....	30
3.1 BCB Construction .....	30
3.1.1 BCB Phase 1: Substructure Development and Flatcar Placement..	31
3.1.2 BCB Phase 2: Development of Longitudinal Flatcar Connections...	37
3.1.3 BCB Phase 3: Installation of the Driving Surface and Guardrails ....	40
3.2 WCB Construction .....	40
3.2.1 WCB Phase 1: Substructure Development and Flatcar Placement.	43
3.2.2 WCB Phase 2: Development of Longitudinal Flatcar Connections..	46
3.2.3 WCB Phase 3: Installation of the Driving Surface and Guardrails ...	51

4. LABORATORY AND FIELD TESTING .....	56
4.1 Laboratory Connection Specimen .....	56
4.1.1 LCS Service Load Torsion Test.....	59
4.1.2 LCS Flexure Test.....	62
4.1.3 LCS Ultimate Load Torsion Test.....	62
4.2 RRFC Bridge Field Testing .....	67
4.2.1 Buchanan County Bridge.....	70
4.2.1.1 BCB Load Test 1 .....	70
4.2.1.2 BCB Load Test 2 .....	75
4.2.1.3 BCB Load Test 3.....	77
4.2.2 Winnebago County Bridge .....	82
4.2.2.1 WCB Load Test 1 .....	82
4.2.2.2 WCB Load Test 2 .....	85
4.2.2.3 WCB Load Test 3 .....	88
5. THEORETICAL ANALYSIS .....	91
5.1 LCS Analysis .....	91
5.1.1 Theory of LCS Behavior .....	91
5.1.1.1 Analysis of LCS Torsion Behavior by Conventional Methods.....	91
5.1.1.2 Analysis of LCS Torsion Behavior by Finite Element Analysis .....	99
5.1.2 Theory of Flexural Behavior.....	104
5.2 Live Load Grillage Analysis of the RRFC Demonstration Bridges.....	107
5.2.1 Grillage Model and Theoretical Results of the BCB .....	111
5.2.2 Grillage Model and Theoretical Results of the WCB .....	116
5.3 Dead Load Analysis of the RRFC Demonstration Bridges.....	126
5.3.1 BCB Dead Load Analysis .....	129
5.3.2 WCB Dead Load Analysis .....	130
6. RESULTS .....	131
6.1 LCS Results .....	131
6.1.1 LCS Service Load Torsion Test.....	131
6.1.2 LCS Flexure Test.....	132

6.1.3 LCS Ultimate Load Torsion Test.....	132
6.1.4 Summary of LCS Performance .....	137
6.2 Field Load Testing of the RRFC Demonstration Bridges .....	138
6.2.1 BCB Field Test Results.....	138
6.2.2 WCB Field Test Results.....	151
6.2.3 Summary of Demonstration Bridge Performances .....	161
7. DESIGN AND CONSTRUCTION OF THE RRFC BRIDGES .....	162
7.1 Construction Time and Expenses.....	162
7.2 Recommendations for Live Load Distribution .....	163
7.3 Suggested Changes in the Construction of the RRFC Bridges.....	167
8. SUMMARY AND CONCLUSIONS.....	169
8.1 Summary .....	169
8.2 Conclusions .....	171
9. RECOMMENDED RESEARCH .....	172
APPENDIX A - CONTACT INFORMATION FOR RAILROAD FLATCAR SUPPLIERS.....	173
APPENDIX B - DETAILS FOR THE LCS CONVENTIONAL OF ANALYSIS.....	175
B.1 W-shape Warping Stresses .....	176
B.2 Compatibility between the W-shapes and the Reinforced Concrete Beam....	179
B.3 Correction for the W-shape Vertical Displacement.....	180
APPENDIX C - DETAILS FOR THE LCS FLEXURAL ANALYSIS .....	185
C.1 LCS Composite Analysis .....	186
APPENDIX D - DEVELOPMENT OF THE DESIGN RECOMMENDATIONS.....	190
D.1 Moment Fraction for the Critical RRFC .....	191
D.2 Inertia Ratios for the Critical Girders .....	194
D.3 Adjustment Factors.....	195
APPENDIX E - SAMPLE CALCULATIONS FOR DETERMINING LIVE LOAD MOMENTS.....	196
E.1 BCB Live Load Moment Calculations.....	197
E.2 WCB Girder Design Moment Calculations .....	199
REFERENCES .....	202
ACKNOWLEDGEMENTS.....	203

## LIST OF FIGURES

Figure 1.1.	Location of the BCB site .....	5
Figure 1.2.	Pin-connected, kingpost pony truss bridge at the BCB site.....	6
Figure 1.3.	Location of the WCB site .....	7
Figure 1.4.	Three-span, timber bridge at the WCB site.....	8
Figure 2.1.	Identification of RRFC structural members .....	10
Figure 2.2.	Details of RRFCs' interior girders .....	11
Figure 2.3.	AF1 – The 56-ft, v-deck RRFC .....	12
Figure 2.4.	AF2 – The 85-ft RRFC.....	14
Figure 2.5.	AF3 – The 89-ft RRFC (Type A) .....	17
Figure 2.6.	AF4 – The 89-ft RRFC (Type B) .....	20
Figure 2.7.	Measuring camber on a RRFC .....	24
Figure 2.8.	The deformed transverse member in AF4 .....	28
Figure 2.9.	The “trimmed” AF1 at the BCB site.....	29
Figure 2.10.	The “trimmed” AF3 at the WCB site.....	29
Figure 3.1.	Side and cross-sectional views of the BCB.....	31
Figure 3.2.	Details of the BCB concrete abutments .....	32
Figure 3.3.	Phase 1 construction on the BCB.....	35
Figure 3.4.	Longitudinal flatcar connection used in the BCB.....	37
Figure 3.5.	Phase 2 construction of the BCB .....	39
Figure 3.6.	Phase 3 construction on the BCB.....	41
Figure 3.7.	Finished Buchanan County RRFC Bridge.....	42
Figure 3.8.	Layout and connection on the WCB .....	42
Figure 3.9.	Winnebago County RRFC abutments and piers .....	44
Figure 3.10.	Exterior girder supports in the WCB .....	45
Figure 3.11.	Phase 1 construction on the WCB.....	47
Figure 3.12.	Longitudinal flatcar connection on the WCB .....	49
Figure 3.13.	Phase 2 construction on the WCB.....	52
Figure 3.14.	Phase 3 construction on the WCB.....	54
Figure 3.15.	Finished Winnebago County RRFC Bridge.....	55
Figure 4.1.	Laboratory connection specimen.....	57
Figure 4.2.	Location of strain gages on the LCS.....	58

Figure 4.3.	LCS Service Load Torsion Test.....	60
Figure 4.4.	Location of displacement instrumentation used in the LCS Service Load Torsion Test .....	61
Figure 4.5.	Location of strain gages used in the LCS Service Load Torsion Test relative to end restraint .....	63
Figure 4.6.	Photograph of the LCS Service Load Torsion Test.....	64
Figure 4.7.	LCS Service Flexure Test .....	65
Figure 4.8.	Location of instrumentation in the Service Load Flexure Test.....	66
Figure 4.9.	Photograph of the LCS under service flexural loads .....	67
Figure 4.10.	LCS Ultimate Load Torsion Test.....	68
Figure 4.11.	Location of displacement instrumentation for the LCS Ultimate Torsion Test .....	69
Figure 4.12.	Location of strain gages used in the LCS Ultimate Load Test relative to the end restraint .....	70
Figure 4.13.	Photographs of the Ultimate Load Torsion Test.....	71
Figure 4.14.	Dimensions and weights of test trucks used in RRFC bridge field tests...	72
Figure 4.15.	Location of instrumentation in BCB LT1 .....	73
Figure 4.16.	Transverse locations of the test truck in BCB LT1 .....	76
Figure 4.17.	North eccentric transverse position of the truck in BCB LT1 .....	77
Figure 4.18.	Location of instrumentation in BCB LT2 and LT3.....	78
Figure 4.19.	Transverse locations of trucks(s) in BCB LT2.....	80
Figure 4.20.	Testing of the BCB after installation of the longitudinal flatcar connections .....	81
Figure 4.21.	Location of instrumentation in WCB LT1 .....	83
Figure 4.22.	Field load testing the unconnected RRFCs during WCB LT1.....	85
Figure 4.23.	Location of instrumentation in WCB LT2 and LT3.....	86
Figure 4.24.	Transverse truck positions in WCB LT2.....	89
Figure 4.25.	Testing the finished WCB immediately following completion of construction.....	90
Figure 5.1.	Composite behavior of the LCS under torsional loading .....	92
Figure 5.2.	Flange torsional warping stresses in the W-shape member of the LCS resulting from a 1 ft-k torsional moment and end warping restraints .....	94
Figure 5.3.	Flange flexural stresses in the W-shape member of the LCS resulting from a 1 ft-k torsional moment and end rotational restraint.....	96



Figure 5.4	Variation in flange stresses in the W-shape of the LCS resulting from a 1 ft-k torsional moment and end restraint.....	97
Figure 5.5.	Variation in axial rotation of the LCS resulting from a 1 ft-k torsional moment and end restraint.....	98
Figure 5.6.	LCS W-shape member analyzed in ANSYS for the Ultimate Load Torsion Test .....	100
Figure 5.7.	LCS partial composite behavior in the Ultimate Load Test.....	101
Figure 5.8.	FEA predicted LCS longitudinal stresses in the analyzed W-shape for the Ultimate Load Torsion Test.....	102
Figure 5.9.	FEA predicted flange stresses for LCS complete and partial composite behavior in the Ultimate Load Torsion Test .....	103
Figure 5.10.	FEA predicted LCS von Mises stresses in the analyzed W-shape for the Ultimate Load Torsion Test.....	105
Figure 5.11.	FEA predicted LCS von Mises concentrated hole stresses in the analyzed W-shape for the Ultimate Load Torsion Test .....	106
Figure 5.12.	LCS service load flexure setup .....	107
Figure 5.13.	Theoretical top and bottom flange stresses for the Service Level LCS Flexure Test ( $P = 1$ k).....	108
Figure 5.14.	Modeling of the BCB cross-section.....	113
Figure 5.15.	Top view of BCB ANSYS grillage model.....	115
Figure 5.16.	Analytical upper and lower bounds for Test 1 in BCB LT1 .....	117
Figure 5.17.	Analytical upper and lower bounds for Test 1 in BCB LT2 .....	118
Figure 5.18.	Modeling of the WCB cross-section.....	120
Figure 5.19.	Top view of WCB ANSYS grillage model.....	122
Figure 5.20.	Relationship between timber plank inertia and interior girder deflections.	124
Figure 5.21.	Analytical upper and lower bounds for WCB LT1 without abutment restraints .....	125
Figure 5.22.	Analytical upper and lower bounds for WCB LT1 with abutment restraints .....	127
Figure 5.23.	Analytical upper and lower bounds for Test 1 in WCB LT2 .....	128
Figure 6.1.	LCS Service Flexure Test strain results.....	133
Figure 6.2.	LCS torsional moments and relative rotations in the Ultimate Load Torsion Test .....	134
Figure 6.3.	Comparison of Ultimate Load Torsion Test analytical and experimental results .....	136
Figure 6.4.	Comparison of BCB LT1 Test 1 midspan deflections and strains .....	139

Figure 6.5.	Comparison of BCB LT1 Test 2 midspan deflections and strains .....	140
Figure 6.6.	Comparison of BCB LT1 Test 3 midspan deflections and strains .....	141
Figure 6.7.	Comparison of BCB LT2 Test 1 midspan deflections and strains .....	143
Figure 6.8.	Comparison of BCB LT2 Test 2 midspan deflections and strains .....	144
Figure 6.9.	Comparison of BCB LT2 Test 3 midspan deflections and strains .....	145
Figure 6.10.	Comparison of BCB LT2 Test 4 midspan deflections and strains .....	146
Figure 6.11.	Comparison of BCB LT2 Test 5 midspan deflections and strains .....	147
Figure 6.12.	Comparison of BCB LT2 Test 6 midspan deflections and strains .....	148
Figure 6.13.	Comparison of BCB LT2 and LT3 midspan deflections and strains .....	150
Figure 6.14.	Comparison of WCB LT1 midspan deflections and strains without abutment restraints.....	152
Figure 6.15.	Comparison of WCB LT1 midspan deflections and strains with abutment restraints.....	153
Figure 6.16.	Comparison of WCB LT2 Test 1 midspan deflections and strains .....	156
Figure 6.17.	Comparison of WCB LT2 Test 2 midspan deflections and strains .....	157
Figure 6.18.	Comparison of WCB LT2 Test 3 midspan deflections and strains .....	158
Figure 6.19.	Comparison of WCB LT2 and LT3 midspan deflections and strains .....	159
Figure 7.1.	Relationships of adjustment factors and inertia ratios for use in Equation 7.1 .....	166
Figure 7.2.	Stay-in-place formwork for the BCB longitudinal flatcar connection .....	168
Figure B.1.	Warping behavior in an unrestrained LCS .....	177
Figure B.2.	Combination of flexure and torsion in the LCS.....	181
Figure B.3.	Excel program flow chart for evaluating LCS rotations and stresses.....	184
Figure C.1.	Simply supported beam subjected to flexure by a concentrated force, P .	186
Figure C.2.	Excel program flow chart for evaluating LCS flexure distribution .....	189
Figure D.1.	Energy of the BCB system for transverse truck positioning .....	192
Figure D.2.	Energy of the WCB system for transverse truck positioning.....	193

## LIST OF TABLES

Table 2.1.	Calculated midspan girder properties for alternative RRFs ..... 25
Table 5.1.	Calculated section properties of the BCB ..... 111
Table 5.2.	Calculated section properties of the WCB ..... 119

# 1. INTRODUCTION

## 1.1 Background

The feasibility of using railroad flatcars (RRFCs) in low-volume road (LVR) bridge superstructures was investigated in a research project completed by the Bridge Engineering Center at Iowa State University (ISU). Railroad flatcars offer several attractive characteristics that make them desirable for superstructures: they are easy and quick to install, can be used on existing or new abutments, are available in various lengths, require low maintenance, and are relatively inexpensive. As will be discussed in the following sections, a 1999 feasibility study [1] collected information on available flatcar types and existing RRFC bridges, field tested an existing RRFC bridge, analyzed its behavior, and determined whether or not flatcars can adequately serve as LVR bridge superstructures.

Through contact with RRFC salvage yard personnel, it was found that RRFCs are removed from service for three main reasons: (1) age, (2) derailments, and (3) economics. For flatcars that have been in service for many years, engineers often question the remaining fatigue life of the RRFC. However, it was determined that fatigue is usually not a concern when RRFCs are used in LVR bridges because of the low average daily traffic on these bridges. Flatcars involved in derailment often have damage to their load-carrying members, and thus, are no longer suitable to support large loads (i.e. traffic loads). Flatcars decommissioned because of economics have been removed from service because new flatcars have been designed, or because their net value has depreciated to essentially zero. Newly designed flatcars are lighter and can haul heavier freight, thus the reason for phasing out the older flatcars. The flatcars that have depreciated to zero value cost more to rehabilitate (usually the wheels, bearings, breaks, etc.) than to completely replace. As a result, a large number of RRFCs removed from service because of age or economics are still structurally sound. Railroad salvage yards selling the decommissioned flatcars often

know the reasons why a particular flatcar was removed from service, and therefore, can assist in the selection of structurally sound, undamaged flatcars [1].

Each RRFC that was evaluated in the feasibility study had one interior and two exterior longitudinal girders. Flatcars reviewed were classified into two categories – those with redundant or non-redundant cross-sections. If all three longitudinal girders in a flatcar had section properties sufficient to support traffic loads, then three longitudinal loads paths were available, and the flatcar was categorized as having a redundant cross-section. In other flatcars, only the interior girder was capable of supporting traffic loads, and therefore, essentially only one longitudinal load path was available. These types of flatcars were categorized as having non-redundant cross-sections. In the feasibility study, it was recommended that only RRFCs with redundant cross-sections be used in RRFC bridges to ensure the presence of safe, structurally sound bridge superstructures [1].

An existing RRFC bridge in Tama County was field tested using a truck carrying Iowa legal traffic loads; during the tests, strains and deflections were measured at critical locations in the main, load-carrying members of the RRFCs. The Tama County Bridge (TCB) spans approximately 42' – 0" and consists of two flatcars aligned side-by-side; a 12' – 0" wide timber deck was positioned on top of the flatcar decks to provide a driving surface and to help distribute traffic load between the two RRFCs. Structural inspection of the bridge revealed obvious damage to load-carrying members, and in addition, each flatcar was supported differently on the abutments. As a result, redundancy and symmetrical behavior of the bridge were questioned [1].

With the test truck positioned at several longitudinal and transverse locations, the TCB was initially tested with no connections between the flatcars; a second field test was performed after connections between the flatcars were installed. By comparing results from both tests, it was shown that the connections between flatcars did very little to redistribute

loads and to reduce strains in the main, load-carrying members. Therefore, it was concluded that the timber deck efficiently distributed the test truck loads [1].

In addition to field testing, a computer model was generated, using beam elements in ANSYS, to simulate the theoretical behavior of the TCB under loading equivalent to that used in the field tests. Results from the field tests and analytical model revealed that maximum strains in the structural frameworks of the RRFCs were well below the yield strength of the steel, and that deflections were relatively small when compared to AASHTO maximum deflection recommendations.

Based on flatcar evaluations along with inspection and testing of the TCB, the ISU feasibility study concluded that through systematic and responsible engineering practices, RRFC bridges can feasibly serve as a low-cost LVR bridge alternative. In addition, recommendations were made for the design and construction of future RRFC bridges. Only flatcars with redundant cross-sections decommissioned because of age or economics should be used. In addition, all structural members in the flatcars should be straight to ensure redundancy in the bridge. Moreover, bearing supports for the RRFCs on an abutment should be the same among all RRFCs to ensure symmetrical behavior of the bridge.

Finally, the feasibility study recommended future research with a demonstration project that included design, construction, and testing of a RRFC bridge. In addition, it was stated that through this process, design recommendations and construction guidelines should be developed for future use by county engineers and construction crews [1]. The results of the demonstration project that followed the previously described feasibility are presented in the remaining portion of this thesis.

## **1.2 Objective and Scope of Demonstration Project**

Addressing the recommendations from the 1999 ISU feasibility study, a follow-up research project was initiated in 2000 to design and construct two RRFC demonstration bridges. The objectives of the follow-up research were to (1) develop a process for selecting structurally adequate flatcars, (2) design, construct, and field test two RRFC demonstration bridges, and (3) develop design recommendations and construction guidelines for these alternative LVR bridges. The following tasks were undertaken to meet the research objectives:

1. Thorough inspection and selection of readily available decommissioned RRFCs.
2. The construction and laboratory testing of a connection specimen that simulated a longitudinal connection between adjacent RRFCs.
3. Design and construction of two RRFC demonstration bridges with different types of flatcars, span lengths, substructures, decks, and longitudinal connections.
4. Field testing of the RRFCs before and after the flatcars were connected.
5. Development of a computer model for each bridge for comparison of theoretical and experimental results.

In addition to the aforementioned objectives, construction time and complete bridge cost were recorded for each bridge during the project to document that these types of alternative LVR bridges cost significantly less and require shorter construction times than conventional bridges.

## **1.3 Selected RRFC Bridge Sites**

Buchanan and Winnebago Counties in Iowa expressed interest in using the RRFC bridge concept because of its potential as an economical bridge replacement system. Each bridge site will be briefly described in the following sections.

### 1.3.1 Buchanan County Site

The Buchanan County bridge (BCB) site selected for one RRFC demonstration bridge crosses an unnamed stream and is approximately 5 miles southwest of Independence, Iowa, on 280<sup>th</sup> Street. A map locating the BCB site is presented in Figure 1.1.

The bridge (constructed in 1898) that was replaced (FHWA No. 081330) on the BCB site spanned a total distance of approximately 38' – 5" from center to center of the abutments, and had a timber deck that was 16' – 0" wide. The timber substructure consisted of two abutments and a pier that supported the timber-decked superstructure which had two spans – the west span was a steel, pin-connected kingpost pony truss spanning 24' – 0", while the east approach span was a 14' – 5" timber stringer structure. Due to severe deterioration in the timber piles in the piers and abutments, the bridge had a



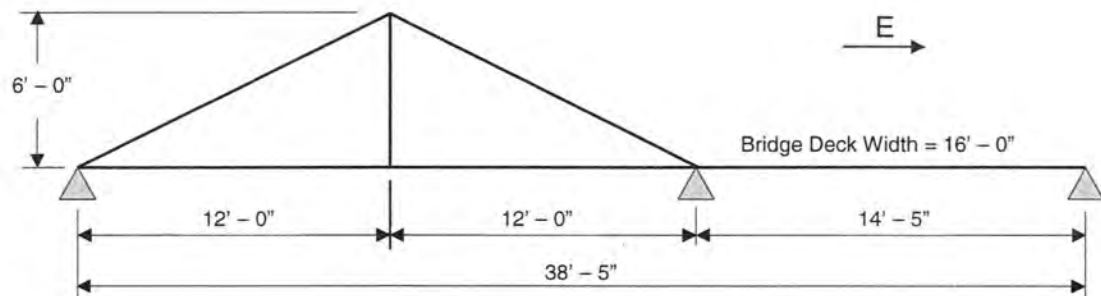
Figure 1.1. Location of the BCB Site [2].



load rating of 10 tons for a tandem truck. Dimensions and a photograph of the replaced bridge at the BCB site are presented in Figure 1.2.

### 1.3.2 Winnebago County Site

The Winnebago County bridge (WCB) site selected for the second RRFC demonstration bridge crosses the North Fork Buffalo Creek and is located approximately



a. Dimensions



b. Photograph of the original bridge

Figure 1.2. Pin-connected, kingpost pony truss bridge at the BCB site.

3 miles east and 3 1/8 miles south of Buffalo Center, Iowa, on 40<sup>th</sup> Avenue. A map locating the WCB site is presented in Figure 1.3.

The replaced bridge (FHWA No. 344610) on the WCB site had a timber deck 20' – 8" wide, spanned a total length of approximately 56' – 0" from center to center of the abutments, and was built in 1949. The substructure consisted of two timber pile abutments and piers, each of which had a 25 degree skew, right ahead; the superstructure consisted of 3 timber stringer spans with each having a length of 18' – 8" as illustrated in Figure 1.4. Due to deterioration in the timber piles, the bridge had a tandem truck load rating of 7 tons.

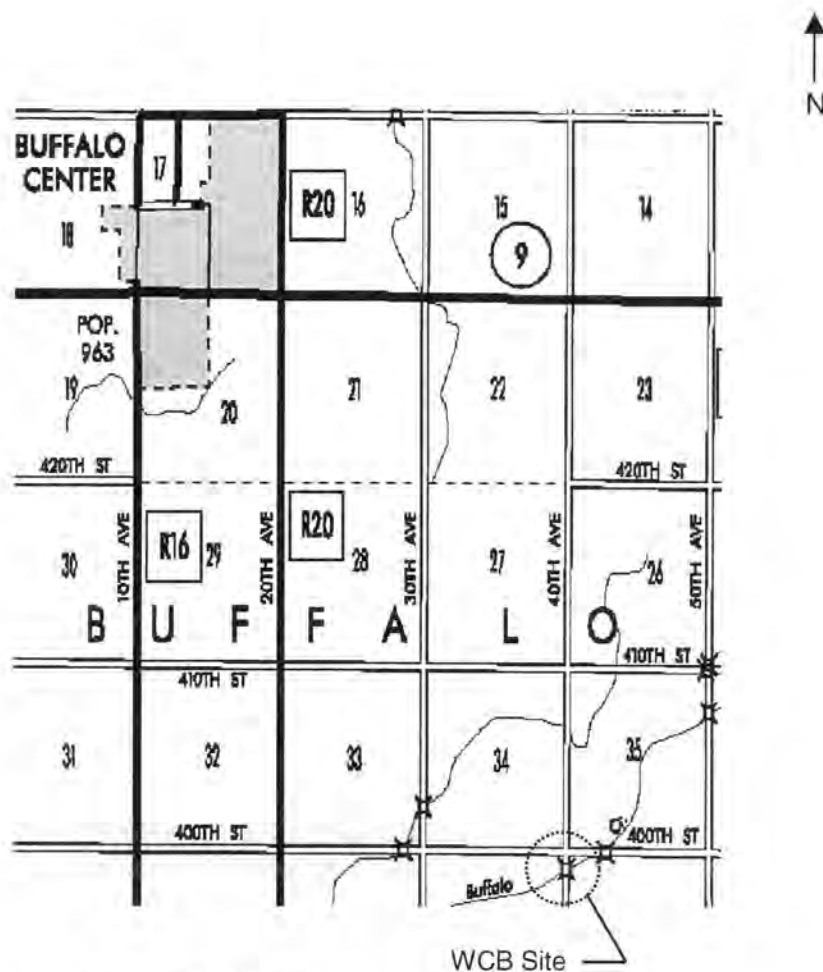
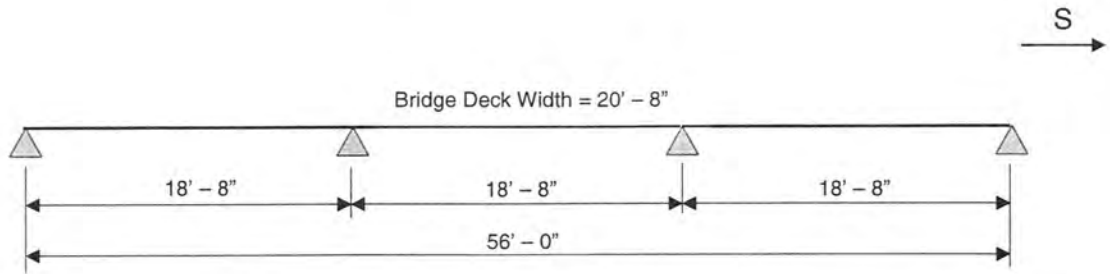


Figure 1.3. Location of the WCB site [3].



a. Dimensions



b. Photograph of the original bridge

Figure 1.4. Three-span, timber bridge at the WCB site.

## 2. RRFC INSPECTION AND SELECTION

### 2.1 Inspection of Alternative RRFCs

Knowing that the demonstration bridges needed to be approximately 38' – 5" and 56' – 0" long (spanning center to center of the abutments) to replace the old BCB and WCB, respectively, contact was made with the Erman Corporation in Kansas City, KS, for assistance with locating appropriate flatcars. The Erman Corporation specializes in collecting, salvaging, and recycling decommissioned RRFCs, and therefore, has vast knowledge in the variety of flatcar structural components, lengths, and availability. In response to the requests, Erman Corporation located four types of flatcars meeting the minimum length requirements for the RRFC bridges – 56-ft RRFCs, 85-ft RRFCs, and two types of 89-ft RRFCs. See Appendix A for a list of RRFC suppliers.

Through inspection of the RRFCs, it was found that although the configuration of the elements in RRFCs may be different, the structural functions of the elements in each configuration remain the same. Therefore, the structural elements of RRFCs can be put into four categories: decking, girders, secondary members, and transverse members. As illustrated in Figure 2.1, the decking is the top plating on each RRFC; girders and secondary members are oriented longitudinally in the RRFC. Girders are the largest members in the RRFC, and thus, will support most of the loads since they will be supported at the piers and/or abutments. Each typical RRFC has three girders – two exterior and one interior. The transverse members are connected orthogonally to longitudinal members, and transfer loads from the secondary members to the girders. Secondary members are the remaining longitudinal members that typically transfer load from the decking to the transverse members.

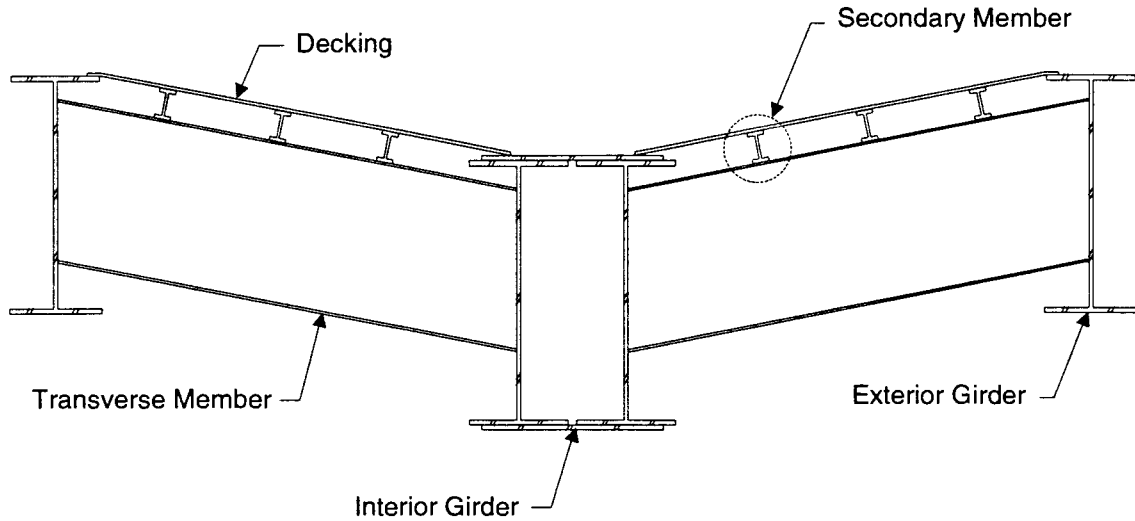
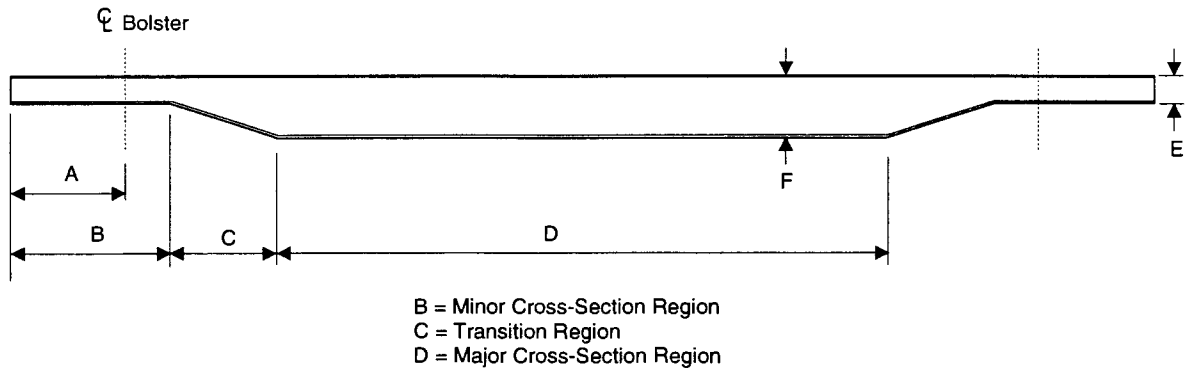


Figure 2.1. Identification of RRFC structural members.

Cross-section structural configurations of each of the four RRFCs previously noted will be discussed in the following paragraphs. Exterior girders have constant cross-sections over the length of the RRFC, and therefore, can accurately be described by one cross-section. However, interior girder cross-sections do not remain constant and vary along the length of the member. Dimensions of the interior girders of the RRFCs reviewed in this investigation are shown in Figure 2.2.

Alternative Flatcar 1 (AF1), the 56-ft v-deck flatcar shown in Figure 2.3, consisted of W-shape girders and secondary members with C-shaped transverse members. There were two sizes of transverse members (Figure 2.3d); they were located on the RRFC approximately as shown in Figure 2.3f. A unique feature of this flatcar was the v-deck resulting from the interior girder being positioned approximately 8 in. below the exterior girders (Figure 2.3b).

Alternative Flatcar 2 (AF2), the 85-ft RRFC presented in Figure 2.4, consisted of an interior box girder, two channels for exterior girders, and Tee-shape secondary members. There are three types of transverse members in this flatcar: S-shape, L-shaped, and U-



RRFC	Dimension					
	A	B	C	D	E	F
56-ft	5' - 0"	7' - 2"	8' - 9"	24' - 2"	1' - 1 1/4"	2' - 3 3/4"
85-ft	11' - 6"	12' - 7"	7' - 5"	45' - 0"	1' - 1 1/2"	2' - 7"
89-ft (Type A)	11' - 6"	12' - 6"	8' - 4"	47' - 4"	1' - 1 3/4"	2' - 6 1/4"
89-ft (Type B)	12' - 0"	13' - 6"	7' - 3"	47' - 6"	1' - 1 1/8"	2' - 6"

Figure 2.2. Details of RRFCs' interior girders.

shaped sections. L-shaped transverse members were positioned at the ends and middle of the major cross-section region (shown in Figure 2.2), while the S-shape transverse members were spaced between the L-shaped members. The U-shaped members were located in the minor cross-section and transition regions of the RRFC. Locations of the transverse members are shown in Figure 2.4j.

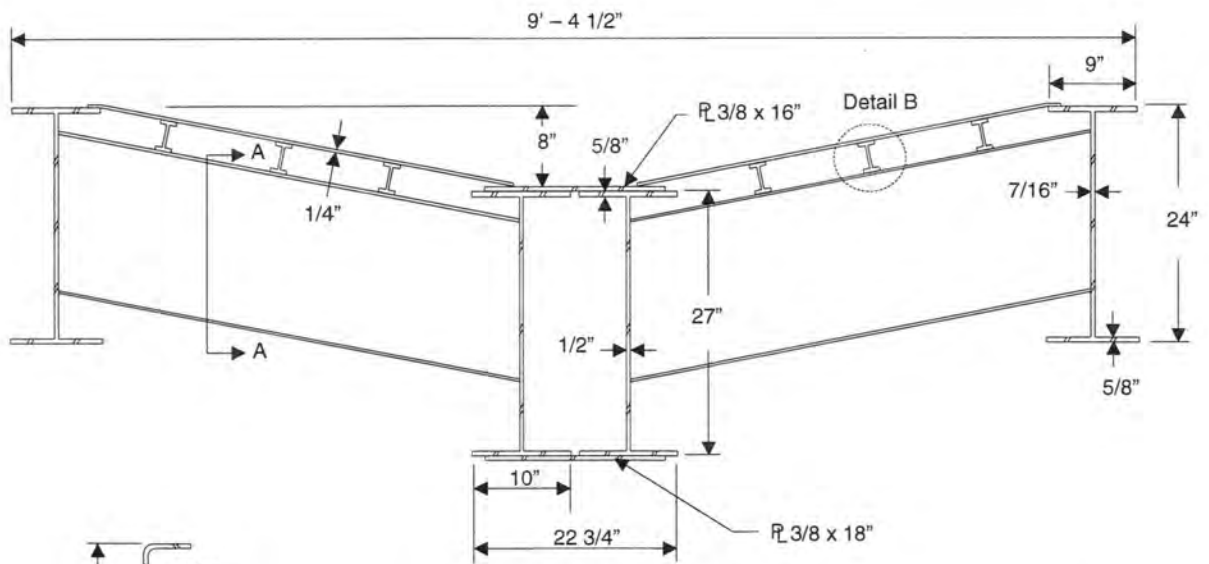
The last two flatcars reviewed were 89 ft long, and will be referred to Type A (Figure 2.5) and Type B (Figure 2.6) for Alternative Flatcar 3 (AF3) and 4 (AF4), respectively. Comparison of the girders, secondary members, and transverse members in Figures 2.4 and 2.5 reveals that the structural configurations of AF2 and AF3 were very similar. AF4 had an entirely different configuration. With the common box girder design for the interior girder, AF4 utilized U-shaped secondary members and unusually shaped



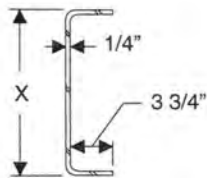
a. The 56-ft RRFC at the Erman Corporation



b. The v-deck



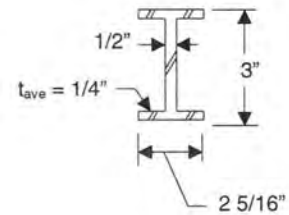
c. Cross-section at midspan



X = 12" for the Small Transverse Member.

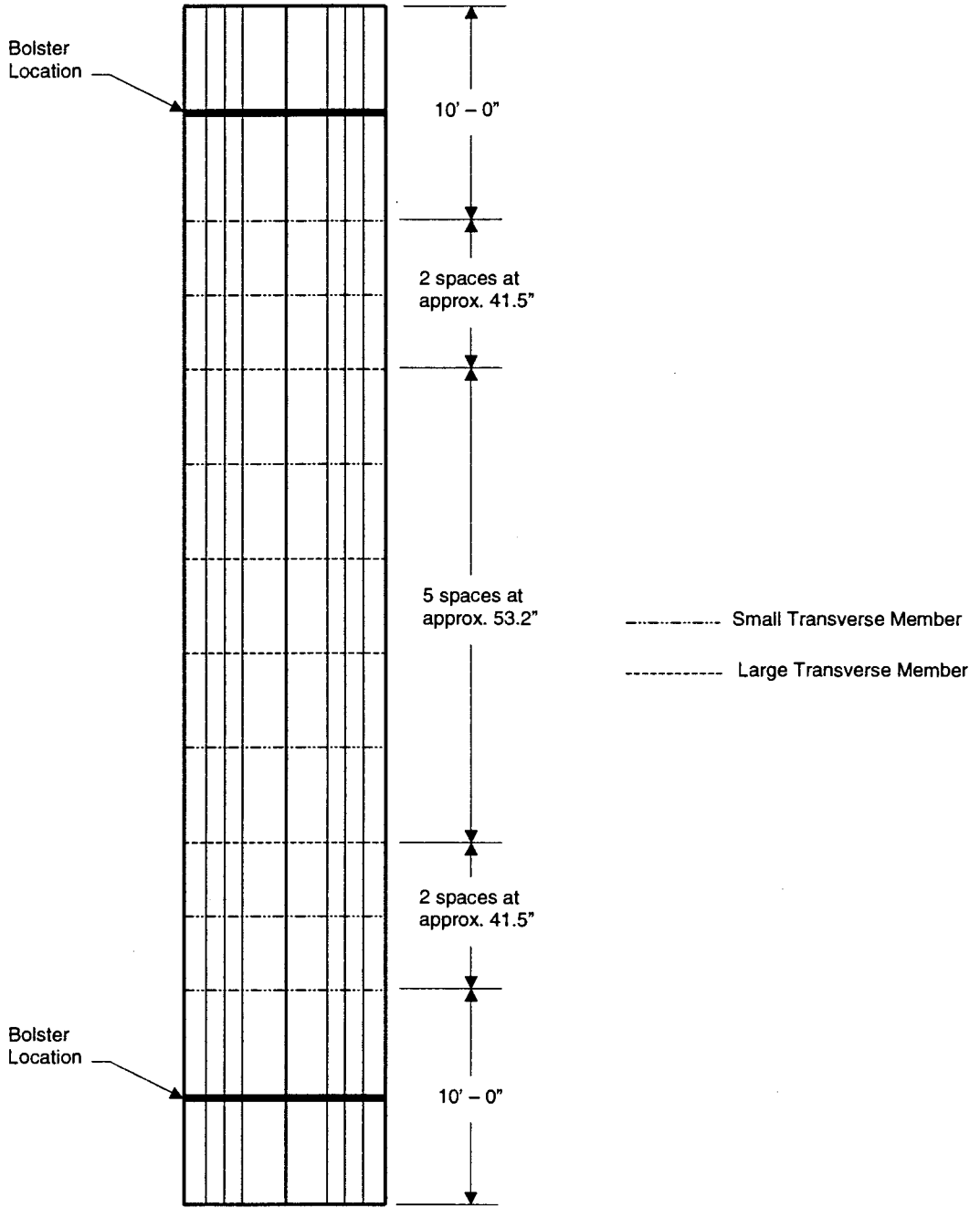
X = 16 3/8" for the Large Transverse Member.

d. Section A - A



e. Detail B

Figure 2.3. AF1 – The 56-ft, v-deck RRFC.



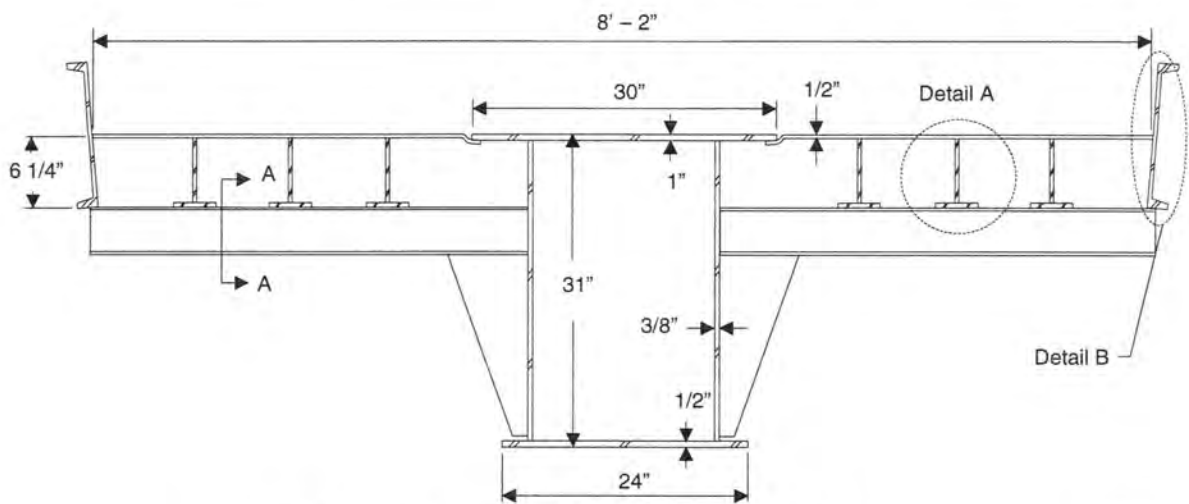
f. Locations of small and large transverse members

Figure 2.3. Continued.

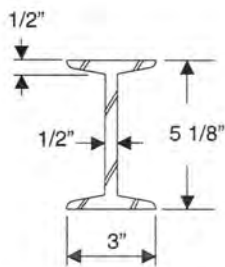




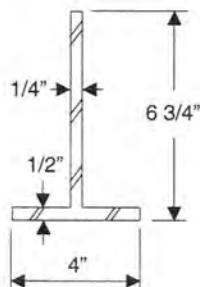
a. The 85-ft RRFC at the Erman Corporation



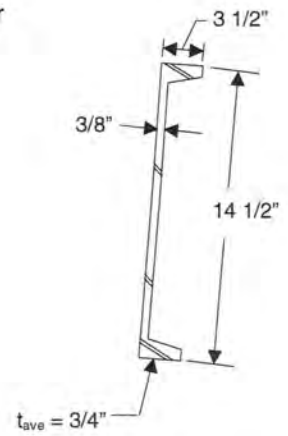
b. Cross-section with S-shape transverse member



c. Section A - A (S-shape)

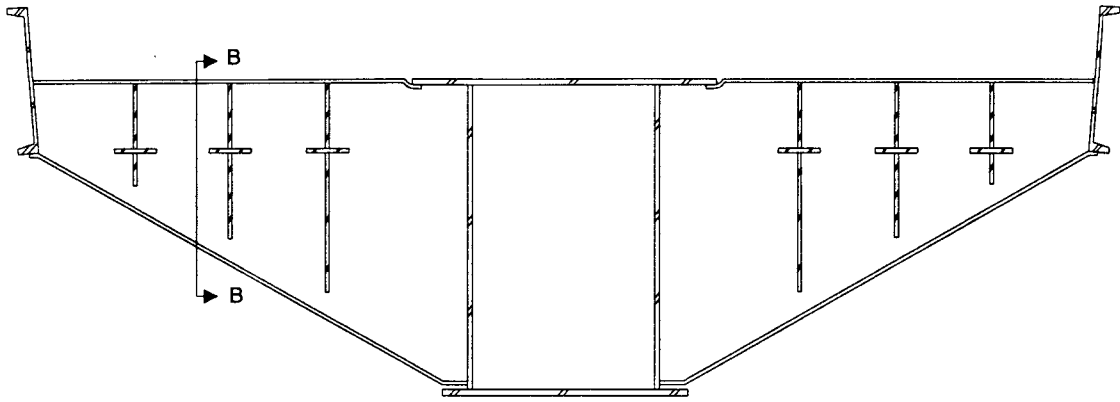


d. Detail A (Tee-shape)

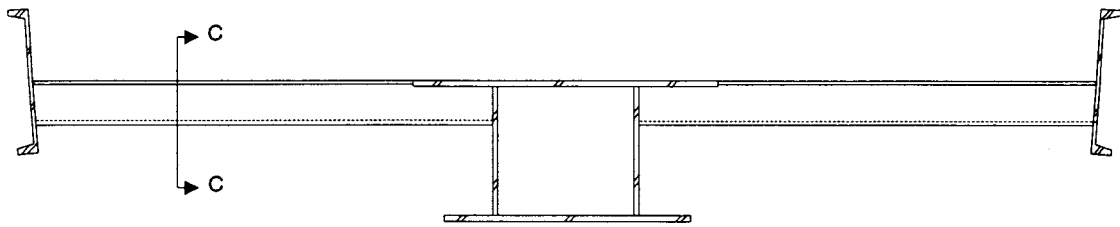


e. Detail B

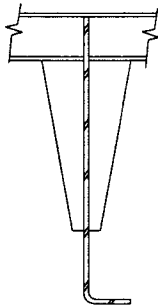
Figure 2.4. AF2 - The 85-ft RRFC.



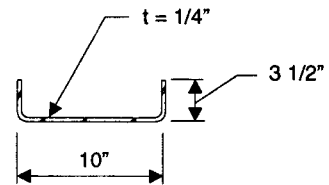
f. Cross-section with L-shaped transverse member



g. Cross-Section with U-shaped transverse member

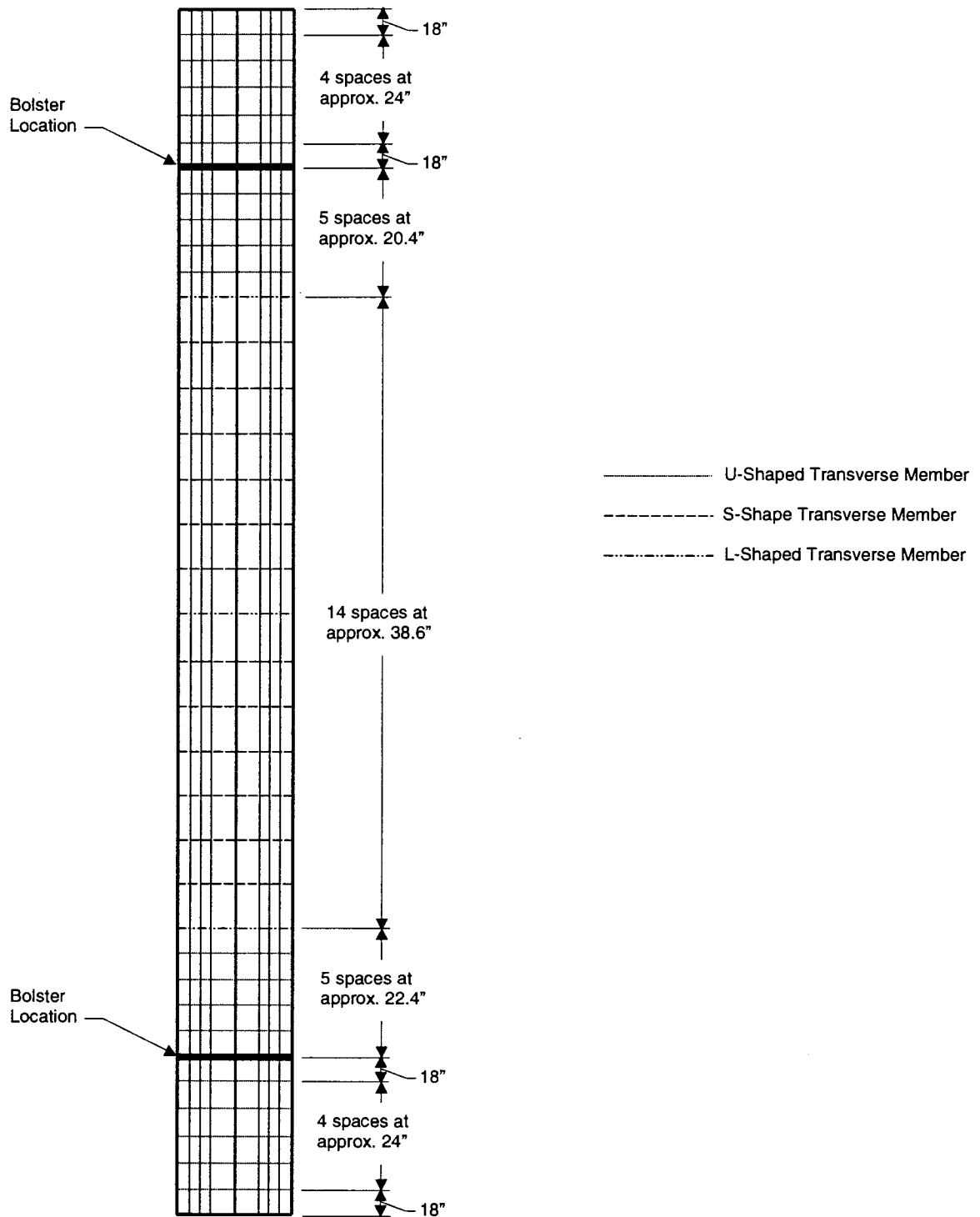


h. Section B - B (L-shape)



i. Section C - C (U-shape)

Figure 2.4. Continued.

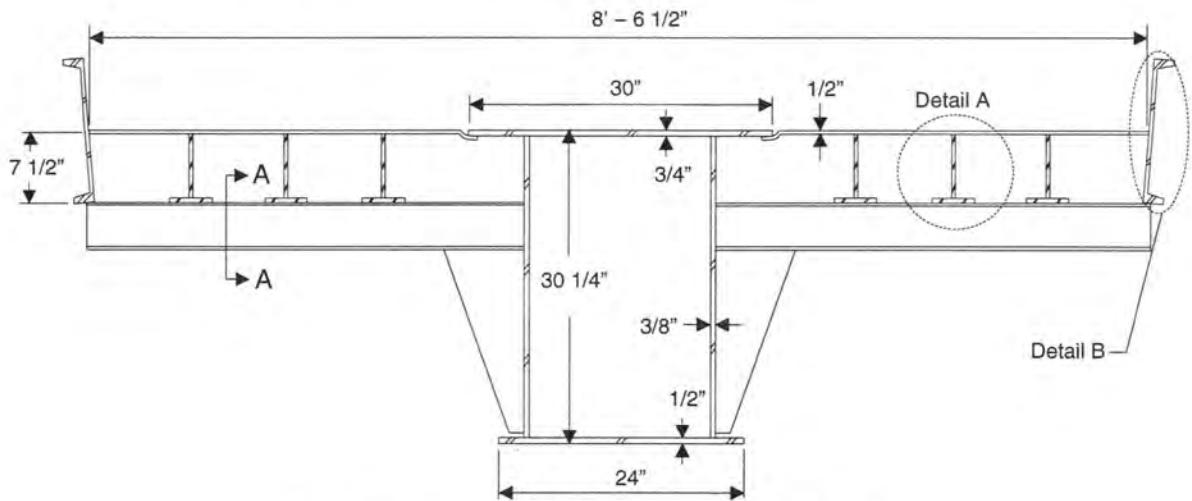


j. Transverse member locations

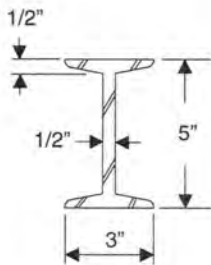
Figure 2.4. Continued.



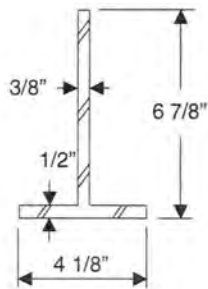
a. The 89-ft RRFC (Type A) at the Erman Corporation



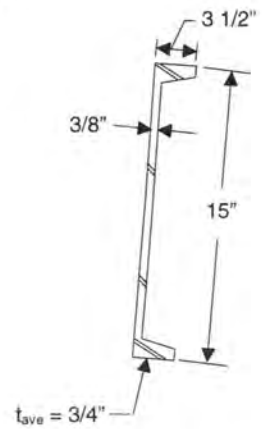
b. Cross-section with S-shape transverse member



c. Section A - A (S-shape)

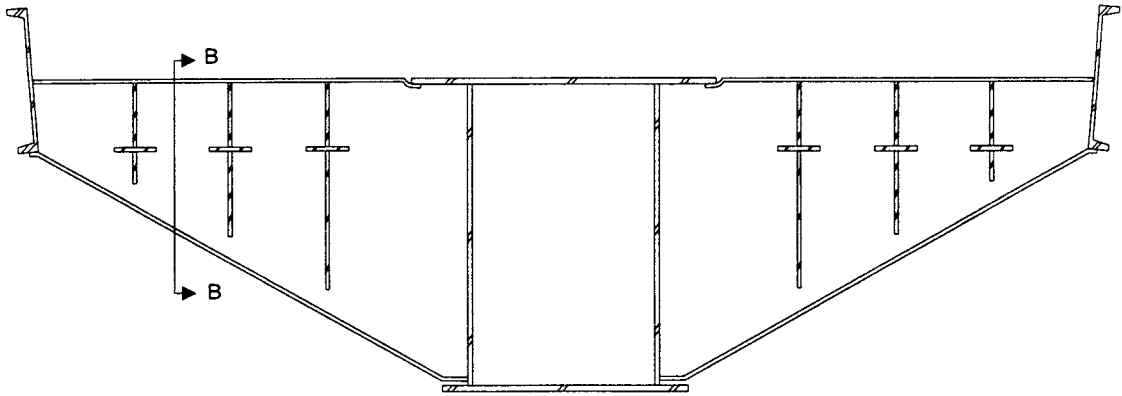


d. Detail A (Tee-shape)

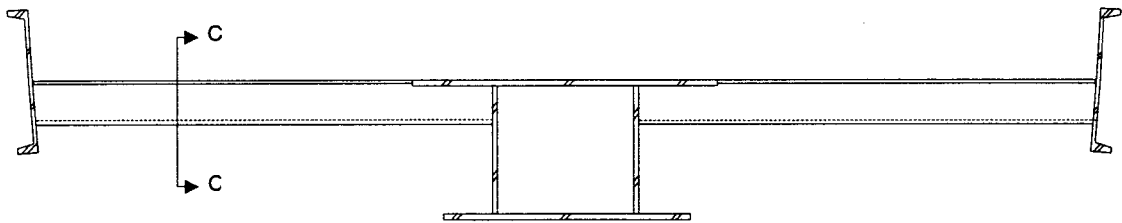


e. Detail B

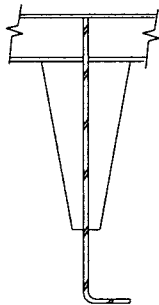
Figure 2.5. AF3 – The 89-ft RRFC (Type A).



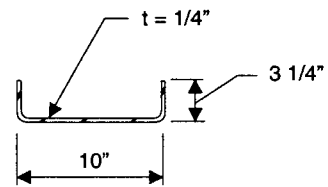
f. Cross-section with L-shaped transverse member



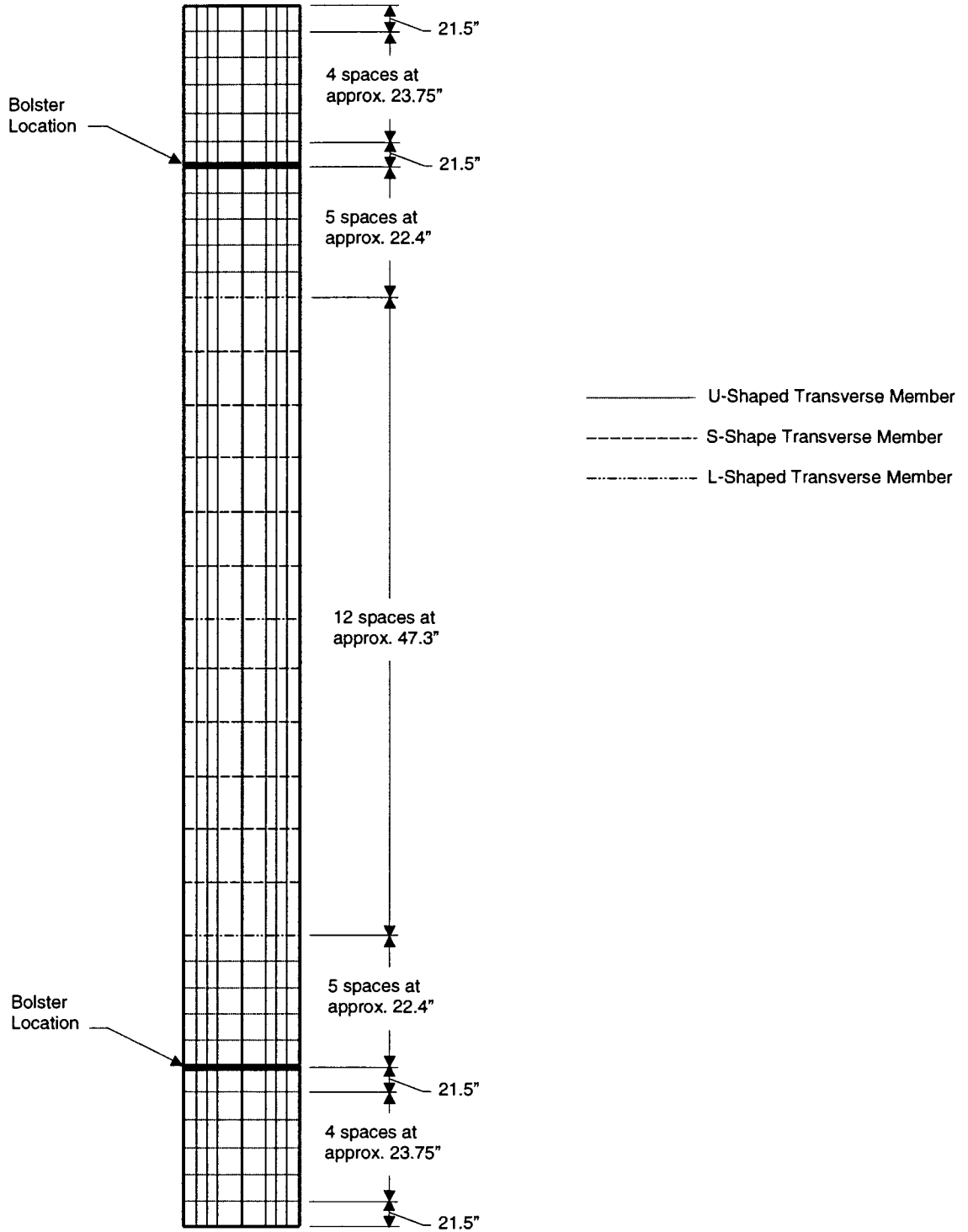
g. Cross-section with U-shaped transverse member



h. Section B - B (L-shape)



i. Section C - C (U-shape)

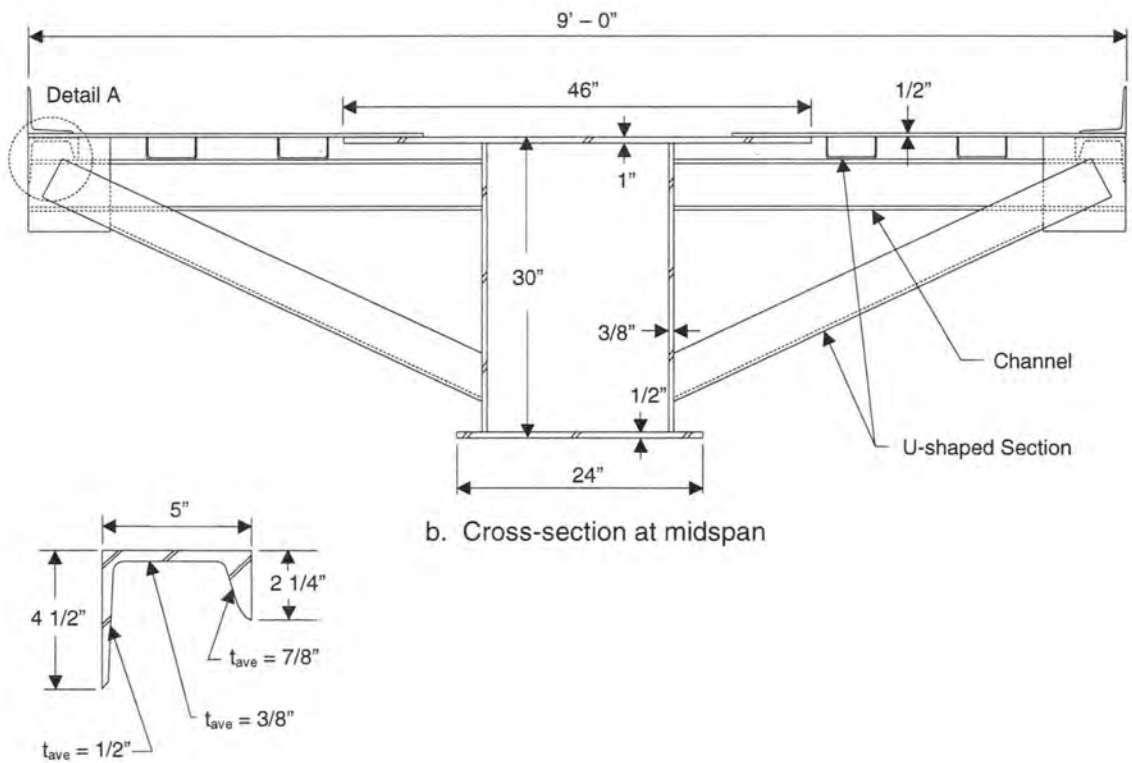


j. Transverse member locations

Figure 2.5. Continued.



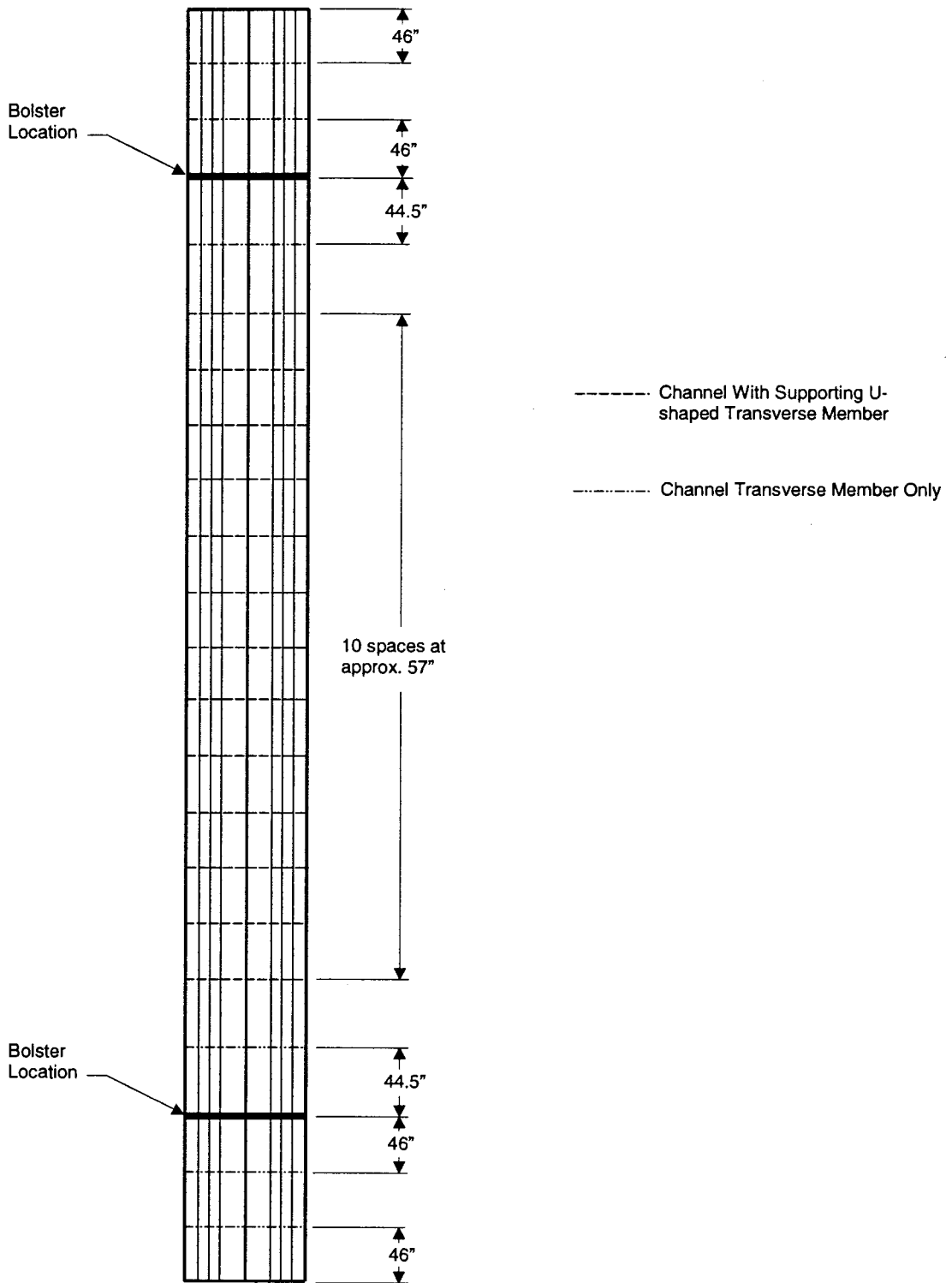
a. The 89-ft RRFC (Type B) at the Erman Corporation



b. Cross-section at midspan

c. Detail A

Figure 2.6. AF4 – The 89-ft RRFC (Type B).



d. Transverse member locations

Figure 2.6. Continued.



exterior girders (Figure 2.6c). The secondary members were supported over the major cross-section region by transverse members consisting of a channel and U-shaped member as presented in Figures 2.6b and 2.6d. In the minor cross-section and transition regions, the diagonal U-shaped support in the transverse member was removed, leaving only a channel for the transverse member.

According to the 1994 LRFD [4] and 1996 LFD [5] AASHTO Bridge Design Specifications, the standard width of a traffic lane is 12 ft. Therefore, regardless of the alternative flatcar chosen, three RRFCs placed side-by-side were required for two full traffic lanes on each bridge.

## **2.2 RRFC Selection Criteria**

Selection of adequate RRFCs is critical to the success of RRFC bridges. Therefore, five criteria were developed and used to extensively evaluate each type of flatcar.

### *2.2.1 Structural Element Sizes, Load Distributing Capabilities, and Support Locations*

If a RRFC is to support lowa legal loads, the members must be of sufficient size to meet strength and serviceability criteria. As discussed in the feasibility study [1], RRFCs with redundant cross-sections offer more longitudinal load paths than RRFCs with non-redundant cross-sections. In other words, a moment on a redundant cross-section will be distributed among three girders, whereas one girder resists a moment in a non-redundant cross-section. As a result, redundant cross-sections generally have a larger flexural capacity, and thus, are more desirable than non-redundant cross-sections for use in LVR bridges.

Although it is not recommended, if flatcars with non-redundant cross-sections are the only RRFCs available for a desired length, it may be possible to use them and still have a redundant bridge superstructure if proper connections are designed to efficiently distribute applied loads to all flatcars in the bridge. Regardless of whether flatcars with redundant or

non-redundant cross-sections are selected, adjacent flatcars must be connected in a RRFC bridge. Therefore, in addition to being structurally adequate to support live loads, the exterior girders in a RRFC must be capable of accommodating longitudinal connections.

In addition to determining flatcars with adequate member sizes, it is important to identify potential areas that have adequate strength to serve as support locations at piers or abutments. For most RRFCs, the girders will be supported by the piers and abutments. If the girders are supported at areas other than the bolster areas, the members need to be checked for adequate strength and stability in the other bearing areas.

### *2.2.2 Member Straightness/Damage*

While many flatcars have been decommissioned because of age or economics, some flatcars have been removed from service because they have been damaged. Deformed members will not adequately carry or distribute loads, and in addition, they may have been yielded or buckled. Therefore, visual inspection, string lines, etc., should be used to determine that all structural members are “perfectly” straight; flatcars with deformed or buckled members, or those with obvious signs of repair, should be rejected.

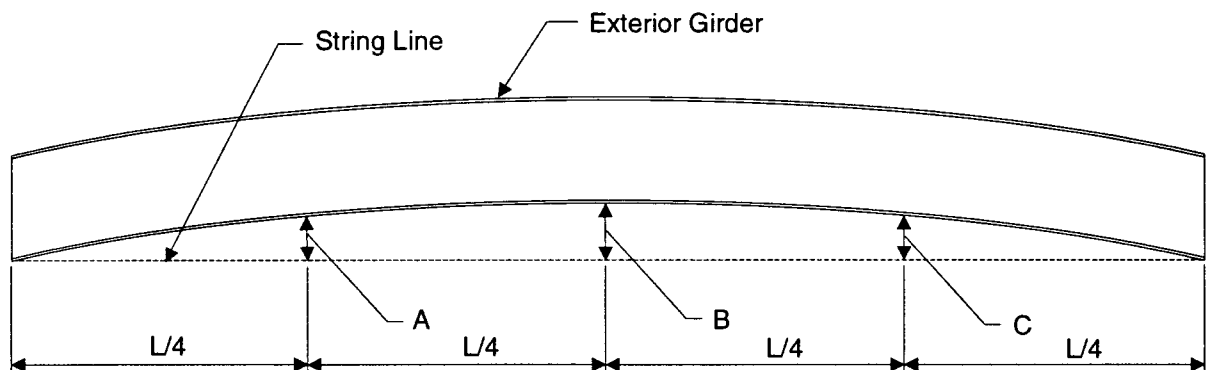
### *2.2.3 Structural Element Connections*

Observations have shown that RRFC members are either connected by rivets or welds. Rivets, however, can lose significant strength over time primarily due to repeated loading or corrosion. Even if all rivets appear to be in good condition at the time RRFCs are inspected, to avoid future problems, it is recommended that only RRFCs with welded member connections be used. Although fatigue issues are not usually a concern with LVR bridges, all welded connections need to be inspected to ensure that fatigue cracks are not already present.

### 2.2.4 Uniform, Matching Cambers

Since several RRFCs will be connected transversely to provide the desired bridge width, careful attention should be given to the camber of each RRFC. Although it was found that cambers are essentially the same for most RRFCs of a particular type, some flatcar cambers do vary. Not only will significantly differing cambers cause problems when connecting the flatcars, but it will also cause difficulties when trying to construct a smooth, level driving surface.

Figure 2.7 illustrates a basic way to measure the camber on RRFCs to ensure that they “match”. After locating the quarter points on each exterior girder, pull a string line from the bottom of one end of an exterior girder to the other. Then, measure the distances “A”, “B”, and “C” indicated in the figure. Distances “A” and “C” should be approximately the same in a given RRFC, and the “B” distance should be approximately the same for each RRFC being considered for use in a particular bridge. It was found during the construction of the RRFC demonstration bridges that  $\pm 1$  in. in camber between adjacent flatcars was



Note: Figure is not drawn to scale; camber is exaggerated.

Figure 2.7. Measuring camber on a RRFC.

manageable during construction. If distances “A” and “C” on a particular RRFC differ by more than 1 in., questions should be raised as to whether or not the RRFC has been damaged.

### 2.2.5 RRFC Availability

The use of RRFCs in LVR bridges is obviously subject to the availability of decommissioned flatcars. As noted previously, structurally sound flatcars are primarily removed from service because of age or economics, and therefore, some flatcars types may be available in limited quantities. If possible, select a type of RRFC that is abundantly available so that identical RRFC bridges may be constructed repetitively without the need for additional designs.

## 2.3 RRFC Selection for the Demonstration Bridges

Midspan section properties listed in Table 2.1 for the girders of each RRFC were calculated and used during the evaluation process. Note that for the exterior girders,

Table 2.1. Calculated midspan girder properties for alternative RRFCs.

RRFC	Girder	Area (in <sup>2</sup> )	I <sub>x</sub> (in <sup>4</sup> )	I <sub>y</sub> (in <sup>4</sup> )
AF1: 56-ft	Exterior	21.1	1,964	76
	Interior	64.4	8,322	2,619
AF2: 85-ft	Exterior			
	- Whole	11.6	334	12
	- Trimmed	5.3	20	6
	Interior	64.1	10,083	4,448
AF3: 89-ft (Type A)	Exterior			
	- Whole	10.8	346	12
	- Trimmed	5.2	25	6
	Interior	56.6	8,999	4,261
AF4: 89-ft (Type B)	Exterior	5.6	10	21
	Interior	79.4	10,775	10,492

“whole” and “trimmed” properties have been calculated. The cross-sections of AF2 and AF3 had exterior girders that extended above the decking. Therefore, in order for those flatcars to be used, the exterior girders of adjacent flatcars at longitudinal flatcar connections needed to be trimmed level with the decking to facilitate a timber deck overlay and/or level driving surface. Therefore, “whole” and “trimmed” refers to section properties before and after the exterior girders were trimmed, respectively.

### *2.3.1 Selection of RRFCs for the BCB*

Since a 38' – 5" span was required for the BCB, AF1 was the most economical flatcar based on length requirements; its adequacy to support live loads needed to be verified. Table 2.1 reveals that the interior and exterior girders of AF1 have significant moments of inertia, which made them capable of supporting live loads. As a result, three load paths were available in the RRFC, and the cross-section was determined to be redundant. In addition, the depth of the exterior girders would easily allow for an engineered, longitudinal connection. Moreover, section property calculations and engineering judgment determined that the transverse members had sufficient flexural strength to transmit loads from the secondary members to the girders.

Visual inspection and use of string lines verified that all structural members were “straight”, and camber among the three RRFCs varied less than 1/2 in. With welded connections between structural elements and Erman Corporation’s assurance that these flatcars were readily available, all criteria were met, and AF1, the 56-ft v-deck RRFC, was selected for use in the BCB.

### *2.3.2 Selection of RRFCs for the WCB*

Although AF1 would have been suitable for the 56' – 0" span length requirement for the WCB, one of the objectives of the project was to construct two demonstration bridges

with differing RRFCs. Therefore, AF1 was rejected. With three alternative flatcars under consideration, attention was once again first given to the girder section properties in Table 2.1. When evaluating the section properties prior to exterior girder trimming, it is apparent that AF2 and AF3 have redundant cross-sections while AF4 offers a non-redundant cross-section. However, after trimming, AF2 and AF3 acquired non-redundant cross-sections due to severe section loss in the exterior girders. As previously mentioned, flatcars with non-redundant cross-sections are not desirable, but they may be adequate for RRFC bridges if proper longitudinal flatcar connections are used to effectively distribute live loads among the three flatcars.

Next, the capabilities of the exterior girders for use in longitudinal flatcar connections were examined. Due to the shallowness and unusual shape of the exterior girder in AF4 (Figure 2.6c), it was determined that this flatcar could not easily accommodate a longitudinal flatcar connection, and thus, it was rejected. However, the remaining portions of the channels below the decking in AF2 and AF3 were considered to be adequate for use in longitudinal flatcar connections.

Both remaining flatcars (AF2 and AF3) had welded connections, and therefore, the camber and straightness of members were next inspected. Visual observations and camber measurements clearly identified a severely deformed exterior girder in AF2; therefore, it was rejected. Although AF4 had already been eliminated, it should be noted that one of its transverse members was severely deformed as illustrated in Figure 2.8, and as a result, load distributing capabilities of the RRFC were limited. An attempt was made to replace the damaged AF4 with an identical substitute, but the Erman Corporation reported that AF4 was not readily available and that it would be difficult finding replacements. AF3 proved to have “straight” members, was verified to be readily available, and the maximum variation in camber among the flatcars was approximately 1 in. Considering 1 in. camber variation to be



Figure 2.8. The deformed transverse member in AF4.

manageable, all selection criteria were met and AF3, the 89-ft (Type A) RRFC, was selected for use in the WCB.

## 2.4 RRFC Preparation and Delivery

While flatcars can often be shipped on the railroad tracks to a railroad yard near the bridge site, the RRFCs must still be transported from the railroad yard to the bridge site. From conversation with Joe Ruttman, Kansas City Plant Superintendent, it was discovered that RRFCs may be transported two ways. If short enough, the RRFCs can be loaded onto drop-deck trailers and be hauled to the site by semi trucks. However, if the flatcars are too long for drop-deck trailers, it is possible to attach dolly axles to the RRFCs and tow them to the bridge site with a semi truck. For this research project, the 56-ft flatcars were hauled with drop-deck trailers, and the 89-ft RRFCs were towed with the semi truck and dolly system.

Most RRFCs will have protrusions on or above the decking of the RRFC that must be removed before the flatcars can be used in a bridge. Except for the trimming required on

the exterior girders that are in longitudinal flatcar connections of the AF3s, Erman Corporation trimmed off all undesirable objects on or above the decking before the RRFCs were delivered to the bridge sites. Figure 2.9 presents AF1 after it has been “trimmed” and transported to the BCB site. Comparison of Figures 2.3a and 2.9 illustrates the amount of material “trimmed” from the AF1. Figure 2.10 presents AF3 after it has been delivered to the WCB site; by comparing Figures 2.5a and 2.10, one can see the amount of material removed from AF3.



Figure 2.9. The trimmed AF1 at the BCB site.



Figure 2.10. The trimmed AF3 at the WCB site.



### **3. CONSTRUCTION OF THE DEMONSTRATION BRIDGES**

In this investigation, the use of two different RRFCs for the superstructures in LVR bridges and the connections between adjacent RRFCs in the bridges were investigated. The demonstration bridges in Buchanan and Winnebago counties were constructed considerably different in terms of the structural materials used, types of RRFCs used, number and length of spans, etc. However, the construction procedures were essentially the same for these two bridges; these procedures can be grouped in three phases:

- Phase 1: Substructure Development and Flatcar Placement
- Phase 2: Development of Longitudinal Flatcar Connections
- Phase 3: Installation of the Driving Surface and Guardrails

Details of each construction phase of the the BCB and WCB are presented in Sections 3.1 and 3.2.

#### **3.1 BCB Construction**

The RRFCs in the BCB were positioned side-by-side so that a non-skewed, two-lane bridge approximately 29 ft wide and 59 ft long (out-to-out dimensions) resulted (Figure 3.1). Each trimmed, 56-ft flatcar weighed approximately 35,000 lb, and each RRFC was placed on the abutments with a backhoe lifting one end of the RRFC and a crane lifting the other end of the RRFC. The flatcars for the BCB were supported at their ends on concrete abutments, which allowed for an integral abutment at the east end of the bridge and an expansion joint at the west end. In addition, longitudinal connections were installed between the adjacent flatcars to create transverse live load distribution. After structurally connecting the RRFCs, a layer of pea gravel was placed to facilitate drainage, an asphalt milling driving surface was constructed, and a guardrail system was installed. In the following sections, details on the construction of this bridge are presented.

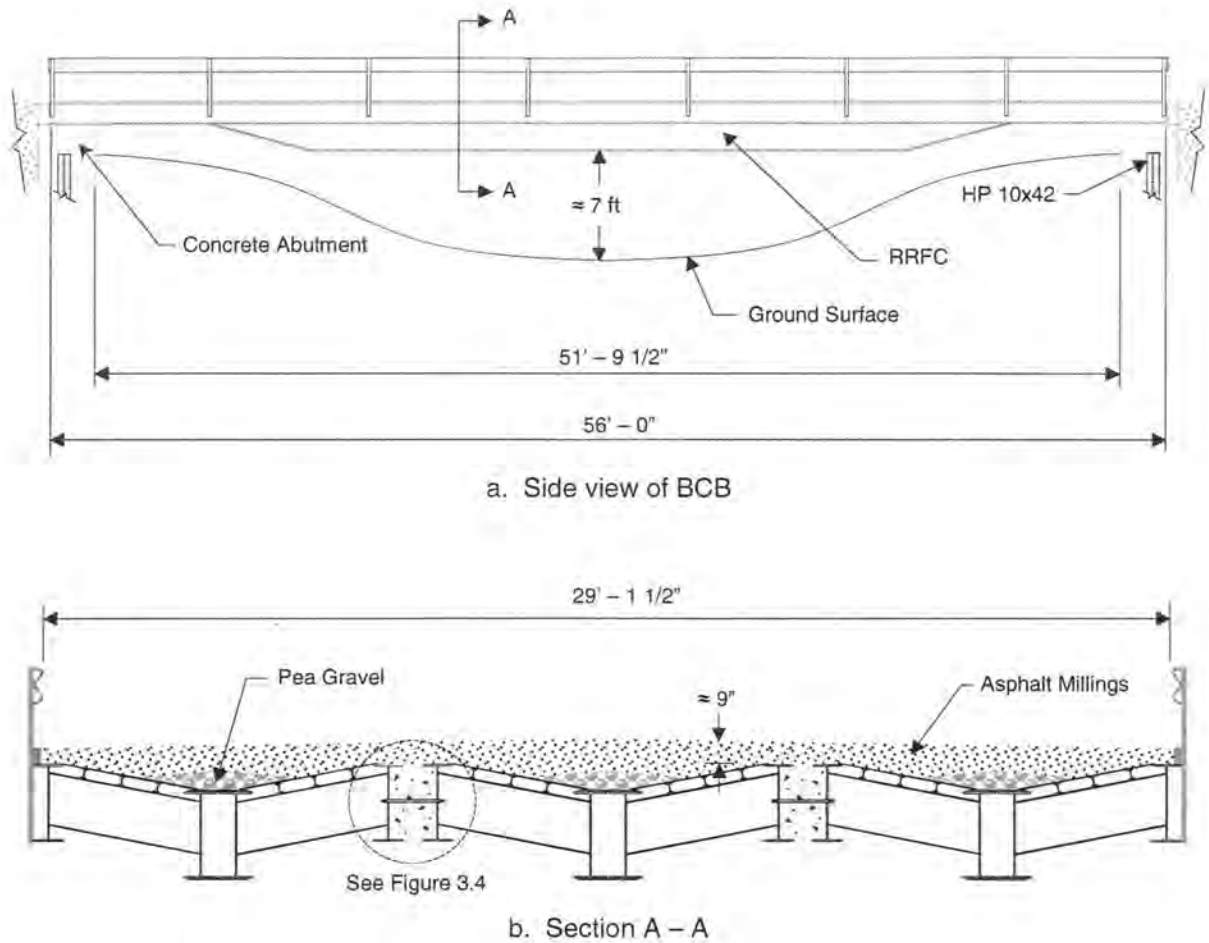
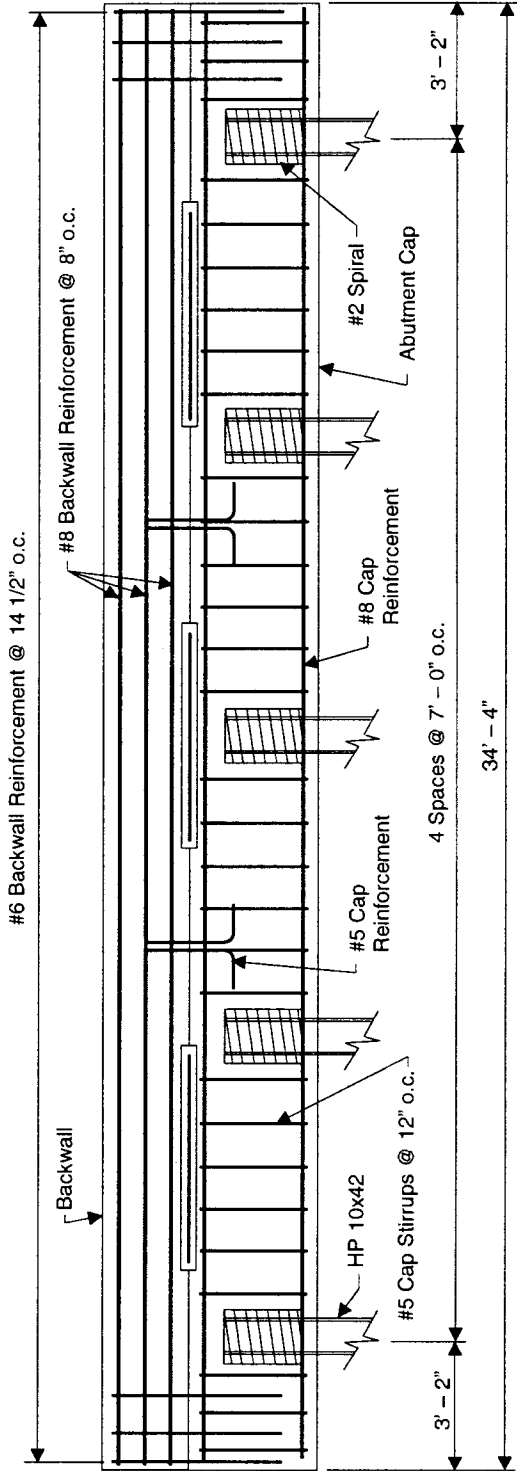


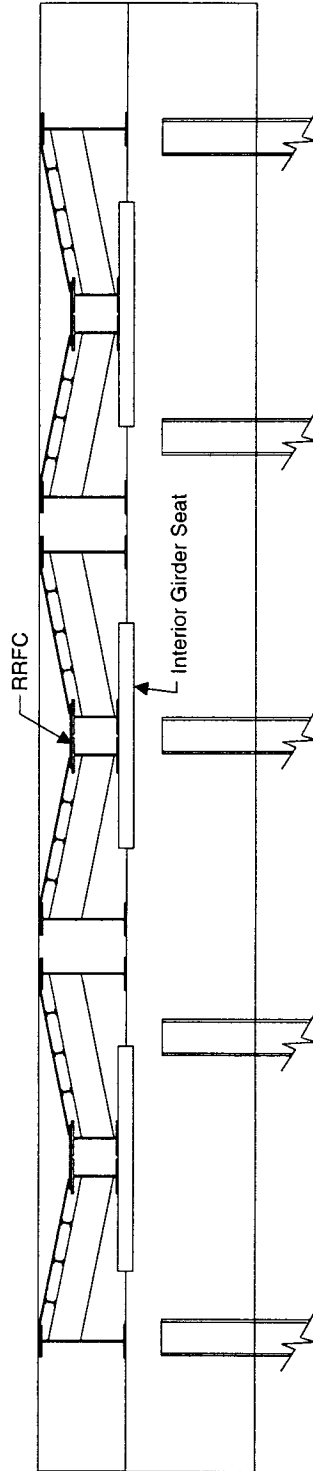
Figure 3.1. Side and cross-sectional views of the BCB.

### 3.1.1 BCB Phase 1: Substructure Development and Flatcar Placement

Abutments shown in Figure 3.2 utilized concrete cap beams with bearing plates and backwalls; these are similar to the Iowa Department of Transportation (Iowa DOT) standard abutments for a continuous concrete slab bridge with zero skew [6]. Five HP10x42s, extending two ft into the concrete cap, were driven to bedrock approximately 30 ft below the ground surface. For the cap, #8 longitudinal reinforcement and #5 stirrups provided flexure



a. End view showing steel reinforcement



b. End view showing RRFC placement

Notes:

All Reinforcing Steel is Grade 60.  
Structural Concrete is Class "C".

Figure 3.2. Details of the BCB concrete abutments.

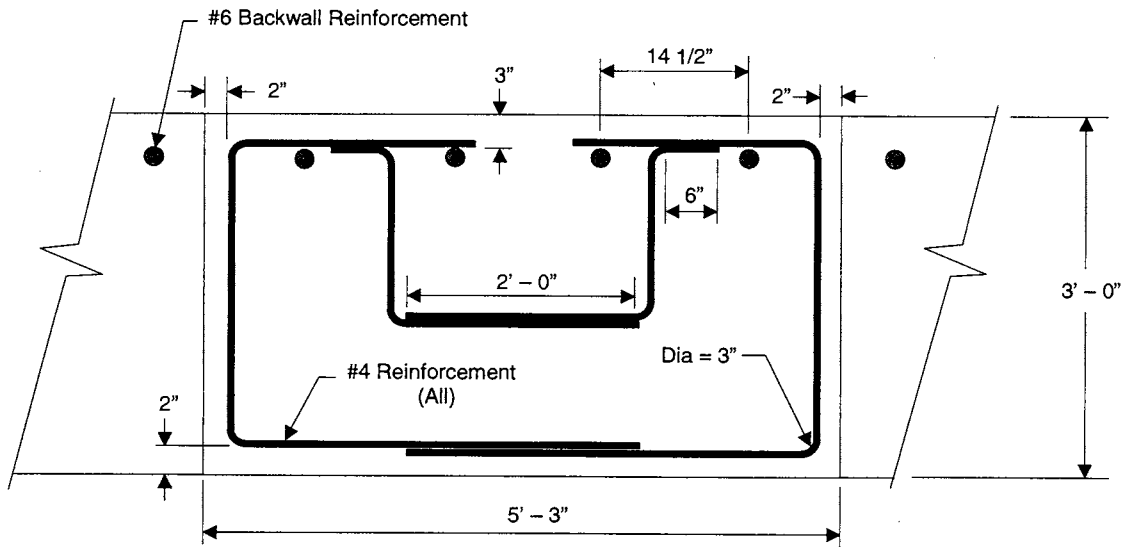
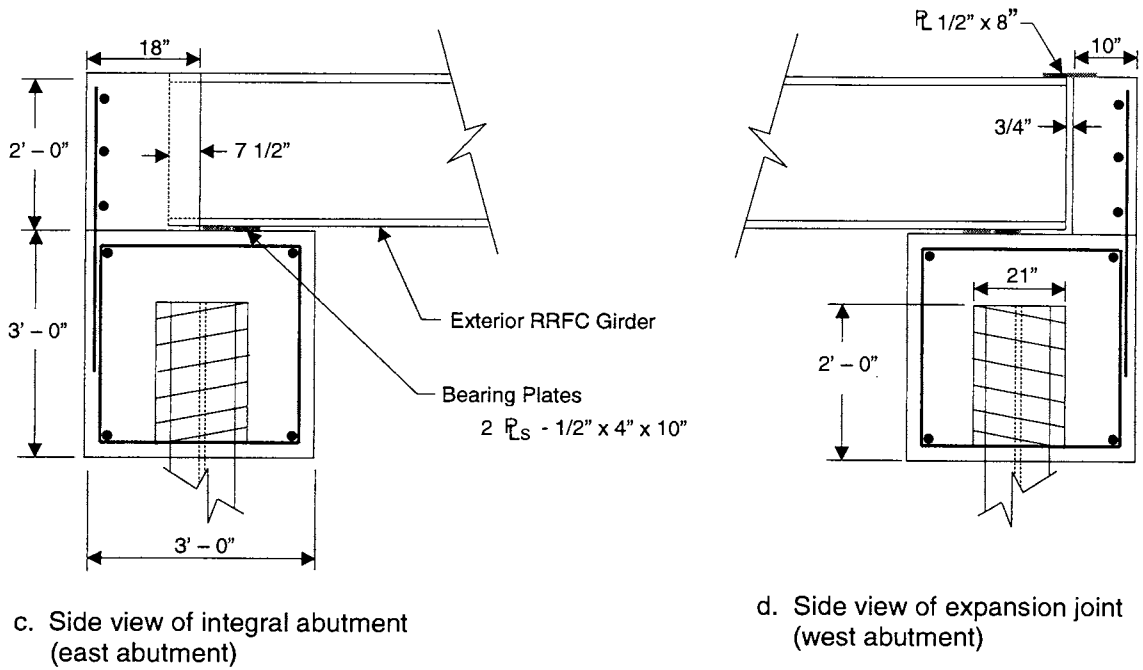


Figure 3.2. Continued.

and shear resistance, respectively. In the east cap, #5 reinforcement with 90 degree hooks on each end extended from the cap into the two longitudinal connections between adjacent RRFCs. Additional details on these connections are presented in Section 3.1.2. The backwall was connected to the cap with #6 reinforcement. The use of reinforced concrete in the substructure made it possible to have an integral abutment (with 7 1/2 in. of the flatcar cast into the backwall (See Figure 3.2c)) at one end of the bridge. An expansion joint (with 3/4 in. gap between the RRFC and the backwall) was constructed at the other abutment (Figure 3.2d). To prevent the future asphalt milling driving surface from falling into the expansion joint, a 1/2 in. thick, 8 in. wide plate was used to cover the 3/4 in. gap.

In each flatcar, the bottom flange of the interior girder was 1 1/2 in. higher than the bottom flanges of the exterior girders. As a result, it was not possible to support all three girders on a level concrete cap beam. To support the interior girders, seats shown in Figure 3.2b were constructed. Rather than attempting to pour these seats monolithic with the cap beam, it was decided to pour them monolithic with the backwall after the three RRFCs were in place; the concrete could thus be placed so that it was in direct contact with the bottom of the interior girders. Since a 1 1/2 in., reinforced concrete seat could possibly crush if subjected to overload, it was decided to construct reinforced seats with a minimum thickness of 5 in. This was accomplished by creating a 3 1/2 in. vertical void in the cap at the seat locations during pouring of the cap beam, placing the reinforcement shown in Figure 3.2e, and then pouring the 5 in. thick seats (3 1/2 in. in the cap beam plus 1 1/2 in. to the bottom of the three interior girders) monolithic with the backwall.

BCB Phase 1 is illustrated in Figure 3.3 and can be summarized as follows:

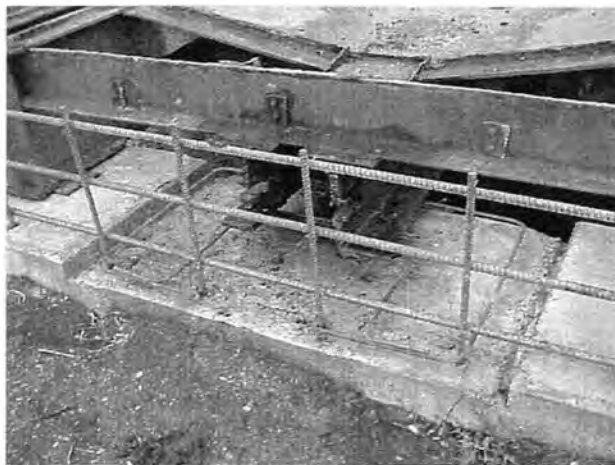
1. The concrete cap beams were constructed with a 3 1/2 in. deep void at the interior girder seat locations (Figure 3.3a).
2. RRFCs were placed on the cap beams after they had cured for 2 1/2 weeks (Figure 3.3b).



a. Concrete cap beam prior to RRFC placement



b. Flatcar placement on the cap beams



c. Backwall and interior girder seat reinforcement

Figure 3.3. Phase 1 construction on the BCB.



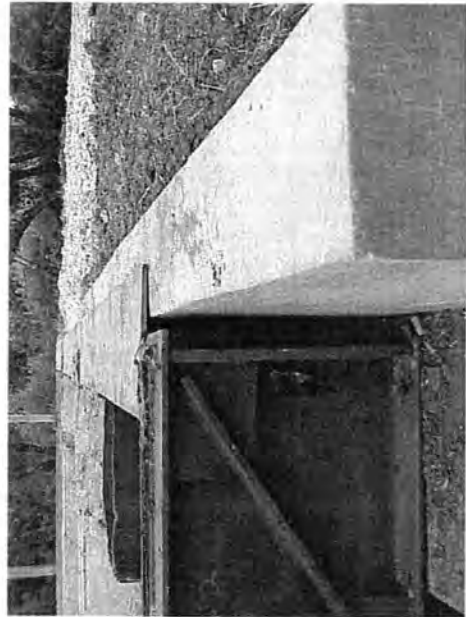
e. Completed interior girder seat



g. Integral east abutment



d. Completed abutment backwall



f. Expansion joint at the west abutment

Figure 3.3. Continued.

3. Interior girder seat reinforcement was installed (Figure 3.3c).
4. The backwall and 5 in. thick interior girder seats were placed monolithically (Figure 3.3d and Figure 3.3e).
5. The west expansion joint was completed (Figure 3.3f). The integral abutment was completed with backwall pour (Figure 3.3g).

### 3.1.2 BCB Phase 2: Development of Longitudinal Flatcar Connections

The 56-ft flatcars have large, exterior girders capable of supporting significant live loads. If one cut off part of the flanges so that adjacent flatcars could be directly bolted together, there would be a significant reduction in the flexural capacity of each RRFC. Therefore, a connection (shown in Figure 3.4) using the exterior girders and a reinforced concrete beam to form a longitudinal, composite connection was developed. The exterior girders of the flatcars were spaced 6 in. apart, thus creating a void that was approximately 14.5 in. wide and 24 in. deep between adjacent RRFCs. Transverse threaded rods (2 ft on center) passing through the mid-height of the webs of adjacent girders (via 13/16 in. holes) prevented transverse separation of adjacent flatcars. Concrete and longitudinal

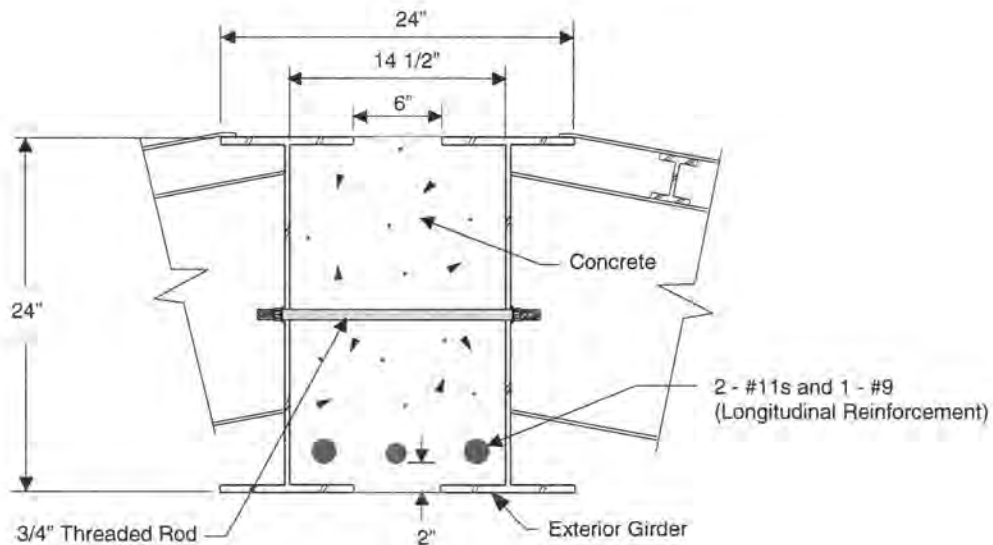


Figure 3.4. Longitudinal flatcar connection used in the BCB.



reinforcement (one #9 and two #11s) were placed in the void to form a reinforced concrete beam; the reinforcement was selected so that the reinforced concrete beam was able to support its self-weight and traffic loads. As briefly discussed in Section 3.1.1, the #5 reinforcement extending from the east abutment were cast into the connection between the two flatcars. To confirm the strength and behavior of this connection, a laboratory connection specimen (LCS) of this type of connection was constructed. This specimen was tested to verify its flexural and torsional strengths; additional details on LCS testing and behavior are presented in Sections 4.1 and 5.1.

For ease of construction, the 13/16 in. diameter holes in the exterior girders of the middle RRFC were drilled before the flatcars were placed on the abutments. After flatcar placement, holes through exterior girders in the two exterior RRFCs were drilled in alignment with those in the middle RRFC. Midspan shoring was used during construction of the longitudinal flatcar connections to reduce the concrete dead load being distributed to the RRFCs.

BCB Phase 2 is illustrated in Figure 3.5 and can be summarized as follows:

1. Holes (13/16 in. diameter) were drilled through the webs of the exterior girders on exterior RRFCs for the transverse threaded rods (Figure 3.5a).
2. Formwork was clamped to the bottom flanges of adjacent, RRFC exterior girders; midspan shoring was erected (Figure 3.5b).
3. Longitudinal reinforcement was positioned in the void between adjacent exterior girders; transverse threaded rods were installed and tightened (Figure 3.5c).
4. Concrete was placed in the void between adjacent flatcars. After two weeks of curing, the forms were removed (Figure 3.5d).

The Buchanan County survey team recorded elevations of the exterior girders in the connections at the 1/4, 1/2, and 3/4 span locations before and after the concrete was placed in the connections. Elevation comparisons revealed that the 1/4 and 3/4 span locations deflected 0.04 in., and midspan deflected 0.05 in. Although the shoring was firmly



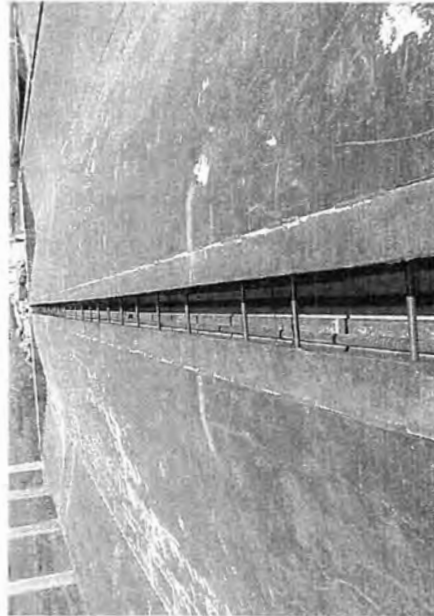
b. Formwork for concrete placement



d. Connection after concrete placement



a. Drilling holes for the transverse threaded rod



c. Threaded rod and longitudinal reinforcement

Figure 3.5. Phase 2 construction of the BCB.

positioned on the sandy base of the stream, it is assumed that the small girder deflections resulted from shoring settlement.

### *3.1.3 BCB Phase 3: Installation of the Driving Surface and Guardrails*

In the first task of Phase 3, guardrail posts were welded to the flanges of the exterior girders at the edges of the bridge. A timber side rail was placed along the top side of each edge girder and nailed to the guardrail posts; these side rails provided lateral support to the asphalt milling driving surface that was used.

To facilitate drainage in the BCB, a layer of pea gravel was first placed on the RRFC decks (See Figure 3.6c) over existing small holes in the decks. This was followed by installation of an asphalt milling driving surface approximately 5.5 in. and 9.0 in. deep at the edges and middle of the bridge (with respect to the top flanges of the exterior girders), respectively. A thrie beam was added to complete the guardrail system.

BCB Phase 3 is illustrated in Figure 3.6 and can be summarized as follows:

1. Guardrail posts were welded to the bridge (Figure 3.6a).
2. Side rails were attached to the guardrail posts (Figure 3.6b).
3. Pea gravel was placed above existing deck holes (Figure 3.6c).
4. The asphalt milling driving surface was constructed (Figure 3.6d).
5. A thrie beam was added to the guardrail posts, which completed the construction of the demonstration bridge.

A photograph of the completed BCB is presented in Figure 3.7.

## **3.2 WCB Construction**

The RRFCs in the WCB were positioned side-by-side so that a non-skewed, two traffic lane bridge approximately 26' – 9" wide and 89' – 0" long (out-to-out dimensions) was obtained (See Figure 3.8). Each trimmed, 89-ft flatcar weighed approximately 42,000lb, and two cranes were used to lift the flatcars onto the abutments and piers. Flatcars were



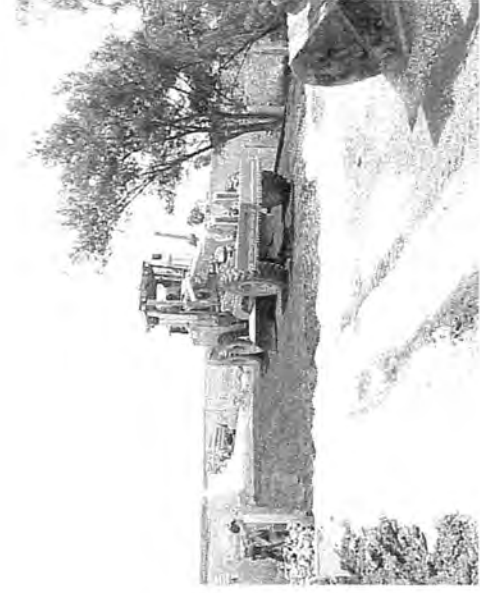
a. Guardrail posts welded on the BCB



b. Nailing on the side rail for the driving surface



c. Laying pea gravel



d. Blading the asphalt milling driving surface

Figure 3.6. Phase 3 construction on the BCB.



Figure 3.7. Finished Buchanan County RRFC Bridge.

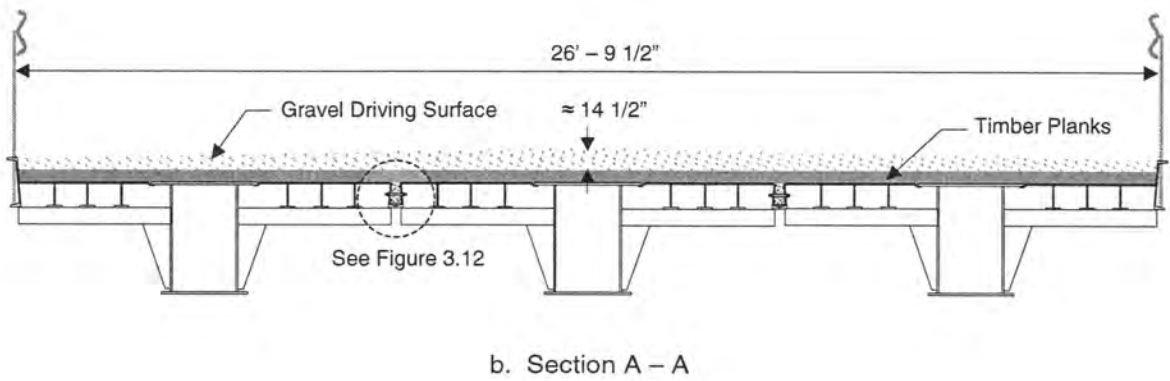
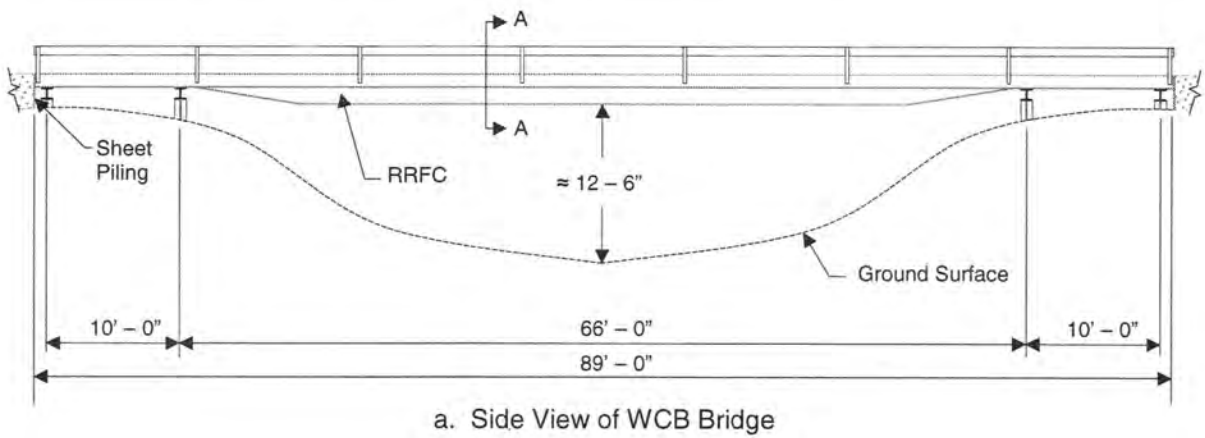


Figure 3.8. Layout and connection on the WCB.

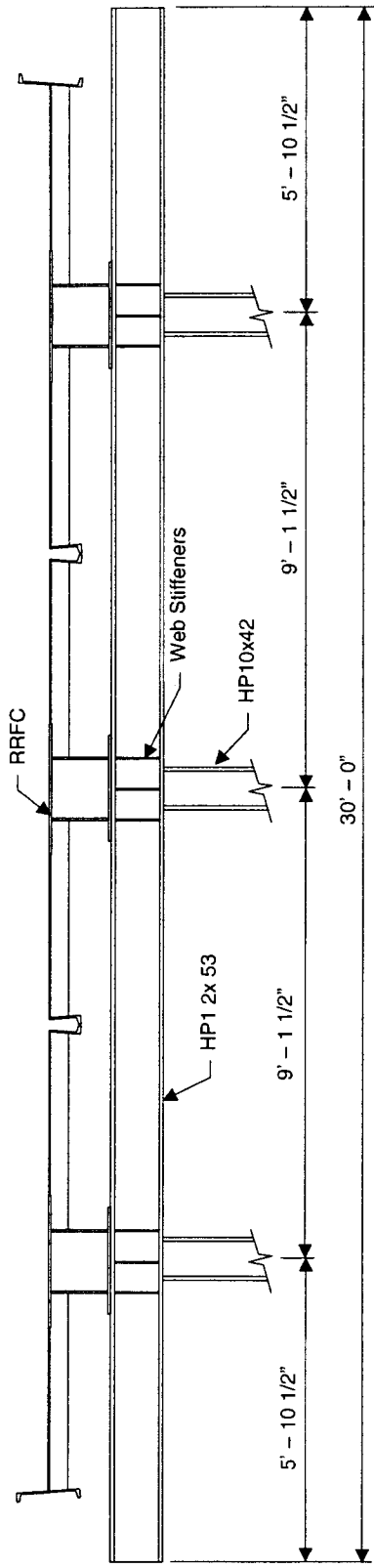
directly welded to the south abutment, preventing translation in all directions; expansion joints were installed at the north abutment and at the piers. Longitudinal flatcar connections and a transverse timber deck overlay were installed to help distribute live loads transversely across the bridge, and a gravel driving surface and guardrail system were added to complete the bridge.

### *3.2.1 WCB Phase 1: Substructure Development and Flatcar Placement*

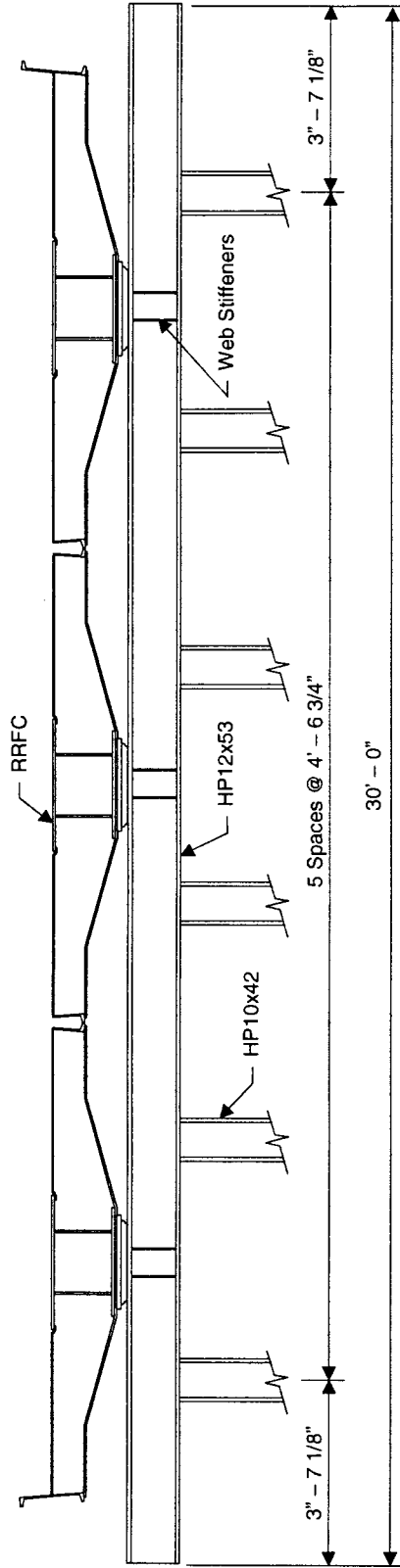
Preliminary calculations determined that the 89-ft RRFCs were inadequate for use in a single span situation. Thus, steel-capped piers and abutments were provided at the RRFC bolsters and ends, resulting in a 66-ft main span and two 10-ft side spans. Pier supports alone would have satisfied strength requirements, but supporting the RRFCs only at the bolsters would have permitted vertical displacements at the ends of the bridge when traffic was on the main span. Displacement of this type would have been a safety threat to vehicles entering the bridge; therefore, abutments were added to prevent vertical displacement at the ends of the bridge. These abutments also helped reduce the deflections resulting from traffic loads at midspan of the main span.

As illustrated in Figure 3.9, the abutments and piers utilized HP10x42s for piling and HP12x53s for the cap beams. For the WCB, friction piles averaged 56 ft in length and 40 tons in bearing capacity at the abutments, and 62.5 ft in length and 45.2 tons in bearing capacity at the piers. Portions of the members extending above the decking were removed prior to flatcar placement to facilitate placement of the transverse timber planks and to simplify construction of the longitudinal connections between adjacent RRFCs. Web stiffeners (3/8 in. thick) were added to the cap beams to prevent web local buckling below the bolsters in the piers and below the interior girders in the abutments.

Since the bottoms of the exterior girders were at a higher elevation than the bottoms of the bolsters and interior girders, exterior girder supports shown in Figure 3.10 were

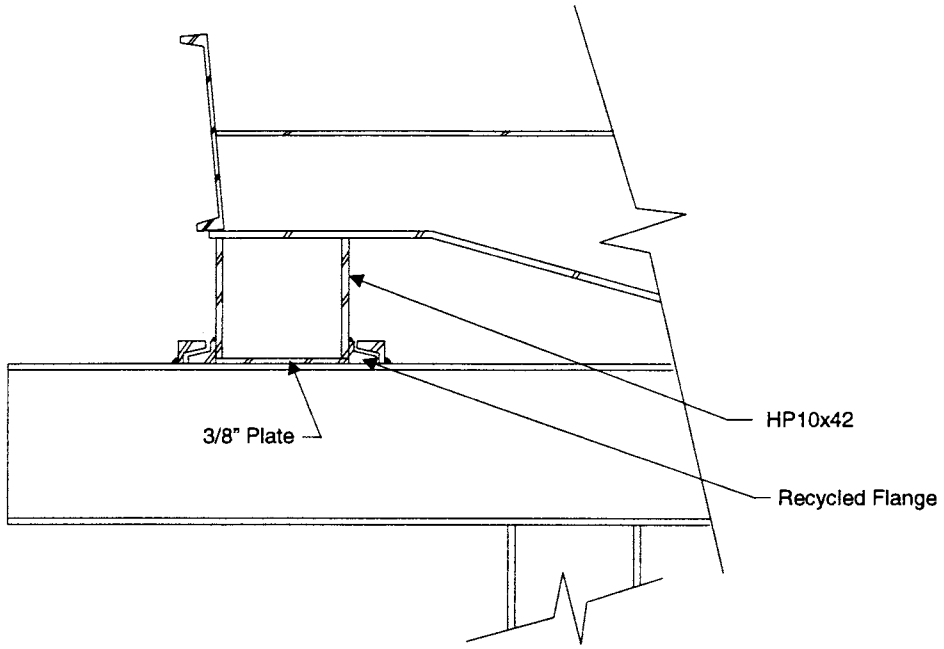


a. End view of an abutment

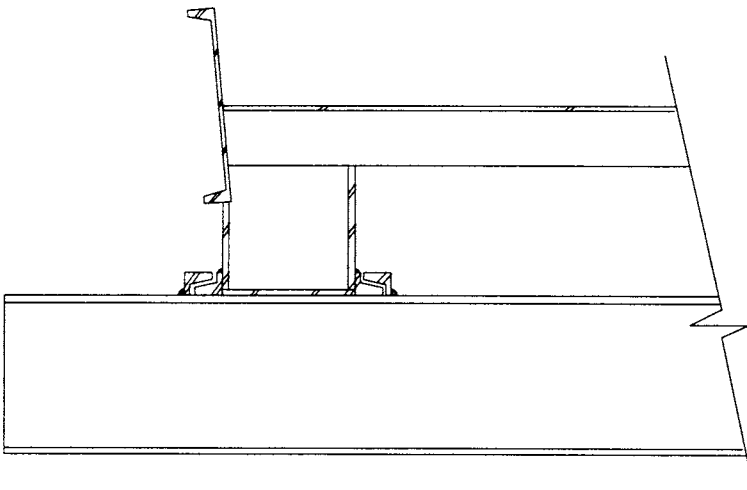


b. End view of a pier

Figure 3.9. Winnebago County RRFC bridge abutments and piers.



a. Exterior girder support at the pier



b. Exterior girder support at the abutment

Figure 3.10. Exterior girder supports in the WCB.



required at the abutments and piers. These supports were constructed by welding a 3/8 in. bearing plate to the bottom of HP10x42 sections; the tops of the HP10x42s were cut to fit the exterior girders that they were supporting. For each support, the one flange of the HP10x42 supported the web of the exterior girder while the other flange and web of the HP10x42 supported the bolster or transverse member (depending on its location). For supports to behave as rollers at the north abutment and piers, recycled flanges from the trimmed portions of the exterior girders were welded as shown in Figure 3.10; this configuration allowed horizontal translation but prevented vertical translation. To behave as pinned supports at the south abutment, the supports were welded directly to the cap beam. To complete Phase 1, sheet pile walls were driven with a backhoe at both ends of the bridge; each sheet pile was 10 ft long and was driven approximately 4 ft into the ground.

WCB Phase 1 is illustrated in Figure 3.11 and can be summarized as follows:

1. The abutments and piers were constructed (Figure 3.11a).
2. Flatcars were placed on the abutments and piers (Figure 3.11b).
3. Exterior girder supports were constructed (Figures 3.11c and 3.11d).
4. Web stiffeners were installed in the HP12x53 caps at the abutments and piers (Figures 3.11e 3.11f).
5. Sheet pile walls were constructed at each abutment (Figures 3.11g and 3.11h).

### 3.2.2 WCB Phase 2: Development of Longitudinal Flatcar Connections

Since the remaining portions of the exterior girders in the longitudinal connections were very shallow, it was not possible to use the reinforced concrete beam concept in the WCB. Thus, the connection presented in Figure 3.12a was designed to utilize torsion properties of a structural tube combined with shear and torsion strength of confined concrete. To construct this connection, 13/16 in. diameter holes were drilled through the webs of each exterior girder in the connection; the holes were drilled approximately 6 in. on



a. WCB north abutment and pier



b. Placement of the 89-ft RRFCs



c. General shape of the exterior girder supports

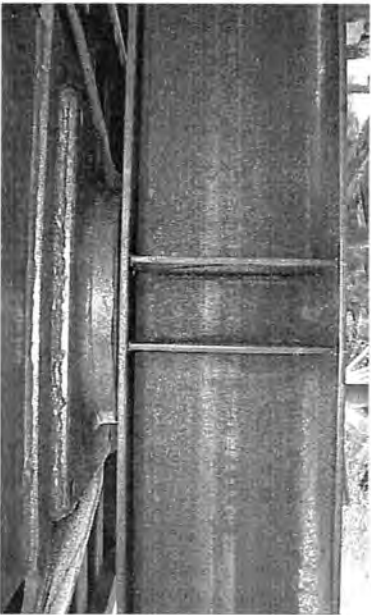


d. Exterior girder support in place at the north abutment

Figure 3.11. Phase 1 construction on the WCB.



f. Web stiffeners under the interior girders at the abutments



e. Web stiffeners under the bolster at the piers



h. Completed sheeting wall

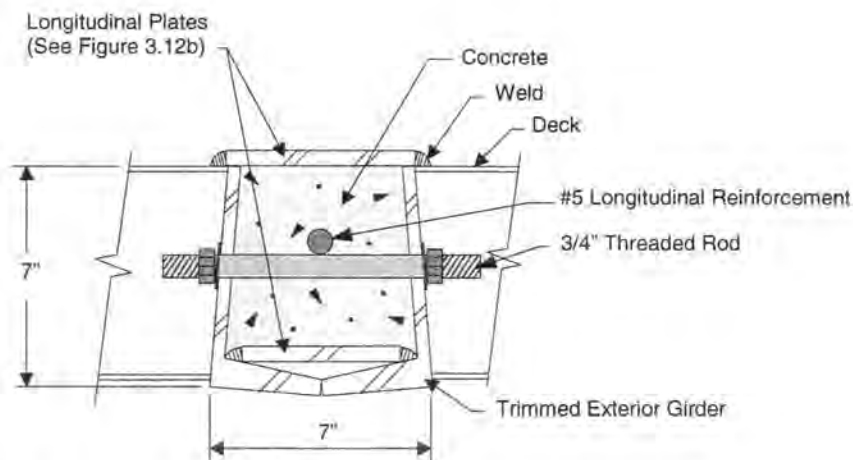


g. Driving sheet piling with a backhoe

Figure 3.11. Continued.

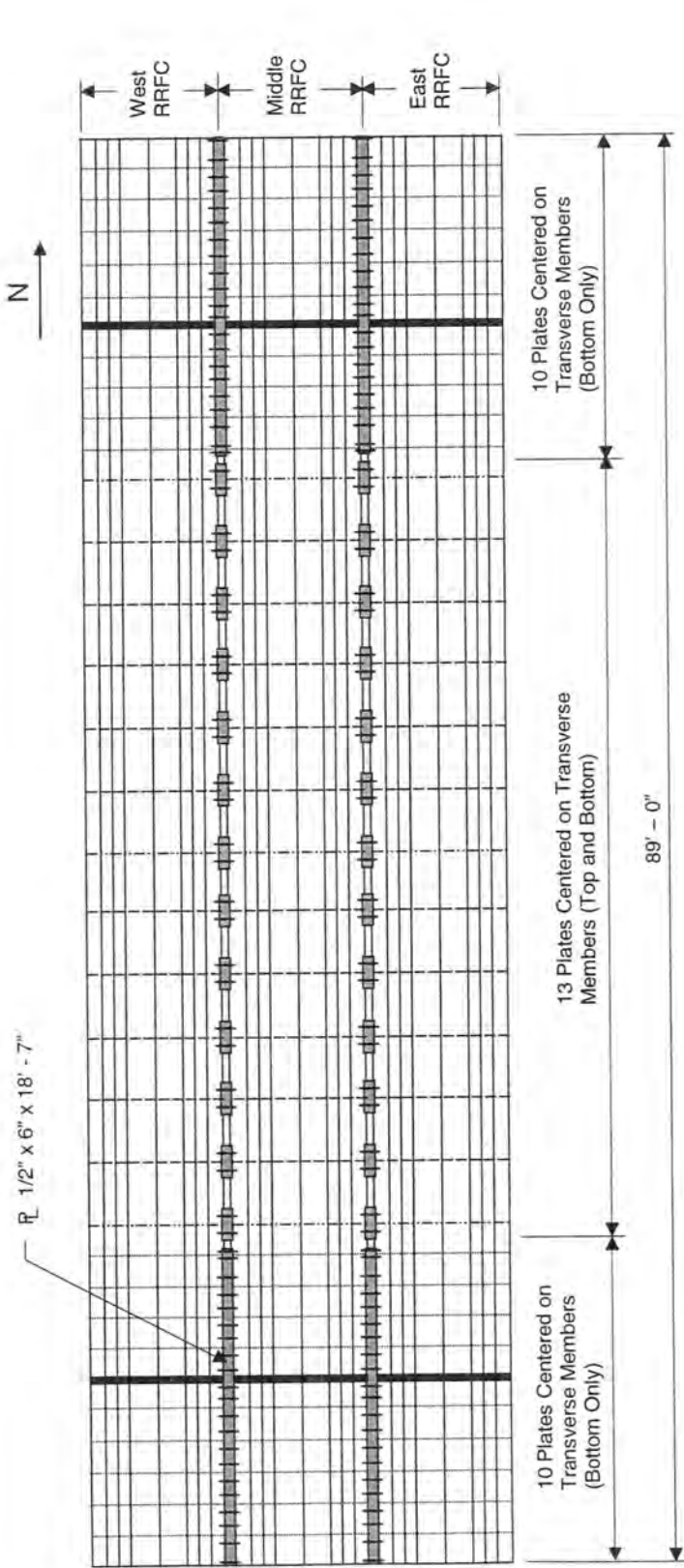
each side of the centerlines for the S-shape and L-shaped transverse members, and approximately 8 in. on each side of the centerlines for the U-shaped transverse members. Space limitations did not allow for the holes to be drilled after the flatcars were placed on the abutments and piers, and thus, all holes were precisely drilled prior to flatcar placement. After the flatcars were positioned on the abutments, 3/4 in. diameter threaded rods were used (via the 13/16 in. holes) to bolt adjacent exterior girders together, and thus, prevent transverse separation between RRFCs.

Following installation of the threaded rod, steel plates, centered on each transverse member, were welded to the bottom flanges of adjacent exterior girders. Dimensions and locations of each plate are given in Figure 3.12b. Following installation of the bottom plates, #5 longitudinal reinforcement was placed on top of the transverse threaded rods, and the connection was filled with concrete. After seven days of curing, steel plates were welded to the tops of adjacent exterior girders directly above the bottom plates in positive moment regions of the connection; in each negative moment region, a continuous steel plate was



a. Cross-sectional view of the longitudinal flatcar connection

Figure 3.12. Longitudinal flatcar connection on the WCB.



Transverse Member	Plate Location	Plate Dimensions (in.)
S-shape	Top	1/2 x 6 x 24
	Bottom	1/2 x 5 x 24
L-Shaped	Top	1/2 x 6 x 24
	Bottom	1/2 x 5 x 24
U-Shaped	Top	None
	Bottom	1/2 x 5 x 30

- U-Shaped Transverse Member
- - - S-Shape Transverse Member
- · - · - L-Shaped Transverse Member
- █ Bolster Location

b. Top view locating connection plates

Figure 3.12. Continued.

welded to the tops of adjacent exterior girders to provide continuous tension reinforcement in the top of the connection (See Figure 3.12b). The addition of the top plates completed the structural tube configuration and confined the concrete in the connection.

After the connections were finished, a transverse timber deck overlay was installed to help distribute traffic loads transversely across the bridge. Instead of bolting each timber plank to the RRFCs, they were “clamped” to the RRFCs by angles that were welded along the longitudinal centerline of the bridge and to the exterior girders at the edges of the bridge.

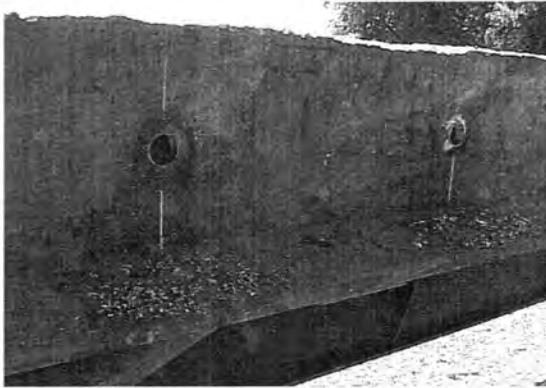
WCB Phase 2 is illustrated in Figure 3.13 and can be summarized as follows:

1. Holes (13/16 in. diameter) were drilled in the exterior girders prior to flatcar placement (Figure 3.13a).
2. Transverse threaded rods were installed and tightened, bottom plates were welded to adjacent girders, and #5 reinforcement was placed in the connection (Figures 3.13b and 3.13c).
3. Concrete was placed in the connection and allowed to cure. Top plates were then welded to adjacent girders to complete the connection (Figure 3.13d).
4. Steel angles were welded along the longitudinal centerline of the bridge and to the exterior girders at the edges of the bridge; next, the timber deck overlay, held in place by the angle, was installed (Figure 3.13e – Figure 3.13g).

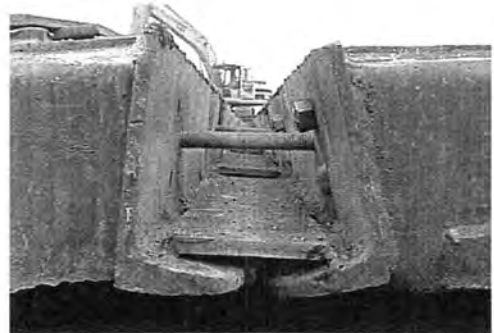
### *3.2.3 WCB Phase 3: Installation of the Driving Surface and Guardrails*

C-shaped sections were used for guardrail posts, and since the exterior girders at the edges of the bridge were rotated approximately 10 degrees, portions of the top flanges were removed to keep the posts essentially vertical. The posts were welded to the flanges of the exterior girders, after which a thrie beam was installed to complete the guardrail system. Visible portions of the RRFC bridge were painted to enhance aesthetics. The thrie beam completed the guardrail system.

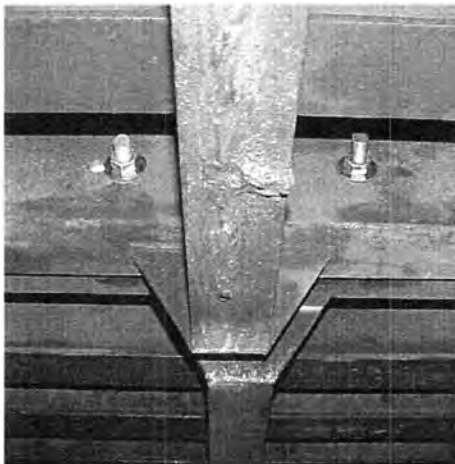
Following installation of the guardrail, a gravel driving surface 14 1/2 in. and 5 in. deep at the centerline and edges of the bridge (Figure 3.8b), respectively, was added.



a. Drilled holes for the transverse threaded rod



b. Bottom connection plates and threaded rod



c. Threaded rod on both sides of the transverse member

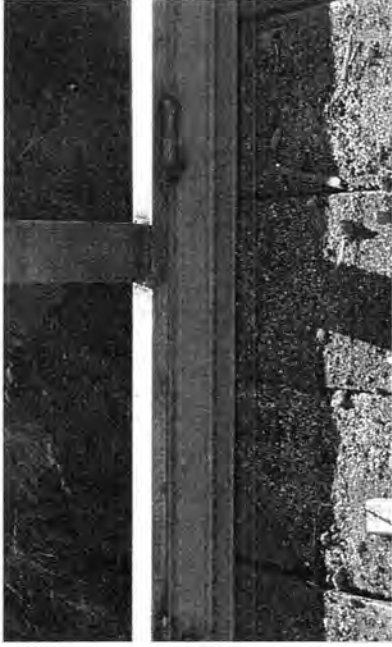


d. Top connection plates after concrete placement

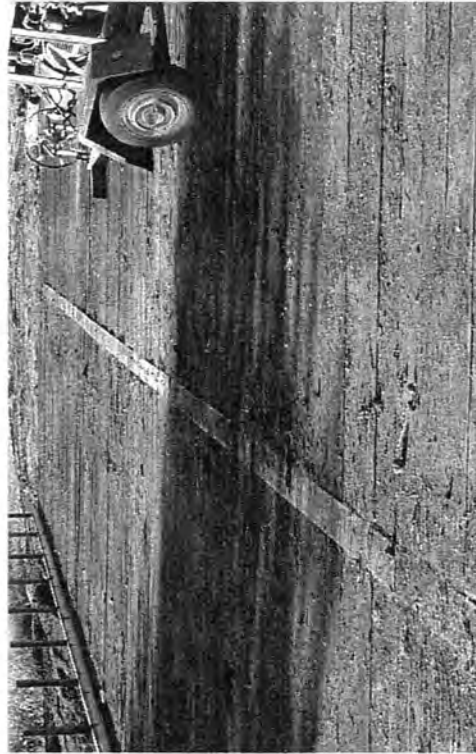
Figure 3.13. Phase 2 construction on the WCB.



e. Angles welded along the longitudinal centerline



f. Angles welded on the exterior girders



g. Placement of the recycled, transverse timber planks

Figure 3.13. Continued.



Drainage through the superstructure was not a concern due to small holes in the RRFC decking, small gaps between timber planks, and porosity of the gravel driving surface.

WCB Phase 3 is illustrated in Figure 3.14 and can be summarized as follows:

1. Guardrails posts were installed, and the bridge was painted (Figure 3.14a).
2. The thrie beam was added to complete the guardrail system (Figure 3.14b).
3. The gravel driving surface was constructed (Figure 3.14c).

A photograph of the completed WCB is presented in Figure 3.15.



a. Addition of guardrail posts



b. Installation of the thrie beam



c. The gravel driving surface

Figure 3.14. Phase 3 construction on the WCB.



Figure 3.15. Finished Winnebago County RRFC Bridge.

## 4. LABORATORY AND FIELD LOAD TESTING

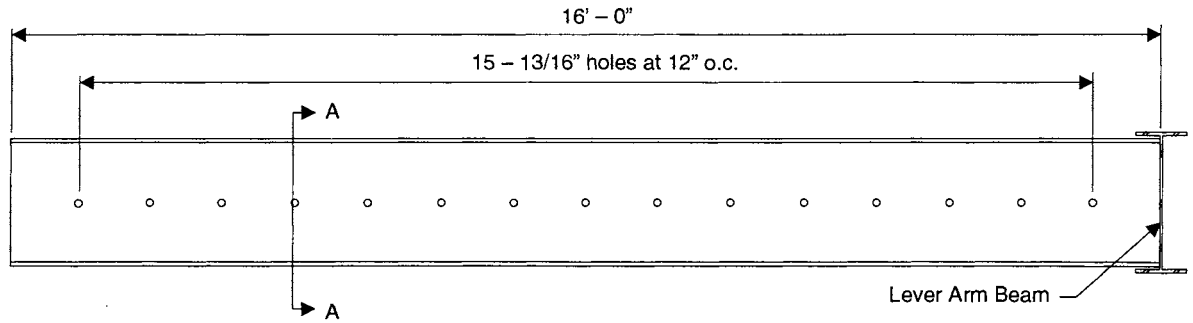
To confirm the strength and behavior of the longitudinal flatcar connection used in the BCB, a laboratory connection specimen (LCS) of this type of connection was constructed and tested. To investigate bridge behavior, each RRFC demonstration bridge was instrumented and field tested with rear tandem trucks carrying gross loads of 51,000-52,500 lbs. Testing procedures for the LCS and demonstration bridges will be described in Sections 4.1 and 4.2, respectively.

### 4.1 Laboratory Connection Specimen

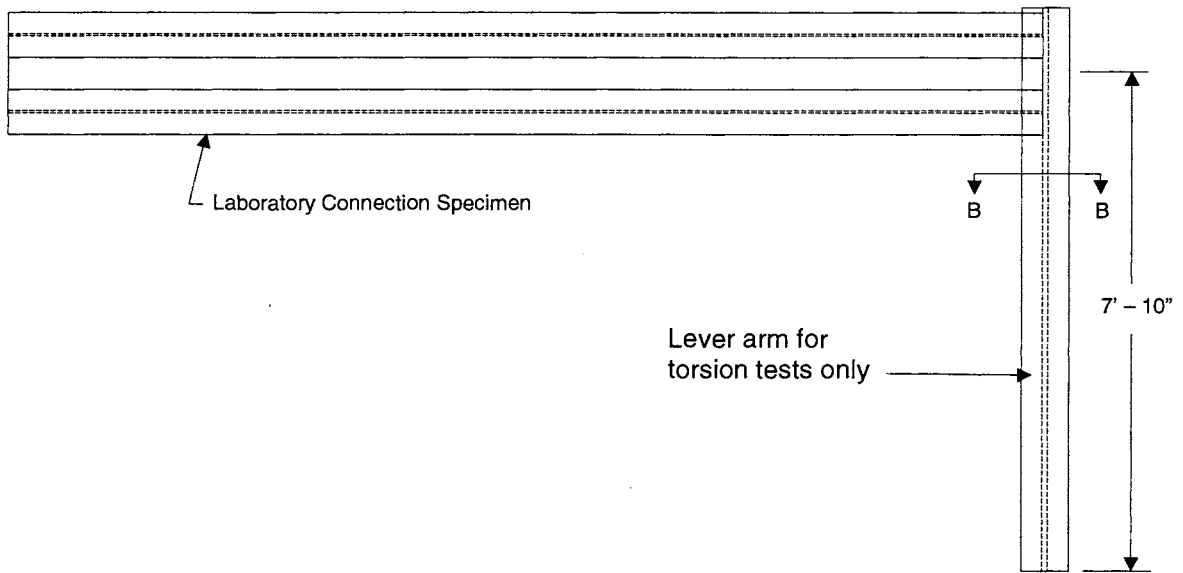
As shown in Figure 4.1, the LCS was constructed by spacing the flanges of two 16-ft-long W21x62 beams 6 in. apart; this void was filled with concrete, which was reinforced with five #8 longitudinal reinforcement bars. Transverse threaded rods sheathed with poly vinyl chloride (PVC) pipe spaced 12 in. on center were included for lateral confinement. The PVC pipe made it possible to remove various bolts, and thus vary the amount of lateral confinement.

The LCS was initially tested in torsion and flexure under service loads; later it was loaded in torsion to failure. In each flexure and torsion test, strains and displacements were measured at critical locations; uniaxial and 45-degree rosette strain gages were used to measure strains, strain potentiometer deflection transducers (SPDTs) were used to measure vertical and lateral displacements, and inclinometers were used to measure longitudinal axis rotations.

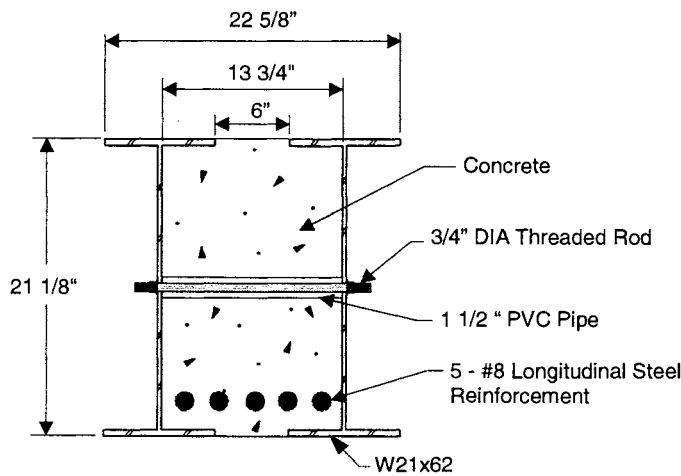
Strain instrumentation was placed on four cross-sections between the rotationally restrained and unrestrained ends of the beam as shown in Figure 4.2. Uniaxial stain gages were placed longitudinally on the top and bottom concrete surfaces, tops of the flanges, top and bottom locations of the webs, on two of the steel reinforcement bars, and on two of the



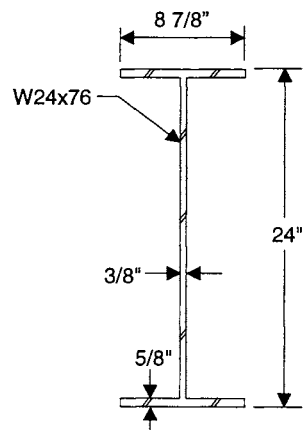
a. Side view



b. Top view



c. Section A - A



d. Section B - B

Figure 4.1. Laboratory connection specimen.

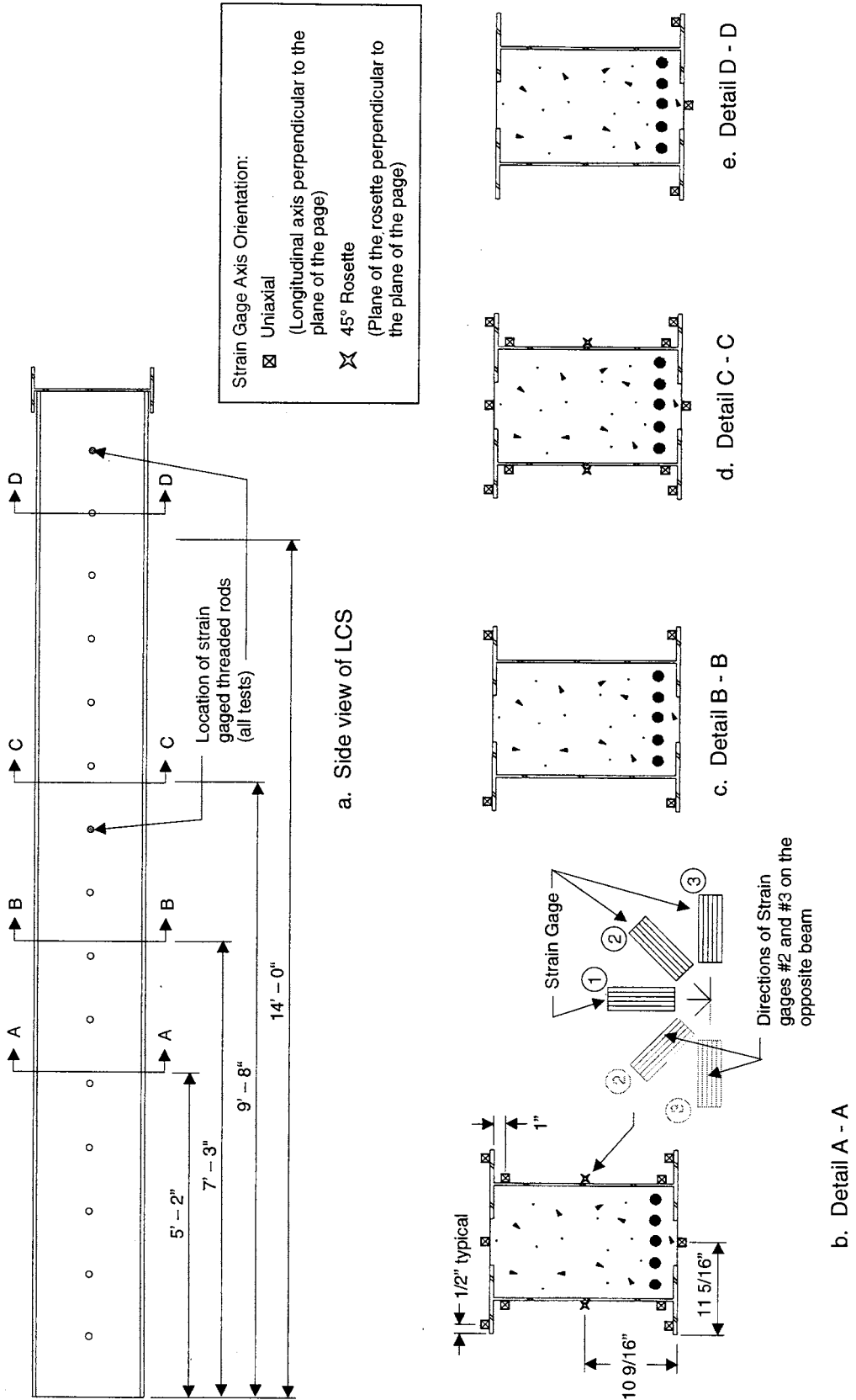


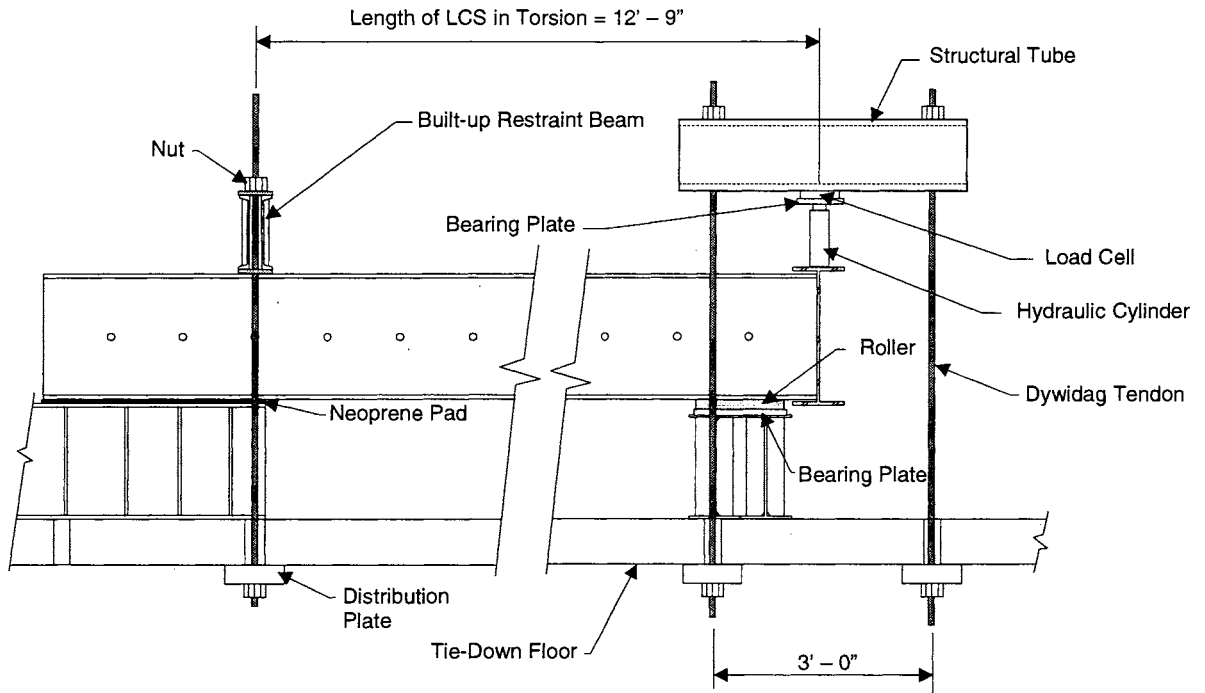
Figure 4.2. Location of strain gages on the LCS.

transverse threaded rods. Strain gages on the threaded rods were positioned parallel to the rod's longitudinal axis; these two rods remained in the first and seventh holes from the lever arm in all tests as shown in Figure 4.2a. As illustrated in Figure 4.2b, the 45-degree rosettes were positioned such that midheight web strains were measured in the horizontal and vertical directions, as well as along a line 45 degrees to these axes. The 45-degree gages on the two beams did not measure strains in the same directions, but rather, in perpendicular directions (See Figure 4.2b). Displacement instrumentation will be discussed along with each testing procedure in the subsequent sections.

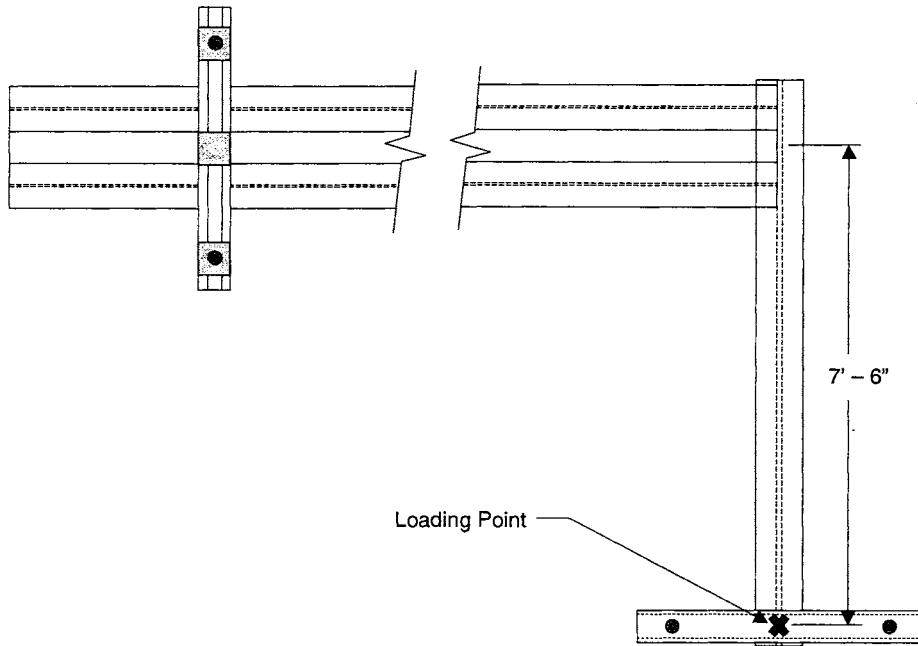
#### *4.1.1 LCS Service Load Torsion Test*

With the objective of determining the behavior of the LCS under service torsion loads, it was also desired to investigate the change in LCS behavior for different amounts of lateral confinement (i.e. transverse threaded rod spacing). Since it was possible to remove the transverse rods, ten tests were performed with different threaded rod spacing – 1 ft, 2 ft, 3 ft, or 6 ft; loading conditions were kept constant in these tests. Three tests were performed for each case with rods spaced on 1-ft, 2-ft, and 3-ft centers, and one test was performed with rods spaced on 6-ft centers. In each torsion test, one end of an 8.5-ft-long W24x76 was connected to the free end of the LCS, while the other end was loaded with a hydraulic cylinder (force = 4 kips, lever arm length = 90 in.); the far end of the LCS was restrained against deflection and rotation as shown in Figure 4.3.

Since it was desired to record LCS rotations along its length in each test, SPDTs were oriented and connected to the beam at several locations to measure vertical and lateral displacements. Using trigonometry, these displacements were converted to rotations. In addition, an inclinometer was fastened to the lever arm beam on the LCS longitudinal axis so rotations could be recorded directly. Figure 4.4 presents the locations where vertical displacements, lateral displacements, and direct rotation readings were recorded, and

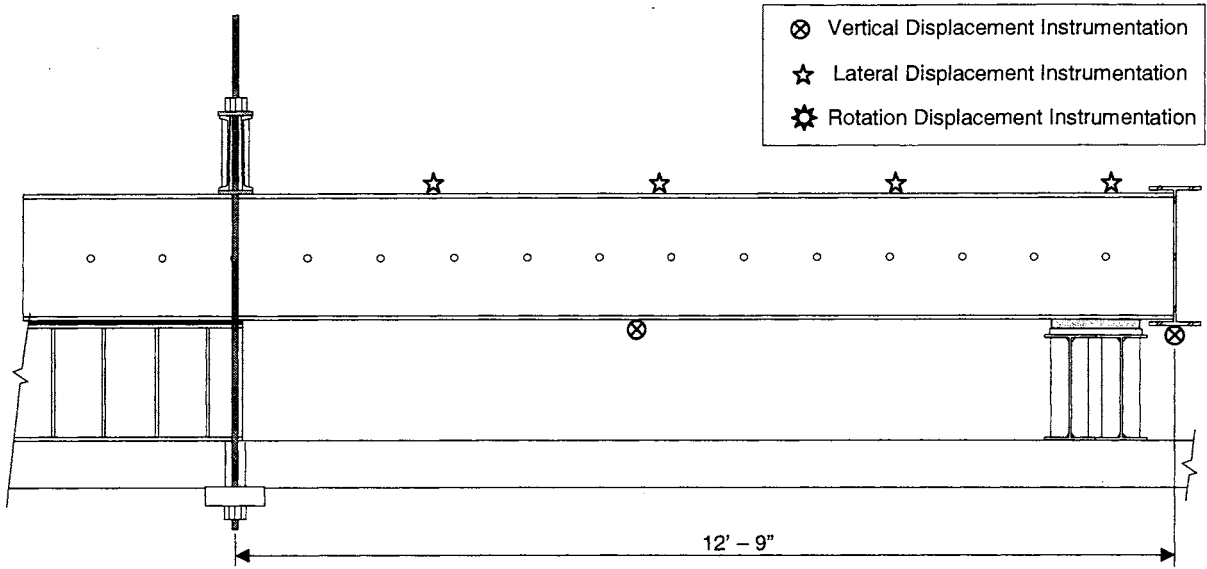


a. Side view

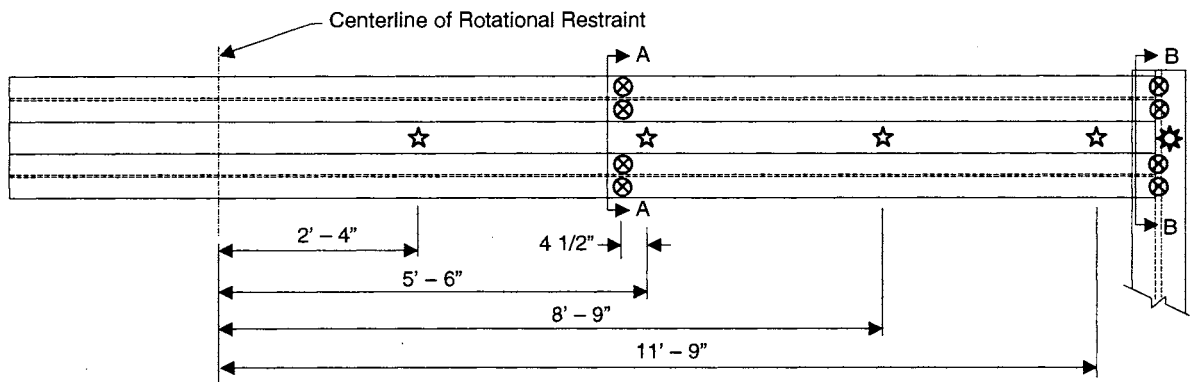


b. Top view

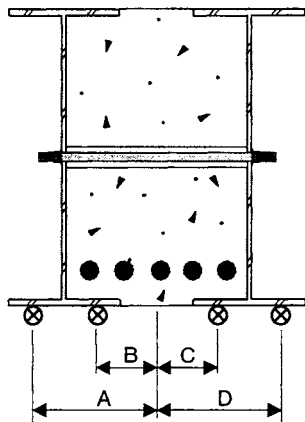
Figure 4.3. LCS Service Load Torsion Test.



a. Side view



b. Top view



c. Details A - A and B - B

Detail	Dimension (in.)			
	A	B	C	D
A - A	9 5/8	4 7/8	4 7/8	9 7/8
B - B	10 1/16	6 5/16	6 3/16	10 1/16

Figure 4.4. Location of displacement instrumentation used in the LCS Service Load



Figure 4.5 illustrates the positions of the strain gages relative to the rotational restraint used in the service load tests. Figure 4.6 illustrates the LCS laboratory service test setup. Prior to testing, the lever arm self weight was supported by an overhead crane as shown.

#### 4.1.2 LCS Flexure Test

Following the torsion tests, the LCS was loaded with service flexural loads to study its flexural behavior. Once again, the spacing of the transverse threaded rods was a variable in the six tests performed; two tests were performed for each case with the rods on 1-ft, 2-ft, and 3-ft centers. In each flexure test, the top of the simply supported LCS was loaded by two slightly asymmetrically positioned hydraulic cylinders spaced 36 in. apart as shown in Figure 4.7, thus, providing a region essentially in pure flexure between the two concentrated forces. The hydraulic cylinders were positioned slightly asymmetrically to avoid strain gages on the top of the LCS.

Due to the basic simple support configuration of the flexure tests, it was only necessary to measure the maximum deflections halfway between the hydraulic cylinders as shown in Figure 4.8a. Figure 4.8b illustrates the location of the strain gages relative to the simple supports, and Figure 4.9 is a photograph of the flexure test setup in the laboratory.

#### 4.1.3 LCS Ultimate Load Torsion Test

Since the flexural behavior of the beam was easier to analyze, the LCS was failed in torsion to gain more understanding of its torsional capabilities. The testing setup was very similar to that of the service tests, however a few changes were made to account for the application of larger forces and the resulting rotations of the specimen. Since lever arm rotations were expected to be significantly greater than those that occurred in the service load tests, the hydraulic cylinders were positioned below the tie-down floor (See Figure 4.10). Load cells were positioned above the structural tube, and a rocker was

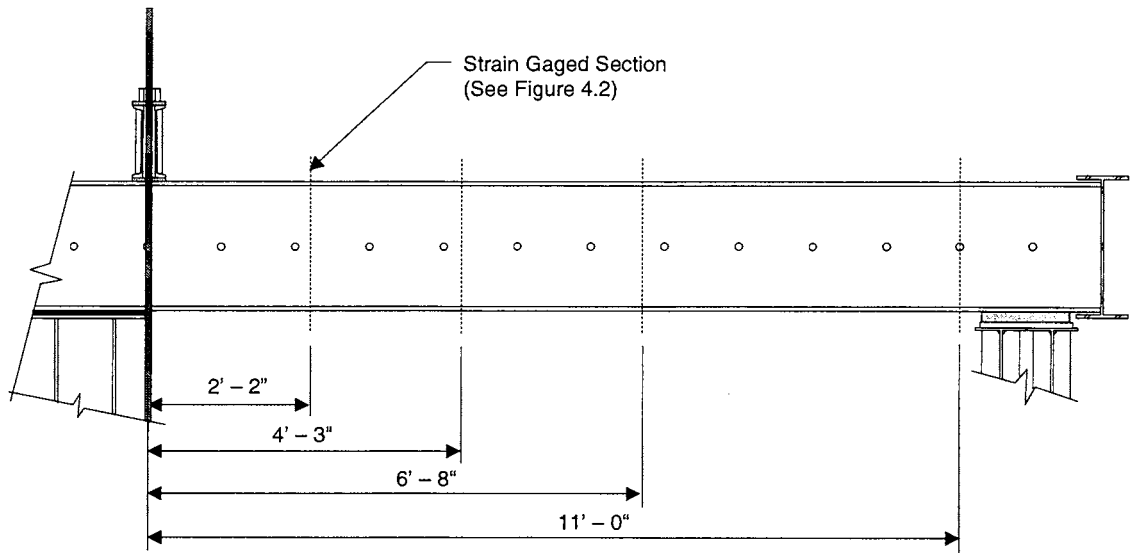
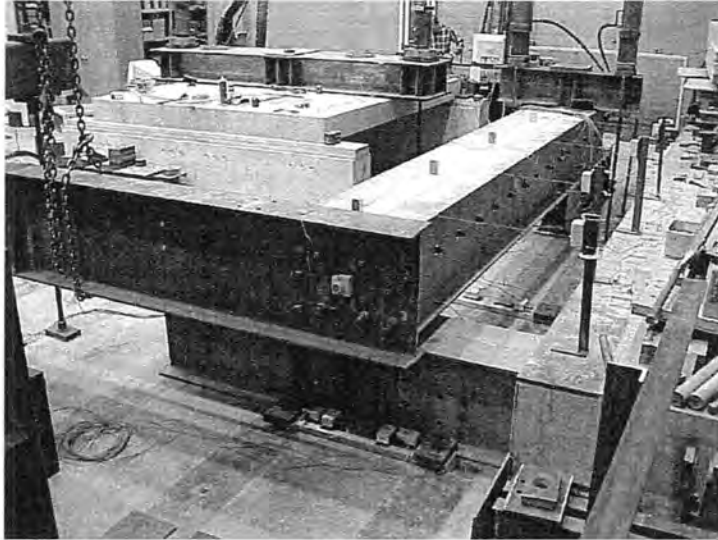


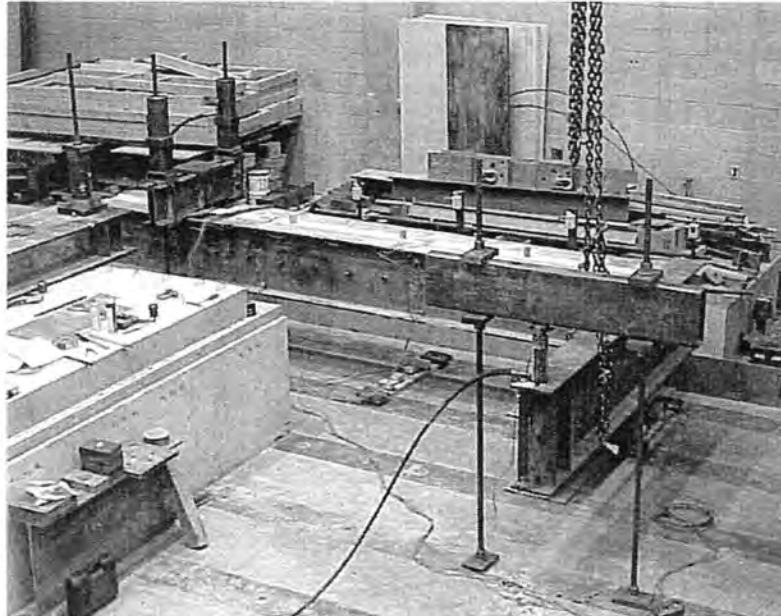
Figure 4.5. Location of strain gages used in the LCS Service Load Test relative to end restraint.

placed between the structural tube and lever arm. To increase the safety in the test, a small vertical *W*-shape section was welded to the lever arm to prevent the rocker and structural tube from sliding on the lever arm. To reduce the possibility of the lever arm failing prior to LCS failure, the lever arm length was reduced to 4' – 6", channels were welded to the top and bottom flanges to increase its inertia, and web stiffeners were added to prevent web buckling. Finally, to minimize rotations on the rotationally restrained end, an additional rotational restraint beam was added (See Figure 4.10).

Displacement instrumentation was essentially the same as that used in the service tests. However, since the restrained end of the LCS rotated a small amount during the service tests, extra SPDTs and an inclinometer (shown in Figure 4.11) were added to the restrained end of the LCS so that the relative rotation between the ends of the specimen could be calculated. Figure 4.12 shows the location of the strain instrumentation relative to the rotational restraint for the Ultimate Load Torsion Test; photographs of the Ultimate Load Torsion Test in progress are shown in Figure 4.13.

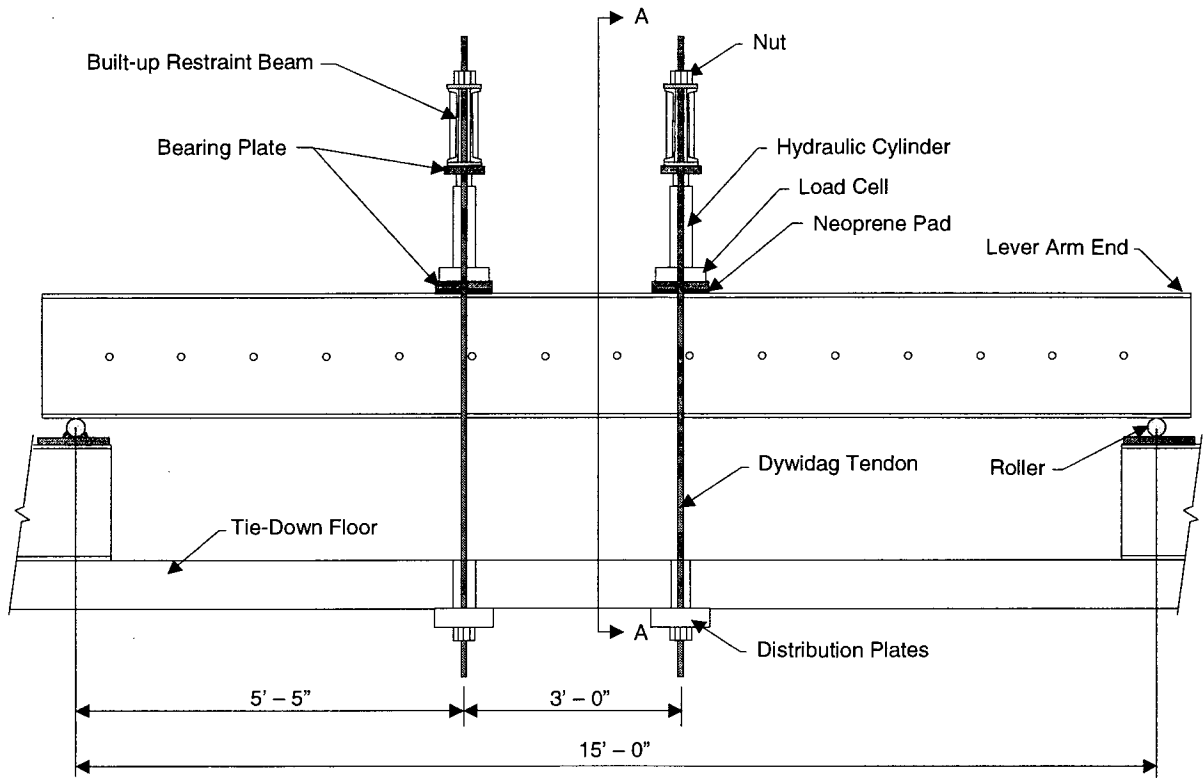


a. SPDT and inclinometer instrumentation

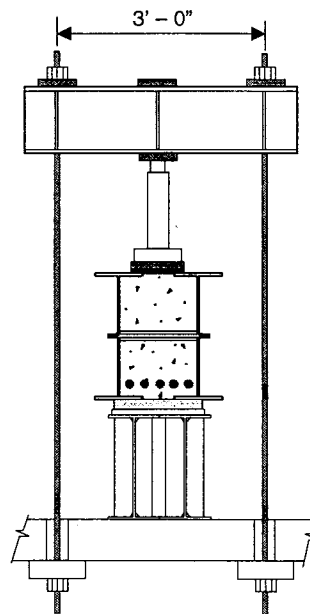


b. Loading arrangement

Figure 4.6. Photograph of the LCS Service Load Torsion Test.

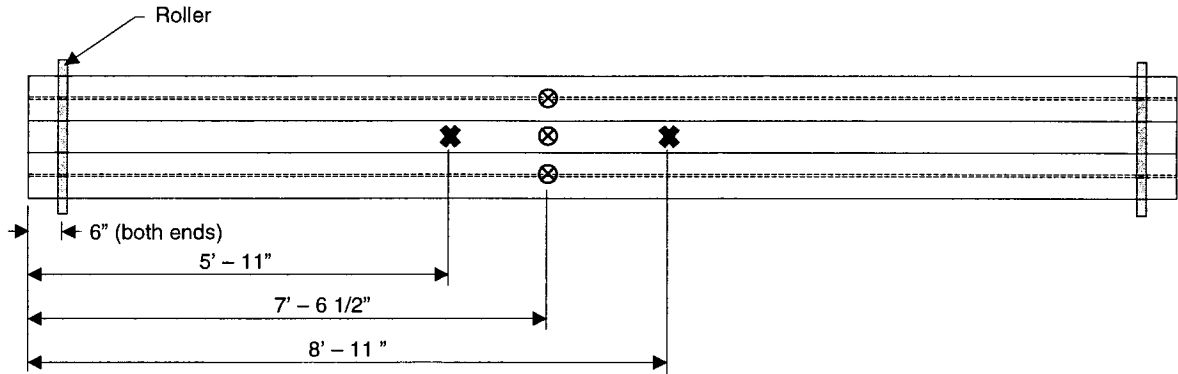
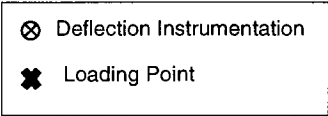


a. Side view

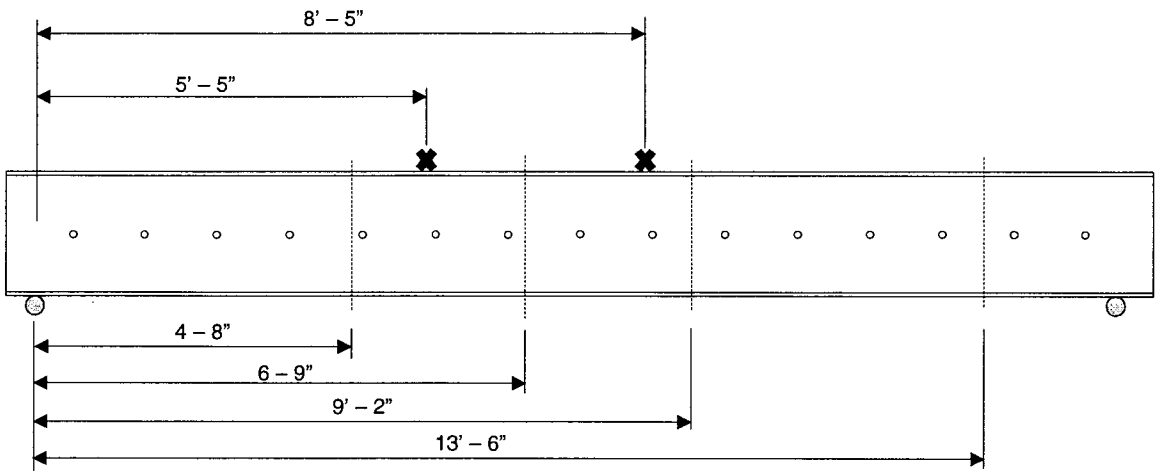


b. Detail A - A

Figure 4.7. LCS Service Flexure Test.



a. Location of deflection transducers



b. Strain instrumentation relative to flexure loading

Figure 4.8. Location of instrumentation in the Service Load Flexure Test.

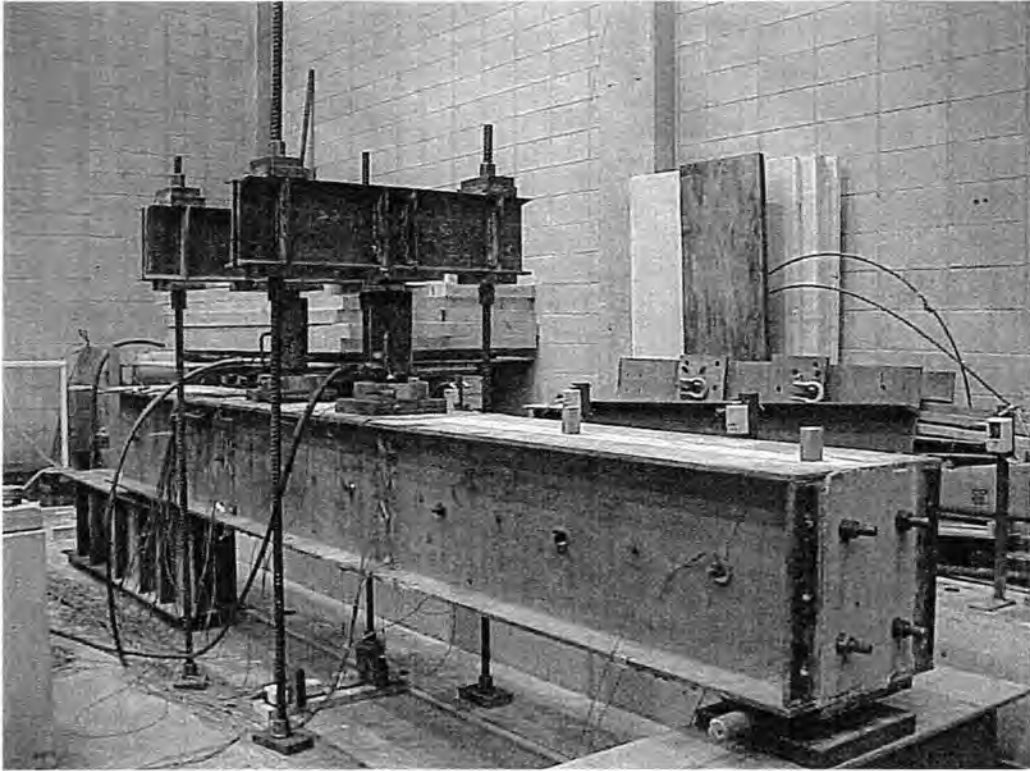
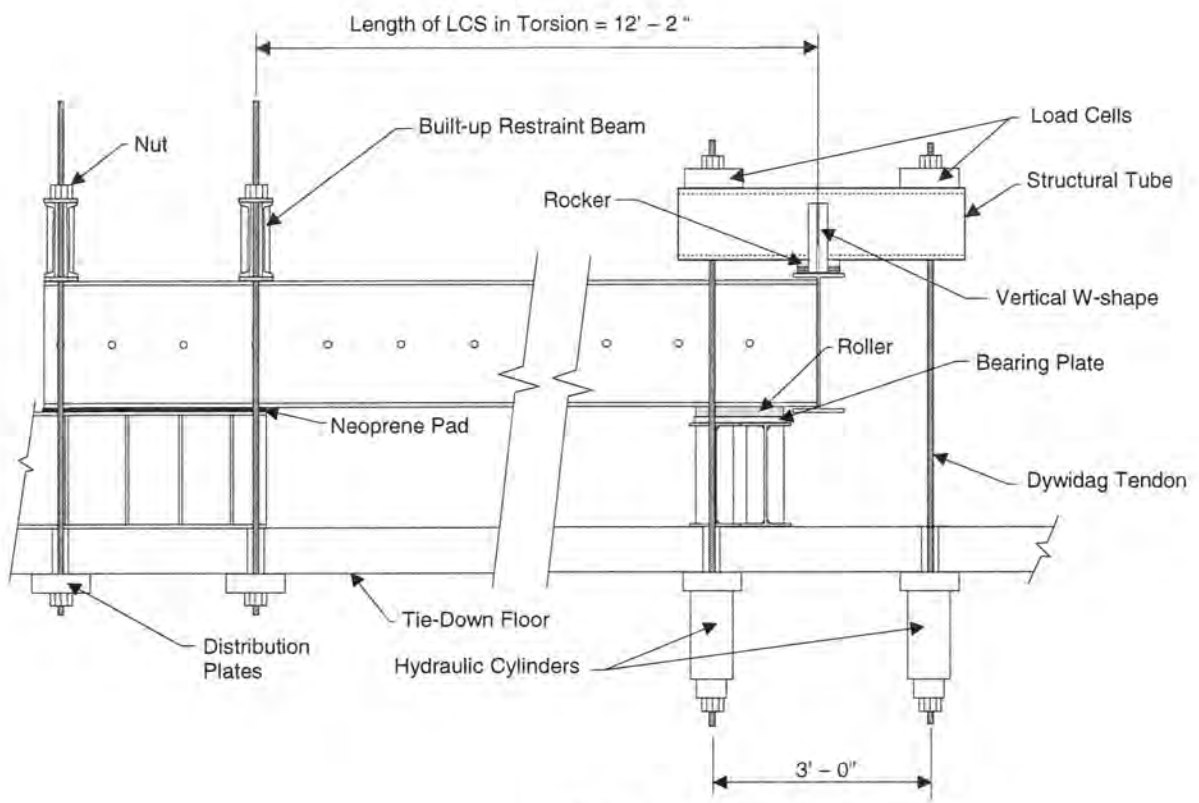


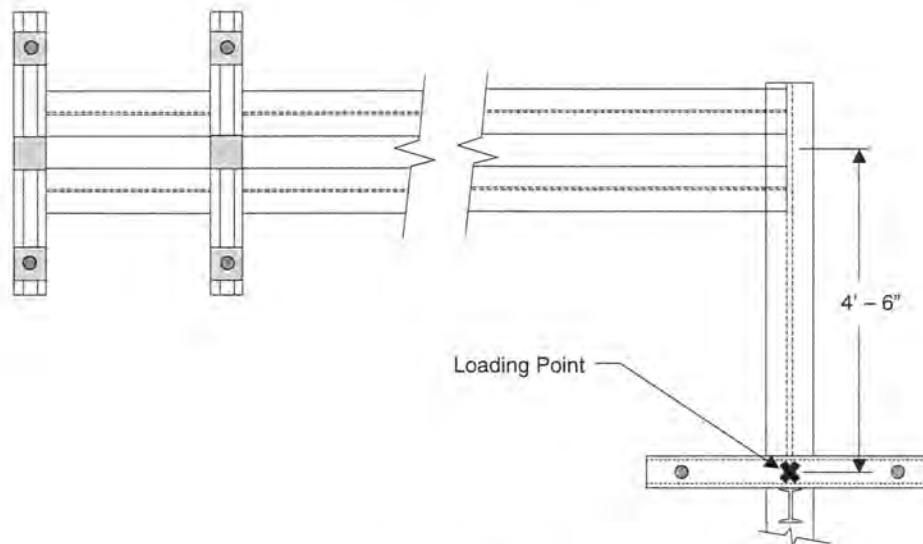
Figure 4.9. Photograph of the LCS under service flexural loads.

## 4.2 RRFC Bridge Field Testing

In order to investigate the behavior of the RRFC bridges, both bridges were load tested with tandem trucks carrying Iowa legal loads. For each bridge, Load Test 1 (LT1) was performed after the flatcars were placed on the abutments and/or piers, but before adjacent flatcars were connected. Load Test 2 (LT2) was performed immediately after the construction of each bridge; Load Test 3 (LT3) occurred approximately one year after the bridges were in service. In each test, strains and deflections at several critical longitudinal and transverse locations resulting from the truck loads were measured and recorded. For information on the test trucks used in each test, refer to Figure 4.14. In each test truck, the front tires were 12 in. wide, the individual tandem tires were 9 in. wide, and the width of a rear set of tandem tires was 1' – 10." The various RRFC bridge tests previously noted will

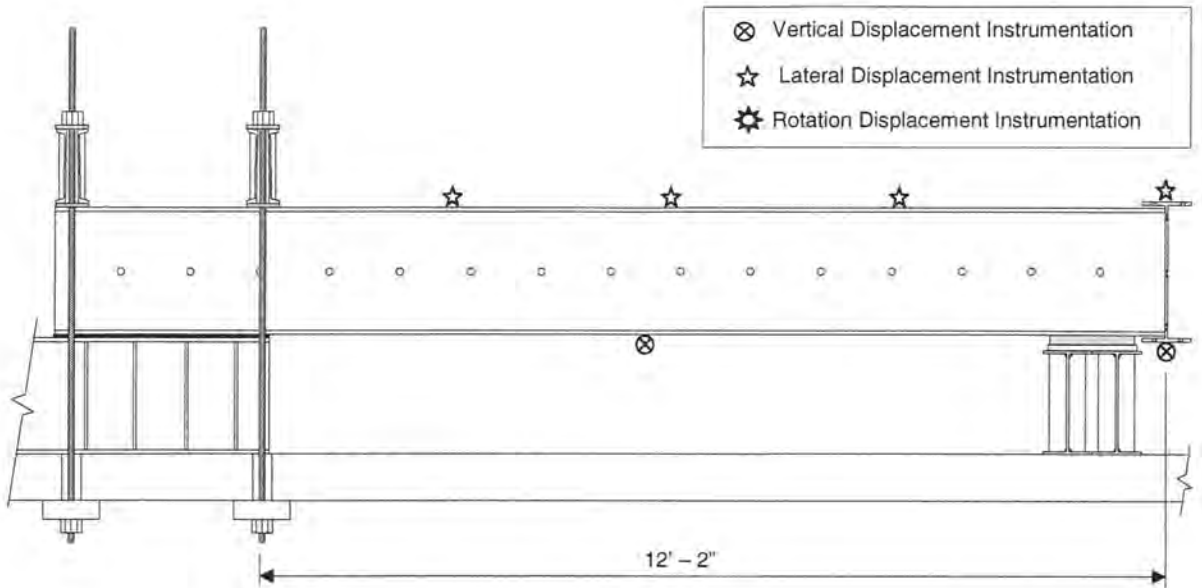


a. Side view

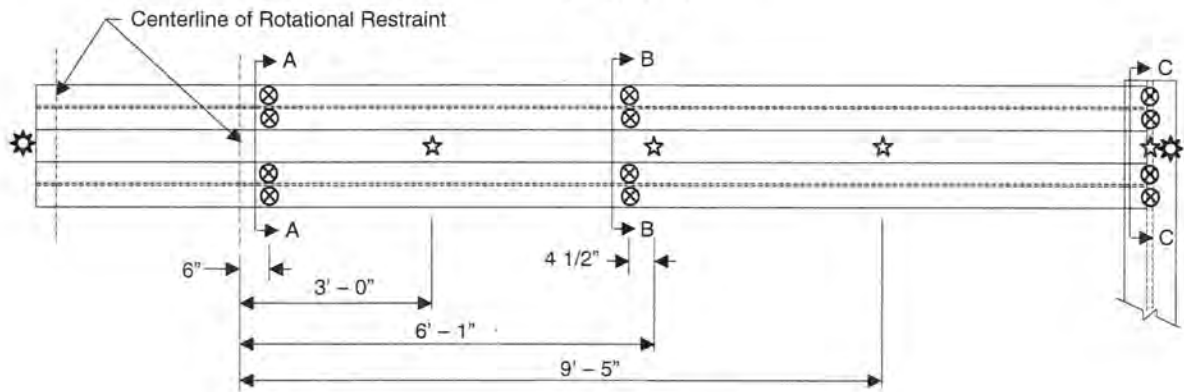


b. Top view

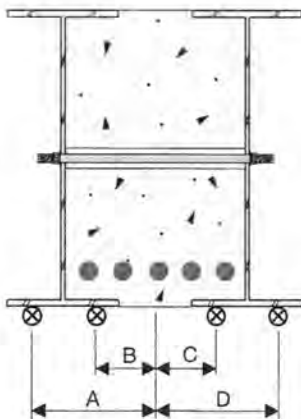
Figure 4.10. LCS Ultimate Load Torsion Test.



a. Side view



b. Top view



c. Details A - A, B - B, and C - C

Detail	Dimension (in.)			
	A	B	C	D
A - A	8 1/4	3 1/2	3 1/2	8 7/8
B - B	9 5/8	4 7/8	4 7/8	9 7/8
C - C	9 3/8	4 3/8	4 3/8	10 3/8

Figure 4.11. Location of displacement instrumentation for the LCS Ultimate Torsion Test.



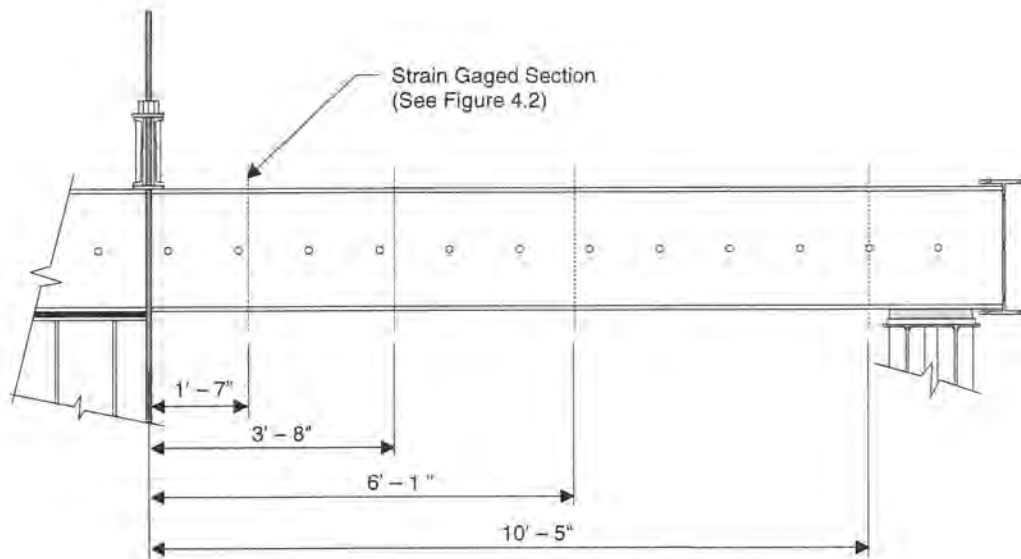


Figure 4.12. Location of strain gages used in the LCS Ultimate Load Test relative to the end restraint.

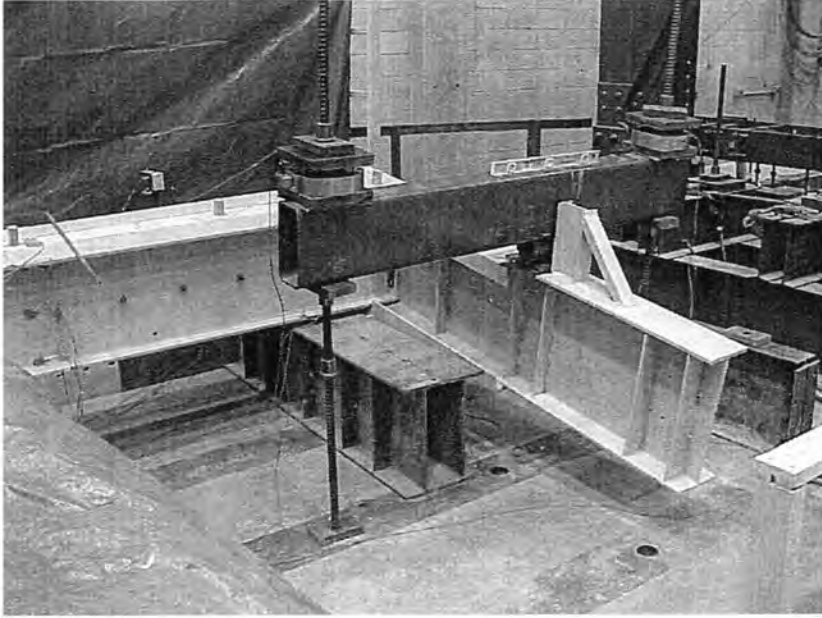
be presented in detail in the following sections.

#### 4.2.1 Buchanan County Bridge

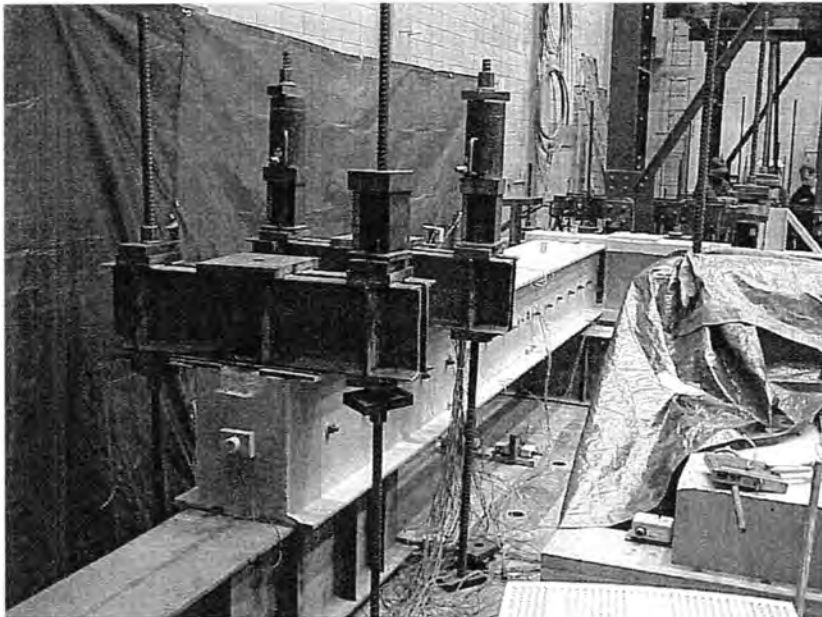
##### 4.2.1.1 BCB Load Test 1

LT1 consisted of 4 tests on the center RRFC with no connection to the outside flatcars. The objectives of LT1 were to verify the initially predicted RRFC maximum midspan strains in the girders, determine the behavior of an individual RRFC to Iowa legal loads, and verify that the RRFCs have more than adequate torsional stiffness.

In order to achieve the first objective, strains were measured in the girders at 1/4, 1/2, and 3/4 span locations during each test. Also, strains at various locations on the RRFC were measured on stringers, transverse members, and directly on the decking. In addition to strains, deflections were measured on the girders at midspan. Location of the strain gage and deflection instrumentation used in LT1 is shown in Figure 4.15. Note that the midspan section (Figure 4.15d) had significantly more strain gages than the other instrumented sections. Due to symmetry, only one exterior girder and the interior girder at the 1/4 span

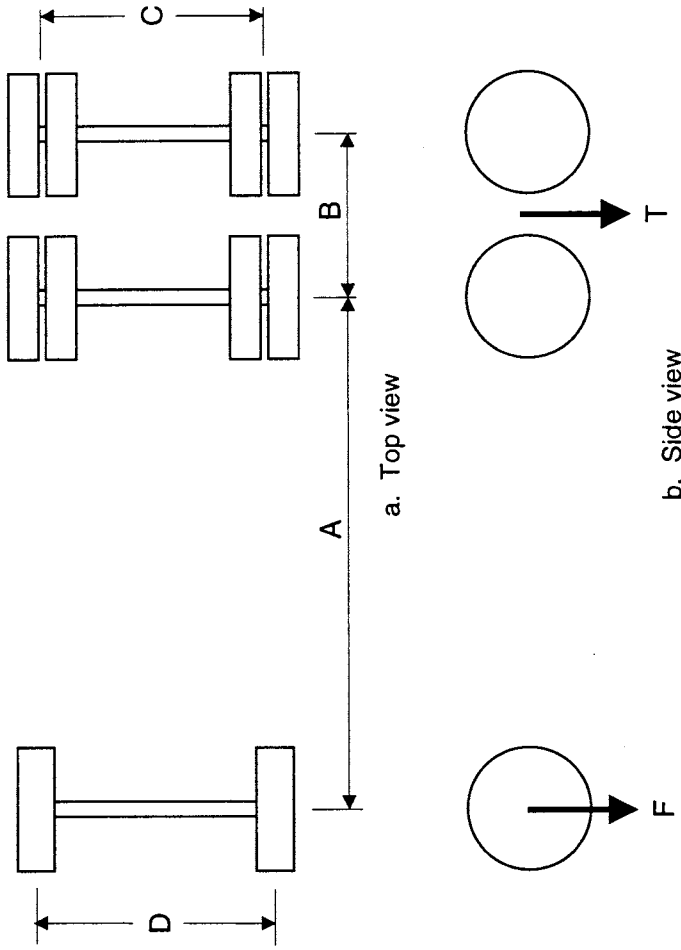


a. Loading system and lever arm rotation



b. Rotationally restrained end of the LCS

Figure 4.13. Photographs of the Ultimate Load Torsion Test.

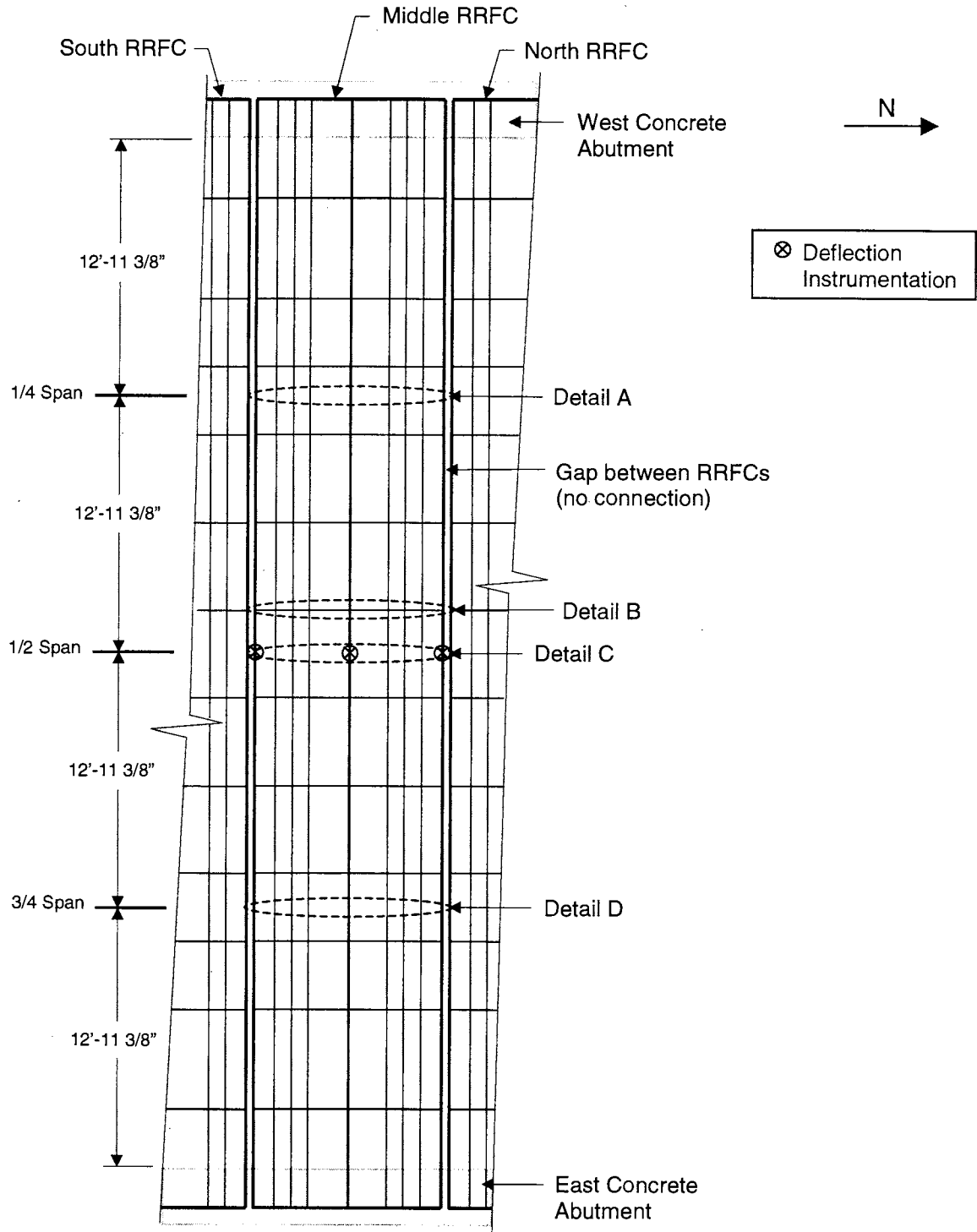


a. Top view

b. Side view

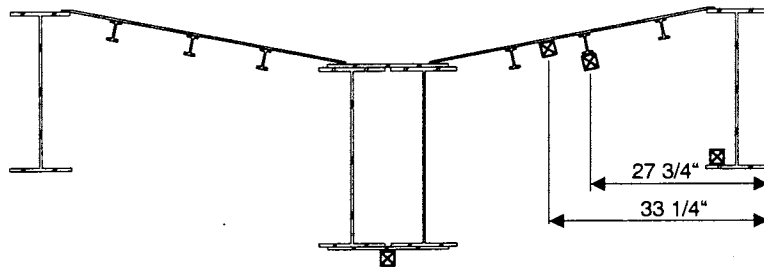
Bridge	Load Test	Truck	Dimensions						Load (lbs)		
			A	B	C	D	F	T	Gross		
BCB	LT1	-	13' - 10 1/2"	4' - 5"	6' - 0"	6' - 11 1/2"	16,240	34,800	51,040		
	LT2	A	14' - 7"	4' - 6"	6' - 0"	6' - 9"	16,100	35,400	51,500		
		B	14' - 2"	4' - 5"	6' - 0"	7' - 1 1/4"	16,080	36,000	52,080		
	LT3	-	14' - 3"	4' - 6"	6' - 0"	7' - 0"	15,000	35,400	50,400		
WCB	LT1	-	14' - 2"	4' - 7"	6' - 0"	7' - 7 1/2"	16,360	35,840	52,200		
	LT2	-	14' - 1"	4' - 7"	6' - 0"	7' - 2 1/2"	18,940	33,380	52,320		
	LT3	-	14' - 10 1/2"	4' - 6"	6' - 0"	6' - 8"	18,040	33,060	51,100		

Figure 4.14. Dimensions and weights of test trucks used in RRFC bridge field tests.

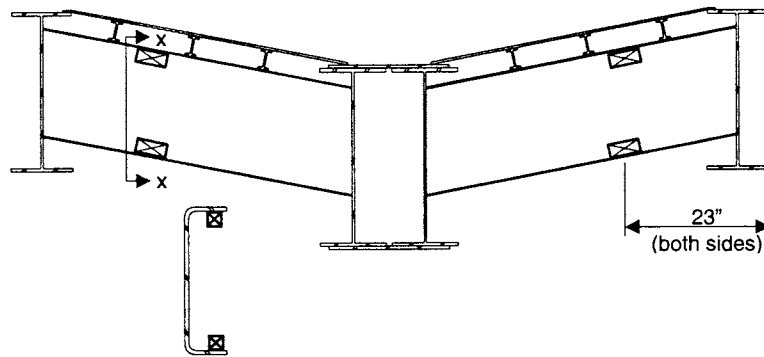


a. Plan view

Figure 4.15. Location of instrumentation in BCB LT1.

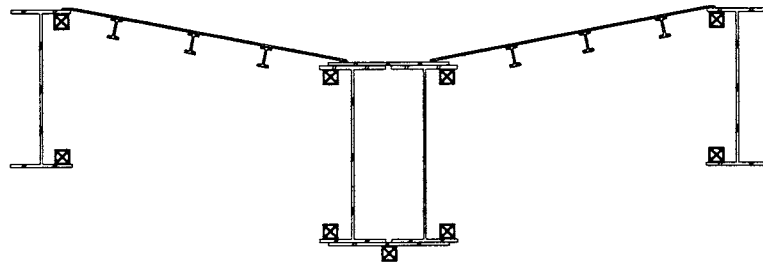


b. Detail A

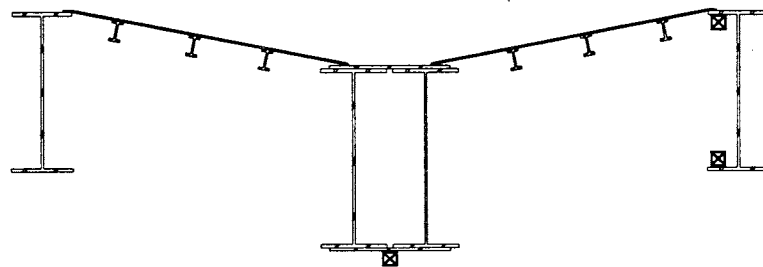


Section x - x

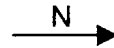
c. Detail B



d. Detail C



e. Detail D



Strain Gage Orientation:



-  Longitudinal axis parallel to the plane of the page
-  Longitudinal axis normal to the plane of the page

Figure 4.15. Continued.

and 3/4 span sections were instrumented.

To determine if there was symmetrical behavior in the RRFC, the transverse position of the test truck was varied. Since the tandem wheel base width (outside-outside of tires) was only 18.5 in. smaller than the width of the RRFC, it was only possible to position the test truck approximately 9.25 in. eccentric to the longitudinal centerline of the RRFC. As a result, Tests 1 and 4 were conducted with the test truck centered on the RRFC, and Tests 2 and 3 were performed with the test truck transversely eccentric at the north and south edges of the RRFC, respectively. In each test, deflections and strains were recorded when the truck was stopped with the centerline of the truck tandem axle at the 1/4, 1/2, and 3/4 span locations. Figure 4.16 illustrates the transverse positioning of the test truck for Tests 1 – 4 in LT1; a photograph of the truck in the north eccentric position is shown in Figure 4.17.

#### 4.2.1.2 BCB Load Test 2

LT2 tests were performed with the longitudinal connections in place between the three RRFCs. As will be discussed in Section 6.2.1, maximum strains in LT1 occurred at midspan of the flatcars, thus the quarter point locations were not instrumented; only the bottom flanges of the girders and the concrete longitudinal flatcar connections were instrumented at midspan in LT2. Strains in the stringers, transverse members, and decking of the RRFCs were also measured at various locations. Following the procedures used in LT1, deflections were only measured at midspan of the girders and flatcar connections. See Figure 4.18 for the location of strain gages and deflection instrumentation used in LT2.

To investigate if the asphalt milling driving surface had any effect on transverse load distribution, identical tests were performed with test trucks positioned in several transverse locations before and after the driving surface was installed. The locations of the trucks used in these tests are illustrated in Figure 4.19. As can be seen, Tests 1 – 4 involved one test truck, while Tests 5 – 6 used two test trucks. In each test, the test truck was driven across

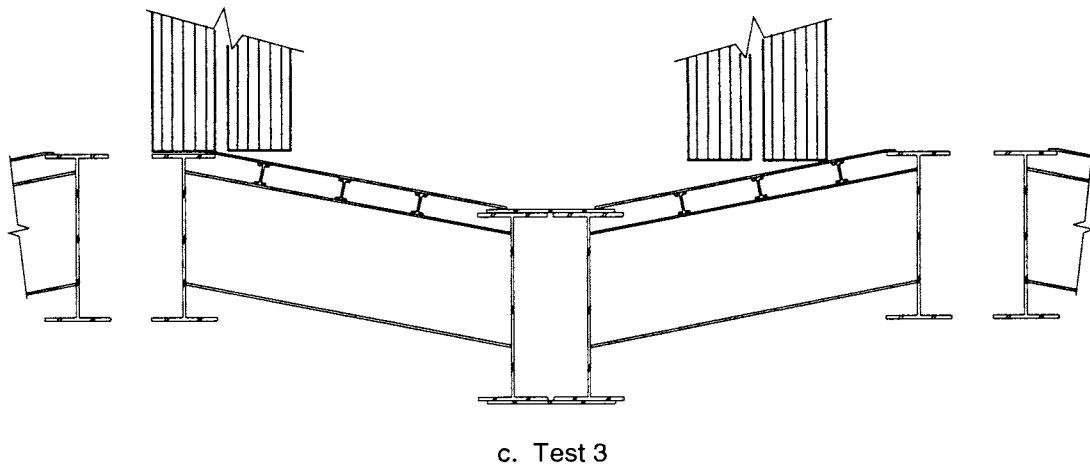
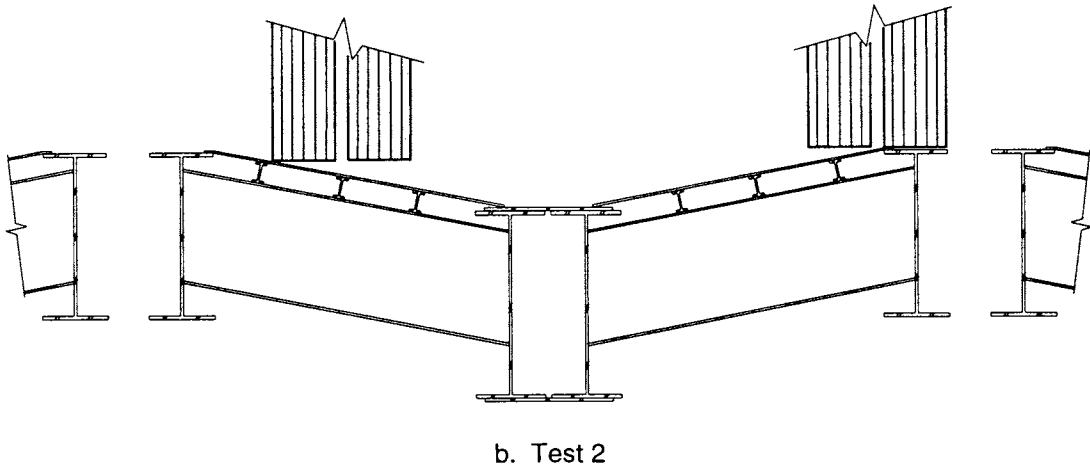
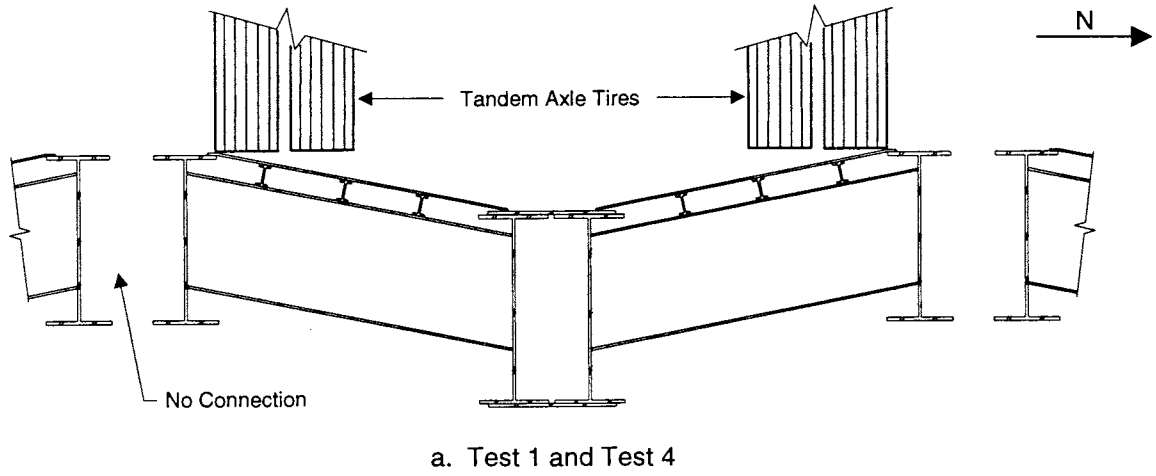


Figure 4.16. Transverse locations of the test truck in BCB LT1.



Figure 4.17. North eccentric transverse position of the truck in BCB LT1.

the bridge, and as the tandem axle reached the 1/4, 1/2, and 3/4 span locations, deflections and strains were measured and recorded. Photographs of these tests prior to and after the addition of the asphalt milling driving surface are presented in Figure 4.20.

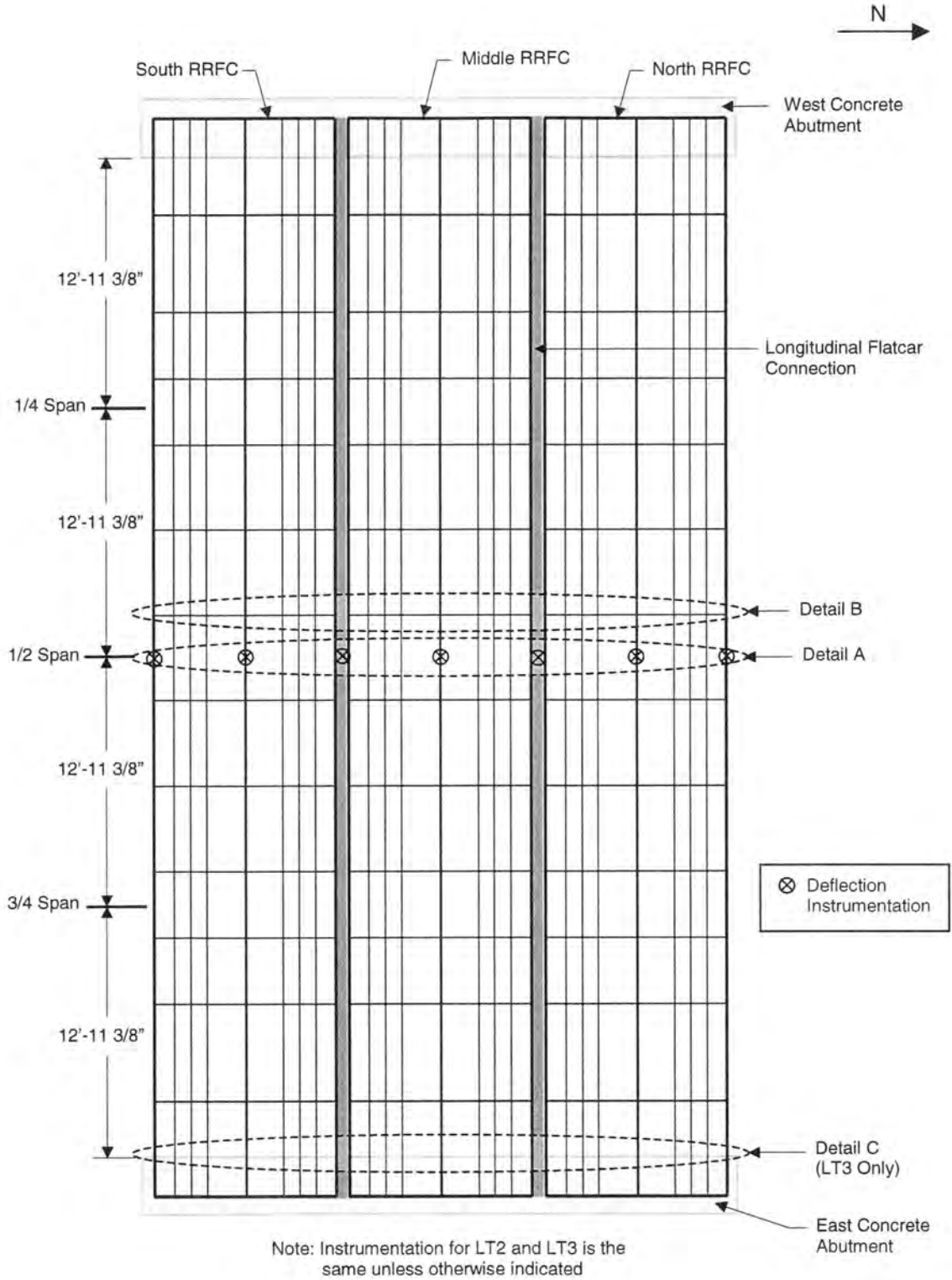
#### 4.2.1.3 BCB Load Test 3

LT3 tests were performed the summer following the completion of construction; thus, the RRFC bridge had been subjected to traffic loads for approximately one year.

Instrumentation used in LT3 was essentially the same as that used in LT2, however more transverse members were instrumented as shown in Figure 4.18. In addition, strain instrumentation was installed on the girders that were cast into the east integral abutment to determine the amount of end restraint provided by the abutment connection.

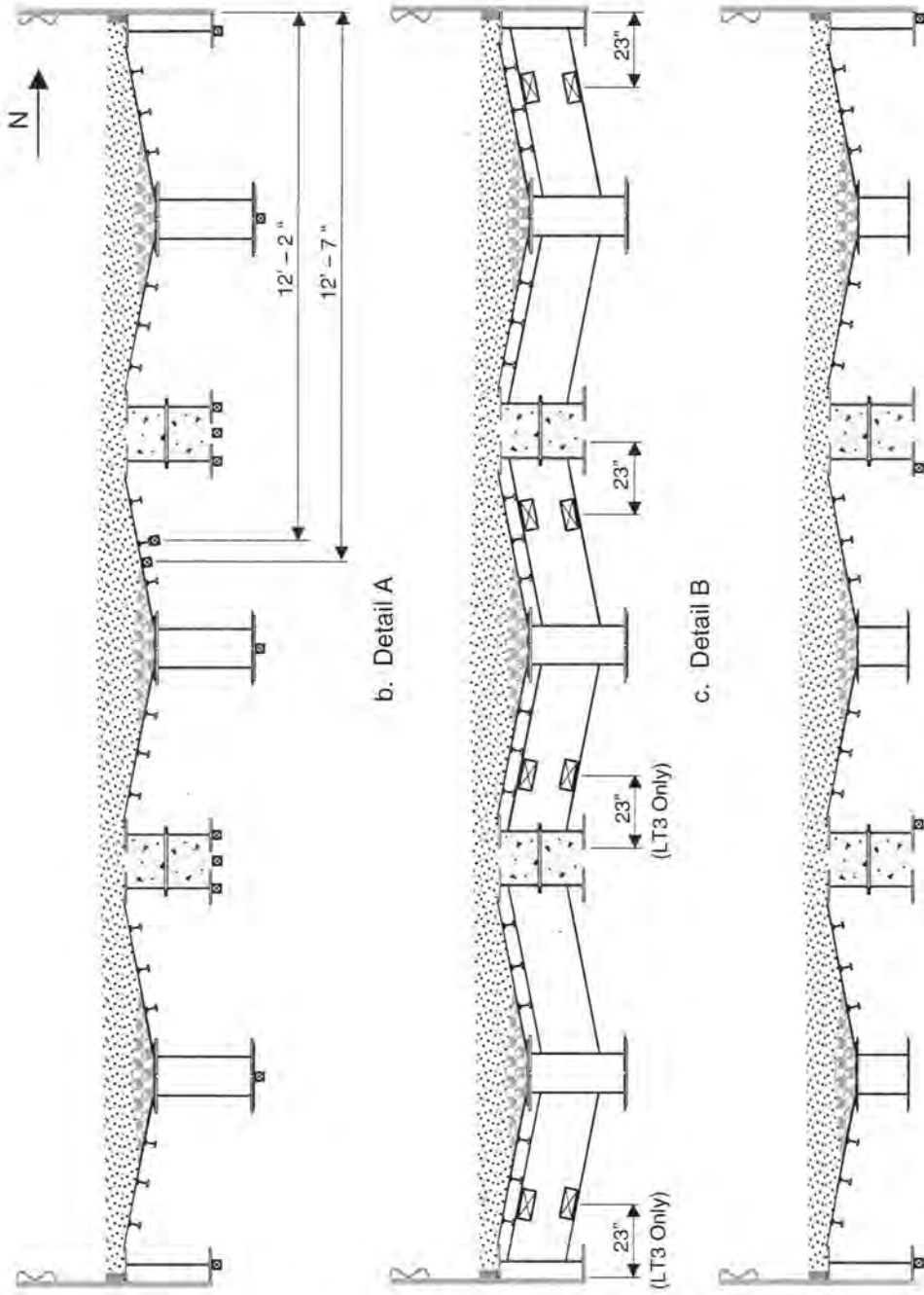
Test truck positions used in LT3 were the same as those used in LT2, however only





a. Plan View

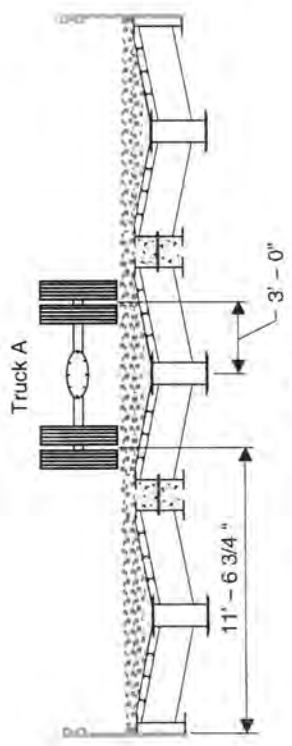
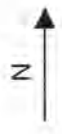
Figure 4.18. Location of instrumentation in BCB LT2 and LT3.



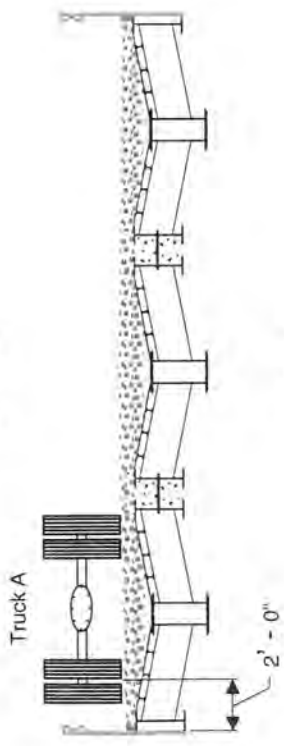
Note: Instrumentation for LT2 and LT3 unless otherwise indicated

d. Detail C (LT3 Only)

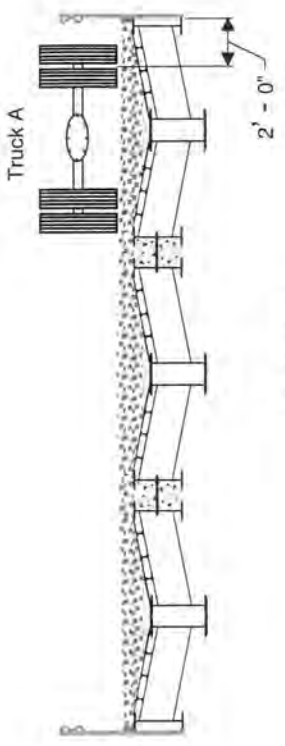
Figure 4.18. Continued.



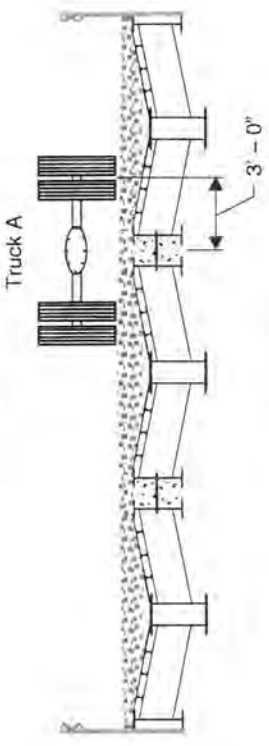
a. Test 1



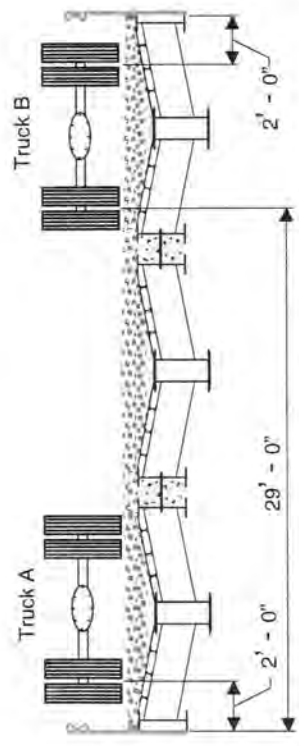
c. Test 3



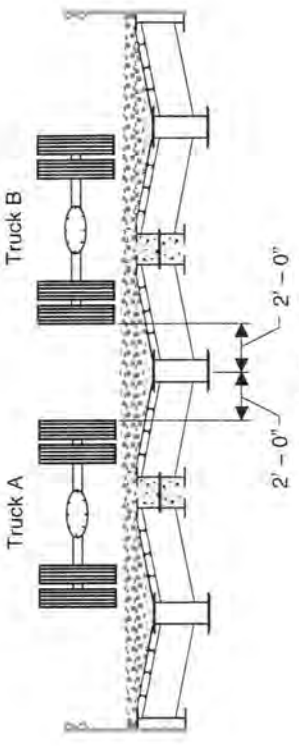
b. Test 2



d. Test 4



e. Test 5



f. Test 6

Figure 4.19. Transverse locations of truck(s) in BCB LT2.



a. Testing prior to placement of the driving surface



b. Testing after placement of the driving surface

Figure 4.20. Testing of the BCB after installation of the longitudinal flatcar connection.

Tests 1 – 4 that involved one test truck were performed (Figure 4.19a – d). The tests involving two test trucks were not performed since the LT2 results indicated that superposition accurately predicted the strains and deflections obtained when two test trucks were on the bridge.

#### 4.2.2 *Winnebago County Bridge*

##### 4.2.2.1 WCB Load Test 1

LT1 consisted of 5 tests on the middle RRFC with no connection to the two outside RRFCs. The objectives of WCB LT1 were very similar to those of BCB LT1, but since the tandem wheel base width was close to the same width of the flatcar, it was not possible to eccentrically load the 89-ft flatcars. In this bridge, vertical restraint was provided at the piers and abutments. To determine the effects of the restraints, three tests were performed with the RRFCs unrestrained at the abutments, and two tests were performed after the addition of the expansion joint and pinned restraint at the north and south abutments, respectively.

Since the WCB has three spans, negative and positive bending moments are present in the structure; without restraints at the abutments, upward displacement at these locations will occur when load is in the main span. In addition, as discussed in Chapter 2, the RRFCs used in this bridge have 3 types of transverse members. As a result, instrumentation was placed on the 89-ft RRFC as shown in Figure 4.21. Assuming symmetrical behavior of the bridge, midspan deflections were measured on the interior girder and only one exterior girder; the deflection on the other exterior girder was assumed to be the same as the instrumented exterior girder.

In each test, the test truck traveled from north to south and was stopped at five longitudinal locations on the RRFC; at each location, strain and deflection data were measured and recorded. The test truck was first stopped as the rear tire of the centerline of the tandem axle was directly above the north abutment with the rest of the truck positioned

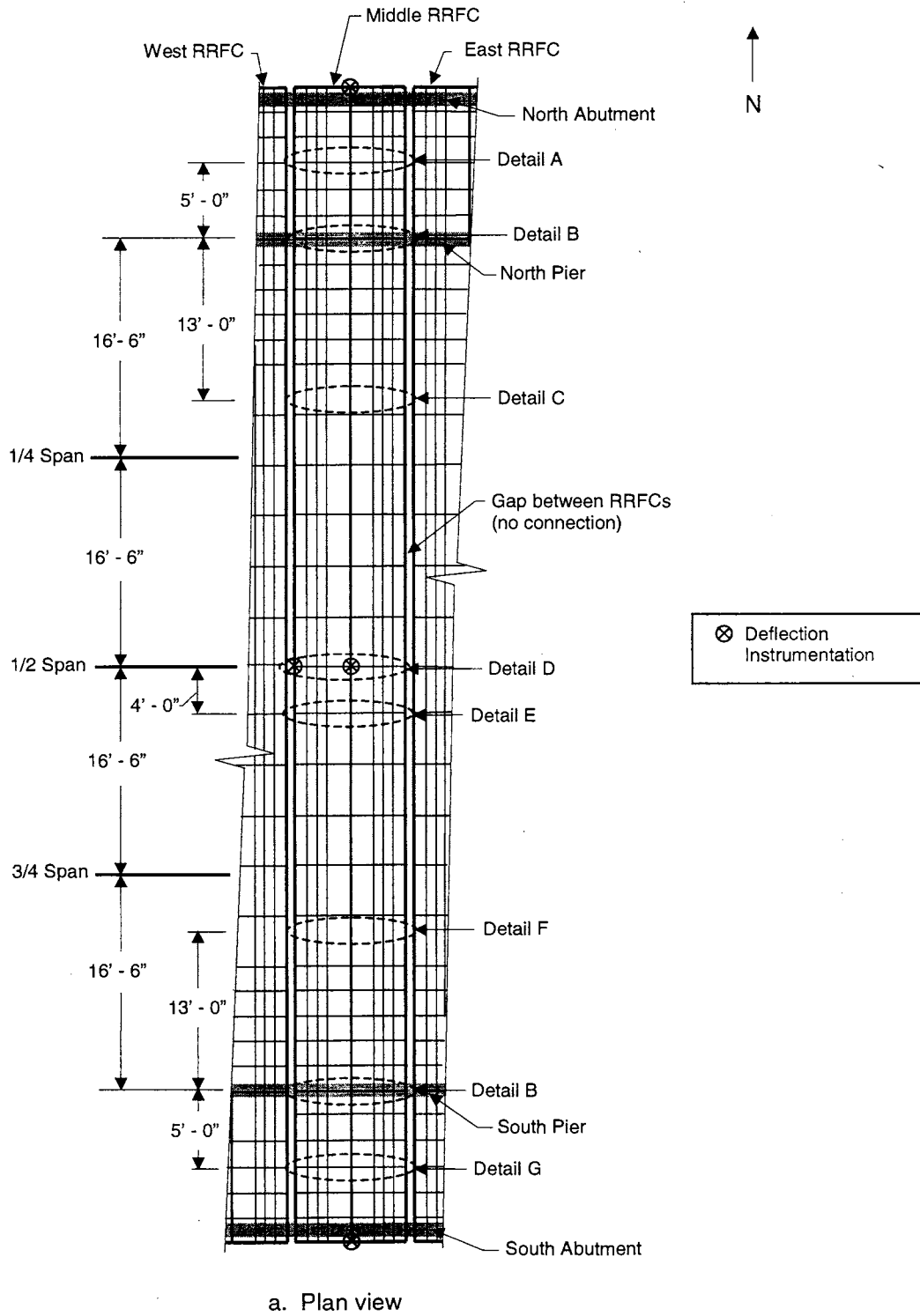
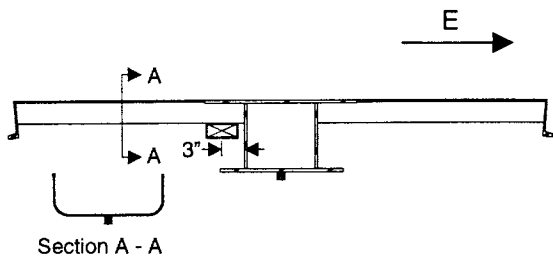
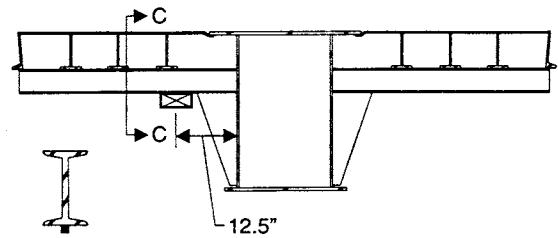


Figure 4.21. Location of instrumentation in WCB LT1.



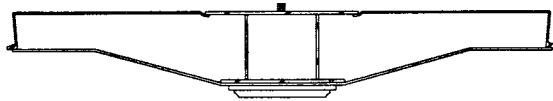
Section A - A

b. Detail A

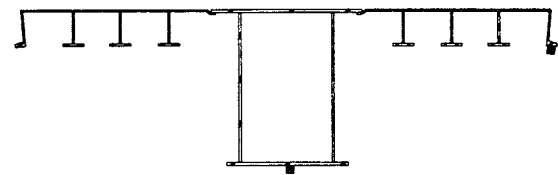


Section C - C

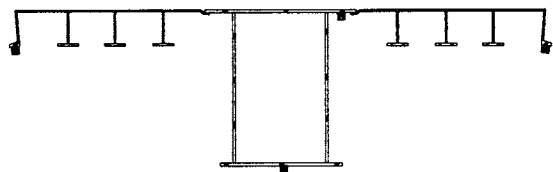
c. Detail E



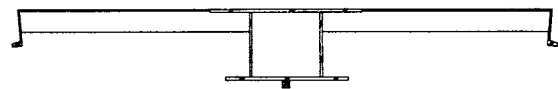
d. Detail B



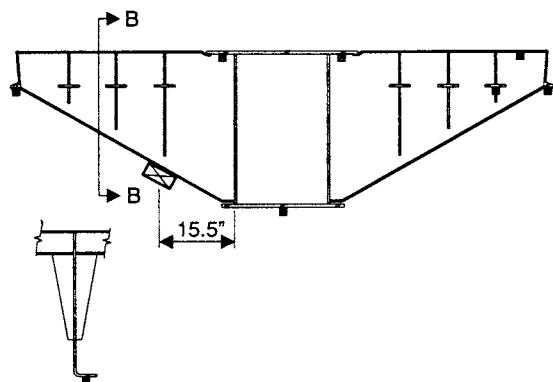
e. Detail F



f. Detail C



g. Detail G



Section B - B

h. Detail D

Strain Gage Orientation:	
	Longitudinal axis parallel to the plane of the page
	Longitudinal axis normal to the plane of the page

Figure 4.21. Continued.

on the bridge. For the next three longitudinal positions, the truck was stopped as the centerline of the tandem axle reached the 1/4, 1/2, and 3/4 points on the middle span. Finally, the last longitudinal location for the test truck to stop was as the front axle was positioned directly above the south abutment. Location of the 1/4, 1/2, and 3/4 middle span locations are illustrated in Figure 4.21, and a photograph of the field testing of the unconnected RRFC in LT1 is shown in Figure 4.22.

#### 4.2.2.2 WCB Load Test 2

LT2 tests were performed with longitudinal flatcar connections between the three RRFCs, the transverse timber planks, and the gravel driving surface in place. As will be discussed in Section 6.2.2, LT1 midspan deflections and strains were larger than those at any other location on the RRFC. Therefore, in LT2, the bridge was instrumented to measure positive moment strains and deflections at midspan, negative moment strains over the north pier, and displacements over the abutments as shown in Figure 4.23.



Figure 4.22. Field load testing the unconnected RRFCs during WCB LT1.



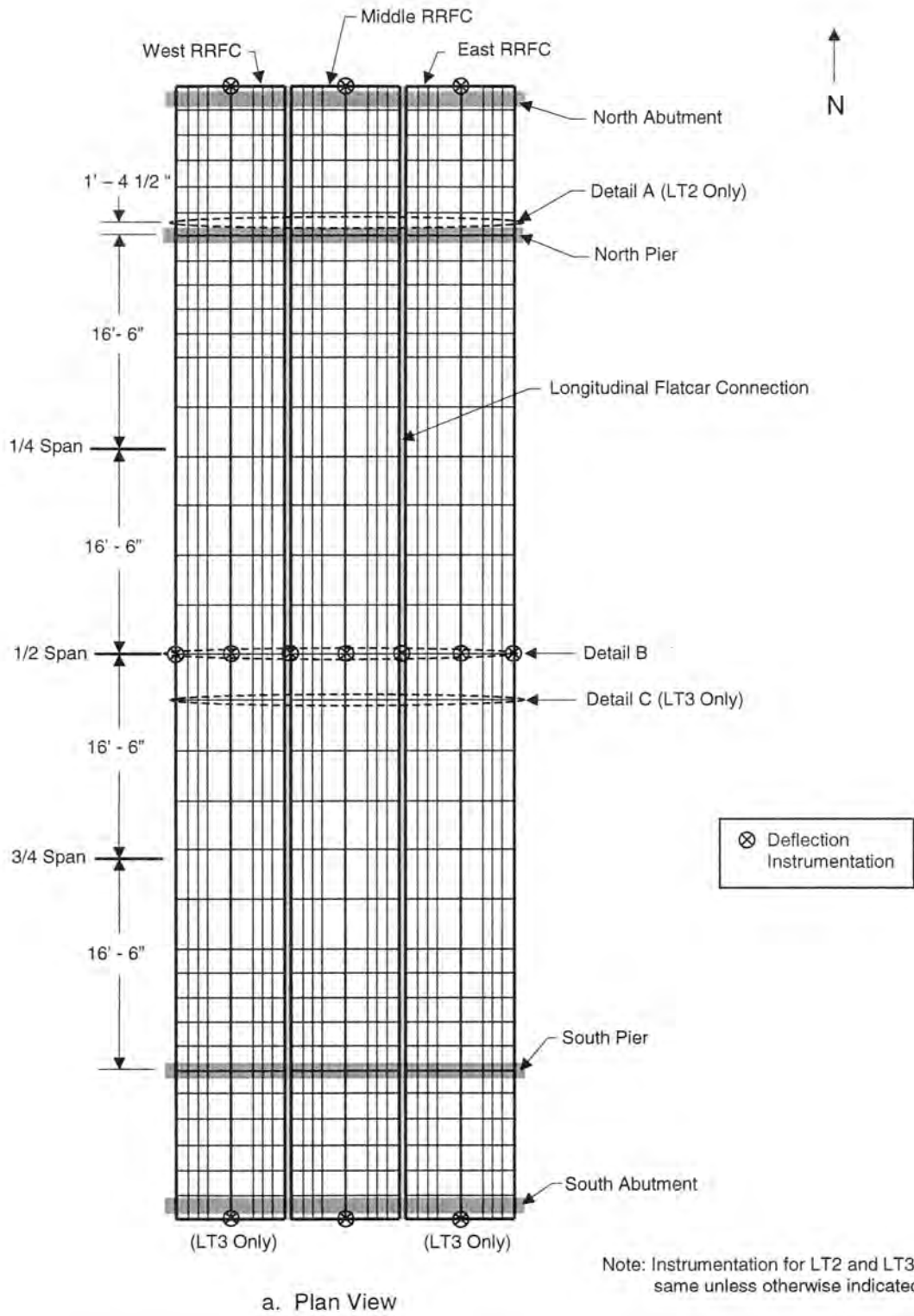
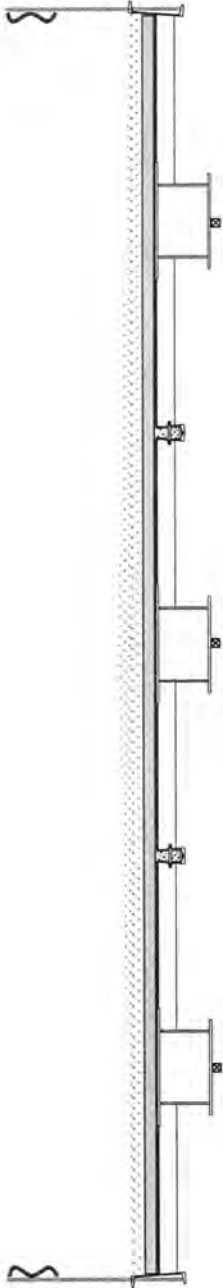
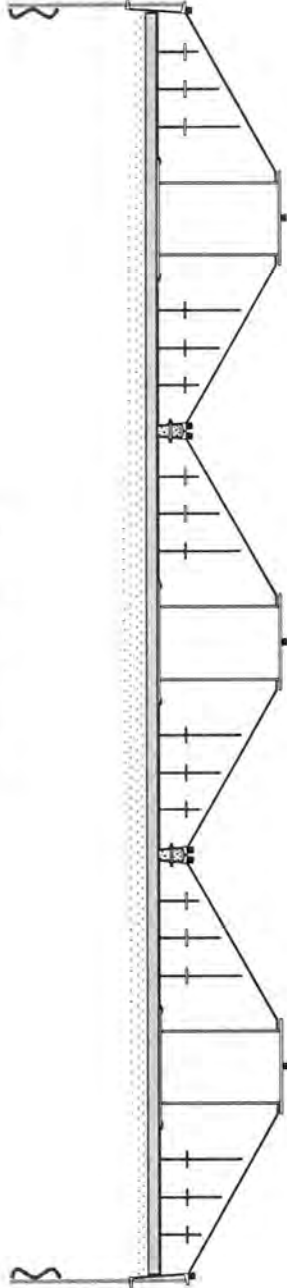


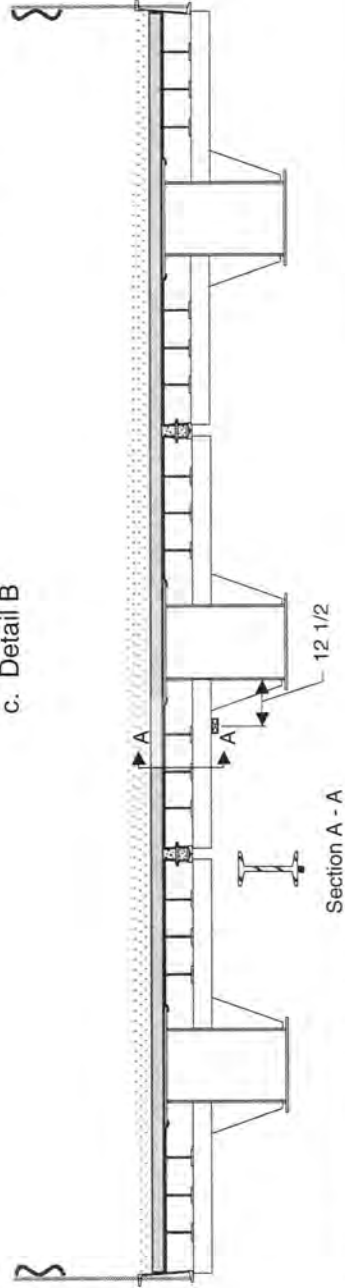
Figure 4.23. Location of instrumentation in WCB LT2 and LT3.



b. Detail A (LT2 Only)



c. Detail B



Strain Gage Orientation:

- ☒ Longitudinal axis parallel to the plane of the page
- ☒ Longitudinal axis normal to the plane of the page

Note: Instrumentation for LT2 and LT3 unless otherwise indicated

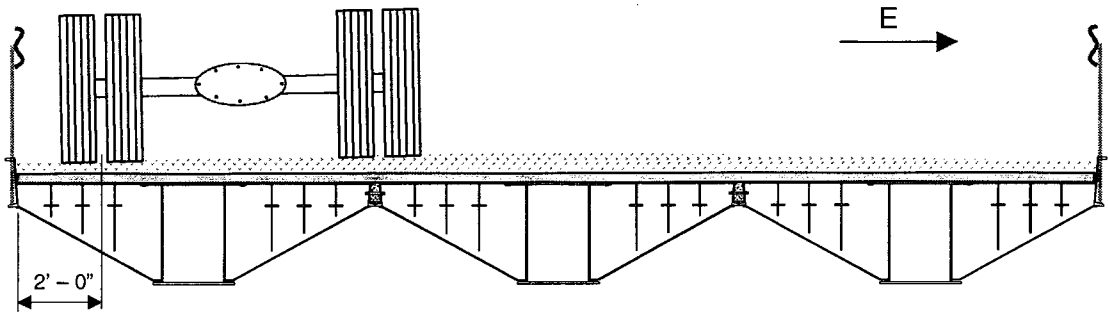
d. Detail C (LT3 Only)

Figure 4.23. Continued.

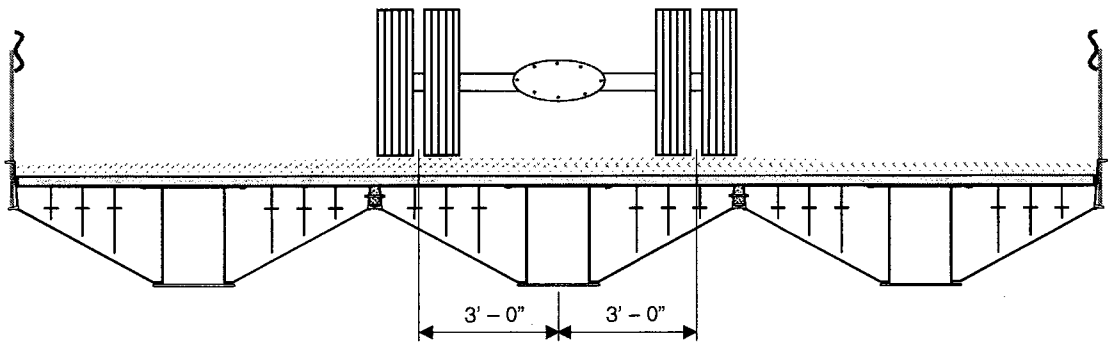
Four transverse truck positions were used in these tests, three of which are shown in Figure 4.24. The fourth position was similar to that of Figure 4.24a, except the space between the guardrail and truck was 2' – 9 1/2" rather than the 2' – 0" that is shown. This truck position was used to investigate the maximum torsion effects on the connection; however, results were essentially the same as those obtained when the truck was positioned as shown in Figure 4.24a. Therefore, results from those tests are not presented in Chapter 5 or Chapter 6. In a given test, the tandem truck was positioned transversely as shown and data were collected with the truck in five longitudinal locations. The first 4 longitudinal locations were identical to those of LT1, but for the fifth location, the data were measured and recorded as the rear tire of the tandem axle was directly above the south abutment with the rest of the truck off of the bridge. A photograph showing a transversely centered truck in the LT2 field load test is presented in Figure 4.25.

#### 4.2.2.3 WCB Load Test 3

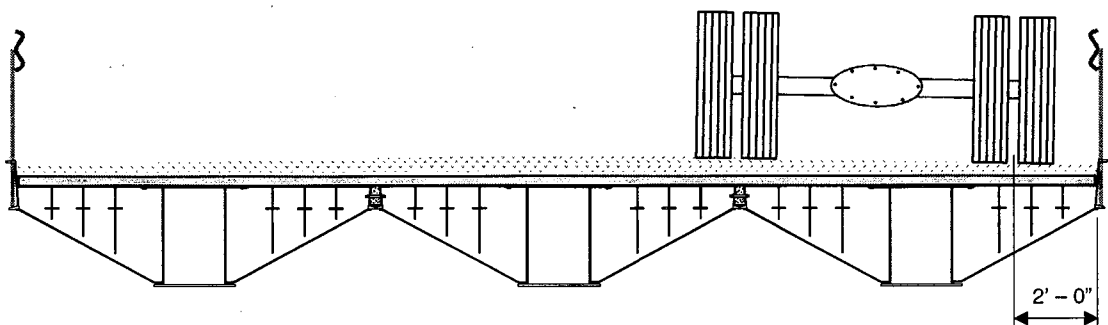
LT3 was performed the summer following the completion of construction; thus, the WCB experienced approximately 9 months of traffic loading. As shown in Figure 4.23, instrumentation used in LT3 was for measuring positive moment strains and deflections at midspan, strains on the two types of middle span transverse members, and upward deflections at the north and south abutments. Since the negative moments above the piers were found to be relatively small during LT1 and LT2, no instrumentation was installed in LT3 to measure strains in these regions. Testing procedures for LT3 were identical to those used in LT2; transverse truck positions used in these three tests are shown in Figure 4.24.



a. Test 1



b. Test 2



c. Test 3

Figure 4.24. Transverse truck positions in WCB LT2.



Figure 4.25. Testing the finished WCB immediately following completion of construction.

## 5. THEORETICAL ANALYSIS

### 5.1 LCS Analysis

To better understand the behavior of the LCS and to be able to predict the behavior of other similar RRFC bridge composite connections, a theoretical analysis was developed. Theoretical results from this analysis will be compared with experimental results in Chapter 6. The following assumptions were made in this analysis:

- Due to the excellent confinement provided by the *W*-shapes, gross section properties for the concrete beam were assumed in the Service Load Torsion Tests for the conventional analysis (See Section 5.1.1.1).
- The longitudinal steel reinforcement make a minimal contribution to the concrete beam torsional rigidity, and therefore, was neglected in the torsion analyses.
- The connection between the *W*-shapes and concrete beam provides composite action along the entire length of the specimen.
- Warping in the steel flanges is not affected by the concrete beam.

A summary of the analytical process and results is presented in the following sections. For more details on the analytical process of LCS torsion behavior, see Appendix B; for more analytical information on LCS flexural behavior, refer to Appendix C.

#### *5.1.1 Theory of LCS Torsion Behavior*

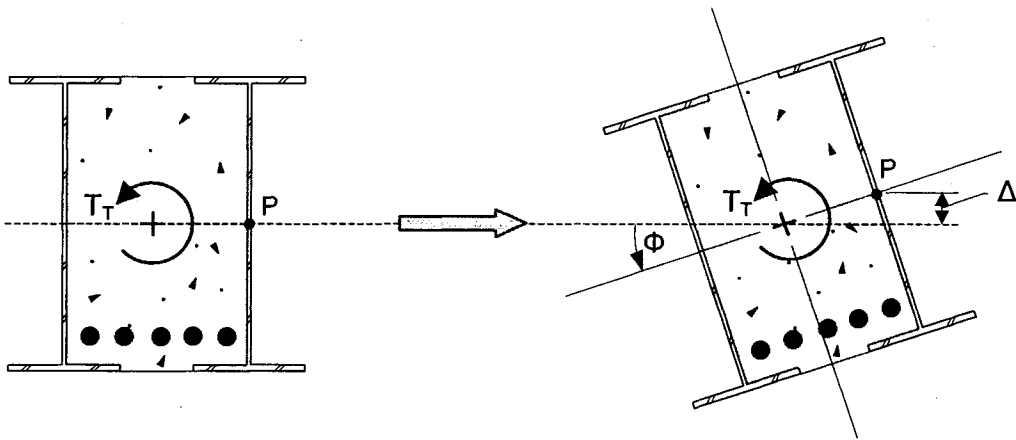
Two methods of analyses were used to examine the torsional behavior of the LCS. The first, described in Section 5.1.1.1, was a conventional method of analysis that was used to investigate the torsional warping and flexural stresses in the *W*-shape flanges. The second analysis, presented in Section 5.1.1.2, was a finite element analysis (FEA) used to investigate the effects of the transverse threaded rods on stresses and strains in the webs and flanges of the steel beams.

##### 5.1.1.1 Analysis of LCS Torsion Behavior by Conventional Methods

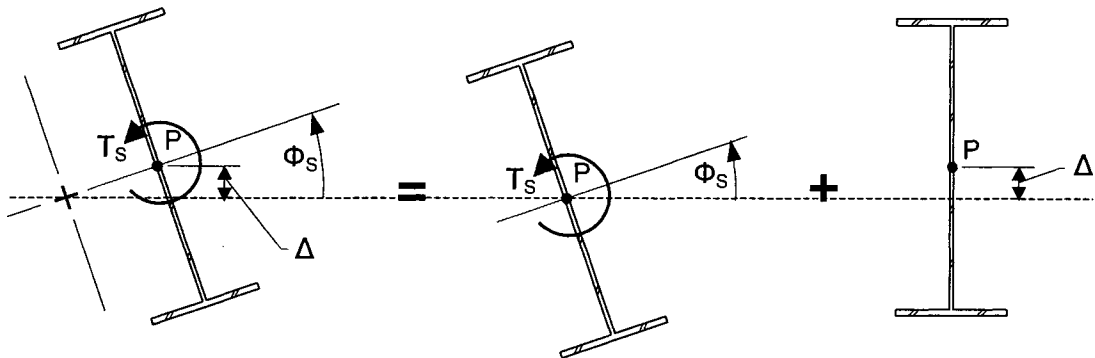
When analyzing a specimen subjected to a torsional moment, stresses will develop from pure torsion effects (St. Venant's stresses) and from warping in the section. St.

Venant's stresses will produce only shear stresses, but warping will result in shear and normal stresses. In beam theory, flexural stresses are usually much larger than shear stresses except in short beams. Since the LCS represents a connection between two adjacent, relatively long girders in a bridge, the primary interest in testing the LCS was the combination of the flexural and warping normal stresses in the *W*-shapes.

A review of the LCS subjected to rotation provides a basic understanding of the analysis that was performed. Figure 5.1a illustrates a composite section of the LCS



a. Composite rotation of the LCS under concentrated torque,  $T_T$



b. Steel beam behavior due to composite action in the LCS

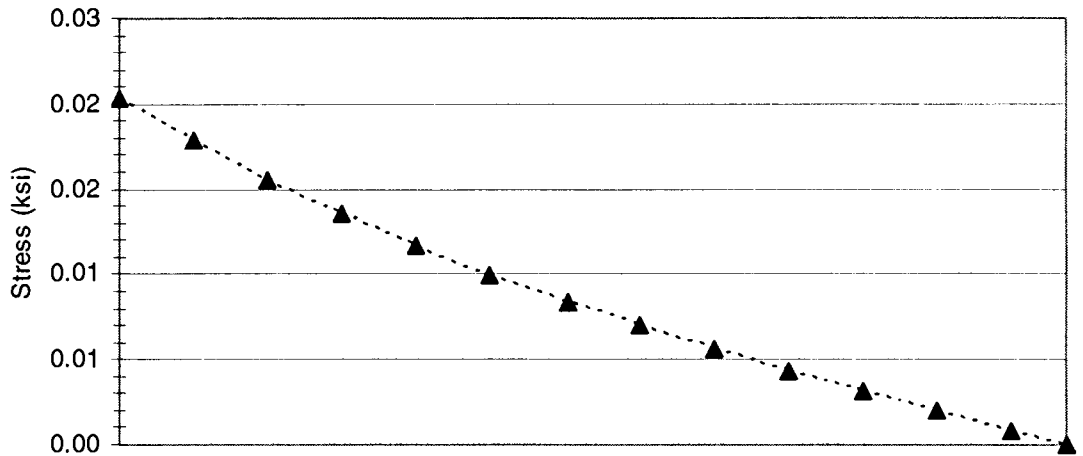
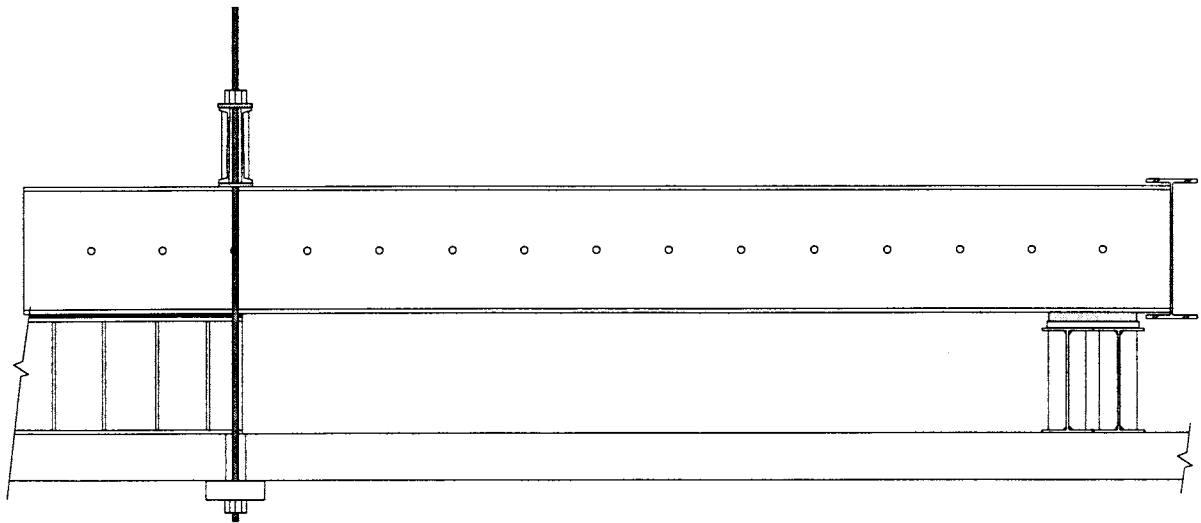
Figure 5.1. Composite behavior of the LCS under torsional loading.

subjected to a torsional moment,  $T_T$ , and rotation,  $\Phi$ ; for the same loading condition, Figure 5.1b isolates a  $W$ -shape from the composite section and illustrates the portion of  $T_T$  and  $\Phi$  resisted by the section,  $T_S$  and  $\Phi_S$ , respectively. Since a composite connection between the steel and concrete is assumed,  $\Phi_S$  and  $\Phi$  are equal. However, the distribution of  $T_T$  between the two  $W$ -shapes and concrete beam is unknown. Therefore, compatibility relationships between the  $W$ -shapes and concrete beam were used to determine the torsional moment distribution. Figure 5.1b also illustrates that for any torque applied to the composite section, the  $W$ -shapes rotate and displace vertically. Therefore, the analyses of the  $W$ -shapes include torsional warping stresses and flexural stresses; their combined effect is obtained through superposition.

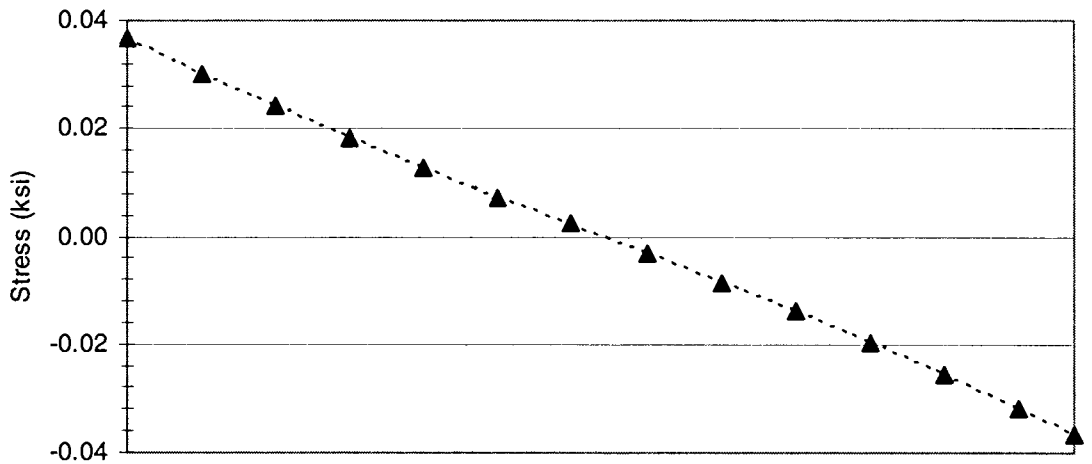
The development and distribution of warping stresses in each section of the  $W$ -shape flanges is directly related to the degree of warping restraint in each section. If warping restraint does not exist, then warping stresses do not develop in a given section. Similarly, if warping is partially or completely restrained in a  $W$ -shape section, then warping stresses develop. The maximum flange warping stresses develop in the tips of the  $W$ -shape flanges.

For an exact evaluation of the torsional warping stresses that develop in the  $W$ -shape flanges of the LCS, the amount of warping restraint at the ends of the LCS must be known. Complete warping restraint was assumed at the rotationally restrained end of the LCS, but only partial warping restraint, caused by the lever arm at the rotating end of the LCS, was assumed. Since the amount of warping restraint in the LCS was not known, two analyses were performed to establish a stress range; the actual warping stress in the flanges should be within the bounded region. Figure 5.2 illustrates the warping flange stress distribution for each analysis resulting from a torque of 1 ft-k on the LCS; this distribution applies to the LCS top right and bottom left flanges shown in Figure 5.1a. The first analysis





a. Fixed-free end warping restraints



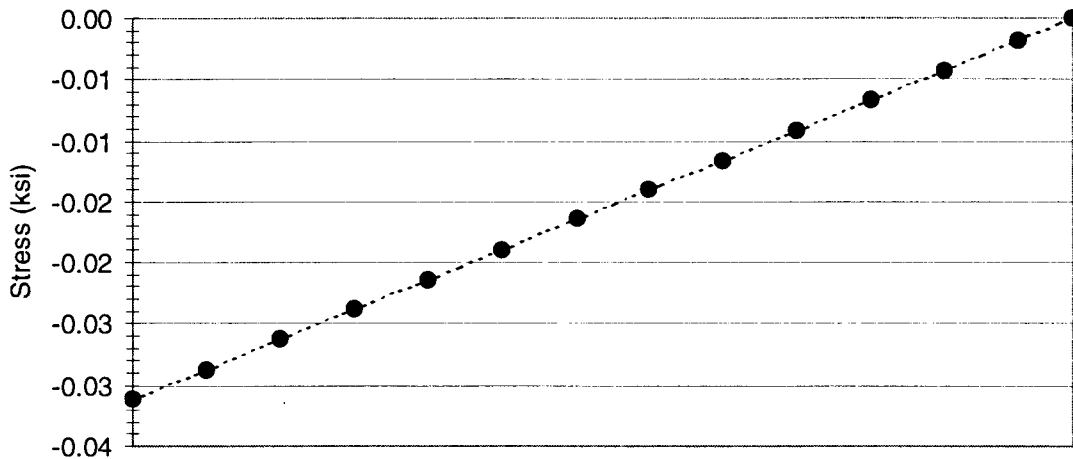
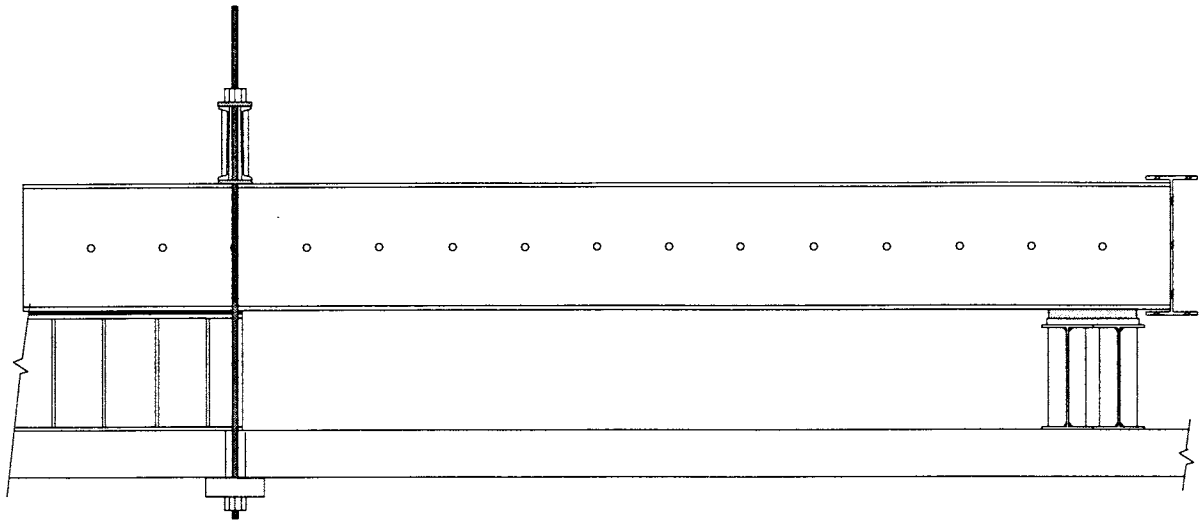
b. Fixed-fixed end warping restraints

Figure 5.2. Flange torsional warping stresses in the W-shape member of the LCS resulting from a 1 ft-k torsional moment and end warping restraints.

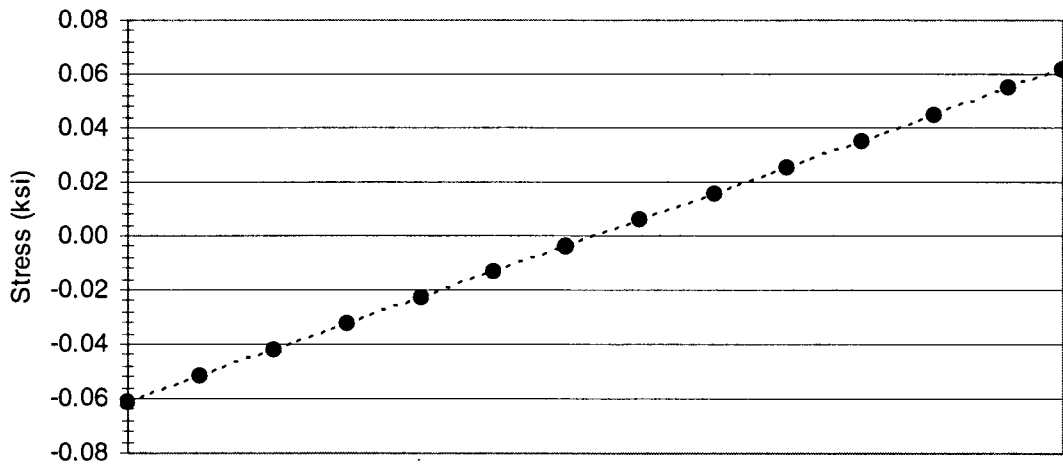
that was performed assumed complete warping restraint at the rotationally restrained end of the LCS and no warping restraint at the rotating end. This analysis is referred to as the “Fixed-Free” analysis. The second analysis assumed complete warping restraint at both ends of the LCS and is referred to as the “Fixed-Fixed” analysis. For both graphs in Figure 5.2, positive values represent tensile stress, and negative values represent compressive stress. At any location along the length of the LCS, flange stresses will be in tension or compression depending on the flange being investigated. See Figure 4.2a for locations of strain gages on the W-shapes.

Similar to torsional warping stresses, the flange flexural stresses that develop from vertical displacement of each W-shape are dependent upon the degree of restraint at each end of the beam. For flexural stresses, rotational end restraint must be present. Following procedures similar to those used in the torsion analysis, two analyses were performed to evaluate the flexural behavior of the W-shapes; these results are presented in Figure 5.3. The end restraints in each analysis are consistent with those used in the torsion analysis; if an end was assumed to have complete warping restraint, then it was also assumed to be completely rotationally restrained. Furthermore, if an end was assumed to have zero warping restraint, then it was assumed to have free rotation. Therefore, the first analysis had fixed-free rotational restraints at its ends, and the second analysis was performed with fixed-fixed rotational restraints at its ends.

Figure 5.4 illustrates the resultant flange stresses obtained by combining the warping and flexural stresses through superposition. As can be seen, warping stresses develop in both ends of the LCS flanges in the “Fixed-Fixed” analysis, but only in one end of the “Fixed-Free” analysis. In addition, Figure 5.5 illustrates the predicted axial rotation for the LCS for both analyses. For both analyses, axial rotation is linear near the middle of the LCS.



a. Fixed-free end warping restraints



b. Fixed-fixed end warping restraints

Figure 5.3. Flange flexural stresses in the W-shape member of the LCS resulting from a 1 ft-k torsional moment and end rotational restraint.

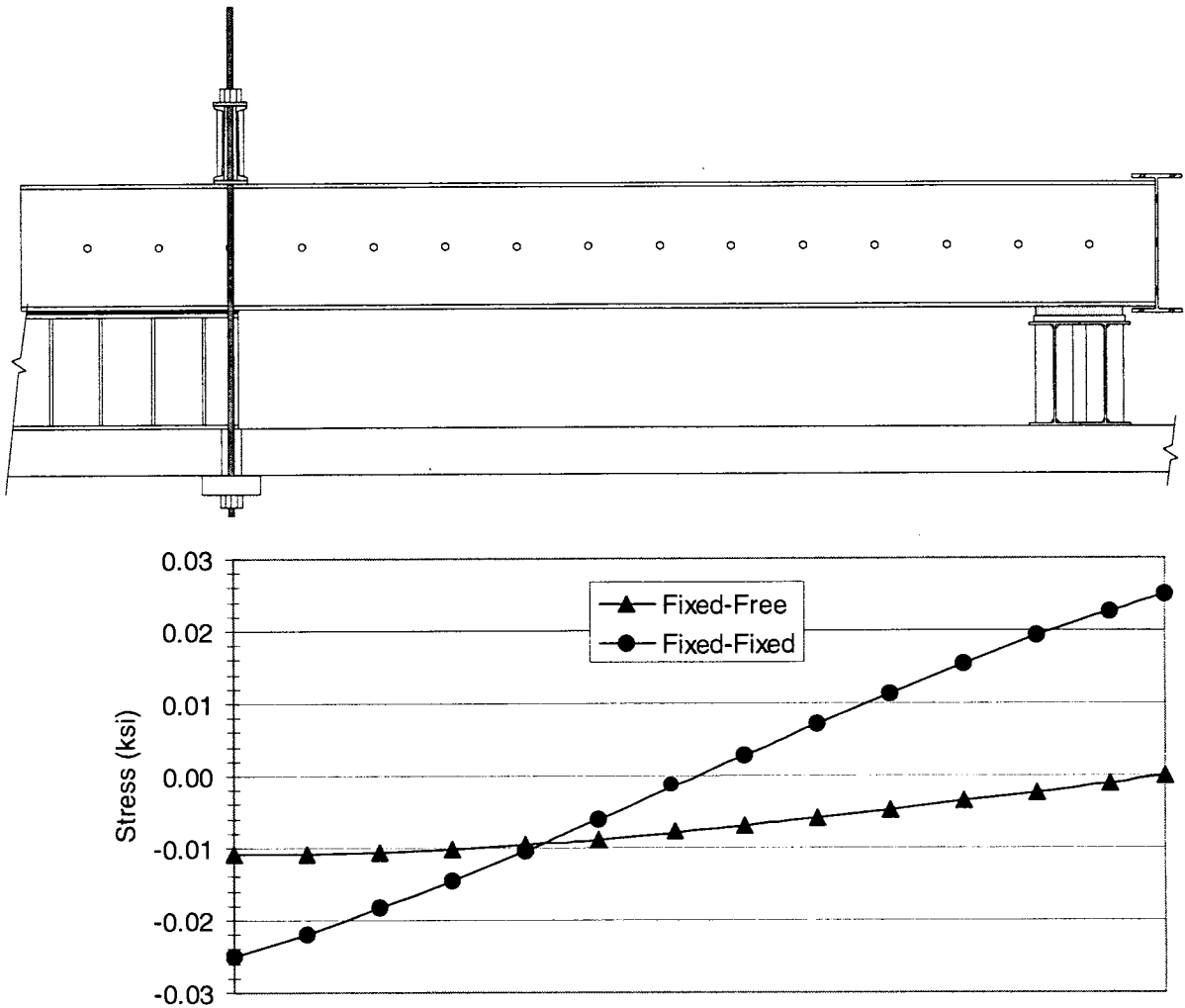


Figure 5.4. Variation in flange stresses in the W-shape of the LCS resulting from a 1 ft-k torsional moment and end restraint.

However, depending on the boundary conditions used in the analysis, nonlinear axial rotation occurs near the ends of the LCS. Since the results in both figures were developed with a unit torsional moment on the LCS, theoretical results prior to yielding for any test may be obtained by multiplying the ordinate values presented in Figure 5.4 and Figure 5.5 by the actual torsional moment on the LCS during the test.

It should be noted that the conventional analysis did not consider any effects from the presence of the transverse threaded rods in the LCS. If the LCS was completely

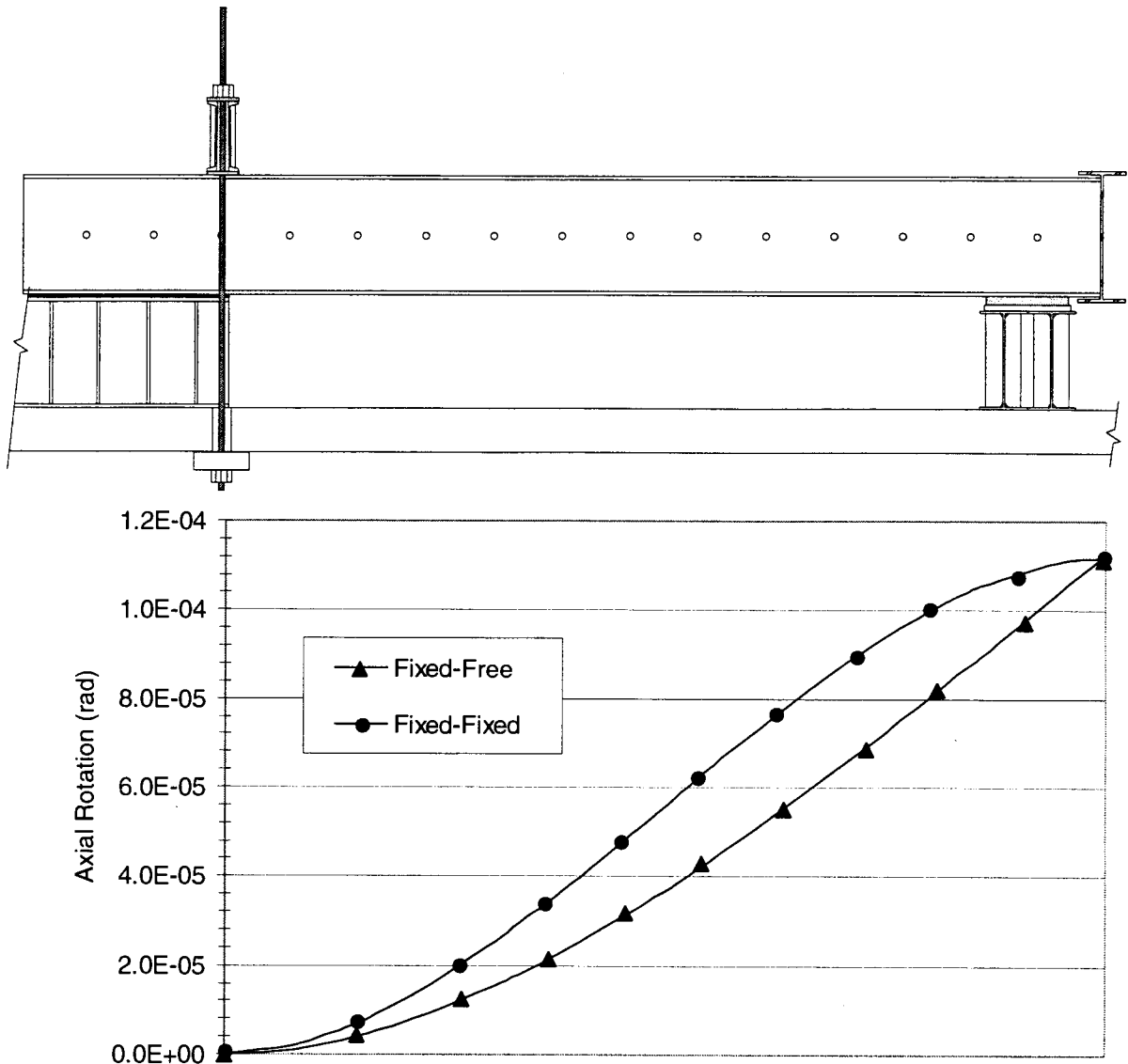


Figure 5.5. Variation in axial rotation of the LCS resulting from a 1 ft-k torsional moment and end restraint.

composite during each of its tests, then the conventional analysis may be accurate.

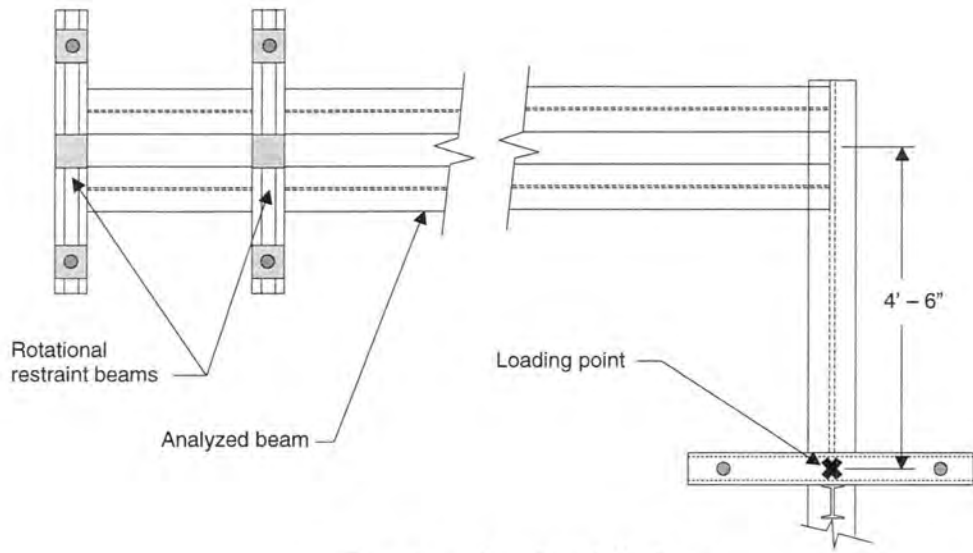
However, as will be discussed in Chapter 6, the LCS was not completely composite when it experienced large rotations, and thus theoretical results from the conventional analysis are not in good agreement with the experimental results. As a result, a FEA was performed to

investigate the influence of transverse threaded rods on web and flange stresses in the W-shapes.

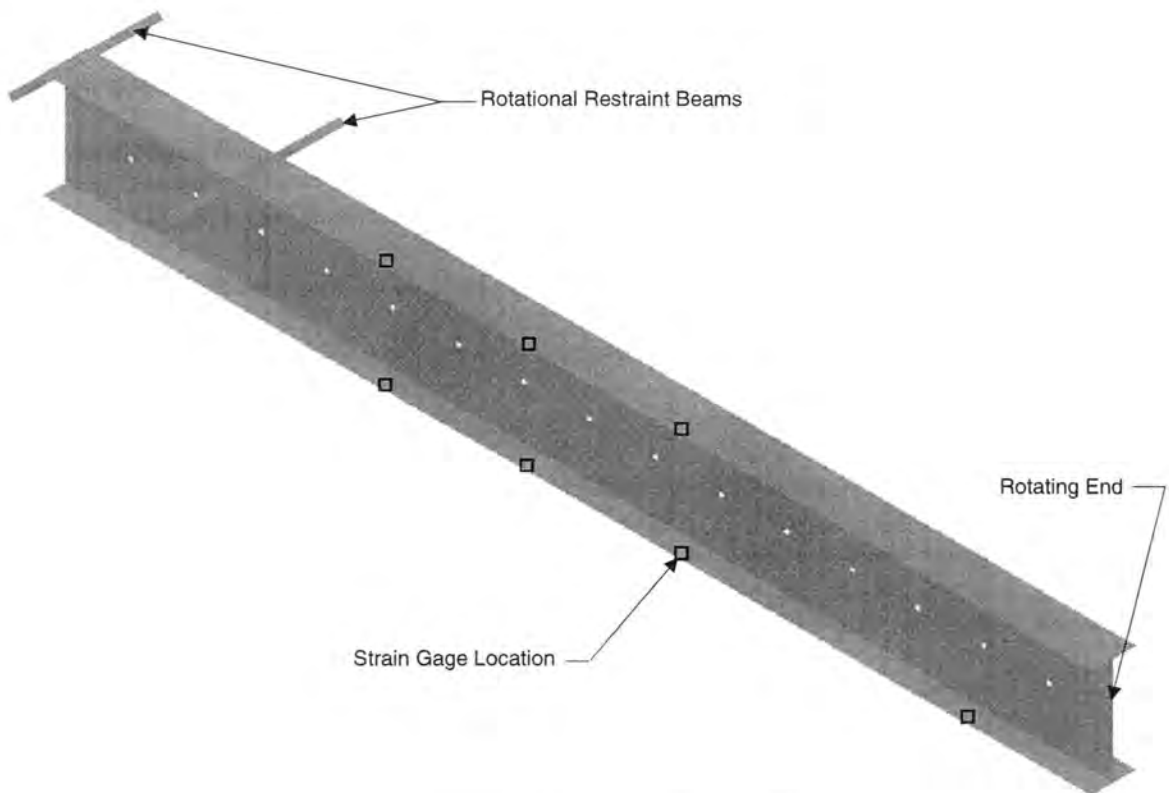
#### 5.1.1.2 Analysis of LCS Torsional Behavior by Finite Element Analysis

The FEA previously noted was performed on one of the W-shapes in the LCS; this W-shape is identified in Figure 5.6a. The modeled W-shape and the location of the strain gages on the flanges of that W-shape are presented in Figure 5.6b. The W-shape was modeled with the element *Shell63* in ANSYS. This element has six degrees of freedom at each node – translations and rotations about the nodal x, y, and z axes; the element is defined by 4 nodes, an element thickness, and material properties. As will be discussed in Chapter 6, the largest measured horizontal, vertical, and rotational displacements during the entire Ultimate Load Torsion Test were 1.67 in., 0.47 in., and 8.6 degrees, respectively. For each FEA, these displacements were applied to the rotating end of the LCS as boundary conditions to accurately reflect loading in the Ultimate Load Torsion Test.

The first condition examined in the FEA was complete composite behavior as illustrated in Figure 5.1a. For this condition, it is assumed that the concrete beam and W-shapes remain in complete contact with each other throughout the entire LCS Ultimate Load Torsion Test, and as a result, no axial force develops in the transverse threaded rods. However, as illustrated in Figure 5.7a, it is evident that complete composite behavior was not present during the laboratory test as W-shapes “separate” from the concrete beam. As a result, the second condition examined was partial composite behavior as illustrated in Figure 5.7b. For the second condition, it was assumed that the W-shape and concrete remain in contact from the transverse threaded rod to the bottom of the LCS, but separation occurs from the transverse threaded rod to the top of the LCS. To examine the sensitivity of the W-shape stresses to the degree of partial composite behavior, the out-of-plane displacement demonstrated in Figure 5.7b at each transverse rod location was assumed to



a. Top view of analyzed W-shape

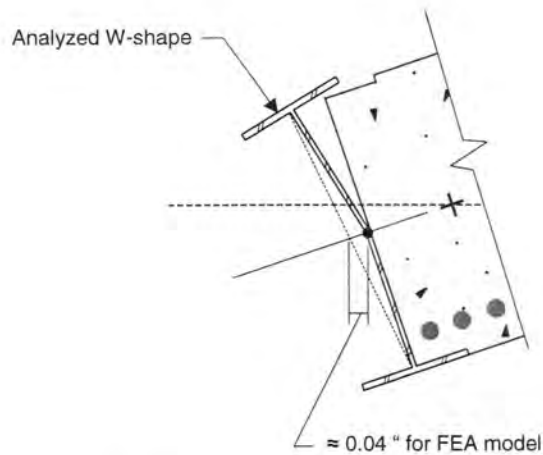


b. Isometric view indicating strain gage locations

Figure 5.6. LCS W-shape member analyzed in ANSYS for the Ultimate Load Torsion Test.



a. Photograph of partial composite behavior



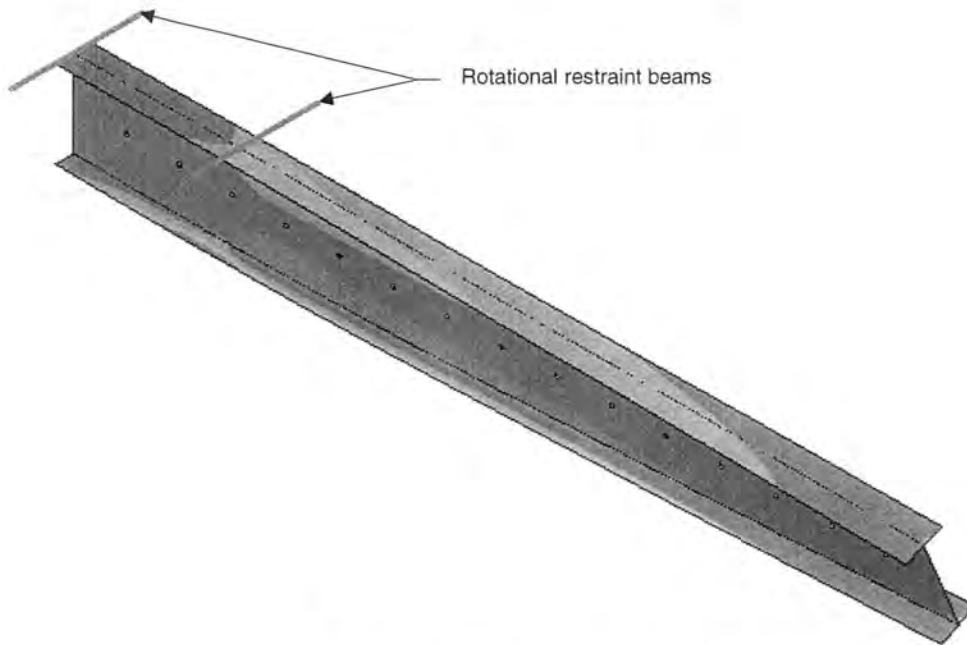
b. Modeling of partial composite behavior

Figure 5.7. LCS partial composite behavior in the Ultimate Load Test.

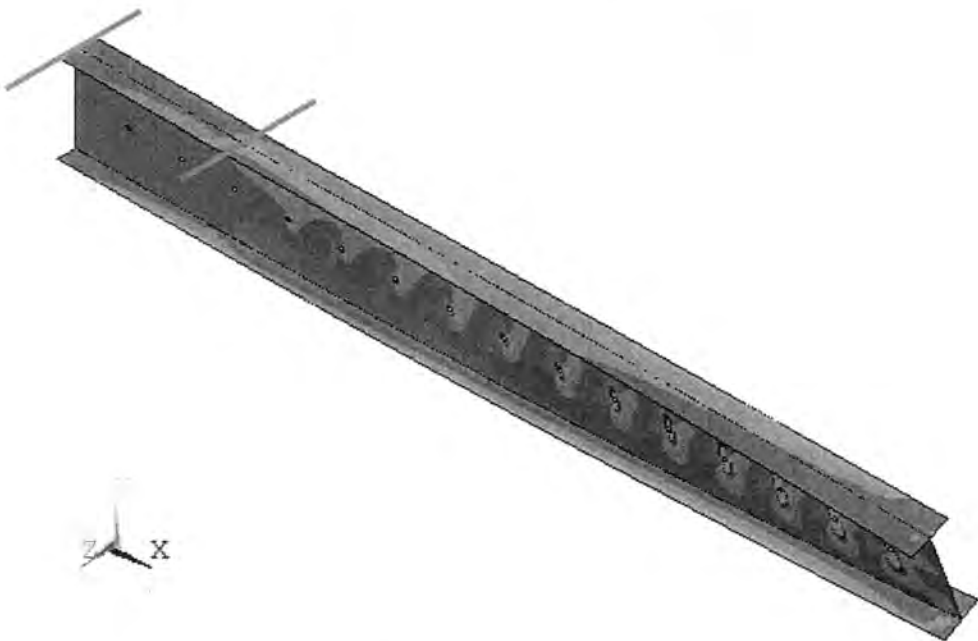
be constant at 0.04 in. This displacement was arbitrarily chosen and serves only to show the relationship between partial composite behavior and W-shape stresses.

Contour plots for longitudinal stresses in the W-shapes for both complete and partial composite behavior conditions are presented in Figure 5.8. As can be seen, the stress contours are different for the complete composite and partial composite analyses. In addition, Figure 5.9 illustrates the difference in longitudinal flange stresses for both





a. Complete composite behavior



b. Partial composite behavior

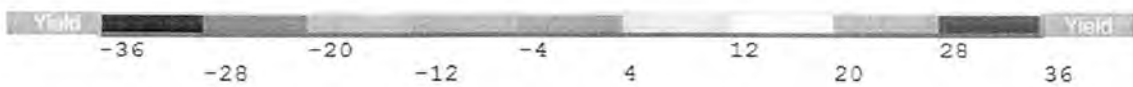
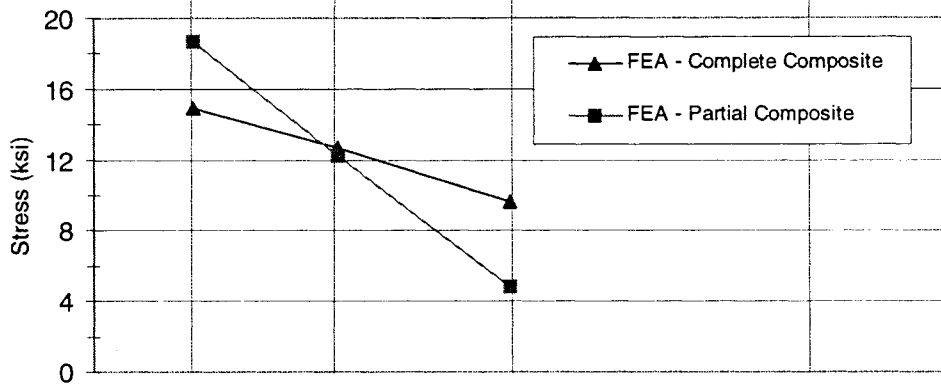
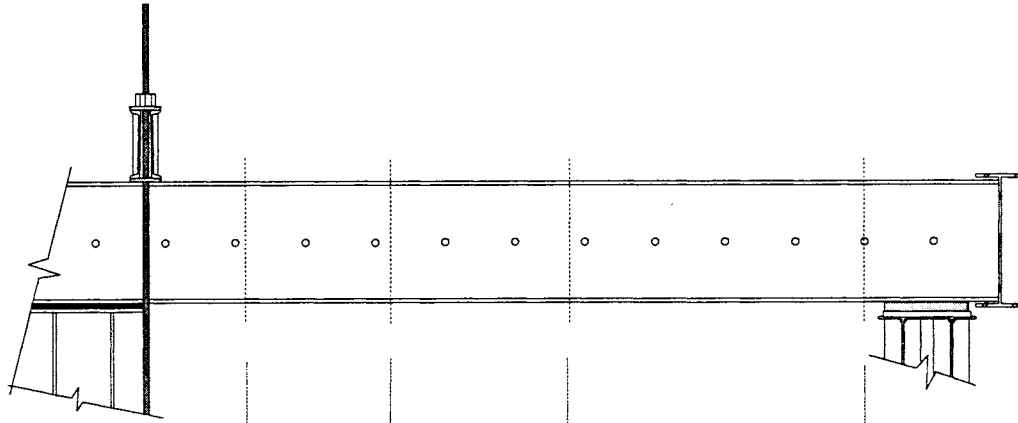
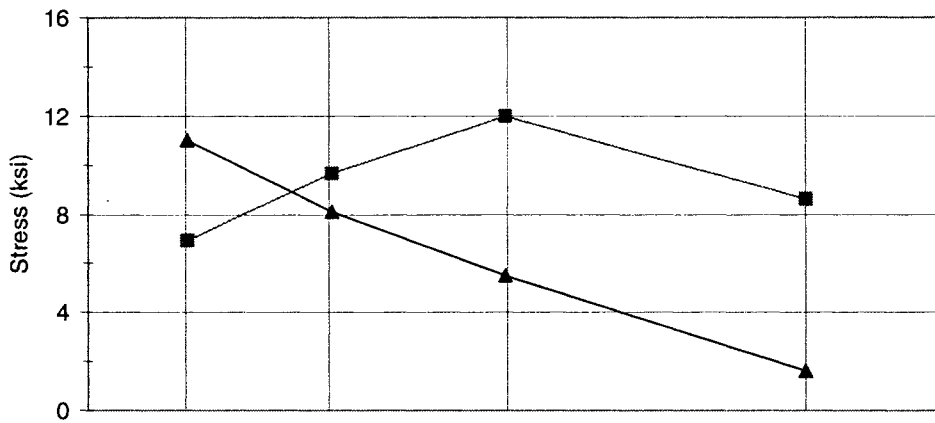


Figure 5.8. FEA predicted LCS longitudinal stresses in the analyzed W-shape for the Ultimate Load Torsion Test.



a. Top flange



b. Bottom flange

Figure 5.9. FEA predicted flange stresses for LCS complete and partial composite behavior in the Ultimate Load Torsion Test.

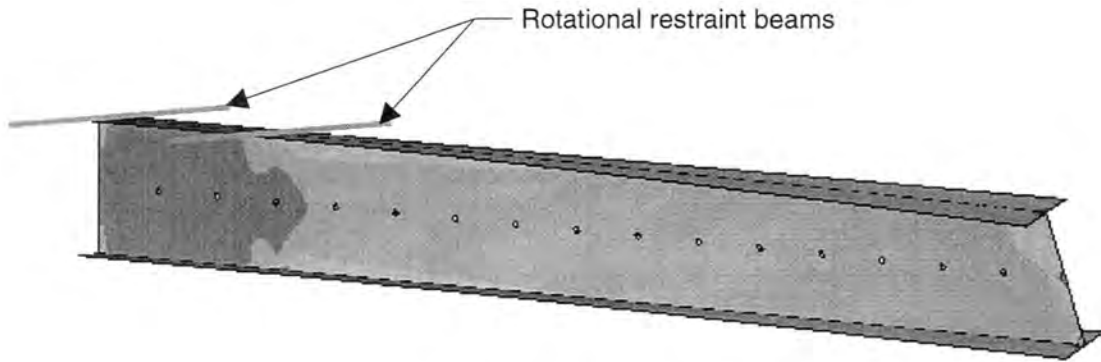
analyses. By reviewing Figure 5.9, flange stresses predicted by the FEA models differed by as much as 7 ksi. As a result, it was concluded that the stresses throughout the LCS W-shapes are influenced by presence of the transverse threaded rods. Since partial composite behavior is a more accurate representation of LCS behavior, results from this model are considered to be more accurate than those from the completely composite section model.

To give a better illustration of the combined effects of normal and shear forces in the W-shape, von Mises equivalent stress contours are illustrated in Figure 5.10. As can be seen, the von Mises stress contours reveal much larger stress concentration around the transverse threaded rods than those shown in Figure 5.8. A close-up view of von Mises stresses in Figure 5.11 illustrates the stress concentrations caused by the presence of transverse threaded rods from partial composite behavior. For the very small out-of-plane displacement used in the partially composite model, stress concentrations propagated many hole diameters away from the hole, and thus, may be measured by the web strain gages shown in Figure 4.2a.

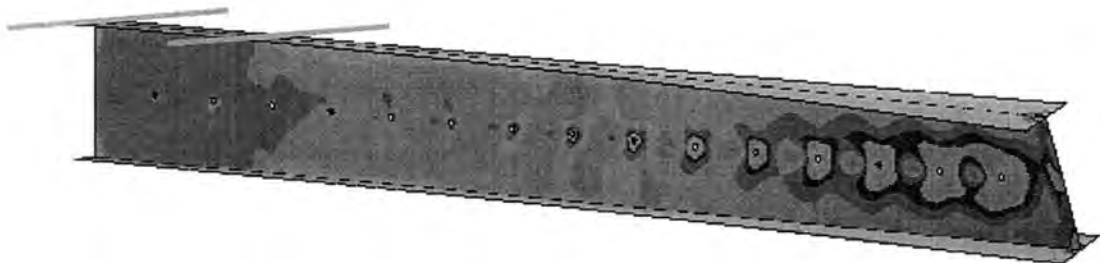
From the FEA, it can be determined that the presence of the transverse threaded rods can affect the stresses in the webs and flanges of the W-shapes in the LCS. Recall that equal out-of-plane displacements were applied at each transverse threaded rod location, and application of this boundary condition assumes equal axial forces in each transverse threaded rod. Since strains were recorded on two threaded rods during the torsion tests, the laboratory test results will validate or disprove this assumption; this will be further discussed in Chapter 6.

### *5.1.2 Theory of Flexural Behavior*

As discussed in Chapter 4, for the service level flexure tests, the composite LCS was simply supported and loaded by two concentrated forces,  $P_1$  and  $P_2$ , as shown in



a. Complete composite behavior



b. Partial composite behavior

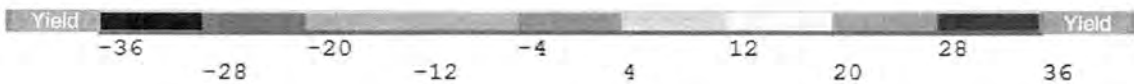
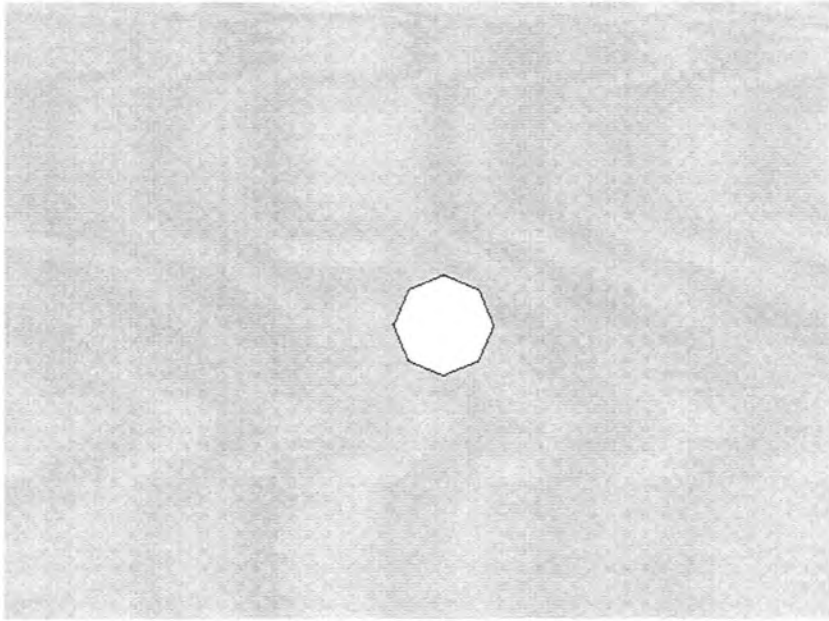
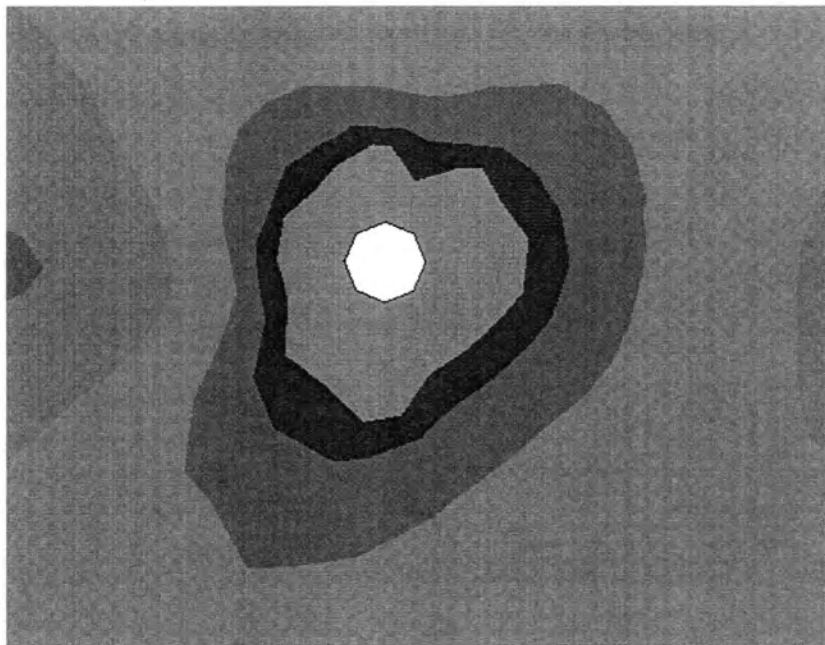


Figure 5.10. FEA predicted LCS von Mises stresses in the analyzed W-shape for the Ultimate Load Torsion Test.



a. Complete composite behavior



b. Partial composite behavior

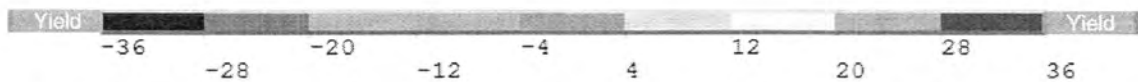


Figure 5.11. FEA predicted LCS von Mises concentrated hole stresses in the analyzed W-shape for the Ultimate Load Torsion Test.

Figure 5.12. The distribution of these forces among the W-shapes and concrete beam was once again unknown. To determine the distribution of the concentrated forces to the W-shapes and concrete beam, compatibility relationships were developed that equated the deflections between the W-shapes and uncracked concrete beam at the SPDTs located by Point G in Figure 5.12. From the relationships, for a given displacement at Point G, the contributions of  $P_1$  and  $P_2$  to the W-shapes and concrete beam were known. Once the distribution analysis was completed, bending moments and strains were calculated at the instrumented sections in the LCS. Figure 5.13 shows the theoretical top and bottom flange stresses for the LCS service flexure test for  $P_1$  and  $P_2$  both equal to 1 kip (i.e. 2 kips applied to the composite LCS). As can be seen in this figure, the longitudinal stress distribution for the LCS subjected to concentrated forces is linear. For this loading, the maximum moment in a W-shape was calculated to be 24.3 in-k.

## 5.2 Live Load Grillage Analysis of the RRFCC Demonstration Bridges

In order to better understand the behavior of the RRFCC bridges, grillage analyses were performed on the BCB and WCB. Results of the analyses are presented later in this chapter and are compared with field test results in Chapter 6. Although a grillage analysis is not the most accurate theoretical analysis, it is easier to construct, requires less computer time for a solution, and therefore, is more economical for obtaining theoretical results than a

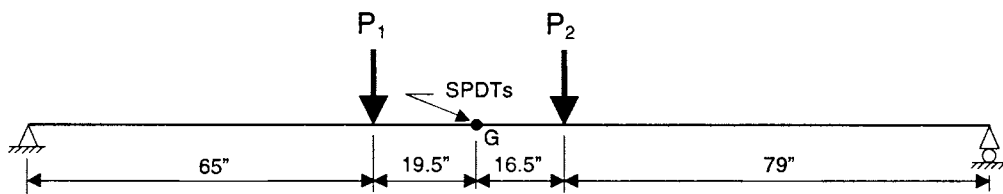


Figure 5.12. LCS service load flexure setup.

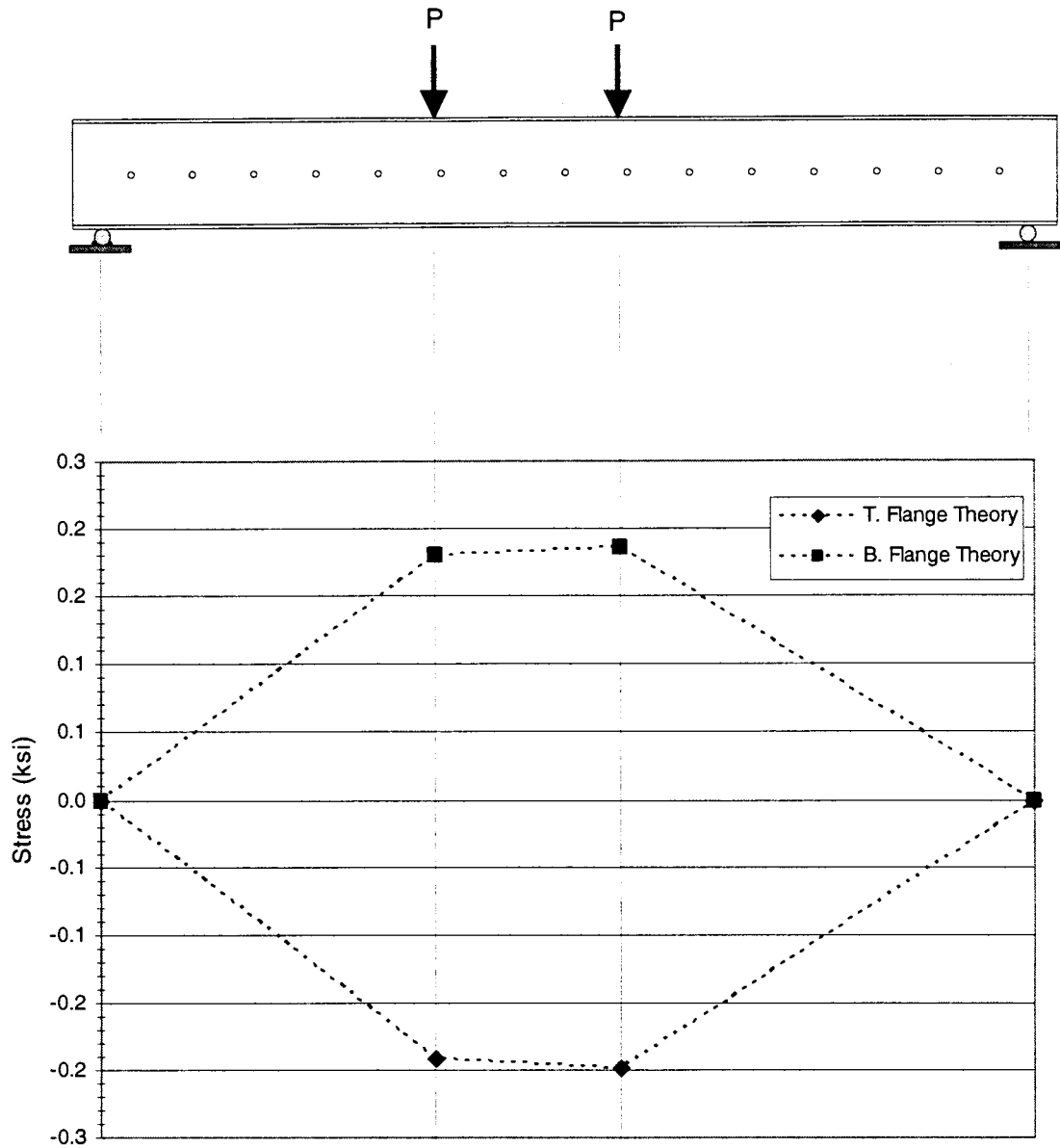


Figure 5.13. Theoretical top and bottom flange stresses for the Service Level LCS Flexure Test ( $P = 1$  k).

more complicated finite element computer model. In addition, the exact section properties for some structural members in the RRFC are not known. Thus a more accurate FEM is not warranted for this reason as well. Since the grillage model is less sensitive to slight errors in

section properties, it was chosen for use in the RRFC bridge analyses. The following assumptions were made in the development of the computer models:

- Corresponding structural members and their spacing among the three flatcars are identical. In addition, using an average spacing between successive, identical members rather than the exact spacing will have negligible effect on the results.
- Steel decking and transverse timber planks do not contribute to the longitudinal stiffness of the bridge.
- Connections between primary, longitudinal members and transverse members in the RRFCs are adequate to support full moment transfer.
- Load distributing capabilities of the asphalt milling and gravel driving surfaces are negligible.
- Rigid links between adjacent exterior girders and the concrete beams created compatible displacements and rotations.
- Gross concrete section properties are applicable for both bridges.
- Timber planks only transfer vertical and horizontal forces to the primary members and flatcar connections of the bridges (i.e., no moment transfer) since they are connected to the flatcars only at the edges and centerline of the bridge.

The analytical models were developed in ANSYS [7], finite element software that has both elastic 3-D prismatic and tapering beam elements. Both beam elements have tension, compression, torsion, and bending capabilities with six degrees of freedom at each node – translations and rotations about the nodal x, y, and z axes. Each RRFC had prismatic members with symmetrical and unsymmetrical cross-sections, and transition (non-prismatic) members with symmetrical and unsymmetrical cross-sections. However, to simplify the model, it was possible to represent every structural member in the RRFCs with a prismatic, symmetrical beam element. The element, *Beam4* in ANSYS, is defined by two or three nodes, a cross-sectional area, strong and weak-axis moments of inertia, a torsional moment of inertia, a width and thickness of the member, and material properties.



$$A_{AV} = \frac{A_1 + \sqrt{A_1 A_2} + A_2}{3} \quad (5.1)$$

$$I_{AV} = \frac{I_1 + \sqrt[4]{I_1^3 I_2} + \sqrt{I_1 I_2} + \sqrt[4]{I_1 I_2^3} + I_2}{5} \quad (5.2)$$

$A_1$  = Cross – Sectional Area at End 1

$A_2$  = Cross – Sectional Area at End 2

$I_1$  = Moment of Inertia at End 1

$I_2$  = Moment of Inertia at End 2

By using section properties at the ends of each transition member, Equations (5.1) and (5.2) obtained from the ANSYS theory manuals were used to calculate an average cross-sectional area and moment of inertia values for each transition member. In order to minimize the error associated with Equations (5.1) and (5.2), ANSYS recommends that the equations be used only over regions where the taper is gradual (i.e.,  $A_2/A_1$  or  $I_2/I_1$  should not be greater than 2.0). As a result, the length of each transition member was selected so that these requirements were met; each transition member was represented by a prismatic beam element.

Prismatic, unsymmetrical members were also represented by prismatic elements; this was accomplished by adjusting each member's section height in ANSYS. To calculate strains on the top and bottom of a prismatic member, ANSYS uses half of the section height as the distance between the neutral axis and the location of the desired strain. As will be discussed in Chapter 6, most strains measured during the field load tests were at the bottom of each longitudinal member. To obtain accurate, theoretical bottom flange strains, the adjusted height of the unsymmetrical structural members was entered into ANSYS as twice the distance from its neutral axis to the bottom of the section. Through this procedure, structural members with prismatic, unsymmetrical cross-sections were represented by

prismatic, symmetrical beam elements in ANSYS. Detailed modeling of each bridge will be discussed in the following sections.

### 5.2.1 Grillage Model and Theoretical Results of the BCB

In order to obtain strains in every member of the flatcar and to accurately obtain information on load distribution in the RRFC bridges, each structural member was modeled regardless of its size. While all of the components of the primary interior girder were modeled as one beam element, all other structural members on the RRFC were individually represented. Table 5.1 lists the cross-sectional area, strong axis ( $I_x$ ), and weak axis ( $I_y$ ) inertia values used in the BCB model. Since there are three load-carrying members in the

Table 5.1. Calculated section properties of the BCB.

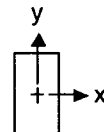
	Area (in <sup>2</sup> )	$I_x$ (in <sup>4</sup> )	$I_y$ (in <sup>4</sup> )
Exterior Girder	21.1	1,964	76
Interior Girder			
- at supports	37.0	643	1,967
- at midspan	64.4	8,322	2,619
- in transition region			
A	52.8	2,468	2,144
B	55.9	3,650	2,271
C	58.5	4,893	2,381
D	62.3	7,017	2,536
Secondary Member	2.4	3	1
Small Transverse Member	5.6	114	8
Large Transverse Member	6.8	243	9
Bolster	66.2	6,968	3,699
Concrete Beam	377.0	18,956	6,180

$I_x$  = Strong-Axis Bending

$I_y$  = Weak-Axis Bending

$E_s$  = 29,000 ksi

$E_c$  = 3,800 ksi

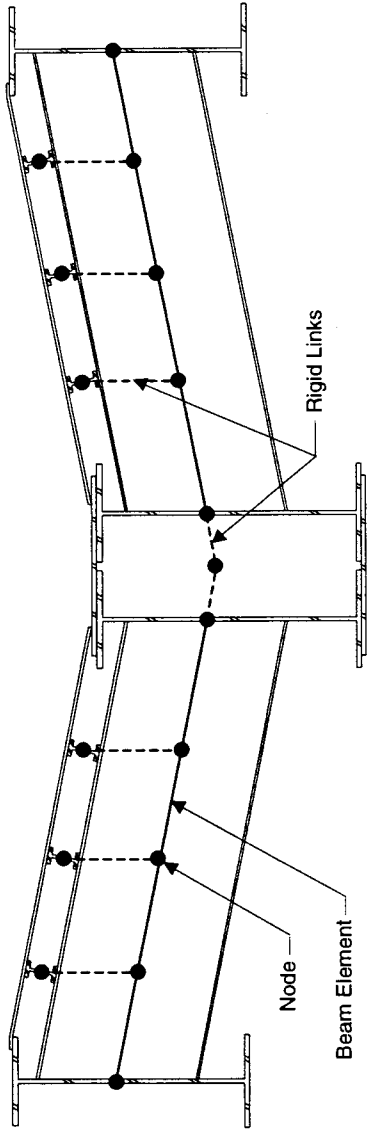


RRFC positioned at different heights within the cross-section due to the v-shape of the RRFC, it was necessary to reflect the v-shape in the model.

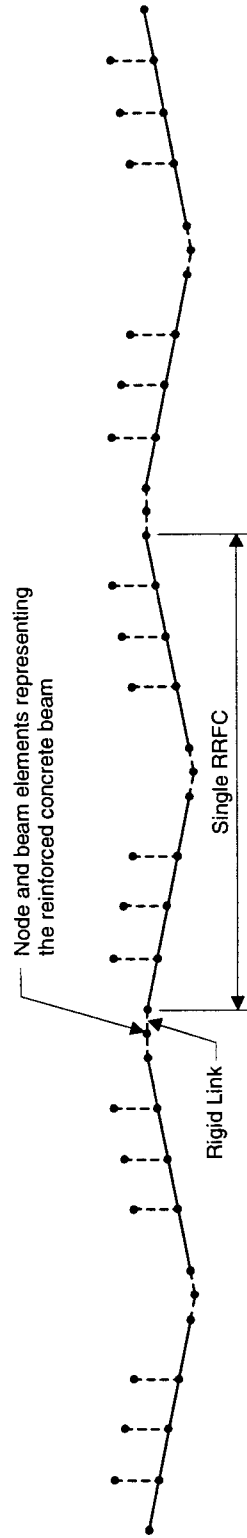
Figure 5.14a illustrates how an individual BCB RRFC was modeled. Each structural member was represented at its centroid by beam elements connected at nodes. The secondary members actually rest on the transverse members in the RRFC, and therefore, they have been connected by rigid links in the model. In addition, the transverse member lengths are modeled as the distance from the centroid of the exterior girder to the centroid of the W-shape within the interior girder. From the W-shape, the transverse member was connected by a rigid link to the element representing the interior girder. Stopping the transverse member at the W-shape rather than directly at the interior girder element avoided adding extra length to the transverse member, and therefore, extra transverse flexibility.

Figure 5.14b illustrates how three individually modeled flatcars were connected to represent the BCB. In order to connect the RRFCs, a concrete beam element was first placed between the exterior girders of adjacent flatcars. Then, the exterior girders on the flatcars were connected to the concrete beam with rigid links at each transverse member location. As noted in the assumptions, the asphalt milling driving surface was neglected in the model since shear transfer among asphalt milling particles is essentially zero.

Since flexural cracking reduces the rigidity of a concrete beam, results from the LCS flexural tests were used to determine an appropriate flexural rigidity for the concrete beam in the model. However, as will be discussed in Chapter 6, using gross section properties for the concrete beam accurately predicted flexural strains in the LCS. In addition, the LCS was subjected to a bending moment larger than the maximum moment created by two tandem trucks carrying Iowa legal loads side-by-side on the BCB. Knowing that the moment from the trucks will be distributed among seven structural members, and that the inertia of the W-shapes in the BCB are larger than those in the LCS justified using gross section properties



a. Single 56-ft RRFC



b. Three connected 56-ft RRFCs

Figure 5.14. Modeling of the BCB cross-section.

for the concrete beams in the BCB.

Figure 5.15 presents the top view of the BCB grillage model. Note the locations of the transition structural members A, B, C, and D. These members are identified in only one region; however, they exist symmetrically across the transverse centerline of the flatcar, in each flatcar (See Figure 2.3e). The lengths of these elements (average length = 26.1 in.) were selected so that  $l_2/l_1$  is less than 2.0 as earlier discussed.

Boundary conditions that were applied to the model to simulate the restraints at the supports are also illustrated in Figure 5.15. Although the flatcars are 56 ft long, the bridge was modeled as spanning 51' – 9", the distance between the abutment faces, since the interior girders were continuously supported on the abutment cap (See Figure 3.3e). While the interior girder seats were being cast on the abutments, concrete was accidentally pushed into the interior girder through openings in its bottom flange. Due to the geometry of the openings, it is assumed that girder movement toward the backwall (expansion of the girder) is possible, however movement away from the backwall is restrained. As a result, the expansion joint was modeled as a pinned support. Also, the fixity of the integral abutment is unknown. Its rotational restraint effects on the structure will be more than that of a pinned support, but less than that of a fixed support. Due to construction details, results were obtained for two sets of boundary conditions. The first set of boundary conditions assumed complete fixity at the integral abutment and pin connection at the expansion joint, while the second set of boundary conditions assumed pinned restraints at both ends of the bridge. Using results obtained from these analyses, upper and lower bounds were established for the field test results.

Since concentrated truck loads can only be applied to the model at node locations, additional nodes, not shown in Figure 5.15, were added so that the truck loads could be applied at correct locations in the grillage model. The number of concentrated forces

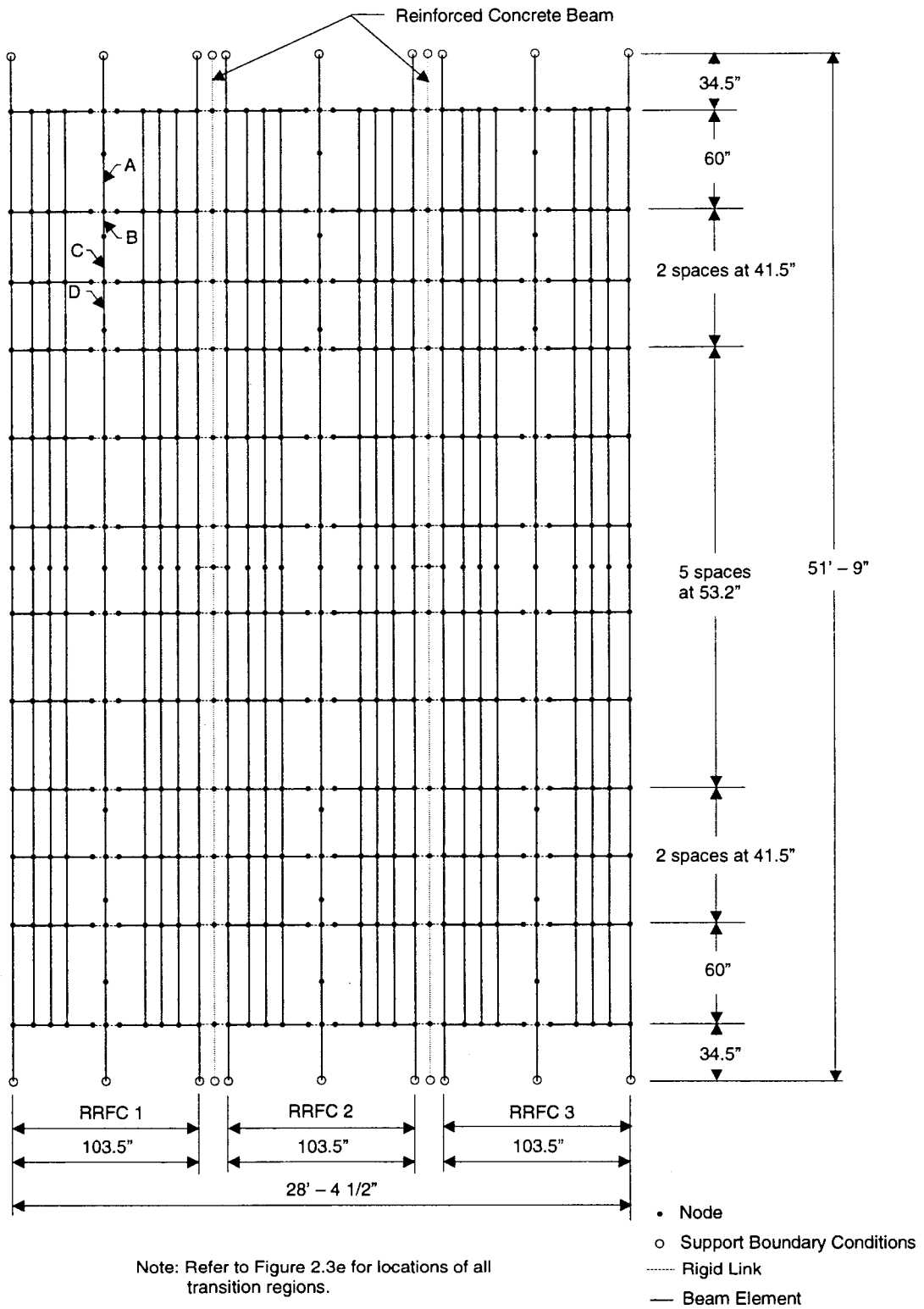


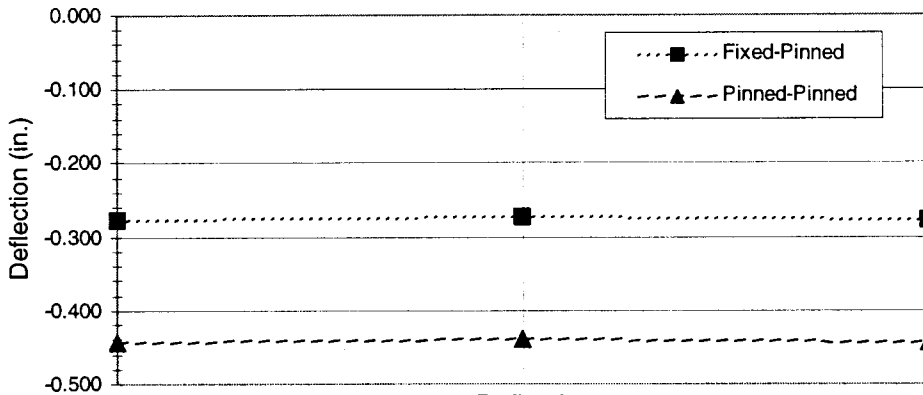
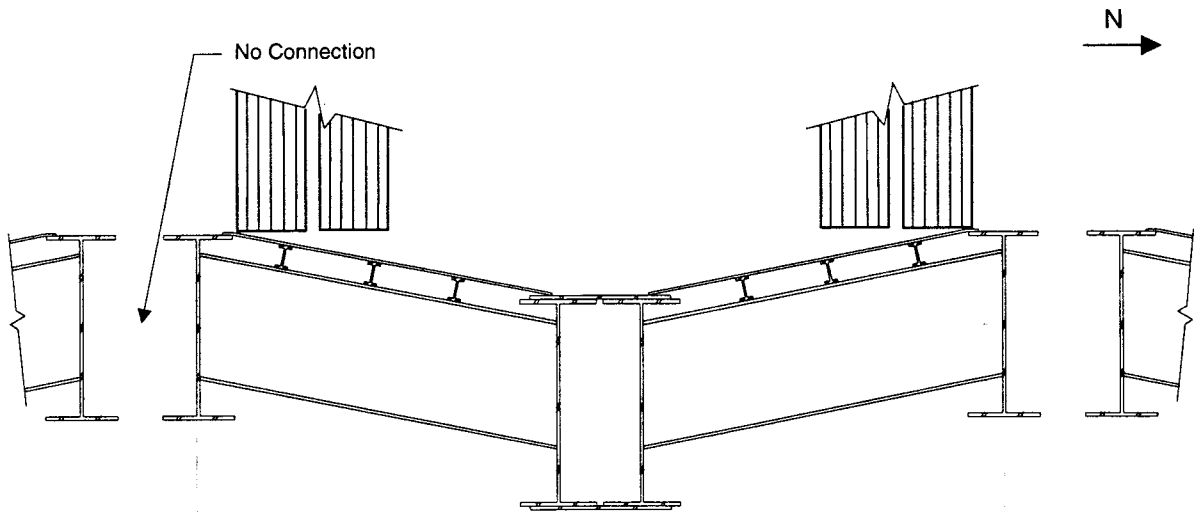
Figure 5.15. Top view of BCB ANSYS grillage model.

representing each wheel load was dependent upon the field test. For LT1, only the edges of the tires were in contact with the steel decking, and therefore, only a few nodes per tire received loads. However, after the driving surface was added in LT2, truck loads were distributed to more nodes since the area of contact between the tire and driving surface increased.

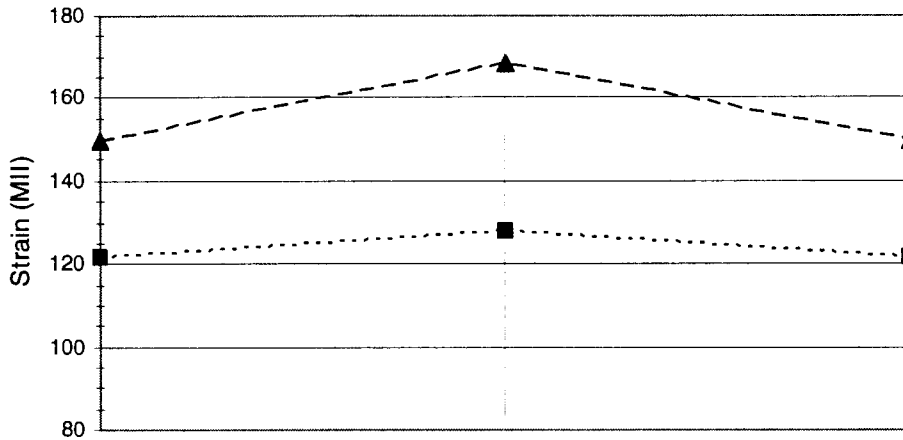
Maximum theoretical midspan deflections and strains for Test 1 in BCB LT1 are presented in Figure 5.16. As can be seen, the model predicts that all three members will deflect approximately the same, but the interior girders will experience larger strains. Maximum theoretical midspan deflections and strains for Test 1 in BCB LT2 are presented in Figure 5.17. Examination of Figure 5.17 reveals symmetrical behavior of the RRFC bridge with girders in the middle RRFC experiencing the largest strains and deflections, which is expected. In addition, adjacent exterior girders in the longitudinal flatcar connections experience approximately the same deflections and strains; strain discrepancies between the girders are explained by evaluating the rotation of the connections. For the deflected shape shown in Figure 5.17a, the strains resulting from connection rotations decrease the tension flexural strains in the exterior girders in the middle RRFC, but increase the tension flexural strains in the girders in the exterior RRFCs. Thus, the rigid links previously described are accurately creating a composite connection (to represent longitudinal flatcar connections). Finally, Figure 5.17 predicts good load distribution to the side RRFCs. Theoretical results for the remaining tests on the BCB will be presented along with the field load testing results in Chapter 6.

### *5.2.2 Grillage Model and Theoretical Results of the WCB*

Procedures similar to those of the BCB were used to model the WCB. All structural members were modeled with prismatic, symmetrical beam elements, and their section properties are listed in Table 5.2. Moreover, as shown in Figure 5.18a, the transverse



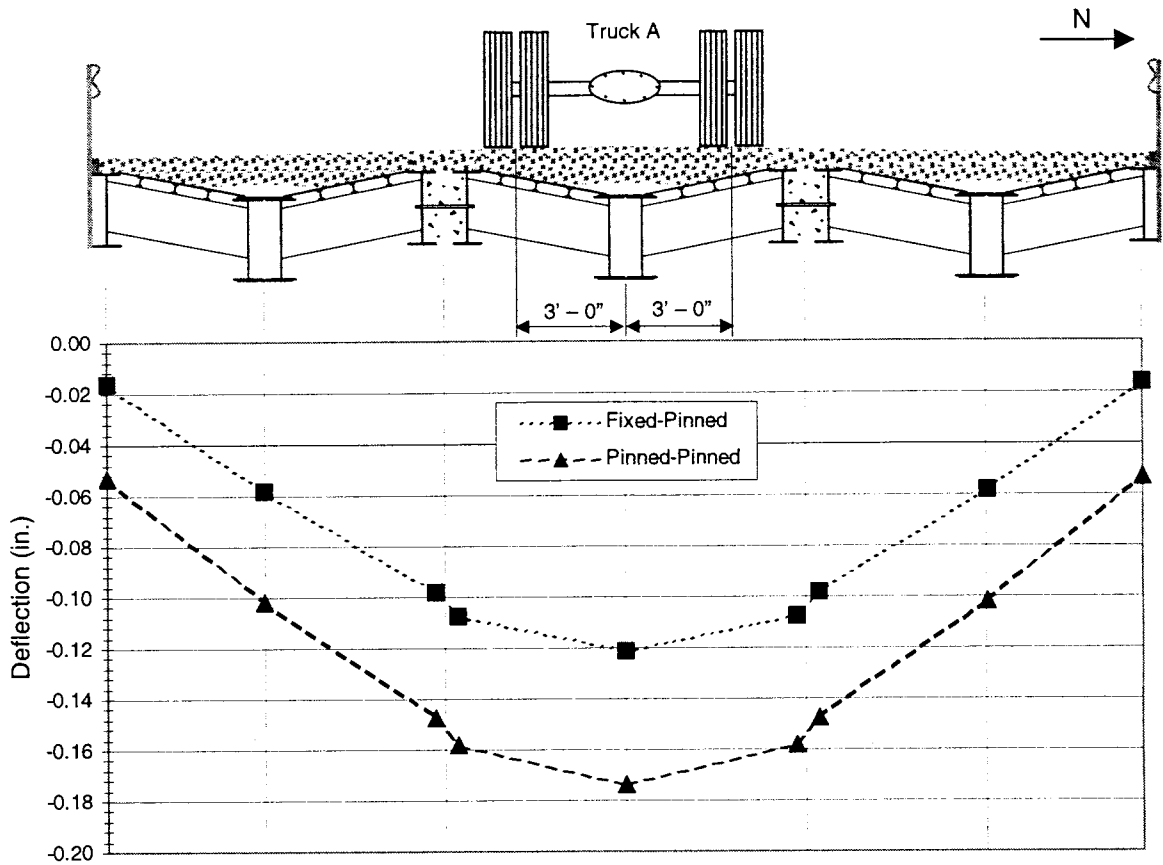
a. Deflections



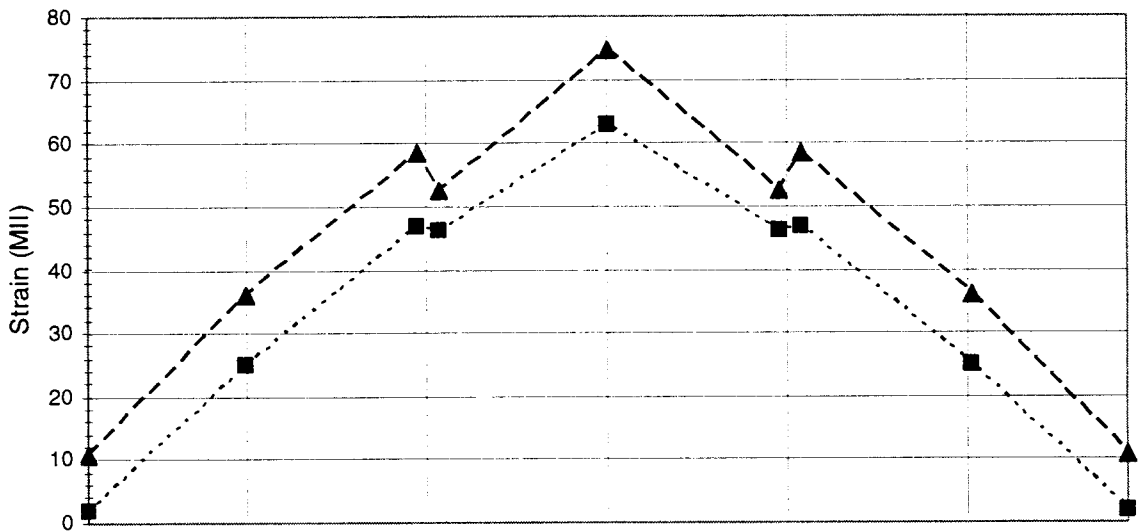
b. Member bottom flange strains

Figure 5.16. Analytical upper and lower bounds for Test 1 in BCB LT1.





a. Deflections



b. Member bottom flange strains

Figure 5.17. Analytical upper and lower bounds for Test 1 in BCB LT2.

members were modeled exactly like those in the BCB. Once again, the exterior members in each flatcar connection were attached to the concrete beam by rigid links. Since the

Table 5.2. Calculated section properties of the WCB.

	Area (in <sup>2</sup> )	I <sub>x</sub> (in <sup>4</sup> )	I <sub>y</sub> (in <sup>4</sup> )
Exterior Girder			
- Whole	10.8	346	12
- Trimmed	5.2	25	6
Interior Girder			
- at supports	43.9	1,503	2,699
- at midspan	56.6	8,999	4,183
- in transition regions			
A	56.5	2,515	3,710
B	58.6	3,647	3,891
C	61.5	5,559	4,138
D	64.3	7,916	4,386
E	67.2	10,740	4,634
Secondary Member	6.5	55	18
U-shaped Transverse Member	4.0	4	56
S-shaped Transverse Member	4.3	15	2
L-shaped Transverse Member			
F	3.4	27	1
G	5.2	93	3
H	6.9	220	6
I	8.9	490	10
Bolster	19.5	193	831
Concrete Beam	42.5	131	174
Timber Planks			
- Rigid	42.0	300,000	504
- Actual Property	42.0	4,980	504

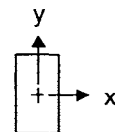
I<sub>x</sub> = Strong-Axis Bending

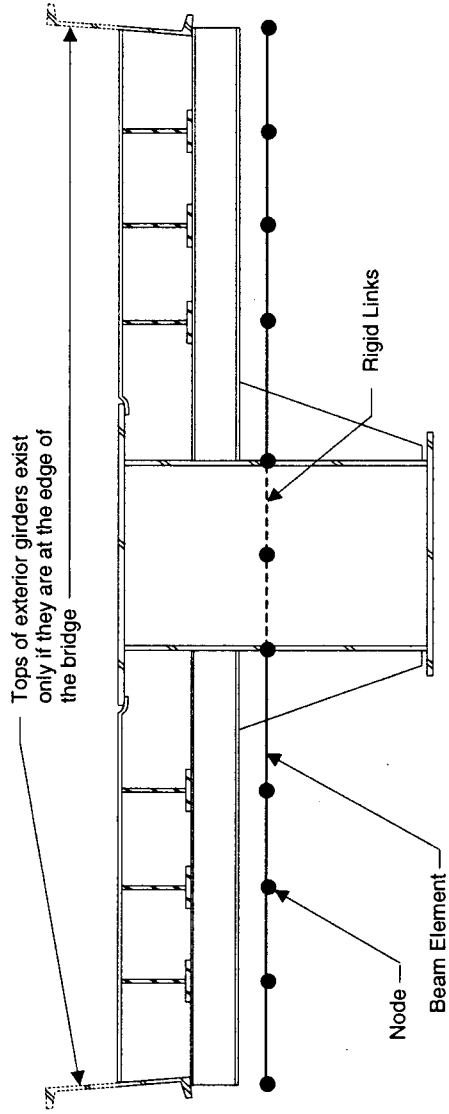
I<sub>y</sub> = Weak-Axis Bending

E<sub>S</sub> = 29,000 ksi

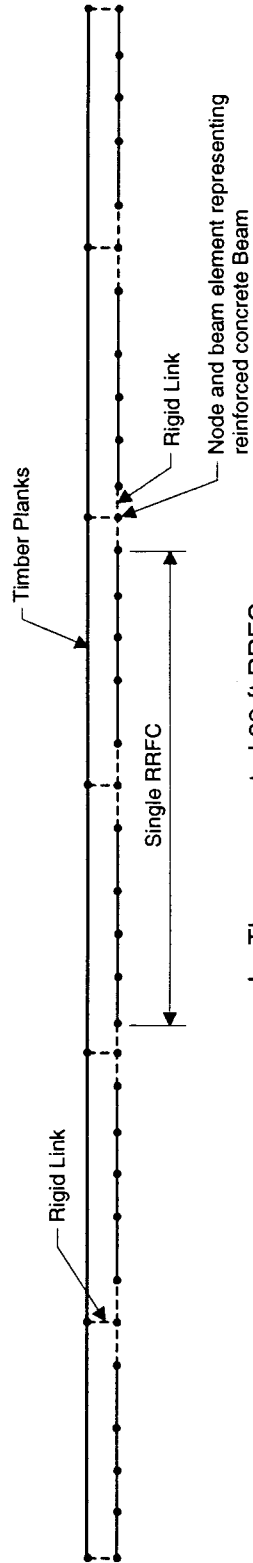
E<sub>C</sub> = 3,800 ksi

E<sub>T</sub> = 1800 ksi





a. Single 89-ft RRFC



b. Three connected 89-ft RRFCs

Figure 5.18. Modeling of the WCB cross-section.

uncracked beam has a very small flexural rigidity and does not have the ability to resist significant loads, using cracked properties for the reinforced concrete beam would have minimal benefits. Therefore, gross section properties for the reinforced concrete beam were used in this model also. Since the 1/2 in. steel plates used in the longitudinal flatcar connections were not continuous, they were neglected in the model.

The timber planks used for load distribution are also illustrated in Figure 5.18b. In the model, truck loads were applied to the timber planks at nodes, and the timber planks distributed the loads to the RRFCs. As stated in the assumptions, since the timber planks are primarily supported by the major longitudinal members of the flatcars, rigid links transferring only vertical and horizontal forces were used to connect the timber planks to the major longitudinal members. It should be noted, however, that the timber planks were only modeled at the sections of the bridge where truck loads were applied. This is justified because the timber planks function primarily to distribute concentrated wheel loads transversely across the bridge. Once these loads have been distributed by the planks on a cross-section, the longitudinal flexural strains and vertical deflections on the longitudinal girders at that section are primarily dependent upon the flexural rigidities of the longitudinal girders. However, if the model had been subjected to a longitudinal distributed load such as AASHTO lane loading, then distribution would be required at every cross-section of the bridge, and thus, all of the timber planks would have required modeling. Since the WCB was only subjected to concentrated wheel loads, thus as previously noted, only the timber planks supporting concentrated wheel loads needed to be modeled.

Figure 5.19 presents a top view of the WCB grillage model. Note the locations of the transition members (A, B, C, D, E, F, G, H, and I) in one region. See Figure 2.5j for the locations of all transition members. The lengths of these elements were selected so that  $l_2/l_1$  is less than 2.0 as earlier discussed, and therefore, elements A, B, C, D, and E averaged

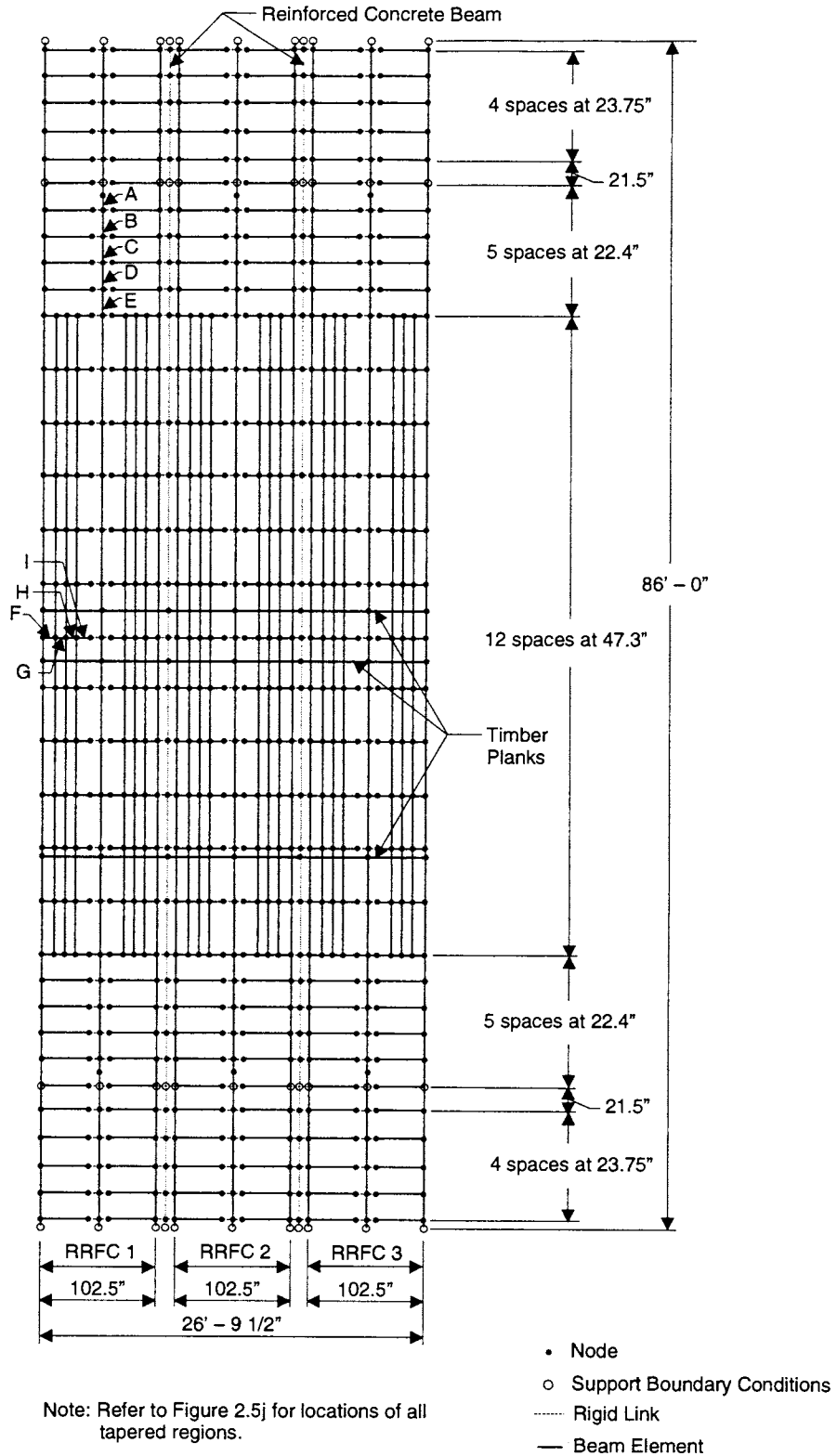


Figure 5.19. Top view of WBC ANSYS grillage model.

20.0 in. in length, and elements F, G, H, and I averaged 10.4 in. in length. Also presented in Figure 5.19 are the locations of the boundary conditions used in the model. Supports at the north abutment and on the piers were modeled as true rollers, but the fixity at the south abutment (where the flatcar was welded directly to the abutment) is unknown. Similar to the integral abutment on the BCB, this support will behave as a rotational spring with an unknown stiffness. Therefore, two sets of boundary conditions were once again applied to the model to represent upper and lower bounds for the deflections and strains in the WCB. The first set of boundary conditions applies complete fixity at the south abutment with rollers at the piers and north abutment; the second set of boundary conditions utilizes a pin at the south abutment with rollers at the piers and north abutment.

In addition to the previously noted boundary condition uncertainty, the flexural rigidity of the timber planks is unknown. In the RRFC bridge, the steel deck supports the timber planks. Since the steel deck was not included in the grillage model, the timber planks in the model behave as if they are only supported by longitudinal members. As a result, using the true section properties of the timber planks would result in planks having more flexibility than they actually have. On the other hand, representing the timbers as rigid elements creates a more rigid section than actually exists.

For a transversely centered truck on the WCB, Figure 5.20 illustrates the relationship between the timber plank inertia and interior girder displacements on the center and side RRFCs. This plot was created by varying the timber plank inertia in the model for the given loading condition, and then plotting the girder displacements versus timber plank inertia from each analysis. Note that as the timber plank inertia is increased, deflection is less for the interior girder in the middle flatcar while the deflection increases for the interior girder in the side flatcars. Since girder displacement is directly related to loading on the member, Figure 5.20 essentially displays the relationship between timber plank inertia and load distribution

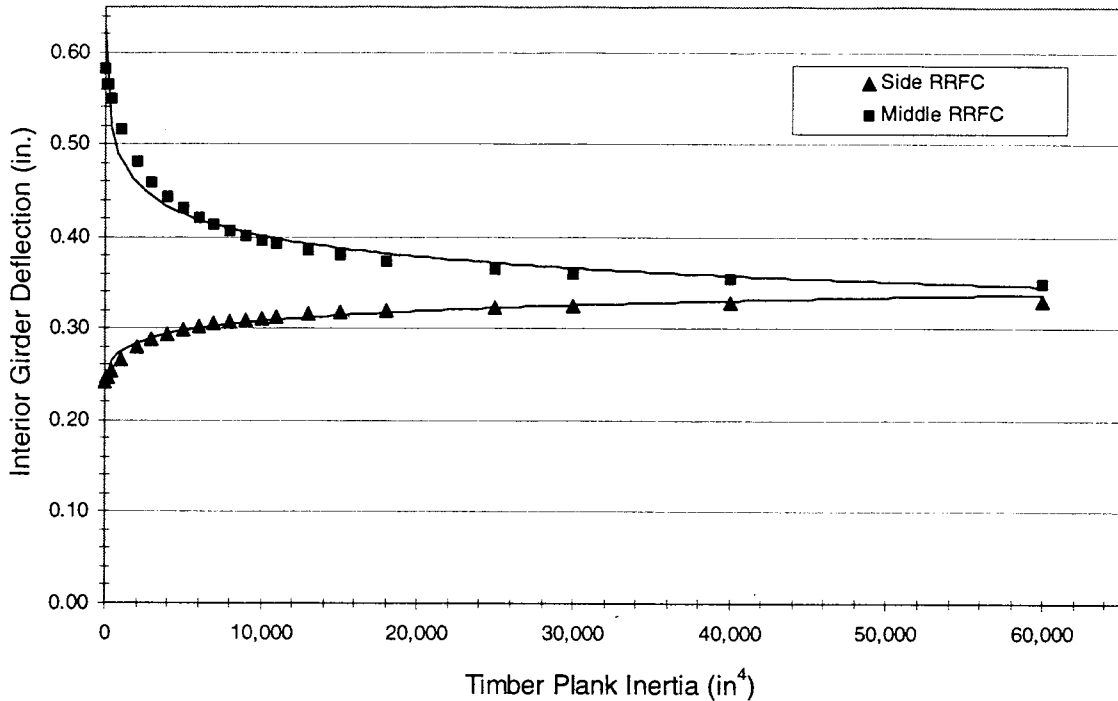
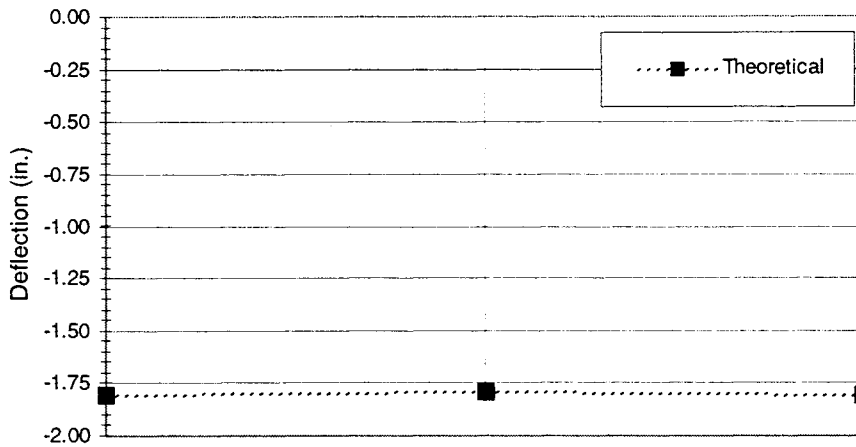
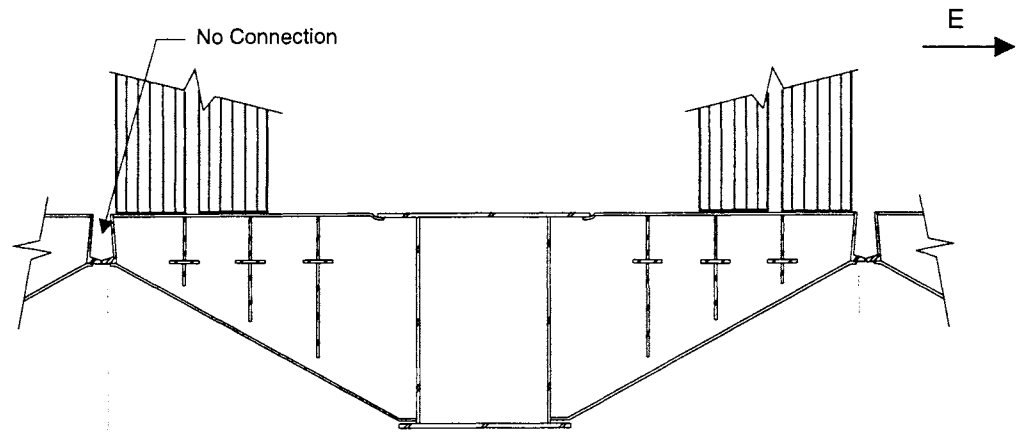


Figure 5.20. Relationship between timber plank inertia and interior girder deflections.

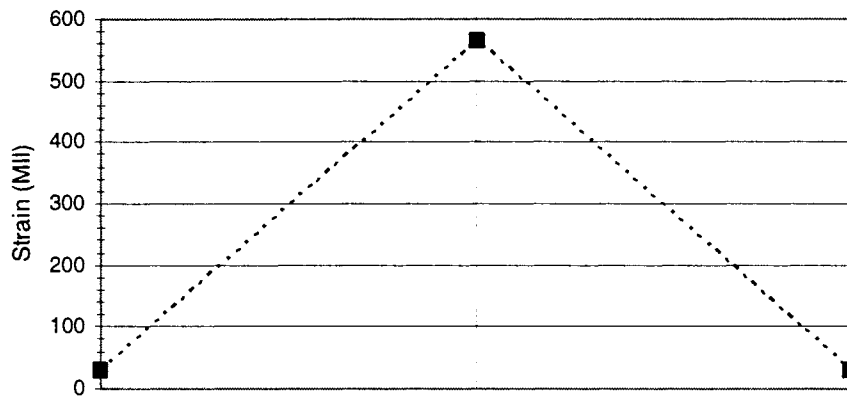
to the three interior girders.

Including the timber plank variable flexural rigidity with the two sets of boundary conditions previously described, upper and lower theoretical bounds were established by performing the analysis with the most flexible bridge possible, and then again with the most rigid bridge possible. The most flexible bridge was represented by a model with a pinned south abutment and timbers with their actual properties; the most rigid model was created with a fixed south abutment and rigid timber planks. The results from the field load tests should be within the bounded range of the analyses.

Theoretical results for the tests of LT1 before the abutment and pier restraints, and before longitudinal flatcar connections were constructed are presented in Figure 5.21. Since this situation clearly reflects RRFCs simply supported at their bolsters, uncertainty with boundary conditions and timber planks did not exist. Therefore, Figure 5.21 does not have



a. Deflections



b. Member bottom flange strains

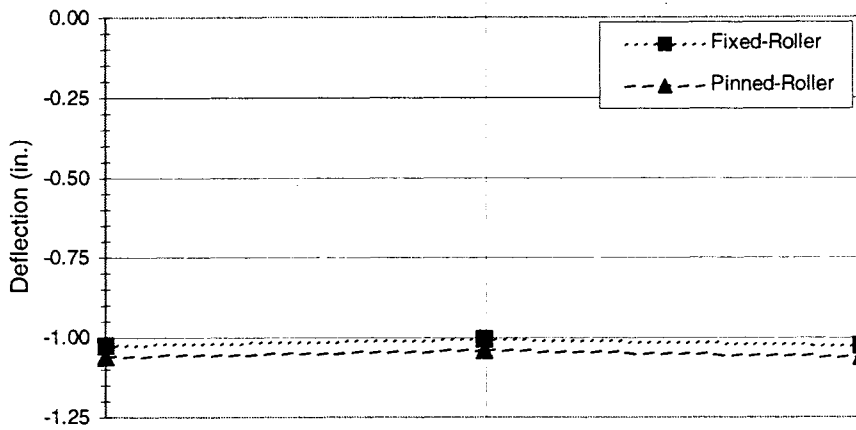
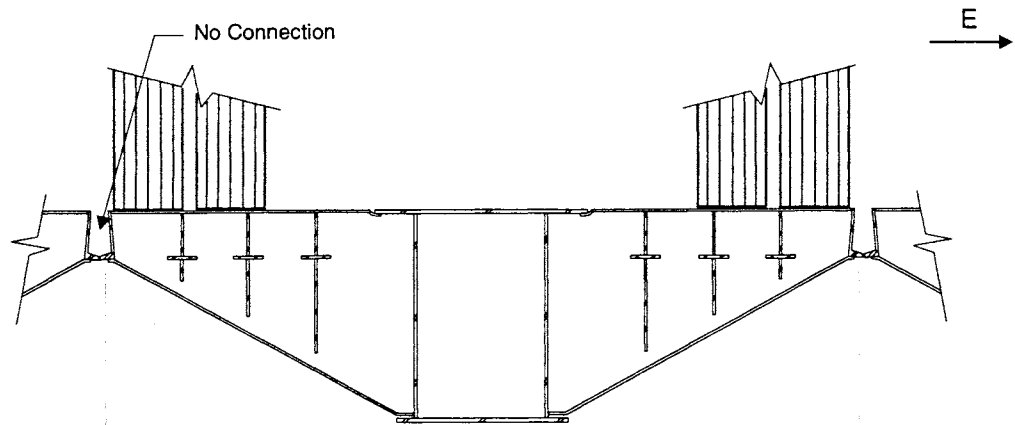
Figure 5.21. Analytical upper and lower bounds for WCB LT1 without abutment restraints.



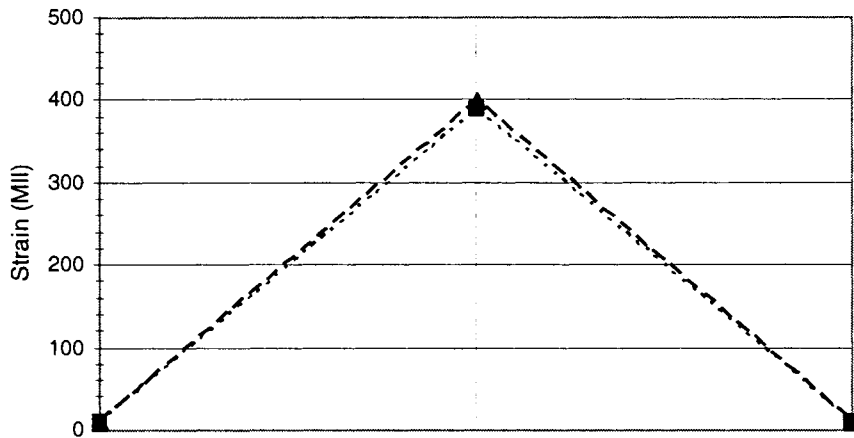
upper and lower bounds, but rather, just the expected theoretical test results. As can be seen in Figure 5.21, the model predicts that the trimmed exterior girders will experience almost zero strain, indicating that nearly all of the truck load is being supported by the interior girder; this reinforces earlier predictions that the 89-ft RRFCs with trimmed exterior girders will behave as flatcars with non-redundant cross-sections (i.e. one longitudinal load path). After the addition of abutment restraints in LT1, boundary condition uncertainty was present. Therefore, Figure 5.22 presents upper and lower bounds for maximum midspan deflections and strains for LT1 after the addition of abutment restraints, but before the installation of longitudinal connections and timber planks. As can be seen, the interior girder strains in Figure 5.22 are still much larger than those in Figure 5.21. However, the models predict that strains and deflections in the interior girder will reduce by approximately 30% by adding abutment restraints. Finally, upper and lower theoretical bounds for maximum midspan strains and deflections in Test 1 in LT2 with the finished bridge are presented in Figure 5.23. As can be seen in Figure 5.23, the girders in the west flatcar experience the largest strains and deflections, but some of the load is predicted to be distributed to the middle and side flatcars via the timber planks and flatcar connection. Once again, deflection and strain results for adjacent exterior girders in longitudinal flatcar connections are nearly identical, thus, indicating that the rigid links accurately represent composite connection between the adjacent exterior girders. Theoretical results for the remaining tests on the WCB will be presented along with the field test results in Chapter 6.

### **5.3 Dead Load Analysis of the RRFC Demonstration Bridges**

Dead load distribution to the primary girders of each demonstration bridge was determined using simplified hand calculations rather than a grillage analysis. As will be discussed in the sections that follow, the bridges were analyzed with span lengths and support conditions that produced maximum, conservative dead load stresses in their

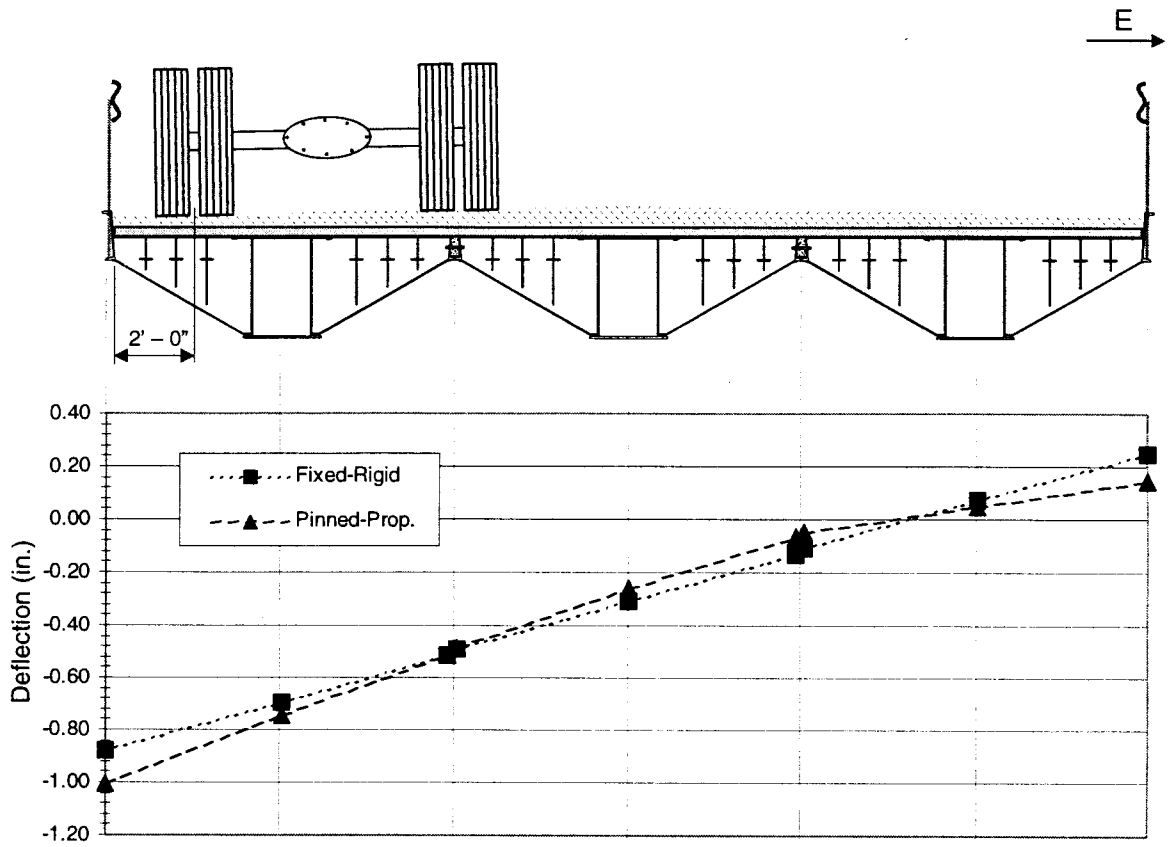


a. Deflections

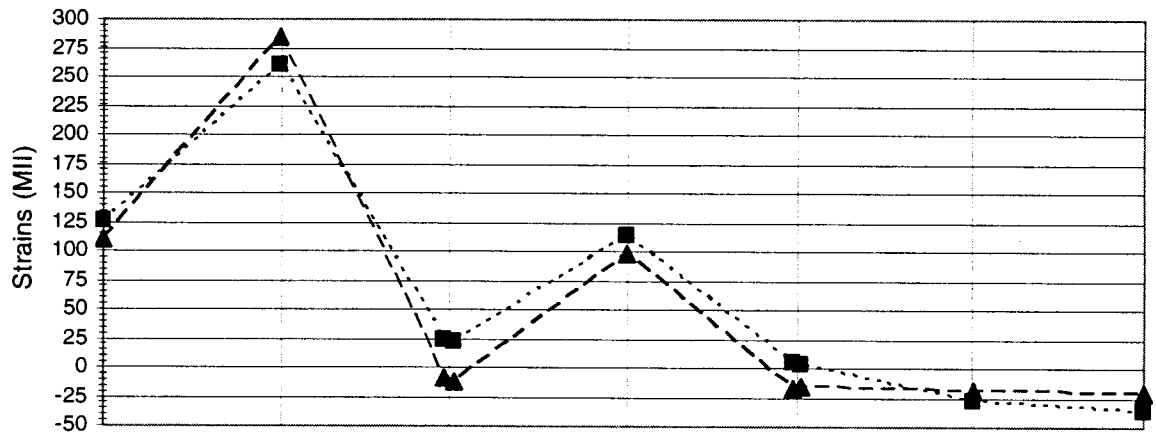


b. Member bottom flange strains

Figure 5.22. Analytical upper and lower bounds for WCB LT1 with abutment restraints.



a. Deflections



b. Member bottom strains

Figure 5.23. Analytical upper and lower bounds for Test 1 in WCB LT2.

girders. The dead load stresses presented are combined with the measured live load stresses obtained from the field tests (presented in Chapter 6) to determine the maximum, critical stresses in each bridge.

### *5.3.1 BCB Dead Load Analysis*

To analyze the BCB primary girders for dead load stresses (and strains), assumptions were made to simplify the analysis. As previously stated, the grillage model assumed that the longitudinal girders in the BCB were simply supported over their clear span (51 ft – 9 in.). However, dead load stresses were calculated using the 56-ft length of the flatcar; using the longer span produced conservative dead load stresses. In addition, each girder was assumed to support its own self-weight and the self-weight of the steel deck, transverse members, and secondary members within its contributory width. Since shoring was used during construction of the longitudinal flatcar connections, the reinforced concrete beam was assumed to carry its own self-weight with no distribution to the exterior girders in the connection. Material weights were assumed to be 490 lb/ft<sup>3</sup> for steel and 150 lb/ft<sup>3</sup> for reinforced concrete.

The total weight of the pea gravel and asphalt milling driving surface was assumed to be uniformly distributed over the plan view area of the bridge. This method of analysis follows conventional methods of bridge design; the connected flatcars were assumed to form a rigid cross-section, and therefore, any added dead load is assumed to be uniform on the bridge. The total weight of the pea rock and asphalt millings was known from truck weight tickets, and thus the gravel and driving surface weights were calculated to be 120 lb/ft<sup>2</sup>. Using these assumptions and girder section properties (See Table 5.1), dead load stresses in the interior girders, exterior girders in longitudinal flatcar connections, and exterior girders at the edges of the BCB were calculated to be 5.5 ksi, 9.6 ksi, and 8.9 ksi, respectively.

### 5.3.2 WCB Dead Load Analysis

Due to the geometry of the 89-ft flatcars and the support conditions of the WCB, the assumptions for the dead load analysis in the WCB were slightly different from those used in the BCB analysis. To simplify the dead load analysis and to produce conservative dead load stresses, the abutment restraints were ignored, and the statically determinate WCB was analyzed as being simply supported at the piers. Again, each girder was assumed to support its own self-weight. However, since exterior girders in longitudinal flatcar connections were trimmed, they were assumed to be incapable of resisting dead load from the decking, transverse members, secondary members, concrete in the longitudinal flatcar connections, and the transverse timber planks. This assumption was developed from the results of the LT1 grillage analysis of the 89-ft RRFC with trimmed, exterior girders; for loading on the main span of this flatcar, 99.9% of the bending moment at each section in the model was resisted by the interior girder.

As a result, the entire dead load from the steel decking, transverse members, secondary members, longitudinal flatcar connections, timber planks, and gravel driving surface was assumed to be supported by the interior girders in the flatcars of the WCB. In addition to the material weights described in Section 5.3.1, a weight of  $36.3 \text{ lb/ft}^3$  was assumed for the timber planks [8]. Assuming  $110 \text{ lb/ft}^3$  for the gravel, the driving surface was calculated to be  $47.25 \text{ lb/ft}^2$ . Using these assumptions and girder section properties (See Table 5.2), dead load stresses at midspan of the main span in the interior girders, exterior girders in longitudinal flatcar connections, and exterior girders at the edges of the WCB were calculated to be 9.7 ksi, 9.1 ksi, and 4.6 ksi, respectively.

## 6. RESULTS

### 6.1 LCS Test Results

As described in Chapter 4, the LCS was tested in both torsion and flexure to determine its adequacy in RRFC bridges. The results for each LCS test are presented in the sections that follow.

#### 6.1.1 LCS Service Load Torsion Test

In each service load torsion test, the LCS was subjected to 360 in-k torsional moment, and the maximum measured rotation at the lever arm end was 0.73 degrees. Due to the small rotation in the LCS, the warping and flexure strains in the W-shapes were small. The maximum recorded flange strain was approximately 50 MII (1.5 ksi), and 94 percent of the recorded strains were less than 30 MII (0.9 ksi). The maximum web principle strains were calculated to be 58 MII (1.7 ksi) from the recorded strains in the 45-degree rosettes. In addition, when the threaded rod spacing was changed to investigate its contribution to LCS behavior, test results revealed that the maximum measured threaded rod strain was 27 MII (0.78 ksi) with the transverse threaded rod spaced on 6-ft centers. However, the threaded rod strain results among all of the tests were scattered (6 MII (0.17 ksi) to 27 MII (0.78 ksi)) and did not reveal a relationship between transverse rod spacing and rod strain.

In any laboratory test in which low strains are measured, the combination of data acquisition “noise” error and strain gage placement error will constitute as a rather large percentage of the output strain. For example, the stability of the strain gages prior to testing revealed that each gage fluctuates approximately 1 MII (0.03 ksi) when no loading is present. Therefore, if only 30 MII (0.9 ksi) is measured in a strain gage during the test, the 1 MII fluctuation in the gage corresponds to approximately three percent error. In addition, misalignment of the gage will introduce error into the strain reading depending on the magnitude of the misalignment. Other areas for potential error include lead wire resistance

effects and transverse sensitivity of the uniaxial strain gages. The data acquisition system used for this test automatically corrects for the lead wire effects. The strain gages located on the W-shape flanges were placed nearly at the tips and were essentially in a uniaxial state of strain, and thus, there was essentially no error due to transverse sensitivity of the strain gage. However, the uniaxial strain gages placed on the webs of the W-shapes were not in a state of uniaxial strain when the LCS was subjected to torsional moment, and thus, there was some error due to transverse sensitivity. As previously stated, the combination of these small errors becomes a significant percentage in the case of small measured strains. As a result, the small strain results obtained from the LCS Service Load Torsion Test were not considered to be accurate enough for comparison with theoretical results. However, it was concluded from these small measured strains that the LCS was structurally adequate to handle expected BCB service torsion loads.

#### *6.1.2 LCS Flexure Test*

The maximum recorded strains in the LCS Flexure Test are presented in Figure 6.1 along with theoretical results; deflection measurements demonstrated the same basic relationship, and therefore they are not presented. For this test, the loads at locations  $P_1$  and  $P_2$  as illustrated in Figure 5.12 were 95 and 94 kips, respectively, and the maximum bending moment in the LCS was calculated to be 2,298 in-k. By observing the good agreement between the theoretical and experimental results presented in Figure 6.1, it is evident that the compatibility analysis that was performed with gross section properties assumed for the concrete beam accurately predicted the LCS flexural behavior.

#### *6.1.3 LCS Ultimate Load Torsion Test*

A graph of the torsional moment versus the measured relative rotation between the two ends of the LCS for the Ultimate Load Torsion Test is presented in Figure 6.2. The straight lines between the data points are only included to illustrate the overall behavior and

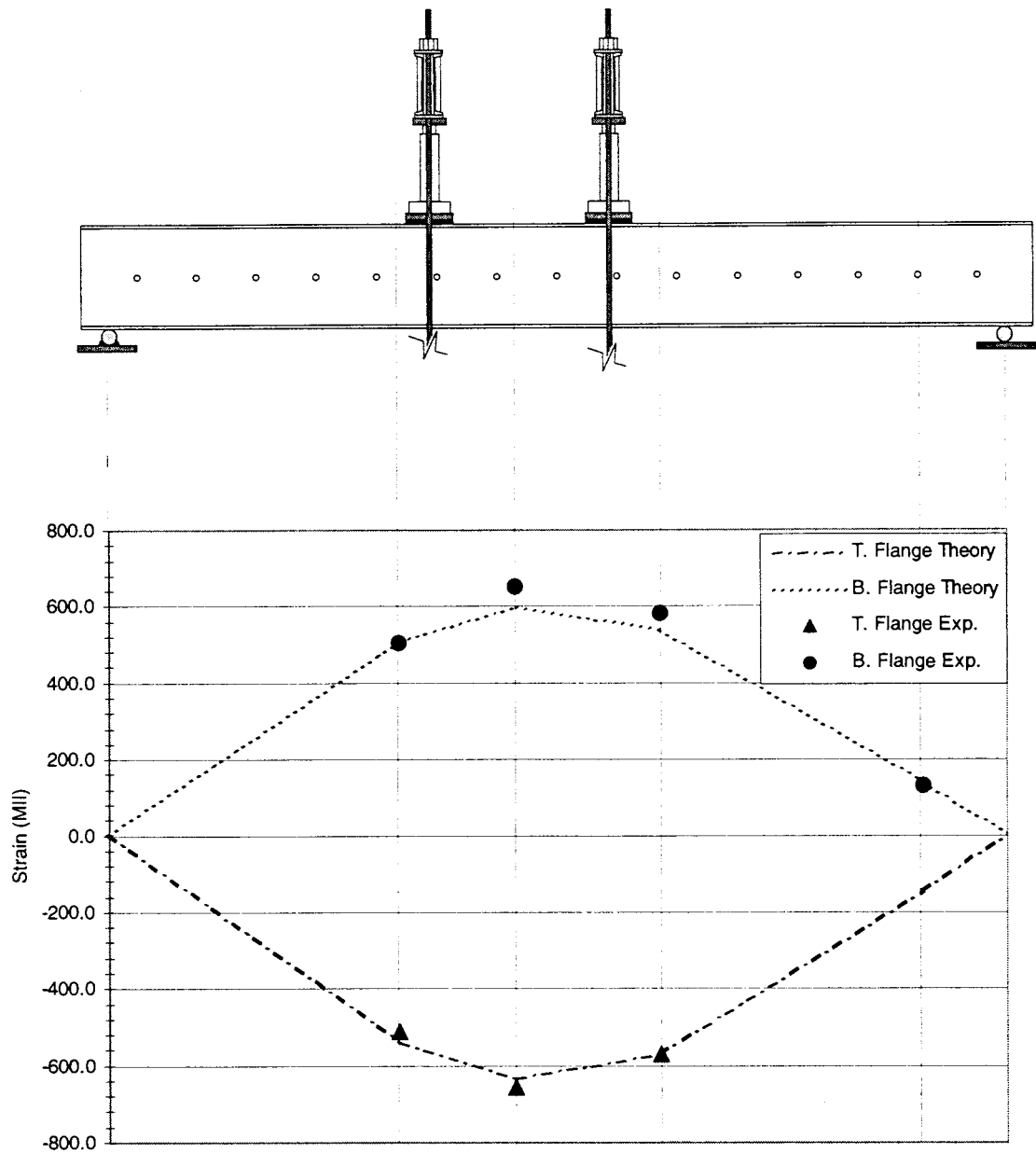


Figure 6.1. LCS Service Flexure Test strain results.



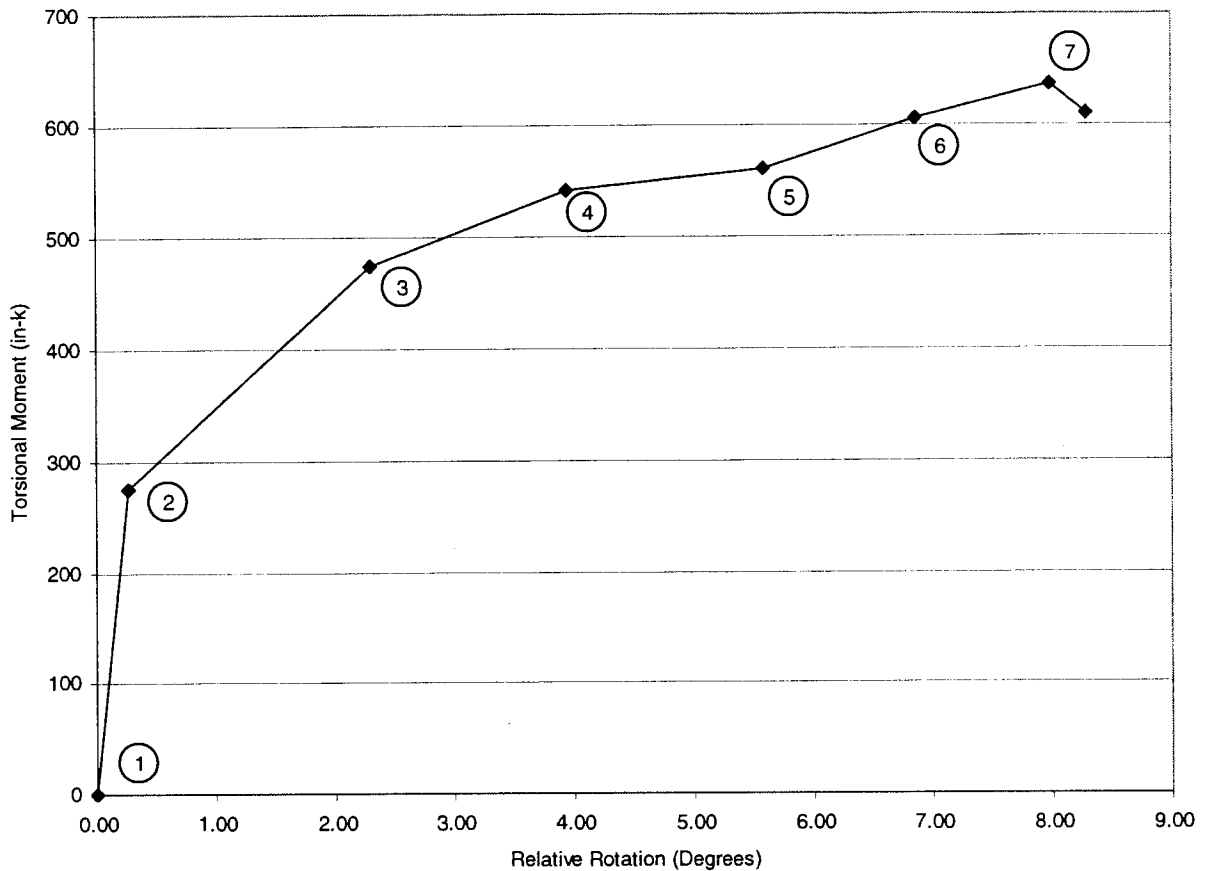


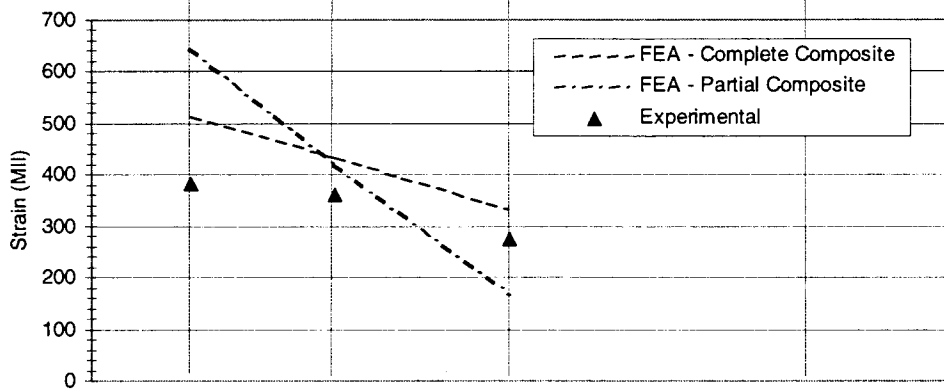
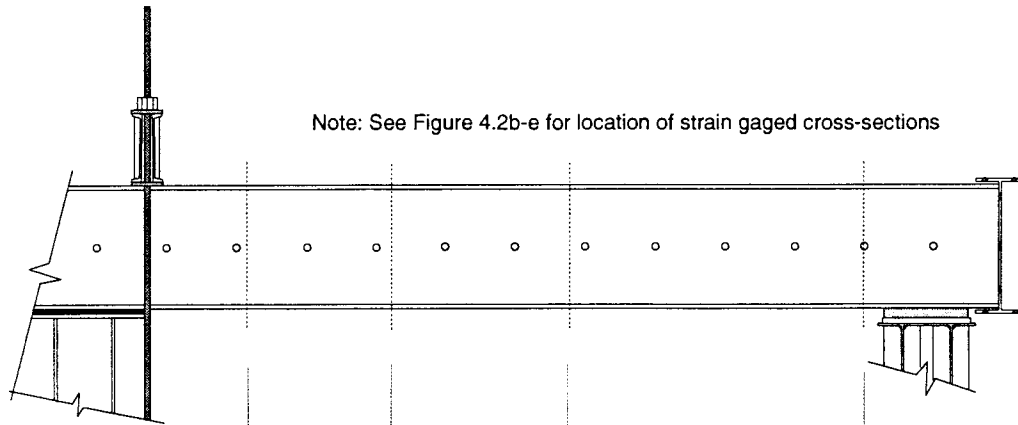
Figure 6.2. LCS torsional moments and relative rotations in the Ultimate Load Torsion Test.

do not to represent the behavior of the LCS between data points. Since three consecutive data points do not form a straight line, it is evident that a nonlinear relationship existed between the torsional moment and LCS rotation. In addition, examining Figure 6.2 reveals that as the rotation of the LCS increases, the slopes of the lines between data points decrease, indicating a decrease in the LCS torsional strength. Moreover, the line between data points 4 and 5 is essentially horizontal, which indicates that a failure mechanism developed. Therefore, Figure 6.2 indicates that yielding in the W-shapes occurred as early as data point 4. The increase in LCS strength between data points 5 and 7 indicates strain hardening in the failure mechanism region.

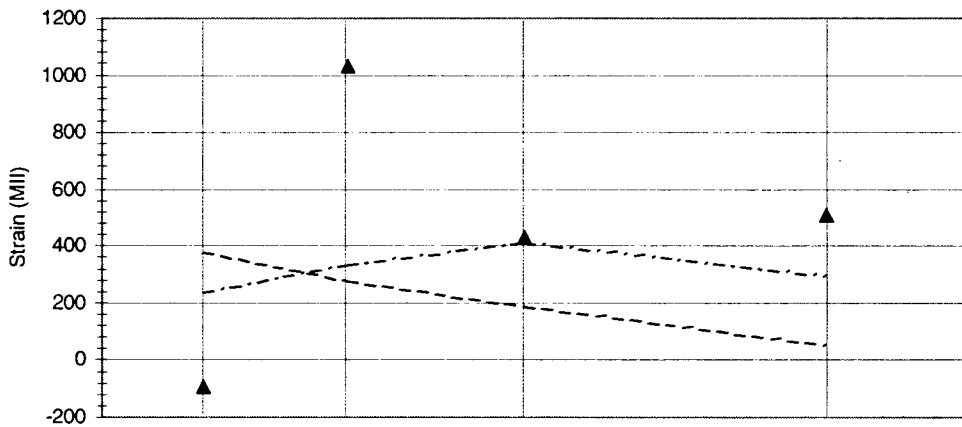
To determine the location of the failure mechanism, strain measurements were reviewed, however all recordings indicated that yielding had not occurred in the flanges. In addition, when the measured flange strains were compared with theoretical strains obtained from the conventional analysis presented in Chapter 5, most experimental strains were not within the theoretical range, and thus, the results are not presented. However, theoretical strains from the FEA partial composite model were compared with measured strains from the laboratory test; these results are presented in Figure 6.3. However, as can be seen, a significant difference still exists between theoretical and experimental results.

The error between theoretical and experimental results may be the result of several factors. As discussed in Chapter 5, the partially composite FEA model assumed equal out-of-plane displacements at each transverse threaded rod. This assumption, however, was proven to be incorrect as the strains in the gaged transverse threaded rods differed by factors of 8.6 in the Service Load Torsion Test and 15.3 in the Ultimate Load Torsion Test. This suggests that in order to accurately predict flange strains when the LCS is subjected to a torsional moment, the exact force in each threaded rod is required in the model. In addition to transverse threaded rod effects, concrete cracking in the LCS causes longitudinal discontinuities in torsional strength; this effect was not addressed in either model. The combination of these two effects are assumed to be the cause of the significant difference between the theoretical and experimental strain results presented in Figure 6.3.

Examination of the test results did reveal, however, yielding at the locations of the rosette strain gages in the web of the left W-shaped section presented in Figure 4.2b (also see Figure 4.5). In fact, principle strains at all four rosette locations on the LCS corresponded to stresses in the range of 26 to 36 ksi. The high stresses in these rosette strain gage regions confirm the existence of stress concentrations around the transverse threaded rods that were predicted by the FEA.



a. Top flange



b. Bottom flange

Figure 6.3. Comparison of Ultimate Load Torsion Test analytical and experimental results.

#### *6.1.4 Summary of LCS Performance*

In the Service Load Torsion Test, it was proven that under small rotations, the LCS experienced small stresses in the flanges and webs of the W-shape because complete composite behavior was present. Because of this behavior, the presence of the transverse threaded rods did not cause stress concentrations in the webs of the W-shapes. As a result, it was determined that stresses that develop from service torsion loads are minimal and are not of concern.

In the Service Load Flexure Test, it was determined that load distribution, and thus flexural stresses in the W-shape flanges, are highly predictable through compatibility relationships between the W-shapes and reinforced concrete beam. As a result, it was proven that longitudinal flatcar connections similar to the LCS that was tested are adequate in flexure.

For the Ultimate Load Torsion Test, it was proven that the partial composite FEA analysis was more accurate than the conventional methods of analysis for predicting LCS torsional behavior. As a result, it can be concluded that web and flange stresses in the W-shapes depend on the forces that develop in the transverse threaded rods. Additional FEA analyses could have been used to examine the effects of variable transverse threaded rod forces and concrete cracking on flange strains, however, such analyses were beyond the scope of this investigation.

The objective of the testing in the LCS was to determine its adequacy for use in RRFC bridges. In RRFC bridges, the connection will experience axial rotations similar to those induced in the Service Load Torsion Test and significantly smaller than those in the Ultimate Load Torsion Test. For this situation, stresses and strains in the W-shapes have been proven to be small (stresses less than 1.5 ksi). However, even under large rotations

and web yielding (i.e. severe overload conditions), the LCS did not collapse and demonstrated its adequacy for use in RRFC bridges.

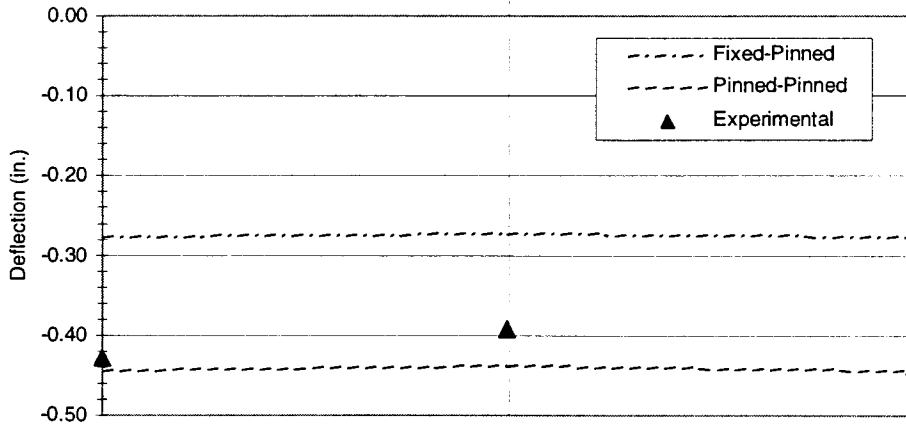
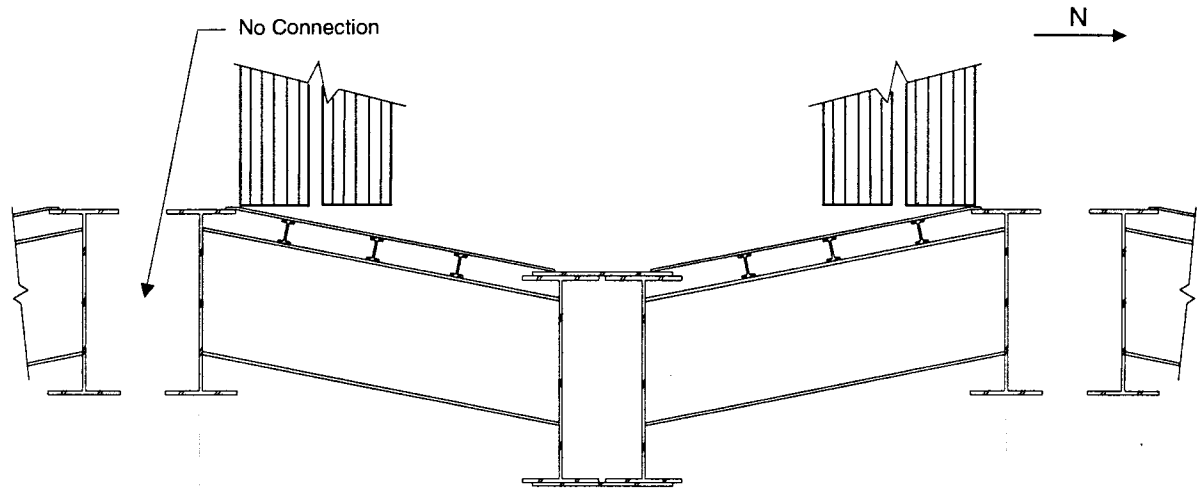
## **6.2 Field Load Testing of the RRFC Demonstration Bridges**

As discussed in Chapter 4, LT1 tests were performed with no longitudinal connection between the flatcars, and LT2 and LT3 tests were performed after the addition of longitudinal flatcar connections. During field load testing of each bridge, LT1 deflections and strains were recorded during static truck loading; results in LT2 and LT3 were recorded while the tandem truck slowly travelled across the bridge. Through a feature in the data acquisition system, it was possible to obtain strain and deflection results at a specific time that corresponded to an individual, longitudinal truck position.

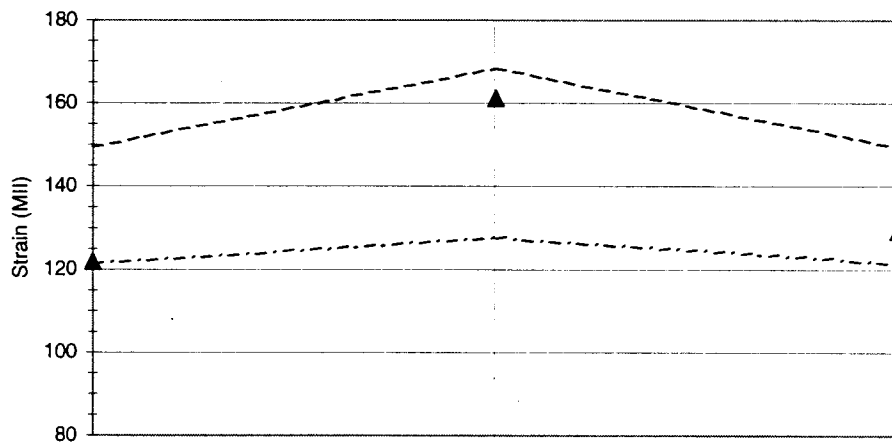
By reviewing the results recorded in each field load test, it was determined that the critical strains and deflections occurred in the longitudinal girders of the flatcars. When excluding the localized effects of the test truck tires, it was also determined from test results that the decking, secondary members, and transverse members experience strains considerably less than those in the longitudinal girders. In addition, the deflections and strains measured in LT2 were verified by those measured in LT3. As a result, RRFC bridge performance will be illustrated with LT1 and LT2 results in Sections 6.2.1 and 6.2.2; LT3 results reveal the RRFC bridge performance after approximately one year of service. The field test results for the BCB and WCB will be presented along with theoretical results in the following sections.

### ***6.2.1 BCB Field Test Results***

In Figures 6.4 – 6.6, the maximum midspan displacements and strains that were measured in all three tests of LT1 are presented along with theoretical results. These displacements and strains occurred when the centerline of the tandem axle was at the midspan of the bridge. As can be seen in each figure, girder displacement patterns are as

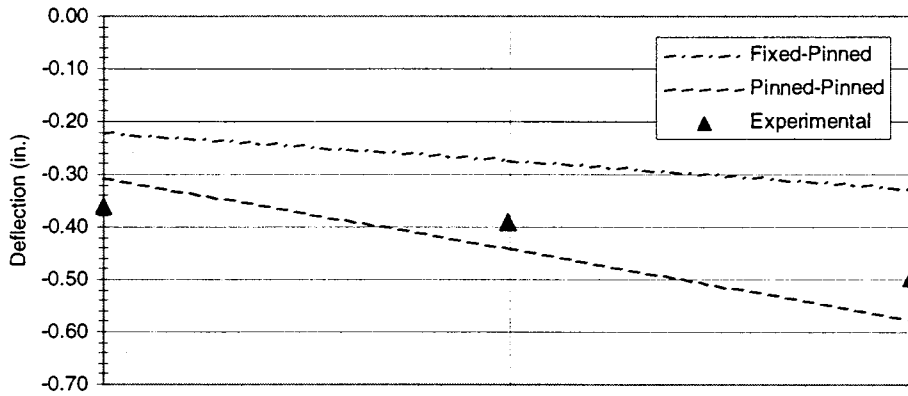
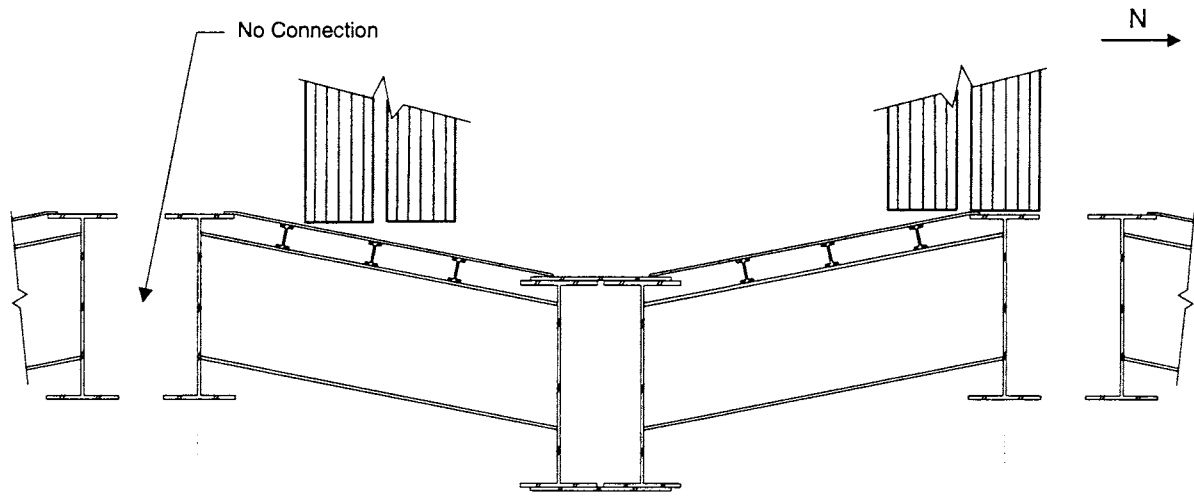


a. Deflections

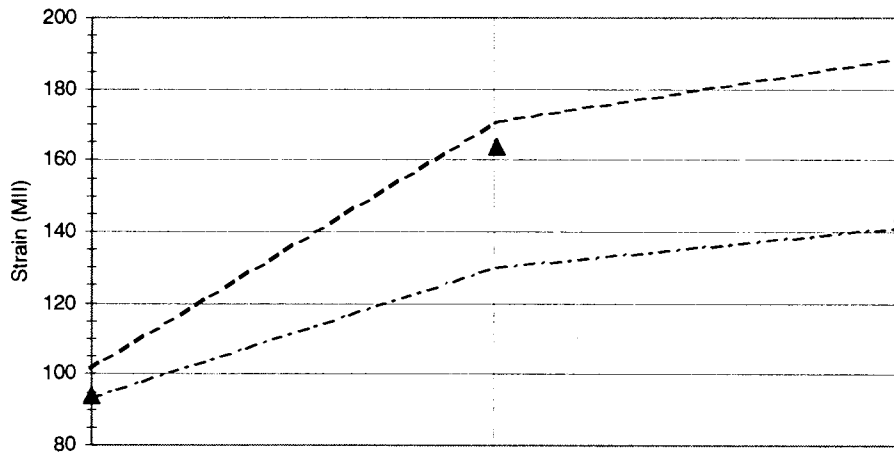


b. Member bottom flange strains

Figure 6.4. Comparison of BCB LT1 Test 1 midspan deflections and strains.

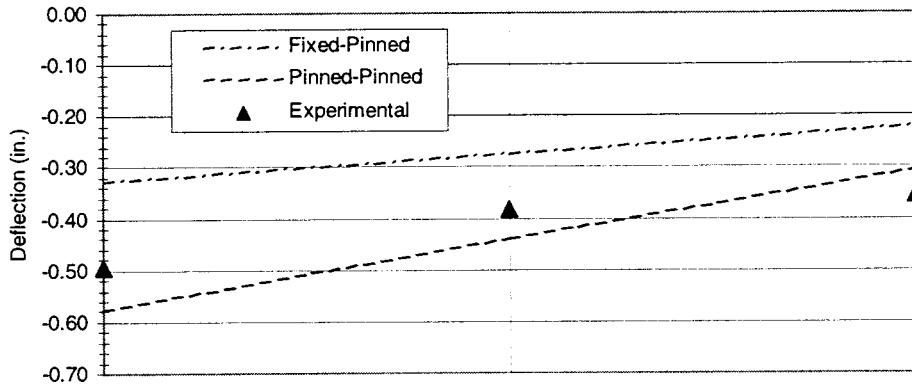
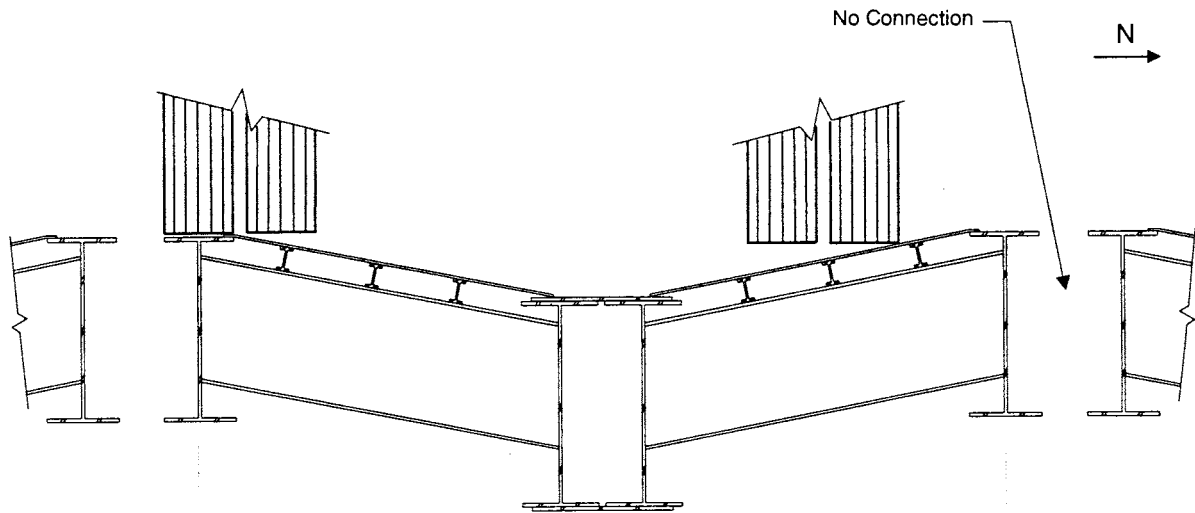


a. Deflections

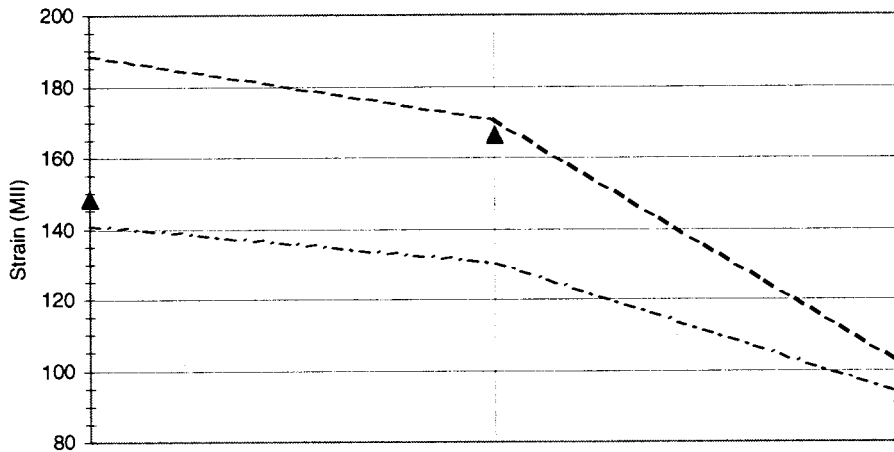


b. Member bottom flange strains

Figure 6.5. Comparison of BCB LT1 Test 2 midspan deflections and strains.



a. Deflections



b. Member bottom flange strains

Figure 6.6. Comparison of BCB LT1 Test 3 midspan deflections and strains.



one would expect; Figure 6.4 reveals a symmetrical displacement pattern, while Figures 6.5 and 6.6 reveal displacement patterns that coincide with the rotation of the flatcar due to the eccentric truck loading. In addition, the interior girder in each test experiences higher strains than either exterior girder. In nearly all of the tests, the measured experimental deflections and strains were within the theoretical range. Comparison of the field test results from the 3 tests in LT1 revealed the following:

- The interior girder's vertical deflections and strains remained nearly the same in all tests since the eccentric loading was so small.
- When comparing deflections in Test 1 (Figure 6.4) with those in Tests 2 and 3 (Figures 6.5 and 6.6), the maximum change in deflection for any longitudinal girder was approximately 0.14 in.; the maximum change in strain was 55 MII (1.6 ksi).
- Displacement and strain patterns for Tests 2 and 3 are nearly mirrored images of each other across the longitudinal centerline of the RRFC. This behavior indicates that the RRFC's have uniform torsional stiffness.
- The maximum deflections on the interior and exterior girders were approximately 0.40 in. and 0.50 in., respectively; the maximum strains were approximately 170 MII and 150 MII (4.9 ksi and 4.4 ksi, respectively).

As discussed in Chapter 4, identical tests in LT2 were performed before and after the driving surface was installed with test trucks positioned in several transverse locations. The results indicated that the driving surface had minimal effect on strains, deflections, and thus, transverse load distribution. Figures 6.7 – 6.12 illustrate midspan deflections and strains for each of the six tests of LT2 after the installation of the driving surface. Once again, these displacements and strains occurred when the centerline of the tandem axle was at the midspan of the bridge. In each figure, it can be seen that girder deflections and strains are maximum directly below the wheel loads and decrease in magnitude as the distance from the wheel loads increases. By comparing these figures, the following observations can be made about LT2 bridge behavior:

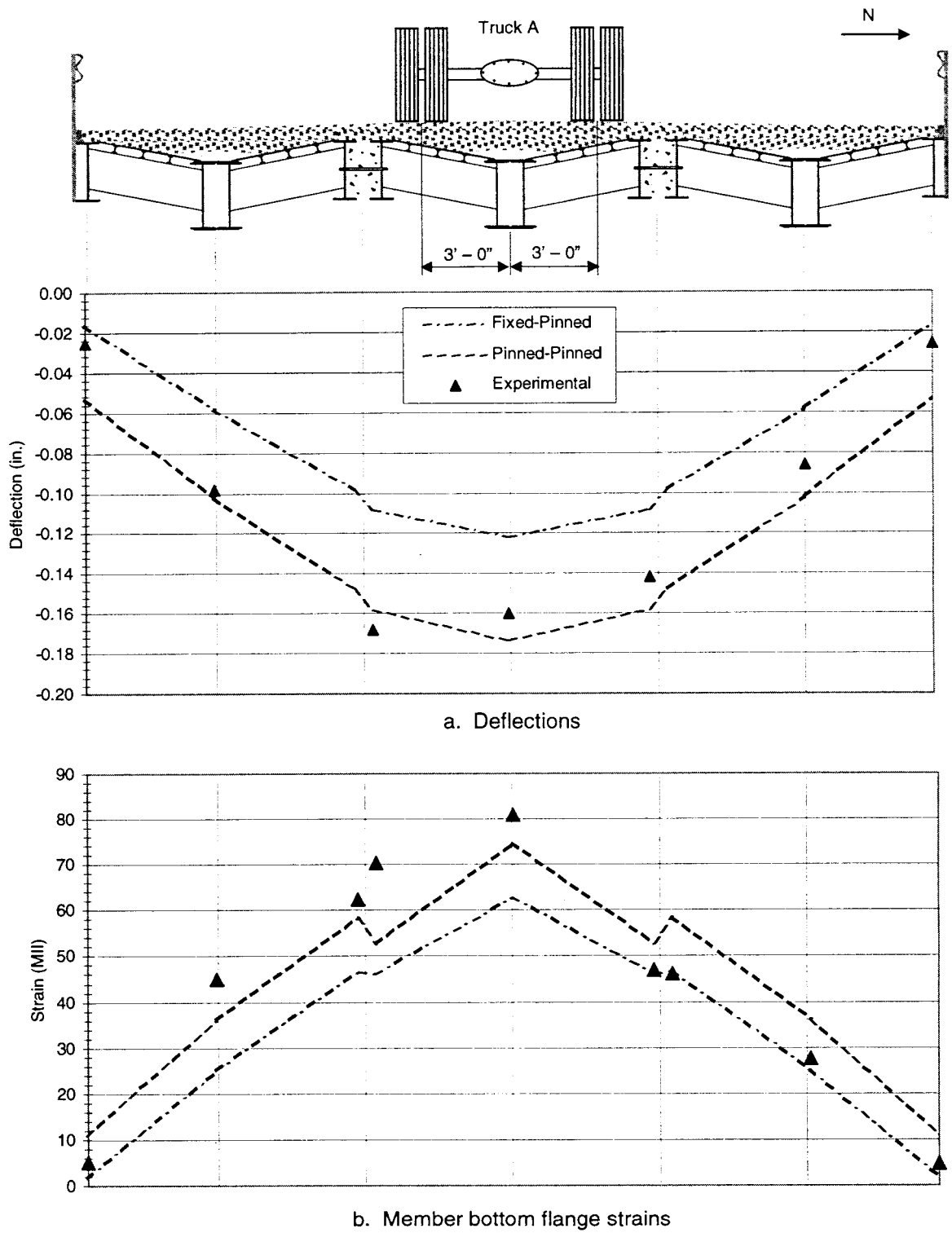
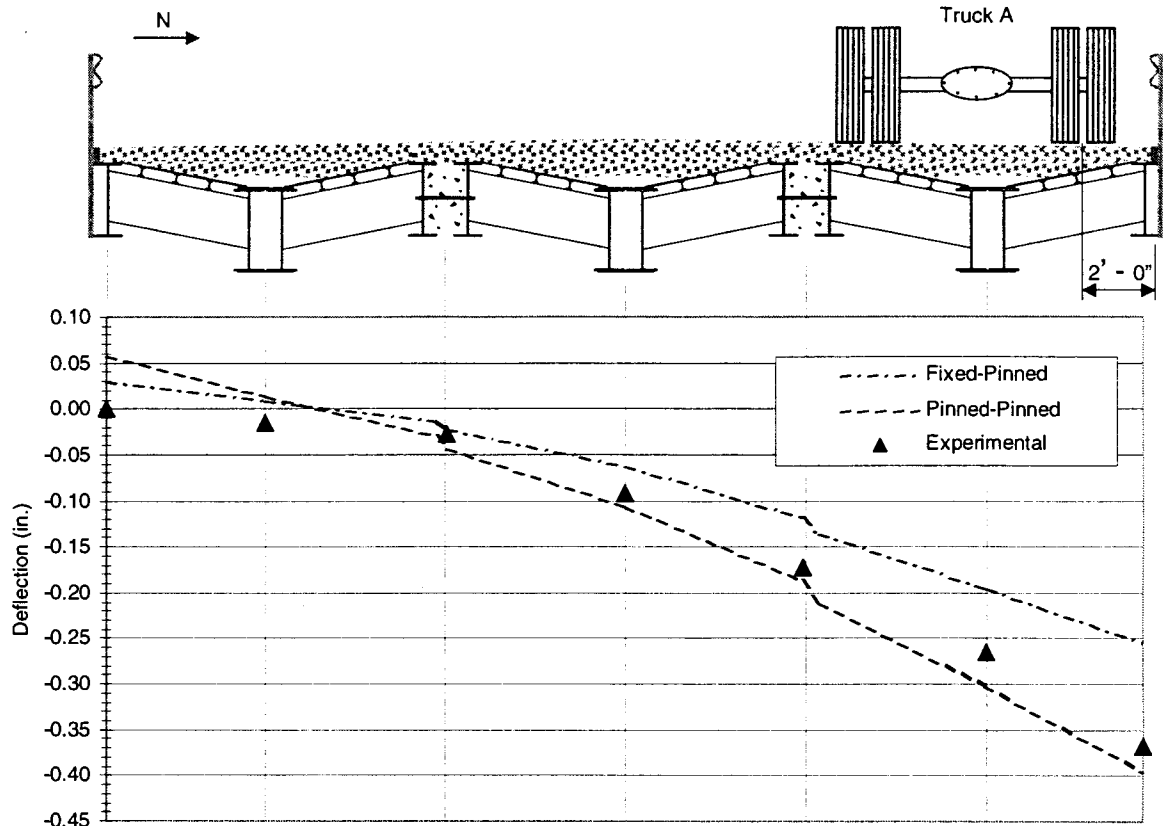
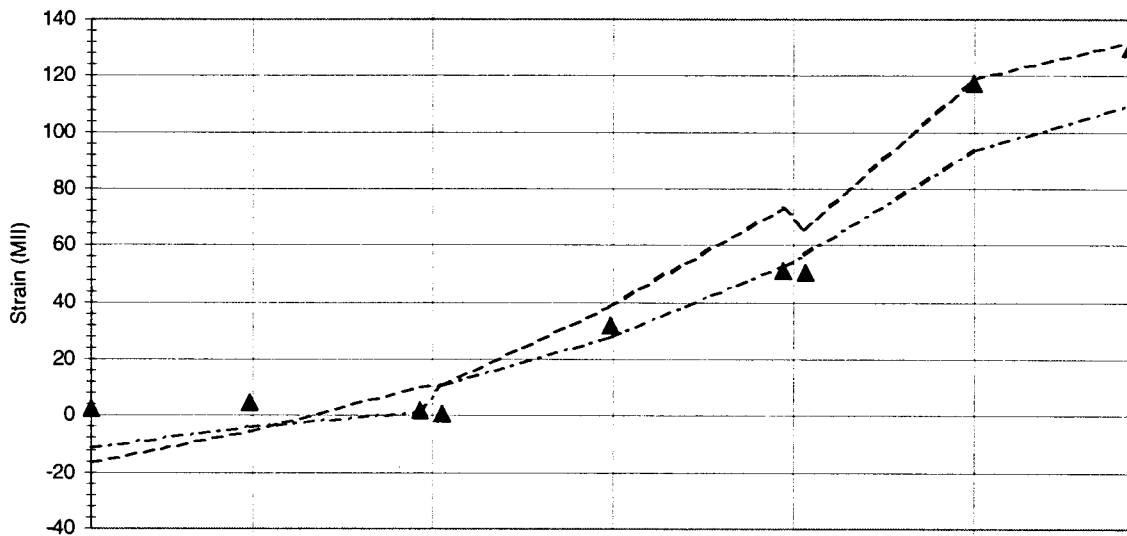


Figure 6.7. Comparison of BCB LT2 Test 1 midspan deflections and strains.

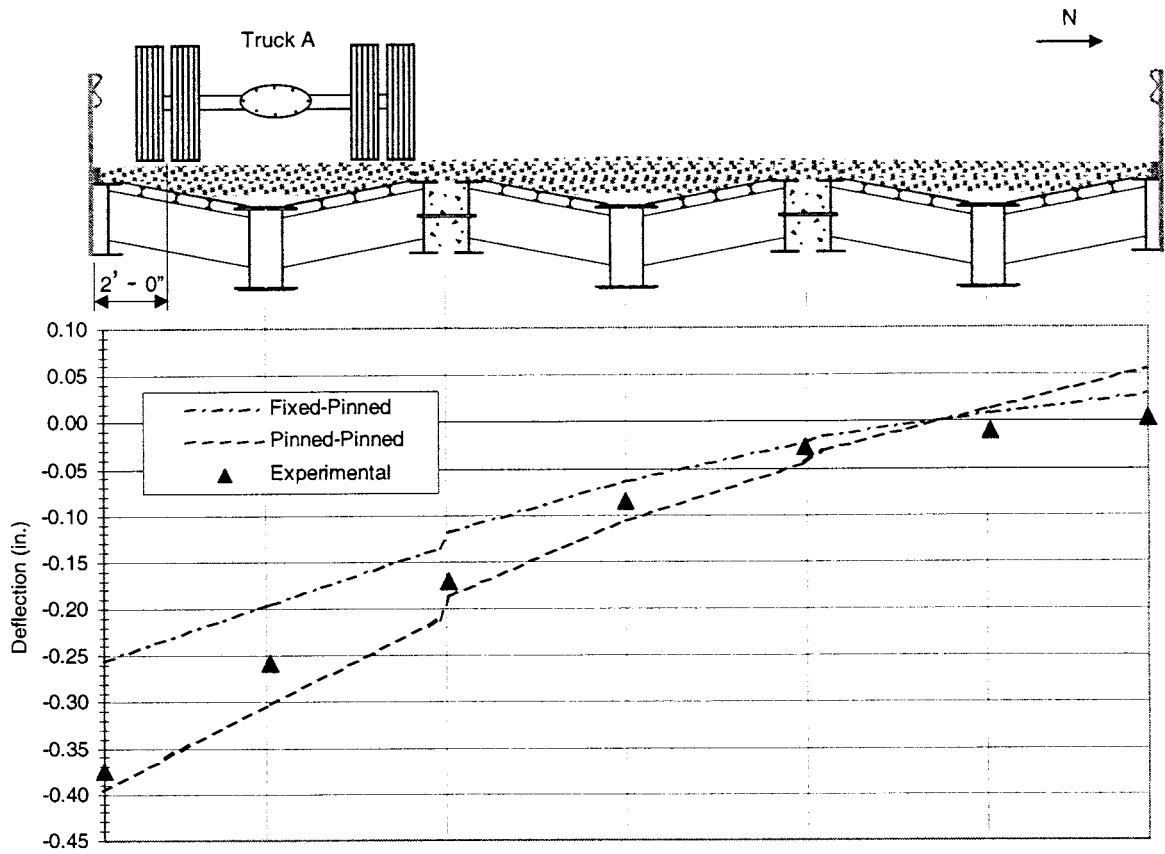


a. Deflections

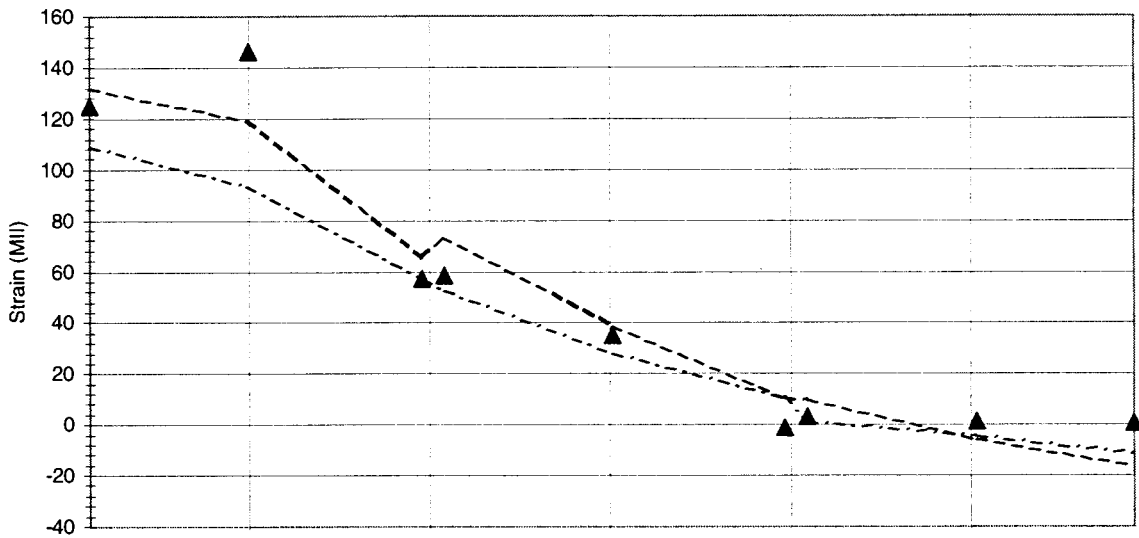


b. Member bottom flange strains

Figure 6.8. Comparison of BCB LT2 Test 2 midspan deflections and strains.

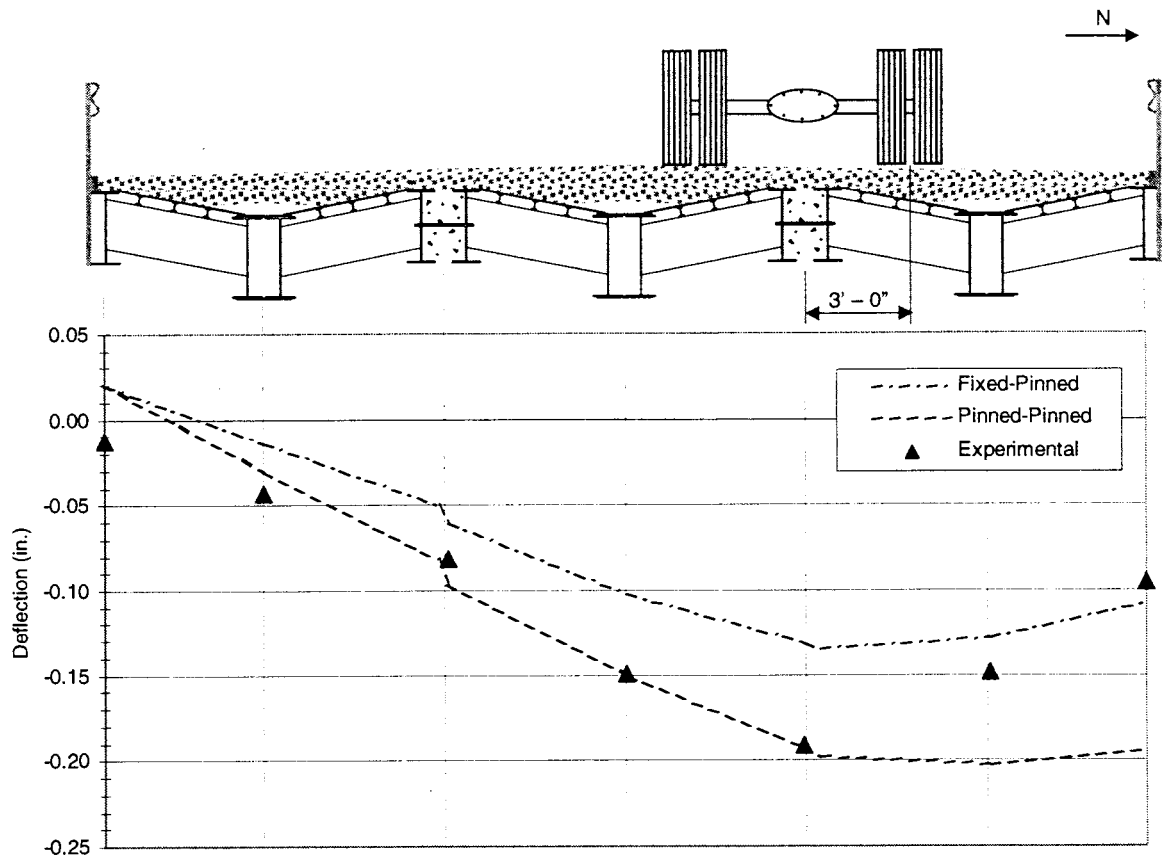


a. Deflections

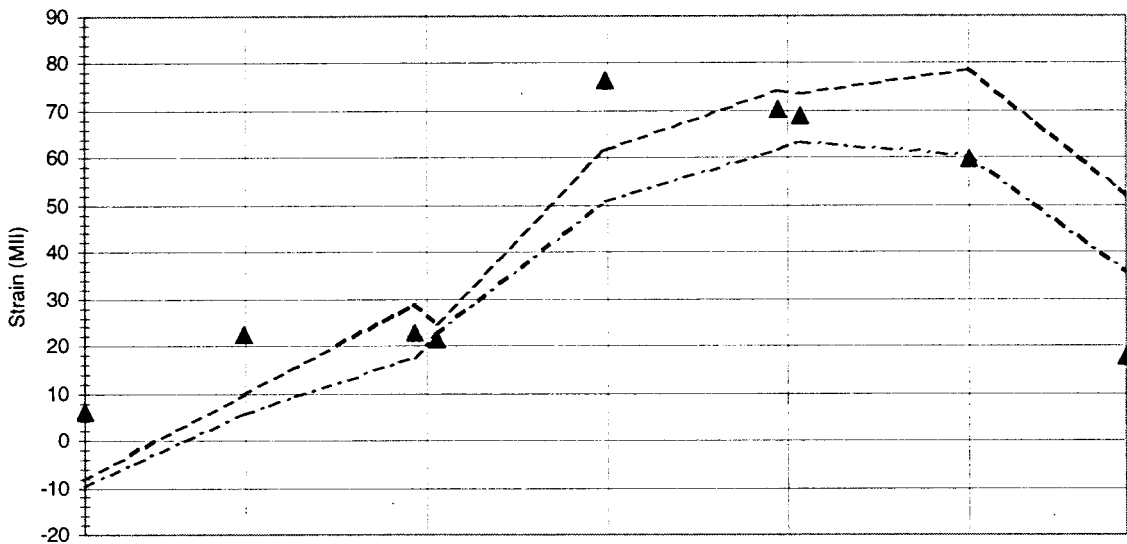


b. Member bottom flange strains

Figure 6.9. Comparison of BCB LT2 Test 3 midspan deflections and strains.

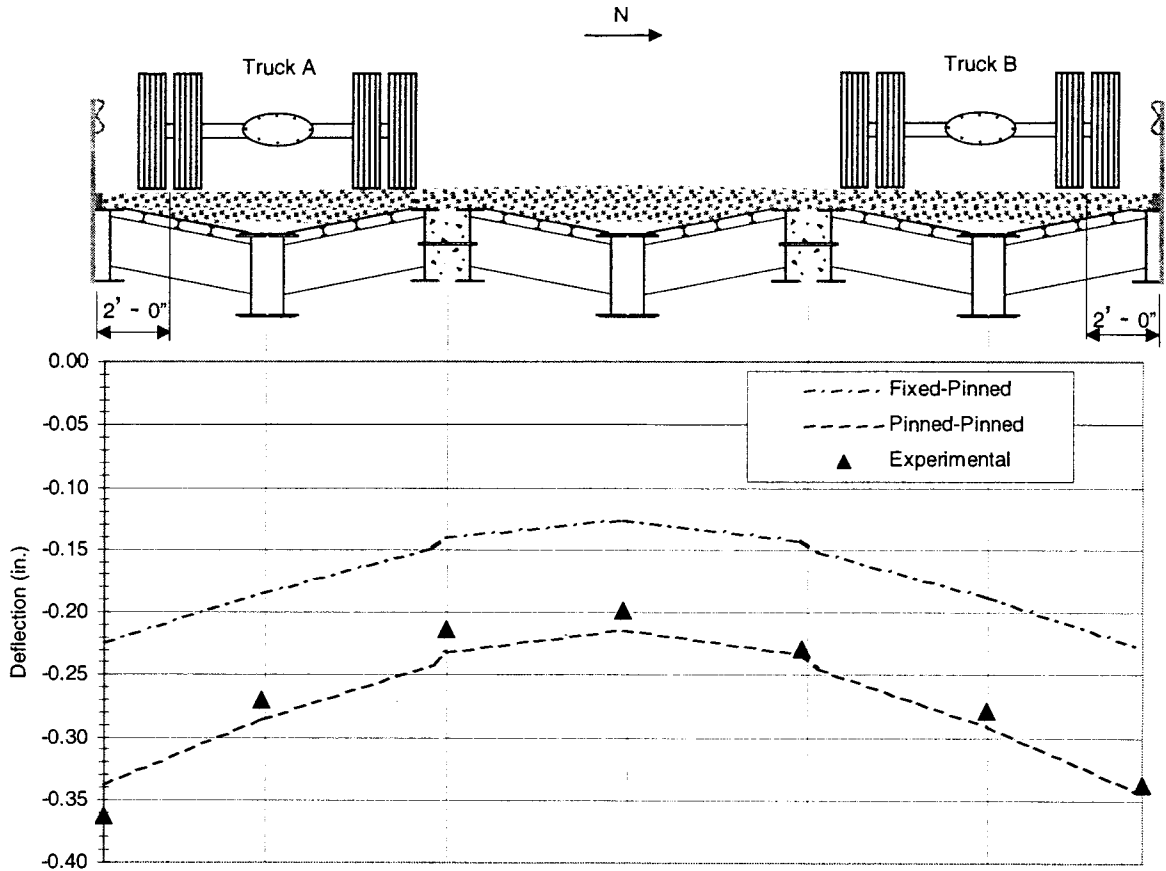


a. Deflections

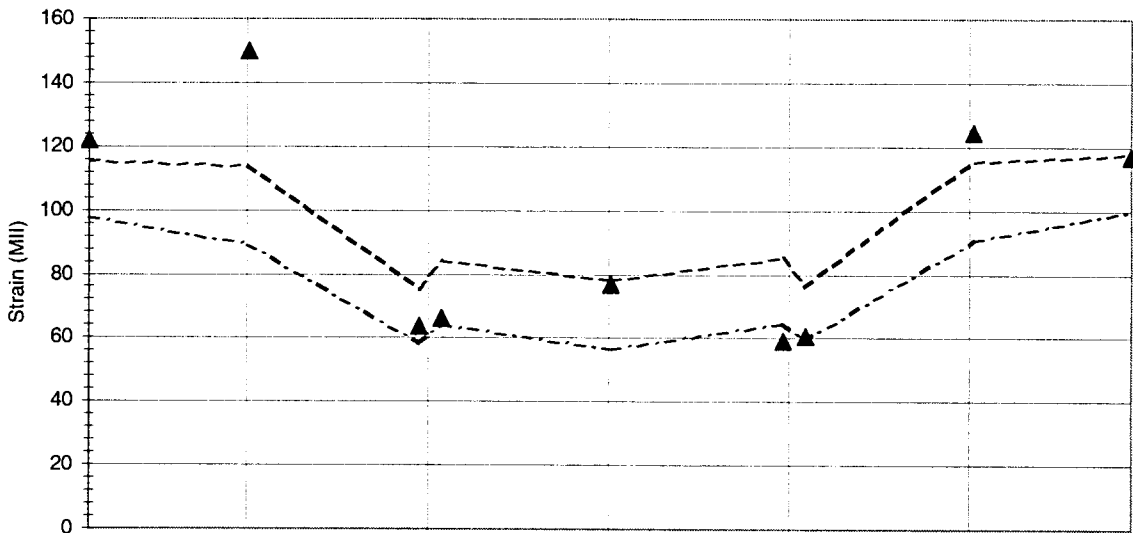


b. Member bottom flange strains

Figure 6.10. Comparison of BCB LT2 Test 4 midspan deflections and strains.

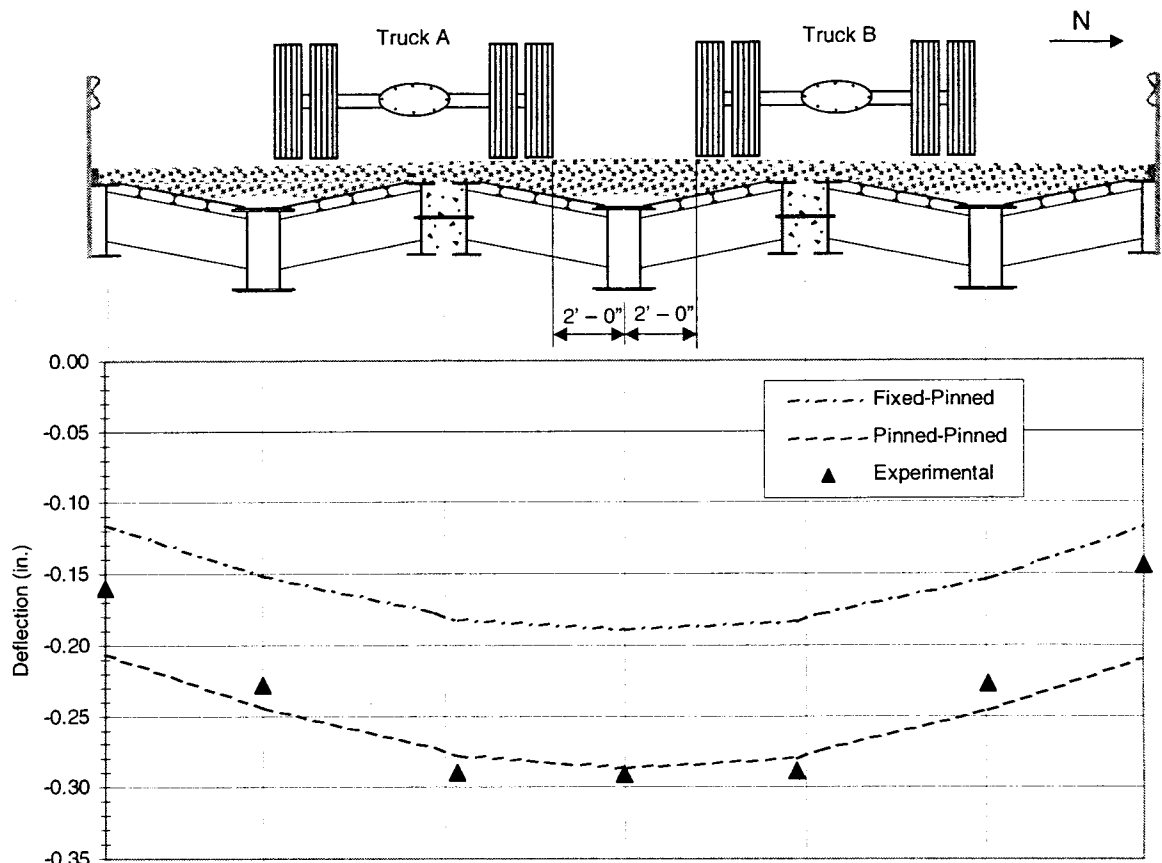


a. Deflections

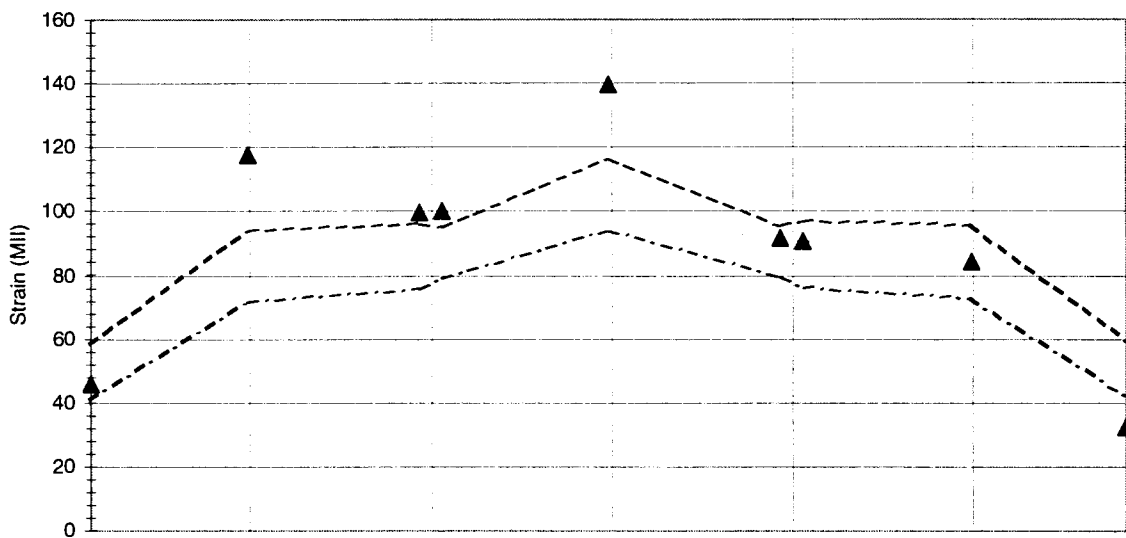


b. Member bottom flange strains

Figure 6.11. Comparison of BCB LT2 Test 5 midspan deflections and strains.



a. Deflections



b. Member bottom flange strains

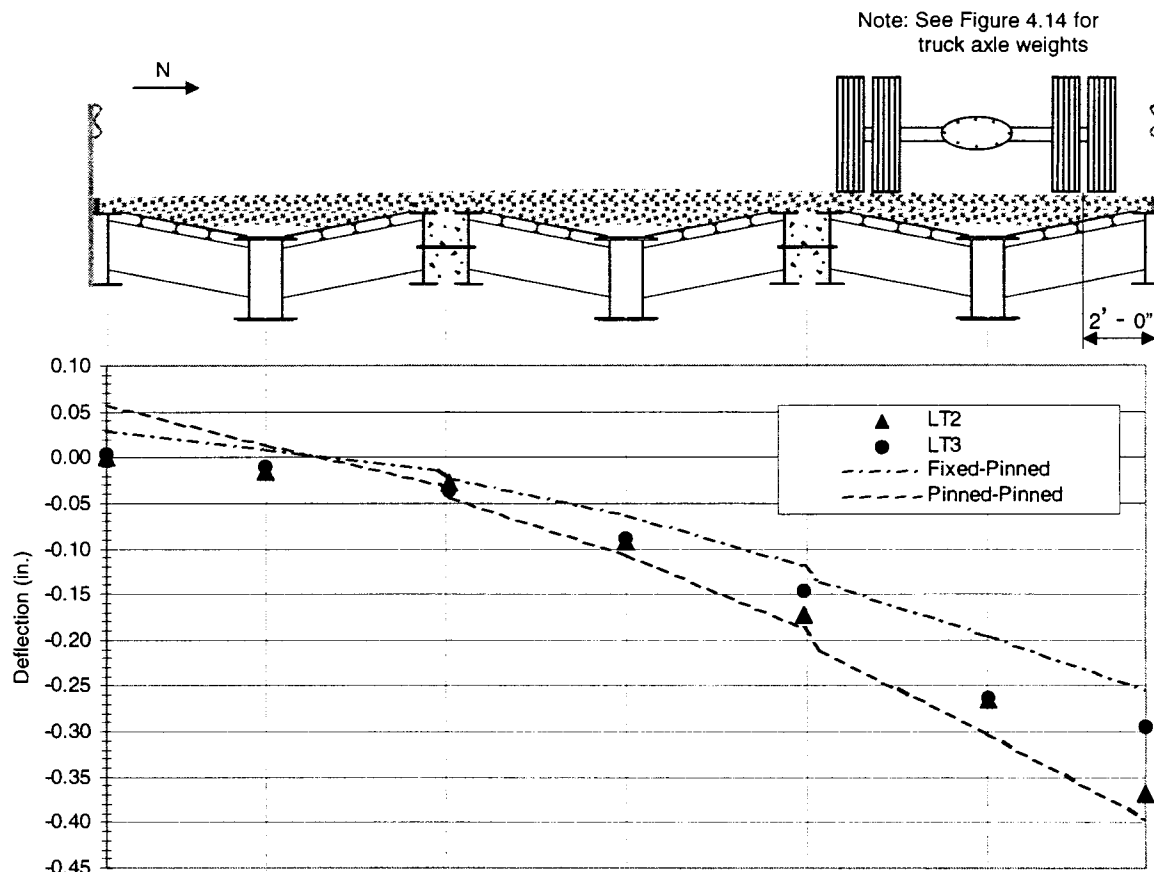
Figure 6.12. Comparison of BCB LT2 Test 6 midspan deflections and strains.

- Deflection and strain patterns for Tests 1, 5, and 6 (Figures 6.7, 6.11, and 6.12) reveal symmetrical bridge behavior, while Tests 2 and 3 (Figures 6.8 and 6.9) illustrate mirrored deflection and strain patterns across the longitudinal centerline of the bridge. Thus, the bending and torsional stiffness of the RRFCs with longitudinal connections remain uniform transversely across the bridge.
- The south and north edges of the bridge deflected upward during Tests 2 and 3, and thus, indicated that the longitudinal flatcar connections distribute load transversely.
- Deflection and strain results for the center RRFC loaded with a transversely centered test truck demonstrated that the addition of the longitudinal flatcar connections reduced deflections and strains by approximately 55-60%. This behavior documented the effectiveness of the connections between adjacent flatcars.

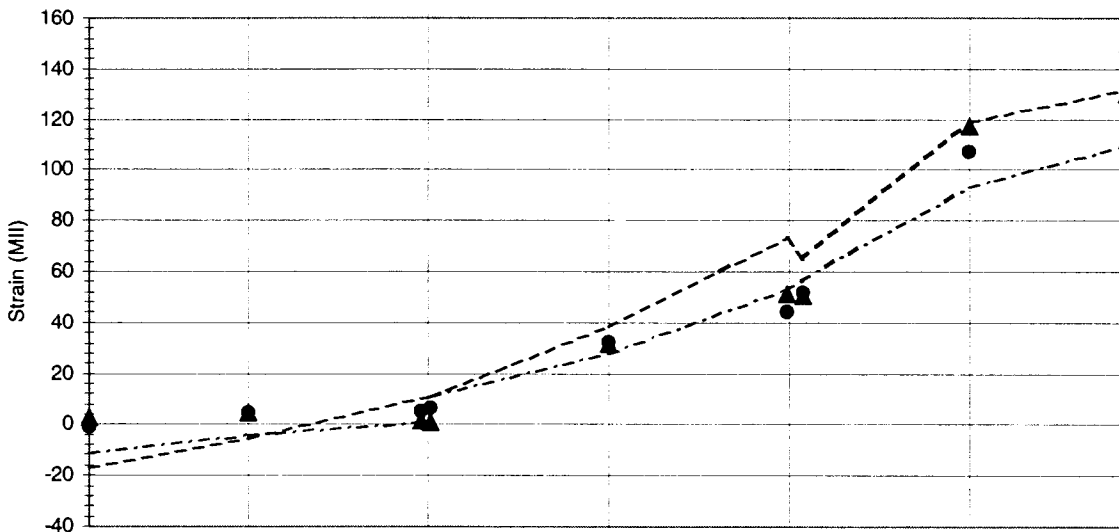
Careful examination of the LT2 test results revealed that strain measurements in the interior girder in the south RRFC are higher than the theoretical results. In addition, when comparing symmetrically identical tests, the strains in the interior girder in the south RRFC do not match those in the north RRFC. However, LT3 strain measurements in the interior girder of the south RRFC are in good agreement with the strain measurements in the interior girder of the north flatcar for both LT2 and LT3. As a result, it can be concluded that the LT2 strain measurements for the interior girder in the south flatcar are most likely high due to instrumentation error.

Figure 6.13 illustrates LT2 and LT3 deflection and strain measurements for transverse truck positioning identical to Test 2 in LT2. As can be seen, a slight variation between strain results occurs at the north edge of the bridge, which is probable due to a slight, accidental difference in the transverse truck position between the two tests. However, good agreement occurs in all other girders, and thus, confirms no change in the RRFC bridge behavior after one year of service. All other tests revealed the same agreement between LT2 and LT3 results, and therefore, have not been presented.





a. Deflections



b. Member bottom flange strains

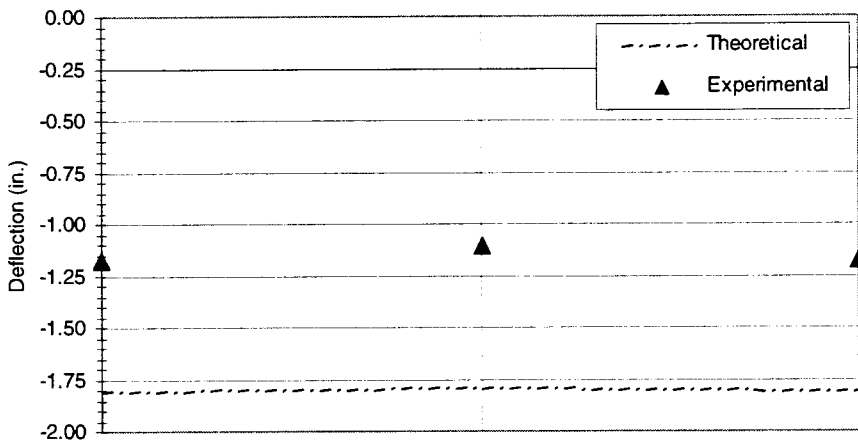
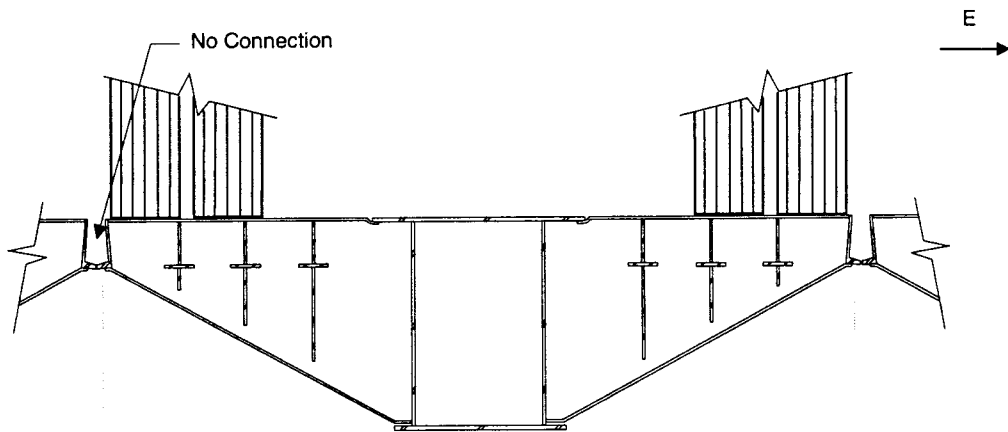
Figure 6.13. Comparison of BCB LT2 and LT3 midspan deflections and strains.

A tensile test was performed in accordance with ASTM A370 [9] on a steel coupon from the 56-ft flatcar. The proportional limit and modulus of elasticity (M.O.E.) from the stress-strain diagram were determined to be 40 ksi and 29,000 ksi, respectively. Thus, a conservative yield strength was assumed to be 36 ksi. Using the coupon M.O.E. and neglecting all strain measurements on the interior girder in the south RRFC (due to instrumentation error), the maximum LT2 flexural stress in the longitudinal girders of the bridge due to test truck loads was approximately 3.8 ksi. As shown in Figure 6.9, the maximum measured deflection was approximately 0.38 in. According to the 1994 LRFD [4] and 1996 LFD AASHTO Bridge Design Specifications [5], the maximum allowable deflection should not exceed 1/800 of the span length, which is 0.84 in. for a 56-ft span.

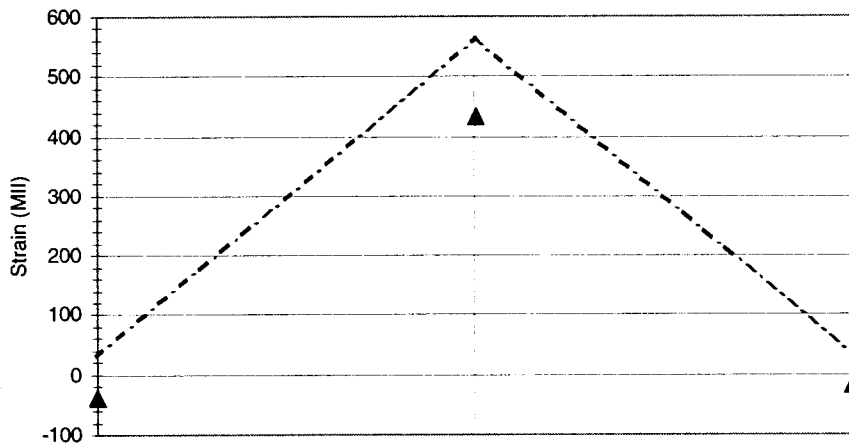
#### *6.2.2 WCB Field Test Results*

The maximum midspan displacements and strains measured for LT1 tests performed with and without abutment restraints are presented in Figure 6.14 and Figure 6.15. By reviewing both figures, it can be seen that the trimmed, exterior girders in the single RRFC experience nearly zero strain, whereas the interior girder experiences over 400 MII (11.6 ksi) in both tests. As a result, it can be concluded that the trimmed, 89-ft RRFCs have a non-redundant cross-section, as predicted by the grillage model. By reviewing Figure 6.14, it can be seen that a significant amount of error exists between theoretical and experimental results for the test without abutment restraints; theoretical results predicted 1.8 in. of midspan displacement, whereas 1.1 in. was measured in the field test. However, theoretical and experimental results presented in Figure 6.15 for the test with abutment restraints are nearly exact.

Due to the good agreement between theoretical and experimental results in Figure 6.15, it can be concluded that instrumentation was properly recording displacements and strains for the LT1 tests, and also that the flatcar members have been adequately

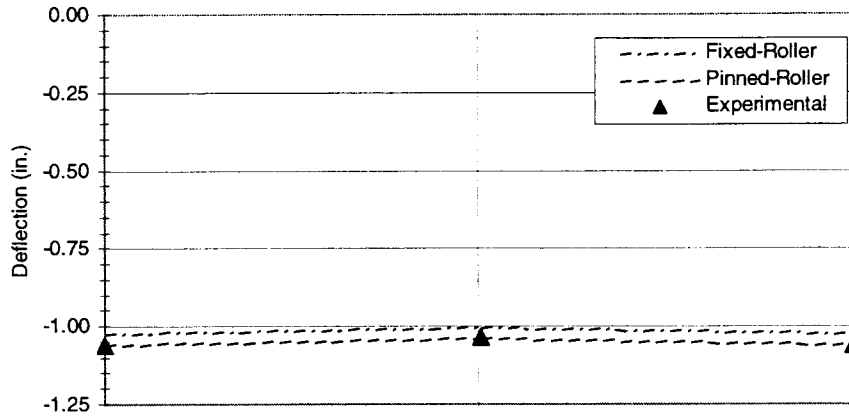
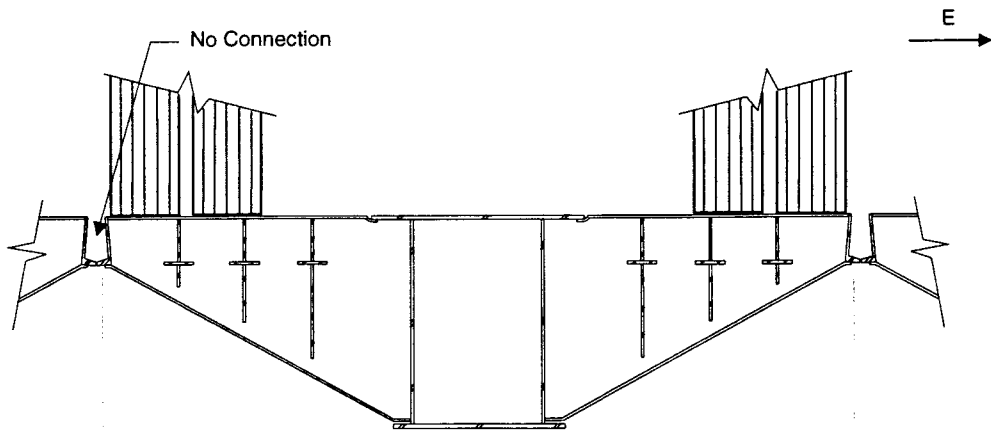


a. Deflections

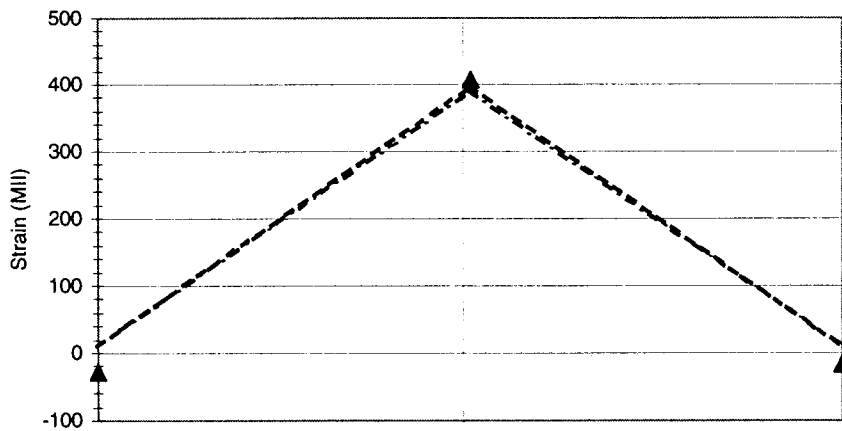


b. Member bottom flange strains

Figure 6.14. Comparison of WCB LT1 midspan deflections and strains without abutment restraints.



a. Deflections



b. Member bottom flange strains

Figure 6.15. Comparison of WCB LT1 midspan deflections and strains with abutment restraints.

represented in the grillage model. In addition, hand calculations for a prismatic beam with equivalent 89-ft flatcar section properties and boundary conditions identical to those of the grillage model for the test without abutment restraints verified the theoretical results shown in Figure 6.14. As a result, it can be concluded that both grillage models were accurately predicting deflections and strains, and the field test instrumentation was operating properly.

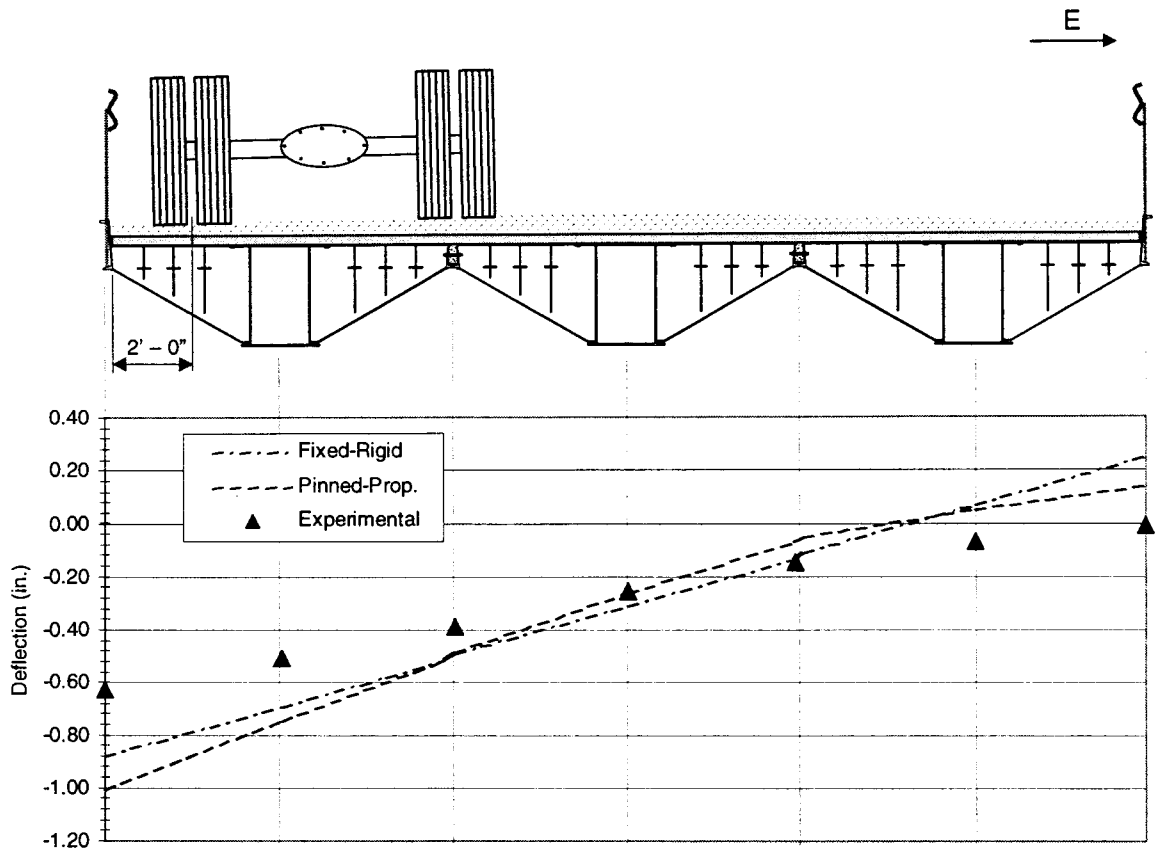
Therefore, the difference shown in Figure 6.14 is probably due to a condition that existed during the test that made the simple support boundary conditions in the theoretical model inappropriate. Since the flatcars were placed directly beside one another, it is possible that there was interaction between the flange tips of adjacent exterior girders. Due to a slight horizontal curvature in the exterior girder, there was a small gap (approximately 1/8 in.) between the flanges of adjacent exterior girders over the main span of the WCB, but these same flanges were in direct contact in the side spans of the WCB. This type of contact may have caused interaction among the three flatcars that cause some rotational restraint, and thus making the simple supports in the grillage model inappropriate. Interaction between the three flatcars would result in lower deflections and strains at midspan of the main span than those that were predicted, which is the case in Figure 6.14. Therefore, most likely the flange-tip interaction between exterior girders in adjacent flatcars caused the error between theoretical and experimental results in Figure 6.14. The following conclusions about LT1 can be made by reviewing Figures 6.14 and 6.15:

- The maximum deflection and strain measured on the longitudinal girders in LT1 was approximately 1.2 in. and 440 MII (12.8 ksi) as illustrated in Figure 6.14.
- The addition of abutment restraints reduced midspan deflections and strains by approximately 6-10%.

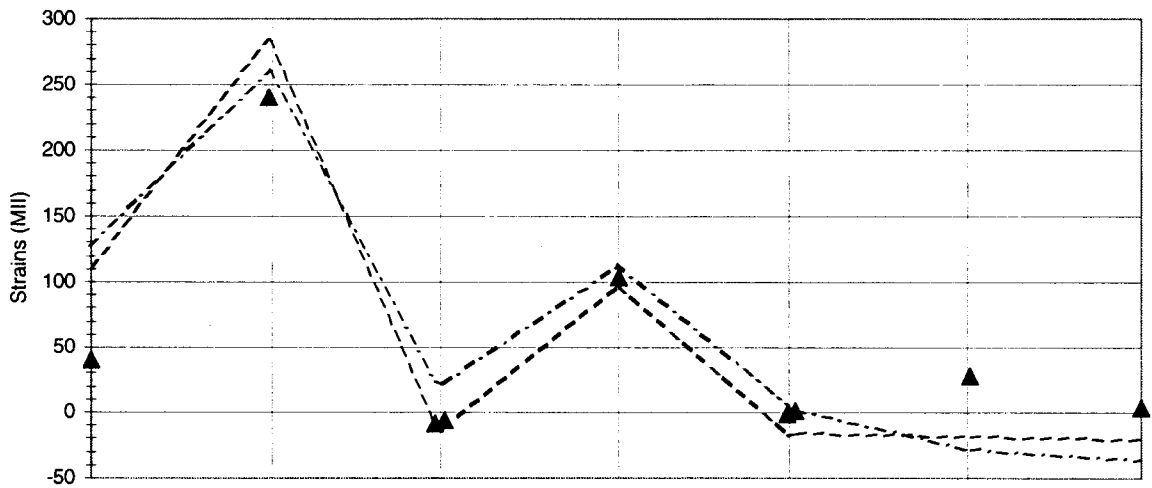
As discussed in Chapter 4, LT1 testing was performed before the addition of abutment restraints so that the vertical displacements at the ends of the flatcar could be measured when a test truck was positioned at midspan of the main span. For this case, LT1

maximum vertical displacements at the north and south ends of the RRFC were 0.06 in. and 0.37 in., respectively. Since the vertical displacement at the north end of the flatcar was small in comparison to the vertical displacement measured at the south end, the north end of the flatcar was inspected, revealing an 1/8 in. gap between the flatcar bolster and the pier cap, however the north end of the flatcar rested directly on the abutment. This undesirable support condition was the reason for the small vertical displacement at the north end of the RRFC; the bolster needed to displace downward to reach the pier before the north end could displace upward at the abutment. The effects of this gap on the vertical displacement results were corrected, and the actual vertical displacements at the north and south ends of the flatcar were corrected to be 0.21 in. and 0.35 in., respectively. This gap did not have any effect on the maximum strain recordings at midspan of the main span since the bolsters of the flatcar were in contact with the piers by the time the midspan strains were recorded. After LT1 field testing, a 1/8 in. steel plate was used to fill the gap between the bolster and north pier.

Midspan deflections and strains measured for each of the three truck positions in LT2 are presented with theoretical results in Figures 6.16 – 6.18. Once again, maximum deflections and strains were recorded in girders immediately under the wheel loads, and other girder strains and displacements decreased in magnitude in relation to the distance from the wheel loads. It should be noted that due to construction time limitations, the guardrail was connected to the WCB prior to LT2 testing; its connection shown in Figure 3.14a is assumed to be rigid. As a result of this connection, the guardrail likely increased the stiffness of the exterior girder at the edge of the WCB. However, this extra stiffness was not considered in the grillage model, and likely caused the difference between the theoretical and experimental results in Figures 6.16 – 6.18. By reviewing the data in LT1 and LT2 tests, the following observations can be made:

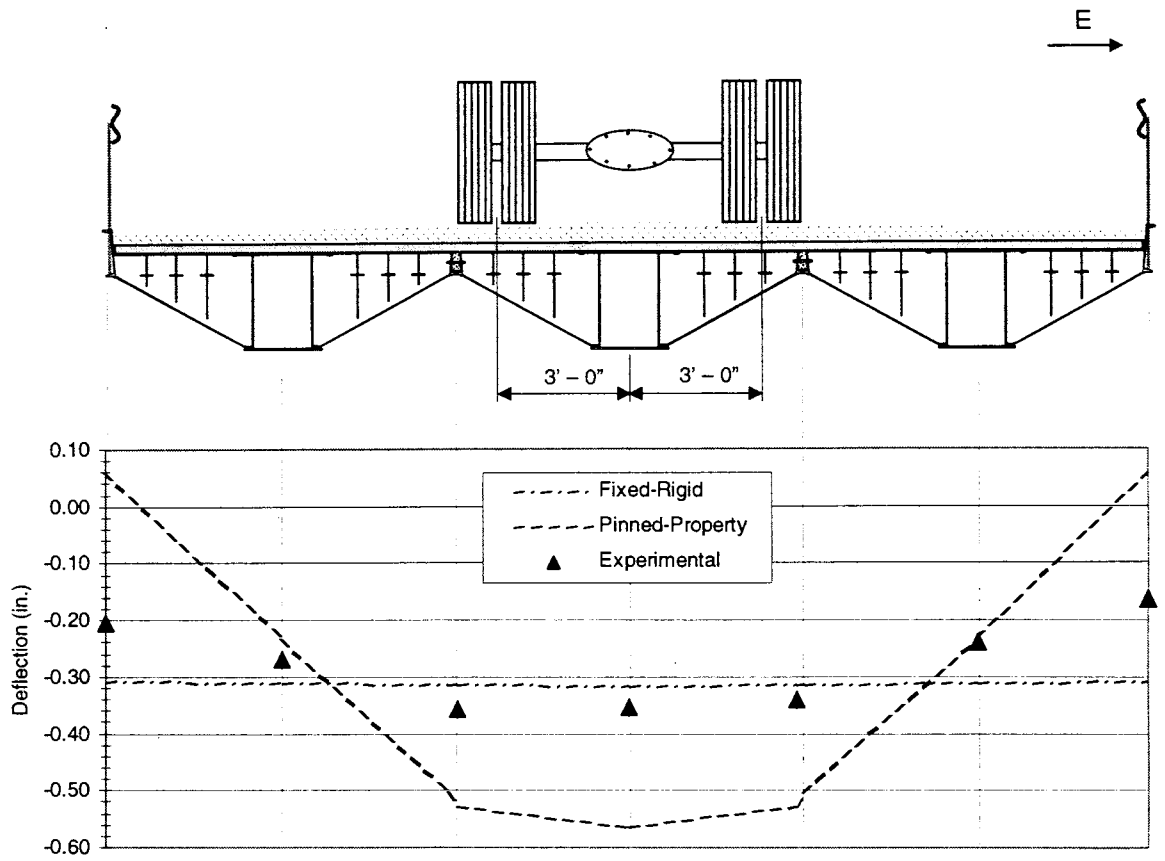


a. Deflections

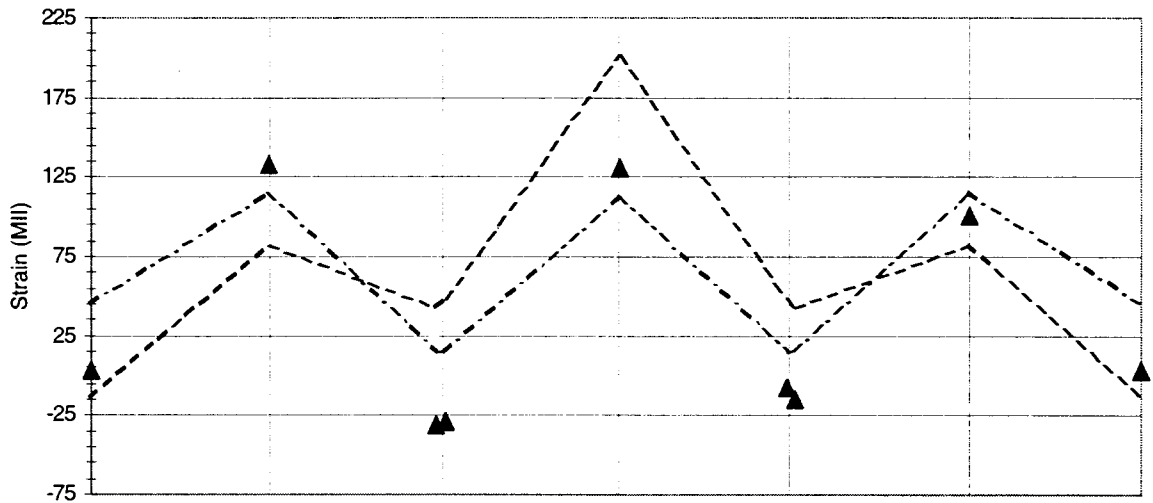


b. Member bottom flange strains

Figure 6.16. Comparison of WCB LT2 Test 1 midspan deflections and strains.



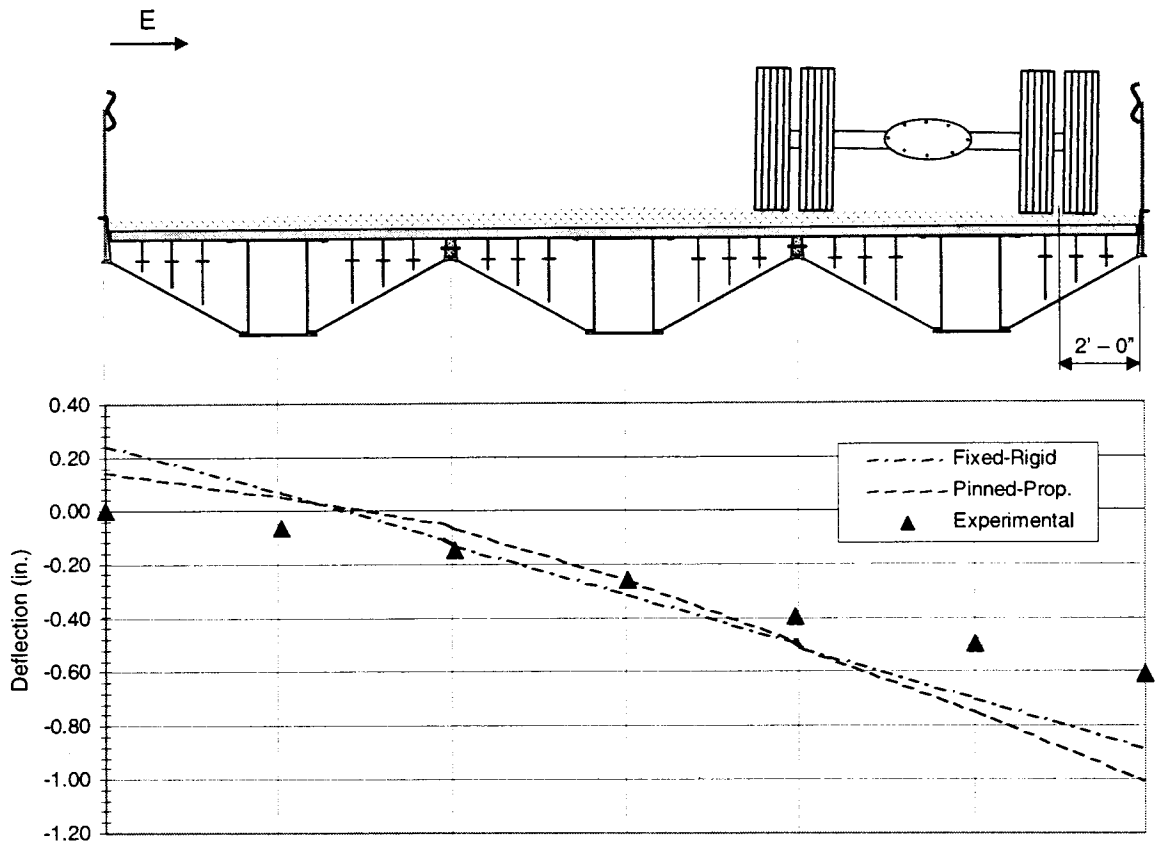
a. Deflections



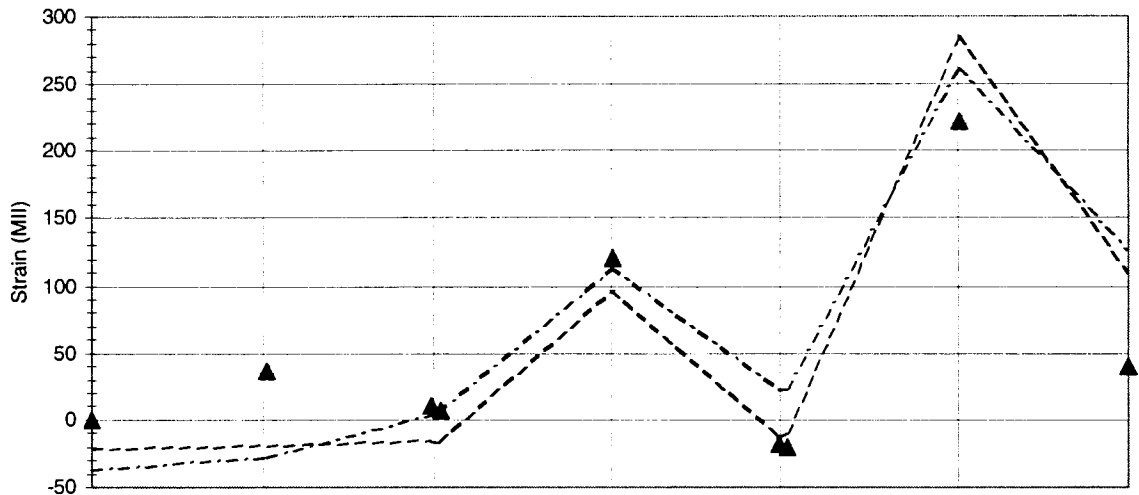
b. Member bottom flange strains

Figure 6.17. Comparison of WCB LT2 Test 2 midspan deflections and strains.



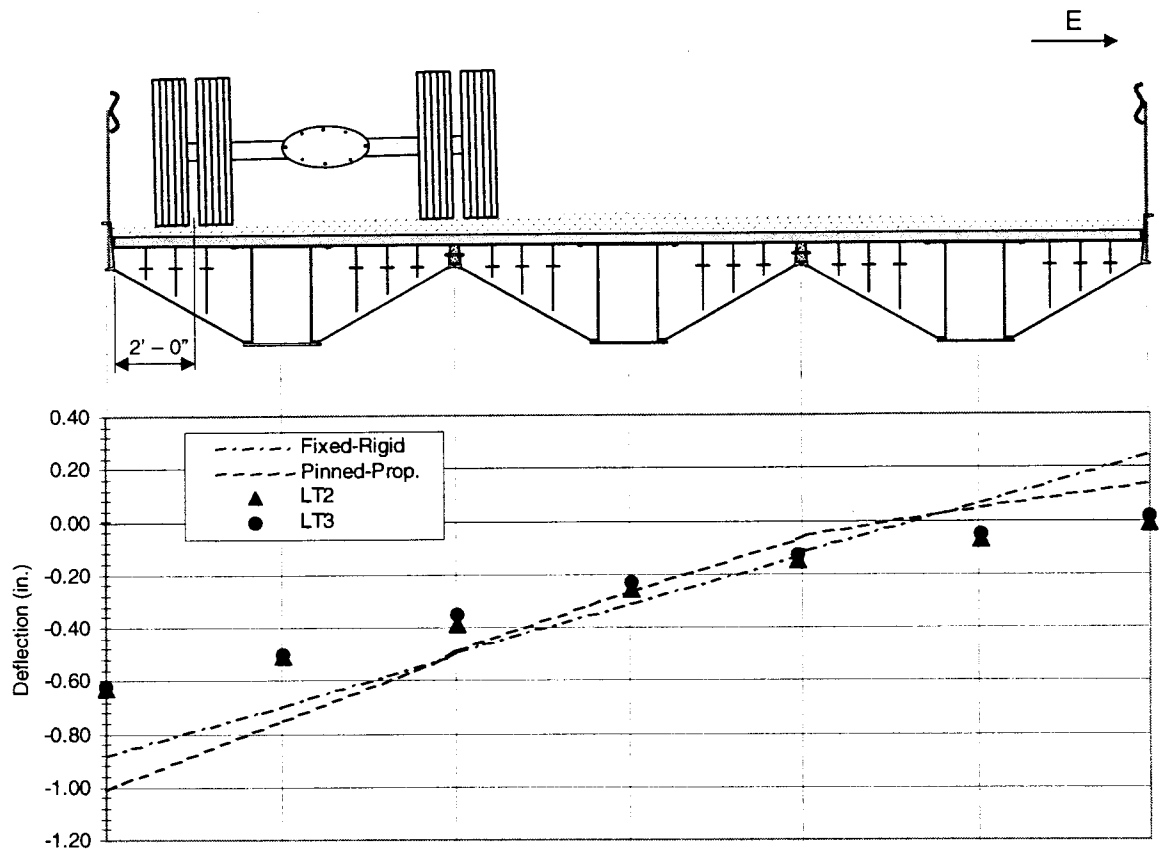


a. Deflections

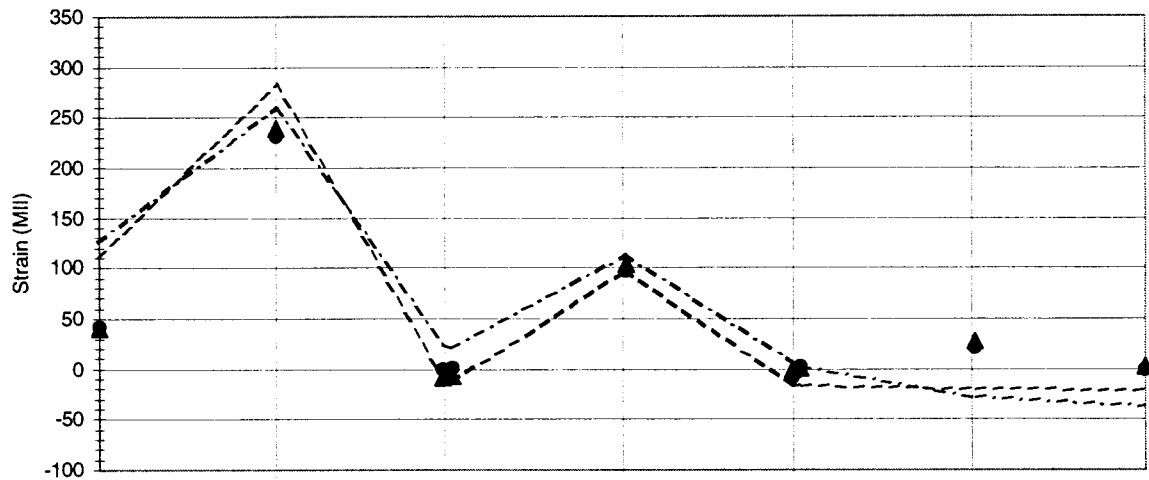


b. Member bottom flange strains

Figure 6.18. Comparison of WCB LT2 Test 3 midspan deflections and strains.



a. Deflections



b. Member bottom flange strains

Figure 6.19. Comparison of WCB LT2 and LT3 midspan deflections and strains.

The east and west edges of the bridge deflected downward during Test 1 and Test 3 (Figures 6.16 and 6.18), and thus, indicated that the longitudinal flatcar connections adequately distribute load transversely.

- Deflection and strain patterns for Tests 1 and 3 in LT2 are nearly symmetrical about the longitudinal centerline of the bridge, which indicated consistent load distribution in both transverse directions across the bridge.
- Comparing the results presented in Figure 6.15 and Figure 6.17, the maximum midspan deflections and strains were reduced by approximately 70% due to the addition of longitudinal flatcar connections and transverse timber planks.

In addition to the tests previously described, a final test was performed with the test truck traveling at 30 mph with transverse positioning identical to that of Test 2 in LT2 (Figure 6.17). The midspan deflection and strain patterns for this test resembled those of Test 2, but the deflection and strain magnitudes were approximately 18% larger due to dynamic effects of the truck.

Deflection and strain measurements recorded in LT2 and LT3 for truck positioning identical to that of Test 1 in LT2 (Figure 6.16) are presented in Figure 6.19. As can be seen, there is good agreement between results from LT2 and LT3, which confirms there was no change in RRFC bridge behavior after approximately one year of service.

Through another ASTM tensile coupon test, it was found that the steel in the 89-ft RRFC had the same yield strength and M.O.E. as the steel in the 56-ft RRFC. When looking at the overall performance of the WCB, it was determined that the maximum flexural stresses in the longitudinal girders from test truck loads were approximately 7.0 ksi. In addition, the maximum deflection was 0.63 in. (illustrated in Figure 6.16), which is less than 0.99 in. (the maximum deflection according to the 1994 LRFD [4] and 1996 LFD AASHTO Bridge Design Specifications [5]) for a 66-ft span.

### *6.2.3 Summary of Demonstration Bridge Performances*

It has been shown through the field load tests of each bridge that providing engineered, longitudinal connections between adjacent flatcars provides significant transverse load distribution just as the grillage models predicted. The LT2 deflection and strain patterns for both bridges proved that both types of longitudinal connections effectively distribute loads transversely in the bridge, and thus, the strength of all three flatcars is used to support the live load.

When the dead load stresses from the theoretical analysis in Section 5.3 are combined with the maximum live load stresses obtained from the field load testing, the maximum resultant stresses in the longitudinal girders of the BCB and WCB were approximately 12.7 ksi and 16.7 ksi, respectively. For the BCB, this maximum resultant stress occurred in an exterior girder at one edge of the bridge when the test truck was transversely positioned at that side of the bridge. Similarly, the maximum resultant stress for the WCB occurred in an interior girder of a side RRFC when the test truck was transversely positioned at that side of the bridge.

In each test, there was good agreement between theoretical and experimental results. As a result, it was concluded that the flatcars behave structurally as basic engineering theory predicts. In addition, the maximum stresses in the longitudinal girders were well below the conservative yield strength of 36 ksi, and the maximum deflections were significantly less than the AASHTO limits. Therefore, the field tests have verified that RRFC bridges can adequately support Iowa legal tandem truck loading.

## **7. Design and construction of RRfc Bridges**

Initial cost of RRFCs and the ease of installing them, which leads to a reduced construction time, makes RRFC bridges economical. Since they are economical, it is expected that several other counties will construct such bridges in the future. To assist in their design, live load distribution recommendations have been developed. Also, recommendations are given to improve the efficiency of the construction process. These topics are addressed in the subsequent sections.

### **7.1 Construction Time and Expenses**

The BCB and WCB were constructed in approximately 8 weeks and 7 weeks, respectively; however, the construction of each bridge was slowed due to the field testing. Therefore, it is envisioned that other RRFC bridges can be constructed in approximately six weeks if there are no field tests or other interruptions. This relatively short construction time reduces the time the road is out of service, and thus, the length of time that local residents are inconvenienced by the closed road.

The economics of the RRFC alternative bridges may be further exemplified by comparing RRFC bridge costs with those of a conventional structure. Each 56-ft RRFC cost \$6,500, and each 89-ft RRFC cost \$9,700; both prices included shipping to the bridge site. If the labor and equipment costs are not included, the BCB and WCB RRFC bridges cost approximately \$20 per square foot and \$26 per square foot, respectively. If the actual costs for the county labor and equipment are included, the BCB and WCB RRFC bridge costs would be \$39 per square foot and \$37 per square foot, respectively. The rationale for excluding the county labor and equipment costs from the RRFC bridge costs is that they were already budgeted expenses. Thus, those costs would have existed throughout the construction season, regardless of constructing the bridges in question. Therefore, only the materials and contracted labor associated with the RRFC bridges were extra expenses to

the counties. The alternative to each RRFC bridge was a concrete slab bridge, which costs approximately \$65 per square foot.

## 7.2 Recommendations for Live Load Distribution

Grillage models were used to investigate live load distribution in each of the RRFC demonstration bridges. However, the model development was very time consuming and required access to and experience with grillage modeling and appropriate computer software. To simplify design of the RRFC bridges, an analysis was developed that utilizes statically determinate structures and design aides to assist in determining the maximum live load moments in the bridge's longitudinal girders.

As was discussed in Chapter 6, the maximum strains (stresses) that occurred in the RRFC bridges were recorded in the interior and exterior girders in an exterior RRFC when the test truck was transversely positioned on that side of the bridge. The live load moments in each girder that caused these strains (stresses) can be calculated by using the following equations:

$$M_{LL} = \frac{2}{3} \psi \omega M_{SD} \quad (7.1)$$

where,

$M_{LL}$  = The actual, maximum midspan live load moment in the girder being investigated resulting from Iowa legal traffic loads

$M_{SD}$  = The maximum, midspan live load moment in the statically determinate RRFC bridge resulting from Iowa legal traffic loads

$\omega$  = Inertia ratio

$$= \frac{I_D}{\sum I_{RRFC}} \quad (7.2)$$

$I_D$  = Strong - axis moment of inertia for the girder being investigated

$$\begin{aligned} \sum I_{RRFC} &= \text{Sum of the girders' strong - axis moments of inertia in one RRFC} \\ &= (2)(I_{Ext}) + I_{Int} \end{aligned} \quad (7.3)$$

$I_{Ext}$  = Strong-axis moment of inertia for the exterior girder

$I_{Int}$  = Strong-axis moment of inertia for the interior girder

$\psi$  = Adjustment factor to correct for the simplified analysis

For interior girders in RRFC bridges with BCB-type connections,

$$\psi = 0.4\omega^2 - 0.7\omega + 1.1 \quad (7.4)$$

For exterior girders in RRFC bridges with BCB-type connections,

$$\psi = -13.7\omega^3 + 10.4\omega^2 - 2.6\omega + 1.2 \quad (7.5)$$

For interior girders in RRFC bridges with WCB-type connections,

$$\psi = -1.7\omega^3 + 4.8\omega^2 - 4.1\omega + 1.9 \quad (7.6)$$

For exterior girders in RRFC bridges with WCB-type connections,

$$\psi = 1800\omega^3 - 270\omega^2 + 20.1\omega + 0.4 \quad (7.7)$$

For more information and details on the development of Equations 7.1 – 7.7, the reader is referred to the supplemental information provided in Appendix D. Sample calculations utilizing Equations 7.1 – 7.7 to determine live load moments and stresses in the BCB and WCB during LT2 testing are presented in Appendix E.

Illustrated above, Equation 7.1 uses statically determinate structures to determine the live load moment in a longitudinal girder. For the BCB, the structure was considered to be simply supported over its clear span, and  $M_{SD}$  was determined at midspan. Similarly, for the three-span WCB,  $M_{SD}$ , at midspan of the main span, was determined from a statically determinate WCB that was simply supported at its piers. Considering the WCB to be simply supported at its abutments would have produced an overly conservative  $M_{SD}$ , and therefore, was not used.

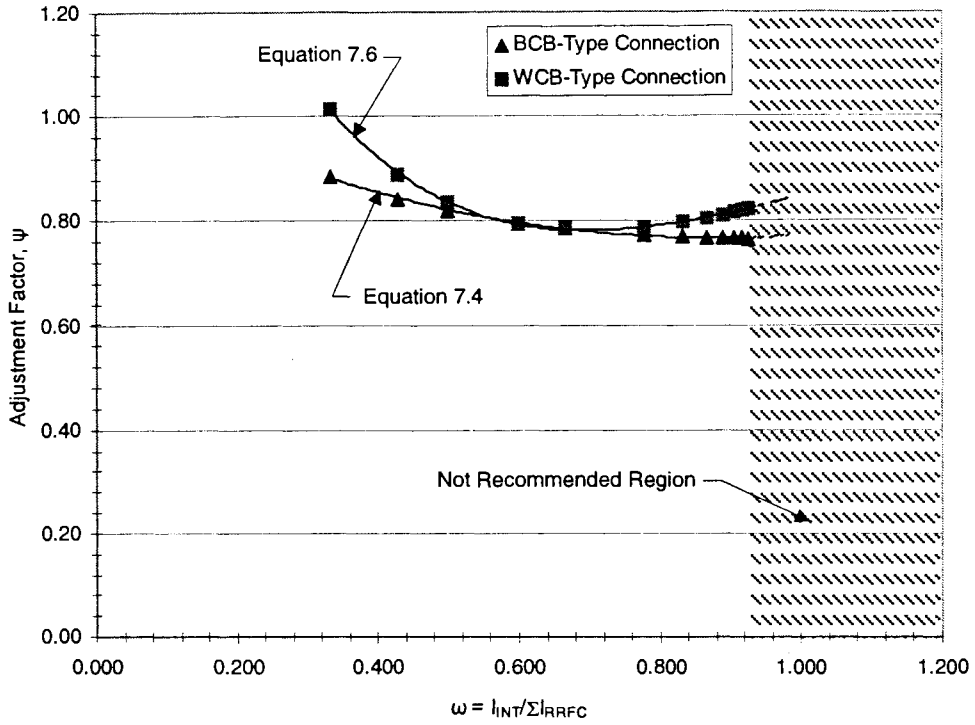
In addition to using statically determinate structures, Equation 7.1 simplifies the analysis through the use of the  $\psi$ -factor. These  $\psi$ -factors are presented in Equations 7.4 –

7.7 and are graphically presented in Figure 7.1. The  $\psi$ -factor adjusts Equation 7.1 for the simplification of using a statically determinate rather than a statically indeterminate structure, and also takes into account the transverse load distribution. Since the longitudinal flatcar connections used in WCB and BCB have different configurations (plus the fact that the WCB has transverse timber planks), transverse load distribution varies between the two RRFC bridges. This difference in behavior is illustrated in Figure 7.1; bridges with identical inertia ratios but different longitudinal flatcar connections (and the presence or absence of transverse timber planks) have different curves. Therefore,  $\psi$ -factors have been given for interior and exterior girders depending on the type of longitudinal flatcar connection used.

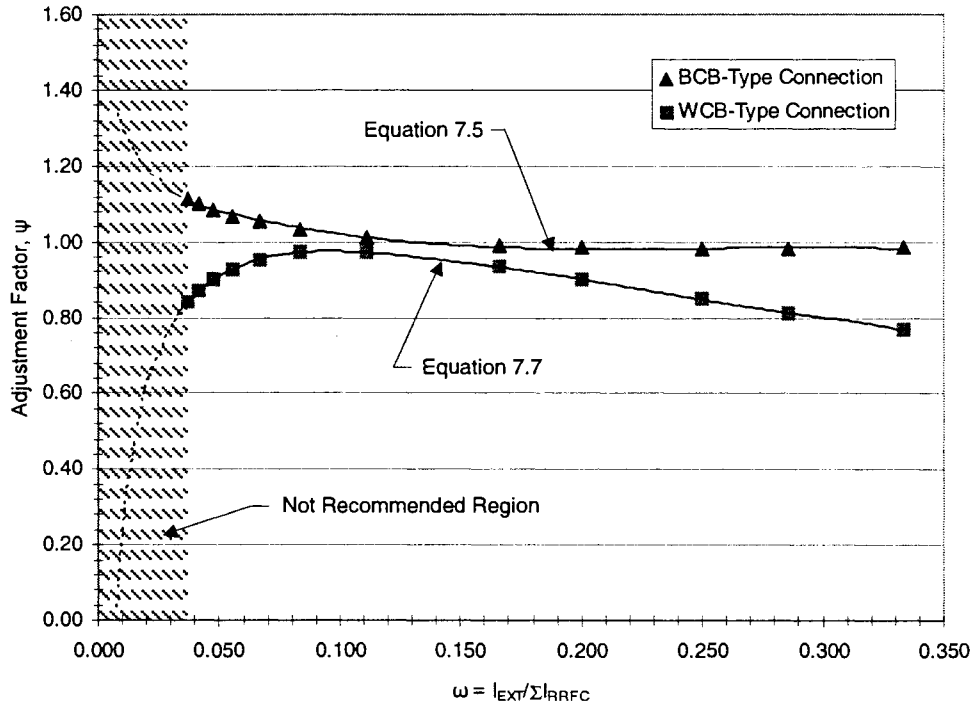
As can be seen in Figure 7.1a, the curve for Equation 7.4 is maximum at the left and decreases as  $\omega$  increases. Also in Figure 7.1a, the curve for Equation 7.6 is maximum at the left and reaches a minimum at  $\omega$  equal to 0.66; from there,  $\psi$  continually increases as  $\omega$  increases. In Figure 7.1b, the curve for Equation 7.5 is maximum at the left and gradually decreases as  $\omega$  increases. Also in Figure 7.1b, the curve for Equation 7.7 increases from the left until it reaches its maximum value at  $\omega$  equal to 0.095, and then it continually decreases as  $\omega$  increases.

Although the design recommendations greatly simplify the calculation of the live load moments in the longitudinal girders, the equations have limitations. First, the adjustment factors are only applicable if  $I_{int}/I_{Ext}$  is less than or equal to 26, which is the  $I_{int}/I_{Ext}$  ratio in the 89-ft RRFCs. Flatcars with  $I_{int}/I_{Ext}$  greater than 26 are not recommended for use in LVR bridge superstructures because more than likely their exterior girders are too small to accommodate longitudinal flatcar connections. As a result, these ranges are shaded and labeled as “not recommended” in Figure 7.1. Moreover, Equations 7.1 – 7.7 are only applicable to RRFC bridges that utilize three identical flatcars placed side-by-side and have longitudinal flatcar connections similar to those in the BCB and WCB (with timber planks).





a. Interior Girder



b. Exterior Girder

Figure 7.1. Relationships of adjustment factors and inertia ratios for use in Equation 7.1.

These equations are not applicable for bridges that use more or fewer than three flatcars because the “2/3” coefficient in Equation 7.1 is dependent upon three flatcars placed side-by-side in a bridge. In addition,  $M_{SD}$  for single-span and three-span RRFC bridges must be determined by using the same statically determinate structures as those described in this chapter and illustrated in Appendix E. Finally, as previously stated, these equations are only applicable to the interior and exterior girders in exterior RRFCs that experience the largest strains (stresses) in the bridge.

It should be noted that Equations 7.1 – 7.7 do not take into account the added flexural stiffness at the edge of the bridge due to the presence of a guardrail system. As a result, predicted girder live load moments will be conservative if the guardrail adds stiffness to the edge of the bridge. If the guardrail system adds minimal stiffness to the bridge, then the results from Equations 7.1 – 7.7 are accurate.

Using the equations previously presented, the section properties of the longitudinal girders, and the maximum live load moment in a statically determinate RRFC bridge, the live load moments and associated moments in critical longitudinal girders can be calculated. Then, live load stresses can be combined with the dead load stresses to obtain the maximum resultant stresses in the bridge. If the resultant stresses are less than the yield strength of the RRFC steel by an appropriate safety factor, then the RRFCs are adequate to support the loading condition causing the resulting stresses.

### **7.3 Suggested Changes in the Construction of the RRFC Bridges**

Based upon the construction of the BCB and the WCB, several modifications can be made in the construction process to improve the economy of the construction procedures in future RRFC bridges:

- If concrete is used in the substructure in future RRFC bridges, the cap beam should be constructed with a constant thickness rather than with steps to accommodate the different girder depths, as was done in the BCB bridge.

“Stepping” the top of the concrete abutment is difficult and requires additional construction time and formwork. Steel supports can be used (as was done in the WCB) to obtain the required elevation at various girder locations.

- All required modifications (such as removing “extra” material) and fabrications (such as drilling holes for transverse rods) on the RRFCs should be completed before the flatcars are installed in the field. This obviously makes work considerably easier (reducing field welds, work above water, making critical measurements easier, etc).
- When constructing longitudinal flatcar connections similar to those used in the BCB, it would be faster and easier to use stay-in-place formwork rather than removable formwork (See Figure 7.2). Removable formwork was used in the demonstration bridge so the concrete beams could be instrumented with strain gages during the field tests. If access to the reinforced concrete beams is not required, then stay-in-place formwork should be used.
- When constructing three-span bridges, support members and restraints at abutments should be constructed after all of the superimposed dead load (i.e. the driving surface) is added to the bridge. Such loading causes RRFC vertical displacement at the abutments, and therefore, changes the height of the required support member.

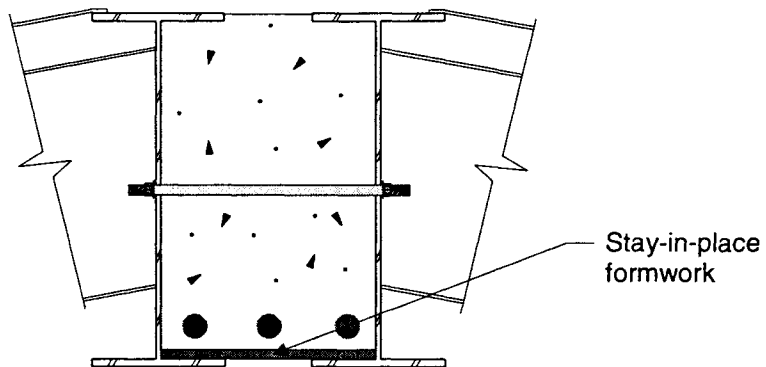


Figure 7.2. Stay-in-place formwork for the BCB longitudinal flatcar connection.

## 8. Summary and conclusions

### 8.1 Summary

In this investigation, the adequacy of RRFCs for use in LVR bridge superstructures was verified. The first task in the project was the inspection and selection of RRFCs for the two bridges. Four alternative flatcars were investigated, and through this process, five criteria were established to aid in the selection process. Using the selection criteria and engineering judgment, two different types of RRFCs were selected for the superstructures in the BCB and WCB.

After identifying the 56-ft RRFCs and the 89-ft RRFCs as potential flatcars for the BCB and WCB, respectively, their adequacy to carry Iowa legal loads was verified through grillage analyses. One flatcar of each type was initially subjected to Iowa legal loads and analyzed with a grillage model; it was determined that each flatcar could individually support an Iowa legal tandem truck. Based on these results, the five selection criteria were proven to be dependable for selecting structurally adequate RRFCs. Next, the grillage models were used to investigate structural connections between the flatcars; the analyses verified that adding longitudinal flatcar connections between the RRFCs provided transverse load distribution and significantly reduced the maximum deflections and strains in the longitudinal girders in the RRFC bridges. As a result, it was decided to use longitudinal flatcar connections in the RRFC bridges to improve the load sharing among the three flatcars.

After completing the analyses and designs, two bridges with different RRFCs, longitudinal flatcar connections, and substructure materials were constructed. The BCB utilized three 56-ft RRFCs that were placed side-by-side on concrete abutments; the two longitudinal connections between the flatcars utilized transverse threaded rods and reinforced concrete beams. A LCS nearly identical to the BCB connection was laboratory tested in torsion and flexure to confirm its structural adequacy and behavior for use as a

longitudinal flatcar connection. Even under extreme loading, the LCS maintained its shape and structural integrity. Thus, the connection was determined to have more than adequate strength for use in the 56-ft RRFC bridge.

In the WCB, three 89-ft RRFCs were placed side-by-side and supported by steel-capped piers and abutments at the bolsters and RRFC ends; this resulted in a 66-ft main span with two 10-ft end spans. The 89-ft RRFCs were connected with transverse threaded rods and the combination of welded steel plates and concrete that resembled a concrete-filled structural tube. Transverse timber planks were also used in the WCB to improve the load distribution. With the exception of the driven steel piling, all construction work for both bridges was completed by county personnel and ISU students. The construction procedures for each bridge are well documented in this thesis for use by other county crews.

Each demonstration bridge was field tested three times. LT1 was performed on a single RRFC before it was connected to adjacent flatcars, while LT2 was performed after the addition of the longitudinal connections, transverse timber planks (WCB only), driving surface, and guardrail (WCB only). Approximately one year later, LT3 was conducted to determine if the RRFC bridges' behavior had changed after being in service. In each test, deflections and strains were measured and recorded at critical locations in the bridge; the experimental results were compared with theoretical results obtained from the grillage models. There was good agreement between experimental and theoretical results, and the comparison between LT2 and LT3 test results did not reveal any change in RRFC bridge behavior after being in service for approximately one year. Most importantly, the RRFC bridges were proven to be more than structurally adequate to support Iowa legal traffic loads.

Finally, design recommendations were established to assist in determining the maximum live load moments in the longitudinal girders in the flatcars of a given RRFC

bridge. Through proper application of the design recommendations, a RRFC bridge can be easily designed to support Iowa legal loads.

## 8.2 Conclusions

Considering all aspects of this investigation, the following conclusions can be made about the use of RRFCs in LVR bridge superstructures:

- Through the design, construction, field testing, and analysis of two RRFC demonstration bridges, it has been determined that RRFC bridges are a viable, economic alternative for LVR bridges.
- The success of the bridges can be directly linked to the careful selection of the RRFCs, design of the longitudinal flatcar connections, and overall design and construction practices.
- Complete RRFC bridge behavior may be predicted using grillage modeling and analysis.
- The design recommendations simplify the live load distribution analysis through use of statically determinate structures and design aids. These recommendations have been verified (through field test results) to accurately predict the maximum live load moments in the girders of longitudinally connected RRFCs.
- Both types of longitudinal flatcar connections provided adequate connection and load distribution among the three flatcars in each bridge. In addition, both types of substructure materials provided sufficient support to the RRFC superstructures.
- With proper equipment and experience, it is envisioned that all construction work for RRFC bridges can be completed with county personnel and equipment.
- RRFC bridge superstructures can be built for less than one-half the cost of a conventional superstructure.

## 9. RECOMMENDED RESEARCH

Additional research is recommended to expand the use of RRFC bridges on low-volume roads. A brief description of several items that should be investigated follow:

- Additional RRFC bridges should be field tested to obtain more strength, behavior and distribution data. This data would make it possible to improve the conservative live load distribution factors obtained in this study that only tested two RRFC bridges.
- A rating methodology or guidelines for RRFC bridges needs to be developed so that county engineers and consultants can rate these bridges. The testing of additional RRFC bridges previously noted would provide a better data base and thus an improved rating procedure.
- Alternative, more economical substructure systems should be investigated for the 89-ft RRFC bridges. In this investigation, two abutments and two piers were used for the 89 ft cars. To reduce the substructure cost for this size of bridge, various substructure configurations should be investigated:
  - Two piers without end abutments.
  - Two piers with sheet pile abutments.
  - Three piers (one at midspan and one at each bolster) and no abutments.
- Other longitudinal connections between flat cars should be reviewed.
  - Can the number of transverse rods that were used in the BCB be reduced? Are there better methods of connecting the flatcars than the R/C beam-threaded rod combination?
  - Develop longitudinal flatcar connections that accommodate RRFCs with extremely small exterior girders (i.e. like those in the WCB) so that the timber planking could be omitted.
- Investigate RRFC bridge replacement alternatives for intermediate span lengths (i.e. between 56 ft and 89 ft). One possibility would be to remove the end regions of 89 ft cars beyond the bolsters. For most RRFCs, this would result in a 66 ft span.
- In some situations, only a single lane bridge is required. Two bridges in Buchanan County have been constructed using only two RRFCs. These bridges, as well as others similar to them should be field tested to learn more about their strength and behavior.
- Different means of obtaining wider bridges with only two RRFC installed could be investigated.

**APPENDIX A**

**CONTACT INFORMATION FOR RAILROAD FLATCAR SUPPLIERS**



**Erman Corporation, Inc.**

6600 Thorn Drive  
Kansas City, KS 66106  
(913) 287-4800

**Skip Gibbs Company**

P.O. Box 260  
Redwood Valley, CA 95470  
(707) 485-5822

**TTX Company**

101 N. Wacker Drive  
Chicago, IL 60606  
(312) 853-3223

**Gateway Pipe & Supply, Inc.**

720 Olive St.  
Suite 2175  
St. Louis, MO 63101  
1-800-489-4321  
(314) 621-6094

**APPENDIX B**

DETAILS FOR THE LCS CONVENTIONAL METHOD OF ANALYSIS

A brief summary describing the development of the results from the LCS conventional method of analysis presented in Section 5.1.1.1 is provided in the following sections.

## B.1 W-shape Warping Stresses

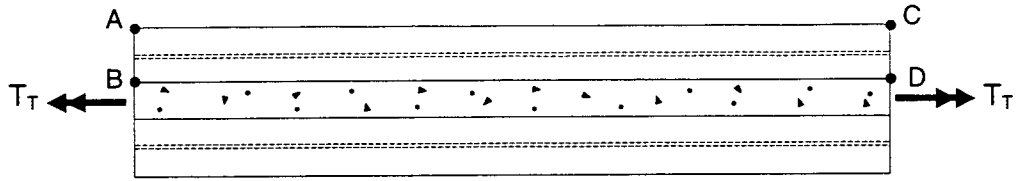
Figure B.1a presents the LCS in an unrestrained condition and subjected to torsional moment  $T_T$ , which is the total torsional moment applied to the LCS (See Figure 5.1a).

Figure B.1b presents one W-shape isolated from the LCS and subjected to  $T_S$ , the portion of  $T_T$  distributed to the W-shape (See Figure 5.1b). For this unrestrained condition, Figure B.1b illustrates the flange warping that develops at the ends of the beam, where the subscripts T and B refer to the top and bottom flanges (i.e.  $A_T$  and  $A_B$ , and  $B_T$  and  $B_B$ , etc. are the stresses in the top and bottom flanges at the four points).

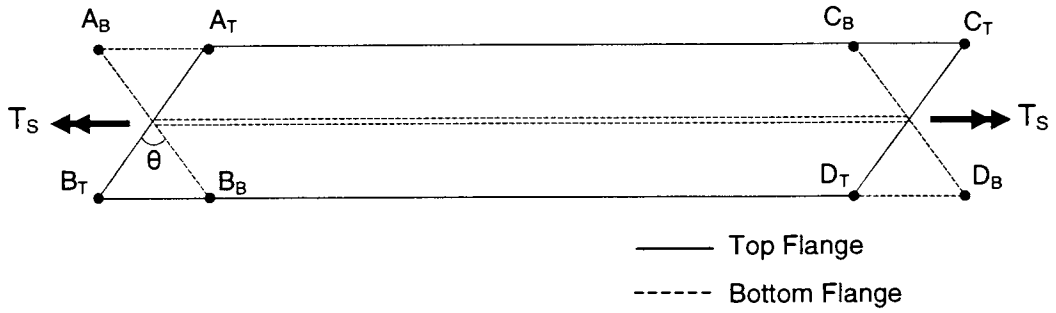
Figure B.1c illustrates the effects of boundary conditions; if warping is restrained at the ends of the member, a moment,  $M_F$ , develops in the flanges and causes tensile and compressive stresses of magnitude  $\sigma_o$  at  $A_T$  and  $B_T$ , respectively. If the warping restraint is present over the entire depth of the member, compressive and tensile stresses develop at  $A_B$  and  $B_B$ , respectively. Thus, to accurately predict warping behavior in the LCS, the boundary conditions need to be defined. As described in Section 5.1.1.1, the rotationally restrained end of the LCS was assumed to have complete warping restraint, but the rotating end of the LCS was assumed to have partial warping restraint. Thus, two analyses were performed with different boundary conditions: one analysis with “Fixed-Free” boundary conditions, and one with “Fixed-Fixed” boundary conditions.

Since the W-shape in Figure B.1b is subjected to constant torsional moment, the rotational and warping behavior of the W-shape can be described by Equations B.1 – B.4.

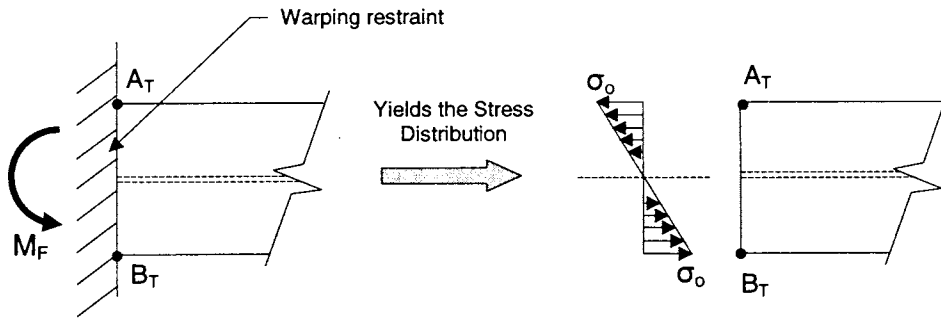
$$\phi_S = A \sinh(\lambda z) + B \cosh(\lambda z) + C + \frac{T_S}{G_S J} z \quad (\text{B.1})$$



a. Top view of the LCS



b. Flange warping of an unrestrained W-shape



c. Stresses resulting from warping-restraint boundary conditions

Figure B.1. Warping behavior in an unrestrained LCS.

$$\phi'_S = A\lambda \cosh(\lambda z) + B\lambda \sinh(\lambda z) + \frac{T_S}{G_S J} \tag{B.2}$$

$$\phi''_S = A\lambda^2 \sinh(\lambda z) + B\lambda^2 \cosh(\lambda z) \tag{B.3}$$

$$\lambda = \sqrt{\frac{G_S J}{E_S C_W}} \tag{B.4}$$

where,

$z$  = Distance from the fixed torsional restraint to a desired cross-section, in.

$\phi_S$  = W-shape rotation on a cross-section, rad.

$J$  = Torsional constant for the section, in<sup>4</sup>

$G_S$  = Shear modulus of elasticity for steel (11,200 ksi)

$E_S$  = Modulus of elasticity for steel (29,000 ksi)

$C_W$  = Warping constant for the section, in<sup>6</sup> =  $\frac{t_f b_f^3 (d - t_f)^2}{24}$

Constants A, B, and C are dependent upon the boundary conditions at the ends of the W-shape. To apply the boundary conditions to Equations B.1 – B.3,  $\phi_S'$  and  $\phi_S''$  must be defined. Simply stated,  $\phi_S'$  is directly related to the warping angle,  $\theta$  (Figure B.1b), between the top and bottom flanges. If  $\theta$  is equal to zero,  $\phi_S'$  is equal to zero. Next,  $\phi_S''$  is directly related to the ability of the warping restraints to develop  $M_F$ . If there is no warping resistance at a boundary (i.e. free boundary condition),  $M_F$ , and thus,  $\phi_S''$  is zero. Thus, the boundary conditions for the “Fixed-Free” analysis are:

$$\text{B.C. \#1: At } z = 0, \phi_S = 0$$

$$\text{B.C. \#2: At } z = 0, \phi_S' = 0$$

$$\text{B.C. \#3: At } z = L, \phi_S'' = 0$$

Application of these boundary conditions to Equations B.1 – B.3 results in the following constants for the “Fixed-Free” analysis:

$$A = -\frac{T_S}{\lambda GJ} \quad (\text{B.5})$$

$$B = \frac{T_S \tanh(\lambda L)}{\lambda GJ} \quad (\text{B.6})$$

$$C = -\frac{T_S \tanh(\lambda L)}{\lambda GJ} \quad (\text{B.7})$$

where,

$L$  = Length of the W-shape in torsion, in.

Similarly, the boundary conditions for the “Fixed-Fixed” analysis are:

$$\text{B.C. \#1: At } z=0, \phi_S = 0$$

$$\text{B.C. \#2: At } z=0, \phi_S' = 0$$

$$\text{B.C. \#3: At } z=L, \phi_S' = 0$$

Application of these boundary conditions to Equations B.1 – B.3 results in the following constants for the “Fixed-Fixed” analysis:

$$A = -\frac{T_S}{\lambda G_S J} \quad (\text{B.8})$$

$$B = \frac{T_S}{\lambda G_S J} [\coth(\lambda L) - \operatorname{csch}(\lambda L)] \quad (\text{B.9})$$

$$C = \frac{T_S}{\lambda G_S J} [\operatorname{csc}h(\lambda L) - \coth(\lambda L)] \quad (\text{B.10})$$

The warping stress,  $\sigma_w$ , in the flanges of the w-shapes is determined using Equation B.11.

$$\sigma_w = \frac{E_S b h}{4} \phi_S'' \quad (\text{B.11})$$

## B.2 Compatibility between the W-shapes and the Reinforced Concrete Beam

Since a complete rigid connection between the W-shapes and concrete is assumed in the conventional method of analysis, the rotation on the concrete beam,  $\phi_C$ , must equal  $\phi_S$  as shown in Equation B.12.

$$\phi_C = \phi_S = \phi \quad (\text{B.12})$$

where,

$\phi$  = Composite LCS rotation, rad.

The concrete torsional moment,  $T_C$ , which is required at the rotating end of the LCS to rotate the reinforced concrete beam  $\phi$  radians, is given by Equation B.13.

$$T_C = \frac{a^3 b G_C \phi \beta}{L} \quad (\text{B.13})$$

$T_C$  = Torsional moment on the reinforced concrete beam, k –in.

$G_C$  = Shear modulus of Elasticity for concrete, ksi

$a$  = Width of the reinforced concrete beam, in.

$b$  = Height of the reinforced concrete beam, in.

$$\beta = 0.196 \text{ for } \frac{b}{a} \approx 1.5 \quad [10]$$

Therefore, the total torsional moment,  $T_T$ , required by the lever arm to rotate the composite LCS  $\phi$  radians is given Equation B.14.

$$T_T = 2T_S + T_C \quad (\text{B.14})$$

### B.3 Correction for the W-shape Vertical Displacement

The relationship between  $\phi$  and  $\Delta$ , the w-shape vertical displacement (where P' is the location of Point P after the LCS rotates  $\phi$  radians), is shown in Figure B.2a.

Equation B.15 relates  $\phi$  and  $\Delta$ .

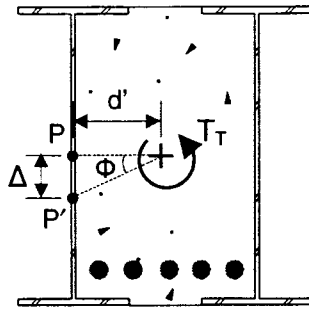
$$\Delta = d' \tan \phi \quad (\text{B.15})$$

With vertical displacement and rotation at one end of the W-shape (assuming a fixed support at the rotationally restrained end of the beam), the flexural behavior is similar to that of a cantilevered beam for the "Fixed-Free" analysis. The displacement at the end of a cantilevered beam,  $\Delta_{\text{End}}$ , due to a concentrated force R shown in Figure B.2b, can be calculated using Equation B.16.

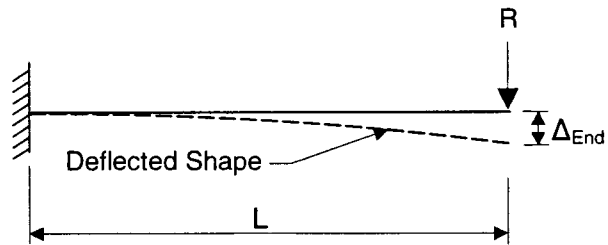
$$\Delta_{\text{End}} = \frac{RL^3}{3E_S I_S} \quad (\text{Fixed-Free}) \quad (\text{B.16})$$

The force R represents the vertical force applied to the end of the W-shape from the lever arm. By equating the displacements in Equations B.15 and B.16, the force R can be expressed as a function of  $\phi$  (Equation B.17).

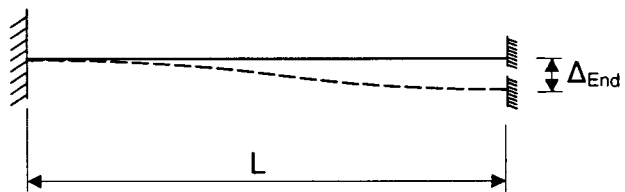
$$R = \frac{3d'E_S I_S}{L^3} \tan \phi \quad (\text{Fixed-Free}) \quad (\text{B.17})$$



a. Relationship between Rotation,  $\Phi$ , and Deflection,  $\Delta$



b. Equivalent Force,  $R$ , on Rotating End of the LCS for Fixed-Free Torsional Boundary Conditions



c. Flexural Behavior of the LCS under Displacement for Fixed-Fixed Torsional Boundary Conditions

Figure B.2. Combination of flexure and torsion in the LCS.



Next, the moment,  $M_D$ , and flexural stress,  $\sigma_D$ , due to force  $R$  may be calculated at any section along the  $W$ -shape member by using Equations B.18 and B.19. Note that Equation B.18 may only be used for the “Fixed-Free” analysis.

$$M_D = R(L - z) \quad (\text{Fixed-Free}) \quad (\text{B.18})$$

$$\sigma_D = \frac{M_D c}{I_S} \quad (\text{B.19})$$

where,

$c$  = Distance from the section neutral axis to the location of stress, in.

$I_S$  = Moment of inertia for the  $W$ -shape, in<sup>4</sup>

As illustrated in Figure B.2c, the flexural behavior of the  $W$ -shape for the “Fixed-Fixed” analysis is not the same as that of a cantilevered beam, and thus, a different  $M_D$  must be calculated for this analysis. Following procedures similar to those for the “Fixed-Free” analysis,  $M_D$  for the “Fixed-Fixed” analysis was developed and is presented in Equation B.20. Application of Equations B.19 and B.20 yields  $\sigma_D$  for the “Fixed-Fixed” analysis.

$$M_D = \frac{6d'E_S I_S}{L^2} \left( \frac{2z}{L} - 1 \right) \tan \phi \quad (\text{Fixed-Fixed}) \quad (\text{B.20})$$

Finally, the total resultant normal stress on a section,  $\sigma_T$ , may be expressed as the addition of the flexural and warping normal stress as shown in Equation B.21, where tensile stresses are assigned positive values, and compressive stresses are assigned negative values.

$$\sigma_T = \sigma_D + \sigma_W \quad (\text{B.21})$$

Using Equations B.1 – B.21, an Excel program was developed to analyze the LCS for any magnitude of  $T_T$ . Figure B.3 illustrates a flow chart for the Excel program. Input for the program includes LCS section properties, an estimate for  $T_S$ , and a torsional moment,  $T_{\text{Desire}}$ , which is the desired value of  $T_T$ . The program calculates  $T_T$  and compares it to

$T_{\text{Desire}}$ ;  $T_S$  is adjusted by the program until  $T_T$  is equal to  $T_{\text{Desire}}$ . Finally,  $\phi$  and  $\sigma_T$  are calculated along the length of the LCS.

It is worthwhile noting that at the rotationally restrained end of the LCS, the flexural and warping normal stresses have opposite signs, and therefore, warping actually reduces the normal stresses at that location. For example, consider  $A_T$  located at the rotationally restrained end of the LCS in Figure B.1b. Boundary conditions and warping cause tensile normal stresses at that point, but flexural compression stresses develop due to upward displacement at the rotating end of the beam due to the torsional moment created by the load applied to the lever arm.

The relationships determined by the conventional method of analysis for the warping and flexural normal stresses along the longitudinal axis for the flange containing points  $A_T$  and  $C_T$  (and the flange containing  $B_B$  and  $D_B$ ) are presented in Figures 5.2 – 5.4. Rotation along the longitudinal axis of the LCS for both analyses is presented in Figure 5.5. As noted in Section 5.1, the conventional method of analysis is limited to small deflections since it assumes complete composite behavior in the LCS.

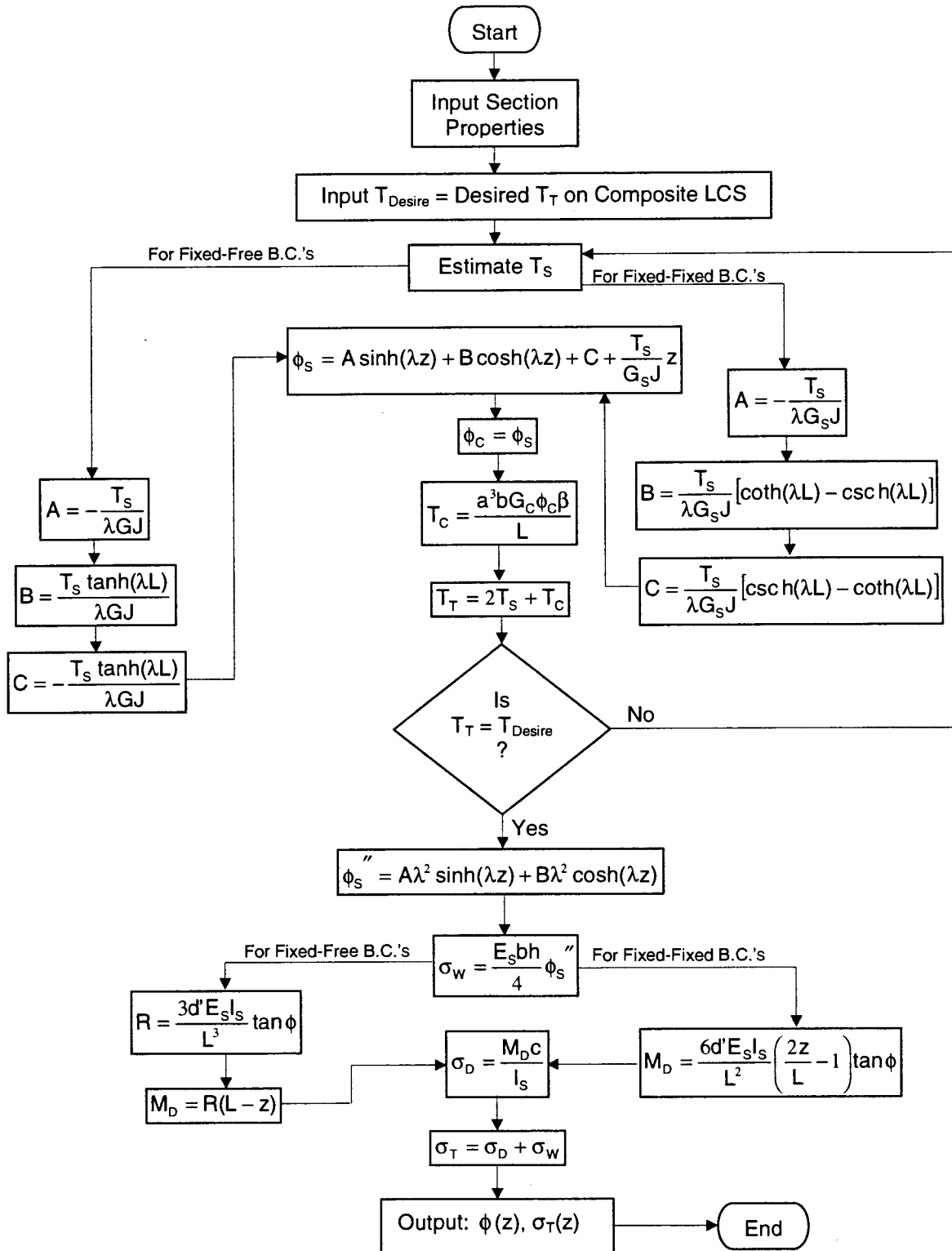


Figure B.3. Excel program flow chart for evaluating LCS rotations and stresses.

**APPENDIX C**

**DETAILS FOR THE LCS FLEXURAL ANALYSIS**

A brief summary describing the development of the LCS composite flexural analysis presented in Section 5.1.2 is provided in the following sections.

### C.1 LCS Composite Analysis

As discussed in Section 5.1.2, the composite LCS was simply supported and subjected to flexure by two concentrated forces,  $P_1$  and  $P_2$ , as illustrated in Figure 5.12. The distribution of these forces among the two W-shapes and concrete beam was unknown. As a result, the flexural analysis was completed using the compatibility of vertical deflections between the W-shapes and concrete beam at the SPDTs located by Point G in Figure 5.12.

Consider the simply supported beam loaded by the arbitrarily positioned, concentrated load,  $P$ , in Figure C.1. If the beam is a W-shape member, Equation C.1 is used to determine the vertical displacement at Point G resulting from the concentrated load.

$$\Delta_G = \frac{K \cdot P}{E_S I_S} \quad (\text{C.1})$$

where,

$\Delta_G$  = Vertical displacement at Point G

$K$  = A constant

$E_S$  = Modulus of elasticity for steel

$I_S$  = Moment of inertia for the W-shape

However, if the beam in Figure C.1 is a reinforced concrete beam, Equation C.2 is used to

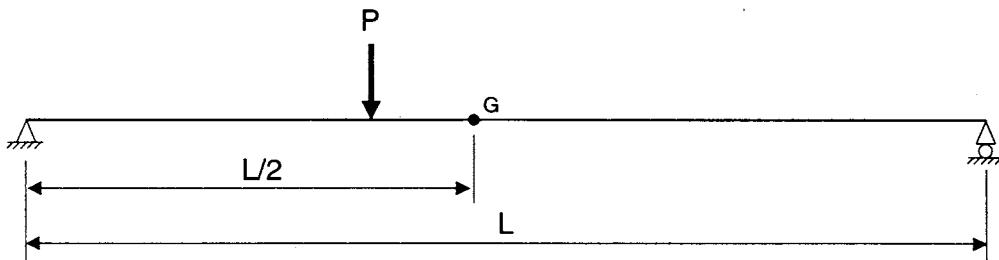


Figure C.1. Simply supported beam subjected to flexure by a concentrated force,  $P$ .

determine the vertical displacement at Point G resulting from the concentrated load.

$$\Delta_G = \frac{K \cdot P}{E_C I_C} \quad (C.2)$$

where,

$E_C$  = Modulus of elasticity for reinforced concrete beam

$I_C$  = Moment of inertia for the reinforced concrete beam

Due to compatibility between the steel W-shapes and reinforced concrete beam in the LCS, the vertical displacement at Point G for the W-shapes and reinforced concrete beam must be equal. By equating the vertical displacements in Equations C.1 and C.2, Equation C.3 results; this expression reveals the theoretical distribution between the W-shapes and reinforced concrete beam when the LCS is subjected to flexural loads.

$$P_C = \frac{E_C I_C}{E_S I_S} P_S \quad (C.3)$$

where,

$P_S$  = Concentrated force distributed to the W-shape

$P_C$  = Concentrated force distributed to the reinforced concrete beam

Thus, Equations C.4 – C.7 were developed for the LCS composite flexural analysis. For location of Point 1 and Point 2, see Figure 5.12.

$$P_{1,C} = \frac{E_C I_C}{E_S I_S} P_{1,S} \quad (C.4)$$

$$P_{2,C} = \frac{E_C I_C}{E_S I_S} P_{2,S} \quad (C.5)$$

$$P_1 = 2P_{1,S} + P_{1,C} \quad (C.6)$$

$$P_2 = 2P_{2,S} + P_{2,C} \quad (C.7)$$

where,

$P_1$  = Total concentrated force at Point 1 on the LCS

$P_2$  = Total concentrated force at Point 2 on the LCS

$P_{1,S}$  = Concentrated force distributed to a W-shape at Point 1

$P_{2,S}$  = Concentrated force distributed to a W-shape at Point 2

$P_{1,C}$  = Concentrated force distributed to the reinforced concrete beam at Point 1

$P_{2,C}$  = Concentrated force distributed to the reinforced concrete beam at Point 2

Using Equations C.4 – C.7, an Excel program was developed to perform distribution calculations for the LCS Service Flexure Tests. A flow chart for the Excel Flexure Program is presented in Figure C.2. Input for the program includes section properties for the W-shapes and reinforced concrete beam, and  $P_{1,Desire}$  and  $P_{2,Desire}$ , which are total concentrated forces for which the LCS is to be evaluated. Then, the program performs calculations to determine the distribution of concentrated loads to the W-shapes and reinforced concrete beam.

After the distribution analysis was complete, moment diagrams were developed and calculations were performed to obtain the stresses and strains in the W-shapes. Figure 5.13 presents the theoretical top and bottom flange stresses in a W-shape for 1 kip force for each concentrated load. Figure 6.1 presents theoretical and experimental results for a LCS Service Flexure Test.

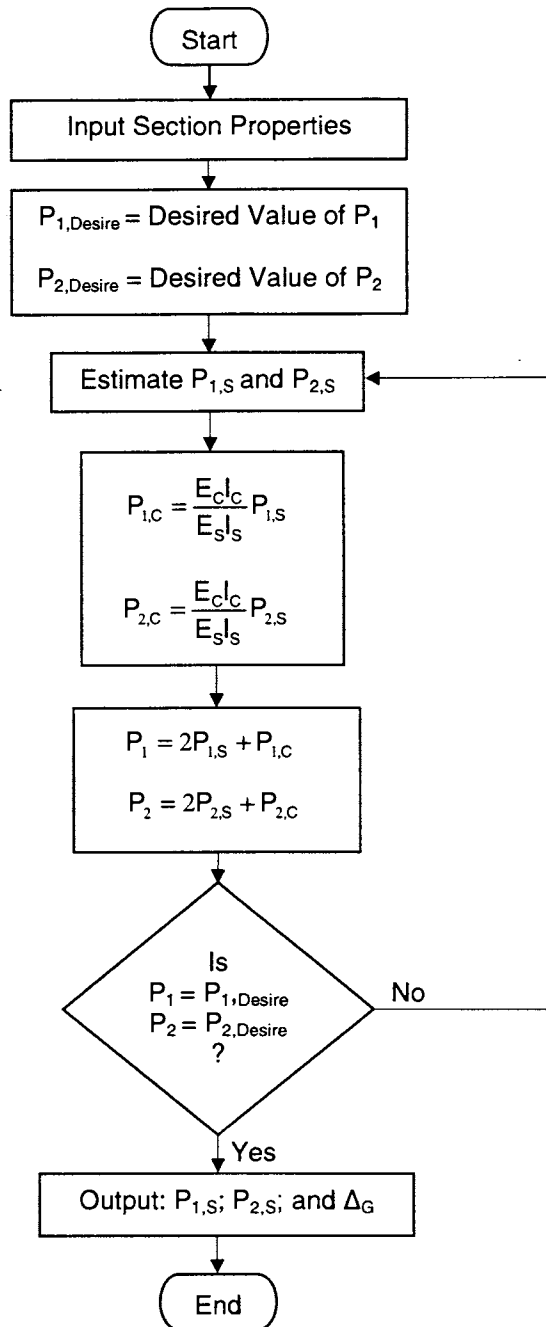


Figure C.2. Excel program flow chart for evaluating LCS flexure distribution.



**APPENDIX D**

**DEVELOPMENT OF THE DESIGN RECOMMENDATIONS**

The design recommendations presented in Chapter 7 were developed by using a combination of basic engineering principles and grillage models for each RRFC (See Chapter 5). Using the design recommendations, one uses the maximum moment in a statically determinate structure, an inertia ratio, and an adjustment factor to calculate the maximum live load moments in the RRFC bridge girders. The development of the design recommendations is presented in the subsequent sections.

### D.1 Moment Fraction for the Critical RRFC

Using Iowa legal truck loads, the maximum moment on the RRFC bridge can be easily determined if the structure is statically determinate. As discussed in Chapter 7, even if the structure is statically indeterminate, it is converted into a statically determinate structure to find the maximum statically determinate moment,  $M_{SD}$ , in the structure. As described in Chapter 7, the adjustment factor,  $\Psi$ , corrects for the simplification.

To determine the moment in the critical girders,  $MF_{RRFC}$ , the fraction of  $M_{SD}$  that is distributed to the critical flatcar (i.e. a side flatcar), must be determined. As presented in Chapter 6, the maximum girder strains occurred in a side RRFC when a truck was transversely positioned at that side of the bridge; thus, this transverse truck positioning will result in the largest moment to be supported by a side flatcar. Consider the BCB subjected to transverse truck loading in Figure D.1; Equation D.1 is a trend line (fit to LT2 experimental deflection data) that describes the deflected shape of the BCB for the given loading condition.

$$y_{BCB} = (-3 \cdot 10^{-6})x^2 + (6 \cdot 10^{-6})x + 0.0003 \quad (D.1)$$

where,

$y_{BCB}$  = Vertical displacement of the BCB at location  $x$

$x$  = Transverse location in the BCB

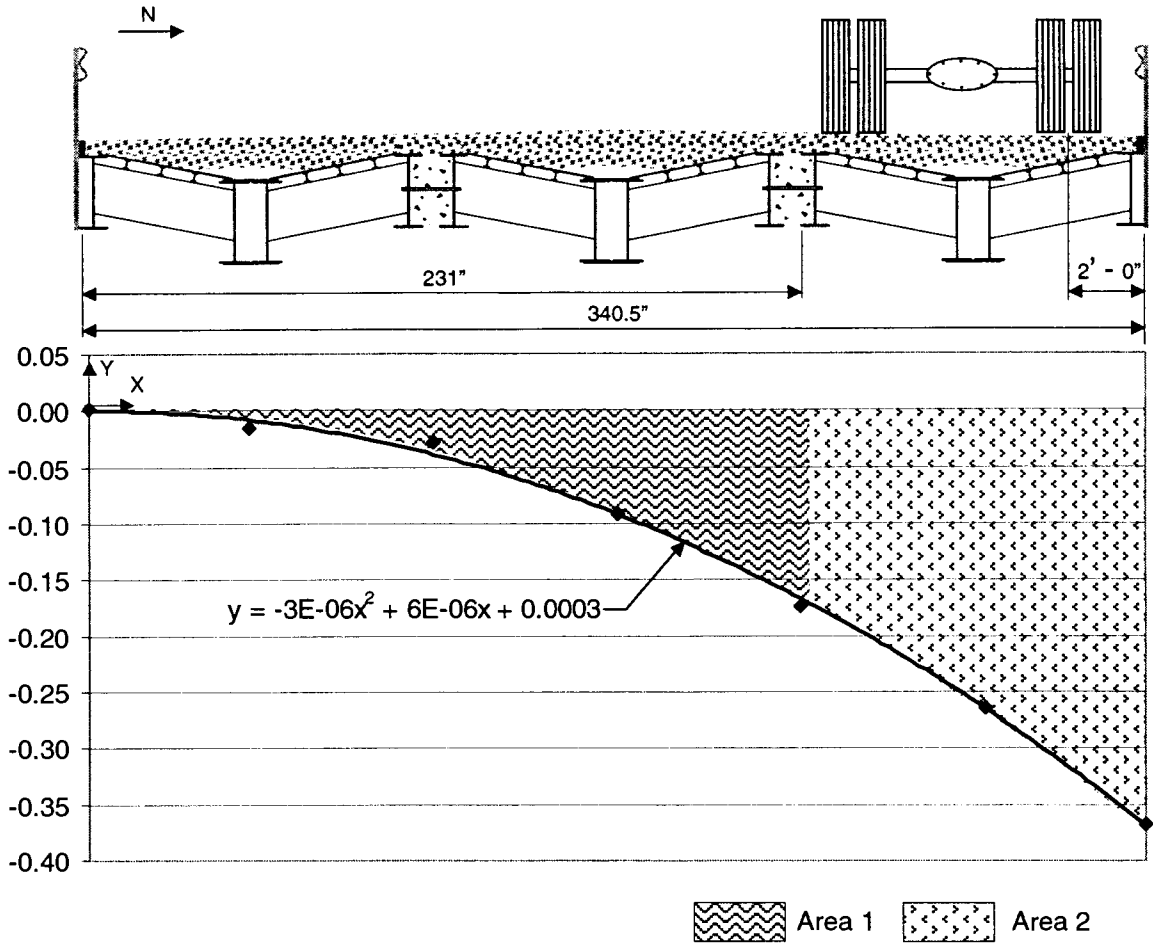


Figure D.1. Energy of the BCB system for transverse truck positioning.

The area under the deflection curve, the addition of  $A_1$  and  $A_2$ , is the total energy of the system. Thus,  $MF_{RRFC}$  is essentially the fraction of the system energy that is bounded within the width of the side RRFC ( $231 \text{ in.} < x < 340.5 \text{ in.}$ ). Thus,  $A_1$ ,  $A_2$ , and  $MF_{RRFC}$  are calculated by equations D.2 – D.4.

$$A_1 = \int_0^{231} (-3 \cdot 10^{-6})x^2 + (6 \cdot 10^{-6})x + 0.0003 \, dx \quad (\text{D.2})$$

$$A_2 = \int_{231}^{340.5} (-3 \cdot 10^{-6})x^2 + (6 \cdot 10^{-6})x + 0.0003 \, dx \quad (\text{D.3})$$

$$MF_{RRFC} = \frac{A_2}{A_1 + A_2} \quad (D.4)$$

Thus, for the BCB:

$$A_1 = -12.097$$

$$A_2 = -26.931$$

$$MF_{RRFC} = 0.69$$

Similarly, for the WCB presented in Figure D.2,  $MF_{RRFC}$  is the fraction of the system energy that is bounded within the width of the side RRFC (215.5 in.  $< x < 325$  in.). Equation D.5 describes the deflected shape of the WCB subjected to the eccentric loading in LT2.

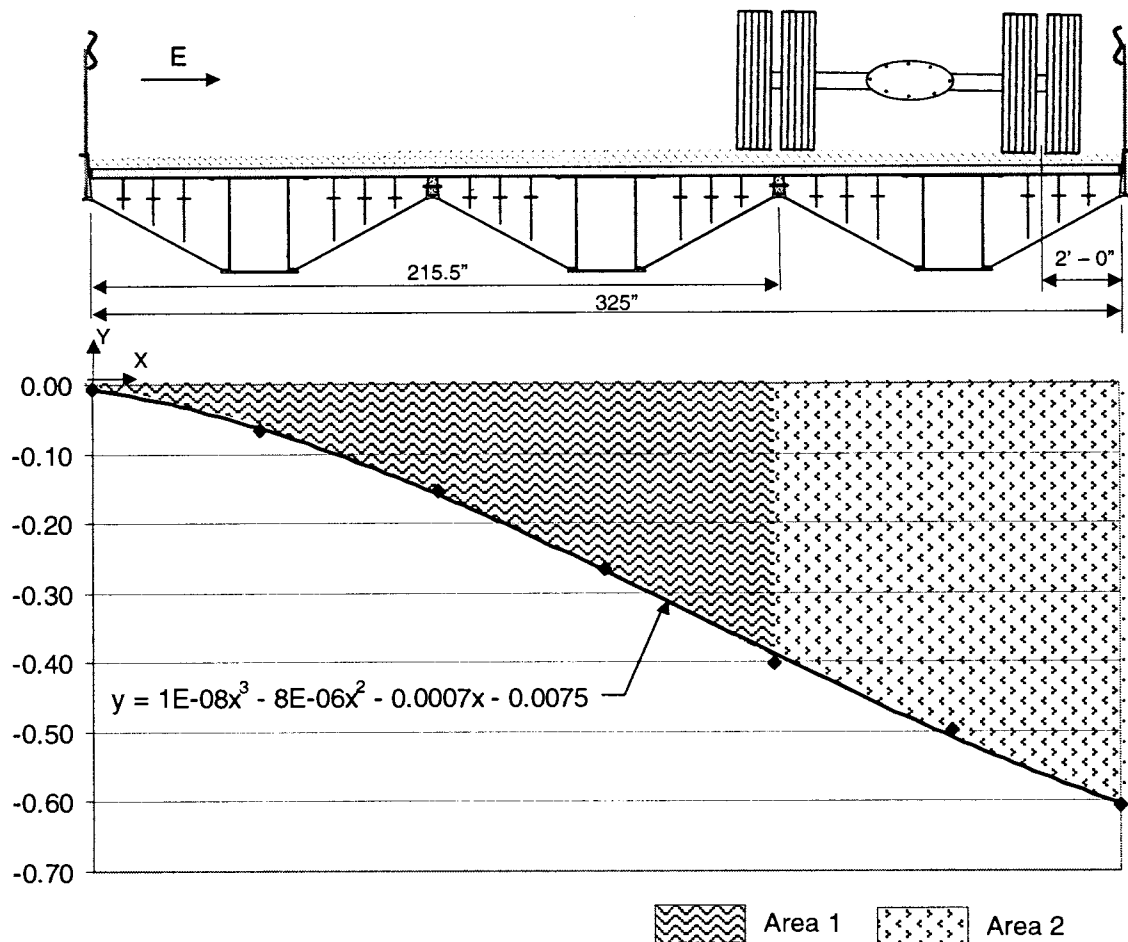


Figure D.2. Energy of the WCB system for transverse truck positioning.

$$y_{WCB} = (1 \cdot 10^{-8})x^3 - (8 \cdot 10^{-6})x^2 - 0.0007x - 0.0075 \quad (D.5)$$

$A_1$  and  $A_2$  for the WCB are calculated by Equations D.6 – D.7.

$$A_1 = \int_0^{215.5} (1 \cdot 10^{-8})x^3 - (8 \cdot 10^{-6})x^2 - 0.0007x - 0.0075 \, dx \quad (D.6)$$

$$A_2 = \int_{215.5}^{325} (1 \cdot 10^{-8})x^3 - (8 \cdot 10^{-6})x^2 - 0.0007x - 0.0075 \, dx \quad (D.7)$$

Thus, for the WCB,

$$A_1 = -39.166$$

$$A_2 = -63.890$$

$$MF_{RRFC} = 0.62$$

The average value of  $MF_{RRFC}$  has been used in the design recommendations.

$$MF_{RRFC,Ave} = 0.655 \approx \frac{2}{3}$$

Thus, Equation D.8 presents  $M_{RRFC}$ , the maximum moment that must be supported by a side flatcar (the critical flatcar).

$$M_{RRFC} = \frac{2}{3}M_{SD} \quad (D.8)$$

## D.2 Inertia Ratios for the Critical Girders

The moment that is carried by each flatcar is distributed to its girders according to each girder's inertia ratio,  $\omega$ . The inertia ratio for each girder is presented in Equation 7.2.

$$\omega = \frac{I_D}{\sum I_{RRFC}} \quad (7.2)$$

where,

$I_D$  = Strong - axis moment of inertia for the girder being investigated

$\sum I_{RRFC}$  = Sum of the girders' strong - axis moments of inertia in one RRFC

$$= (2)(I_{Ext}) + I_{Int} \quad (7.3)$$

Thus, Equation D.9 approximates the moment that is distributed to each girder.

$$M_{\text{Girder}} = \frac{2}{3} \omega M_{\text{SD}} \quad (\text{D.9})$$

### D.3 Adjustment Factors

The moments calculated by Equation D.9 do not consider the effects of transverse load distribution caused by the longitudinal flatcar connections, and they also have not been corrected for the simplification of using a statically determinate rather than a statically indeterminate structure. Thus, an adjustment factor has been used in the design recommendations to account for these issues.

The grillage models described in Chapter 5 accurately predicted bottom girder strains that resulted from the live load moment in each girder for each bridge. Thus, these models were utilized to develop adjustment factors (See Section 7.2) for use in the design recommendations. The adjustment factor is defined in Equation D.10.

$$\psi = \frac{M_{\text{Grillage}}}{M_{\text{Girder}}} \quad (\text{D.10})$$

Adjustment factors were calculated for the critical girders (interior girder and exterior girder at the edge of the bridge) in each bridge. In addition, section properties for the RRFCs were altered, and additional analyses were performed with the grillage models to develop adjustment factors for RRFC bridges constructed with other types of flatcars. These adjustment factors were plotted for each critical girder and are presented in Figure 7.1. Trend lines were fit to each plot and are listed as Equations 7.4 – 7.7.

By incorporating the adjustment factor into equation D.9, the maximum live load moments for each girder can be calculated through application of Equation 7.1.

$$M_{\text{LL}} = \frac{2}{3} \psi \omega M_{\text{SD}} \quad (\text{7.1})$$

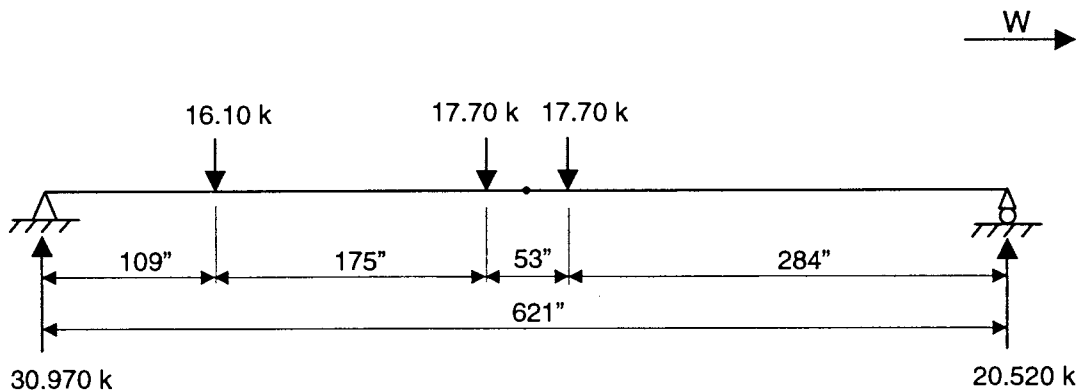
**APPENDIX E**

**SAMPLE CALCULATIONS FOR DETERMINING LIVE LOAD MOMENTS**

In the sections that follow, the equations from Chapter 7 are used to determine maximum live load moments in the longitudinal girders in the BCB and WCB. To verify that the design recommendations are conservative, LT2 truck loads will be applied to each bridge to determine  $M_{LL}$ , the live load moment in the girder being investigated. Then,  $M_{LL}$  and girder section properties will be used to calculate strains that result from the truck loads, and these strains will be compared to those recorded in LT2 to verify the conservativeness of the design recommendations. For design purposes, the same calculations are performed, however Iowa legal traffic loads need to be applied to the bridge rather than the truck loads used in the field tests. As previously stated, the equations do not account for increased bridge stiffness due to the presence of guardrails.

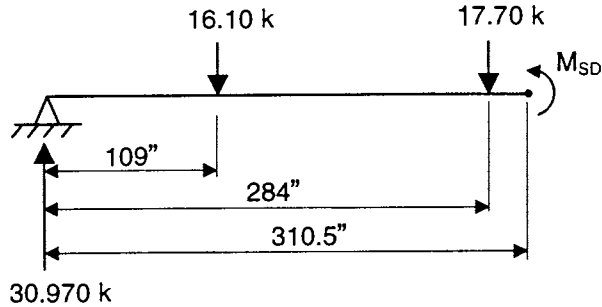
### E.1 BCB Live Load Moment Calculations

Develop a statically determinate structure for the BCB. Using the LT2 axle loads given in Figure 4.14, center the tandem axles on the span and analyze the BCB as simply supported over its clear span:



Determine the largest live load moment,  $M_{SD}$ , at midspan in the statically determinate BCB.





$$M_{SD} = (30.970\text{ k})(310.5\text{ in.}) - (16.10\text{ k})(310.5 - 109\text{ in.}) - (17.70\text{ k})(310.5 - 284\text{ in.}) = \underline{5,904.2\text{ in} \cdot \text{k}}$$

Determine section properties for the longitudinal girders in the BCB RRFC (Previously listed in Table 5.1):

$$I_{\text{Int}} = 8,322\text{ in}^4$$

$$I_{\text{Ext}} = 1,964\text{ in}^4$$

$$\frac{I_{\text{Int}}}{I_{\text{Ext}}} = \frac{8,322}{1,964} = 4.24 < 26 \quad \therefore \text{OK} \quad (\text{Limitation check})$$

Determine the maximum live load moment in the interior girder at midspan of the bridge:

$$\Sigma I_{\text{RRFC}} = (2)(1,964) + 8,322 = \underline{12,250\text{ in}^4} \quad (7.3)$$

$$\omega = \frac{I_{\text{Int}}}{\Sigma I_{\text{RRFC}}} = \frac{8,322}{12,250} = \underline{0.679} \quad (7.2)$$

$$\psi = (0.4)(0.679)^2 - (0.7)(0.679) + 1.1 = \underline{0.809} \quad (7.4)$$

$$M_{\text{LL}} = \frac{2}{3}(0.809)(0.679)(5,904.2\text{ in} \cdot \text{k}) = \underline{2,163.4\text{ in} \cdot \text{k}} \quad (7.1)$$

$$\sigma_{\text{LL, Midspan}} = \frac{(M_{\text{LL}})(c)}{I_D} = \frac{(2,163.4\text{ in} \cdot \text{k})(13.7\text{ in.})}{(8,322\text{ in}^4)} = \underline{3.56\text{ ksi}}$$

Compare the interior girder's theoretical strain with its LT2 experimental strain:

$$\epsilon_{\text{Theoretical}} = \frac{(M_{\text{LL}})(c)}{(E)(I)} = \frac{(2,163.4\text{ in} \cdot \text{k})(13.7\text{ in.})}{(29,000\text{ ksi})(8,322\text{ in}^4)} (10^6) = 123\text{ MII}$$

$$\epsilon_{\text{Experimental,LT2}} = 117.5 \text{ MII}$$

Thus, the live load moment is conservative.

Determine the maximum live load moment in the exterior girder at midspan of the bridge:

$$\omega = \frac{I_{\text{Ext}}}{\sum I_{\text{RRFC}}} = \frac{1964}{12,250} = \underline{0.160} \quad (7.2)$$

$$\psi = -(13.7)(0.160)^3 + (10.4)(0.160)^2 - (2.6)(0.160) + 1.2 = \underline{1.107} \quad (7.5)$$

$$M_{\text{LL}} = \frac{2}{3}(1.107)(0.160)(5,904.2 \text{ in} \cdot \text{k}) = \underline{\underline{697.1 \text{ in} \cdot \text{k}}} \quad (7.1)$$

$$\sigma_{\text{LL, Midspan}} = \frac{(M_{\text{LL}})(c)}{I_D} = \frac{(697.1 \text{ in} \cdot \text{k})(12.0 \text{ in.})}{(1,964 \text{ in}^4)} = \underline{\underline{4.26 \text{ ksi}}}$$

Compare exterior girder's theoretical strain with its LT2 experimental strain:

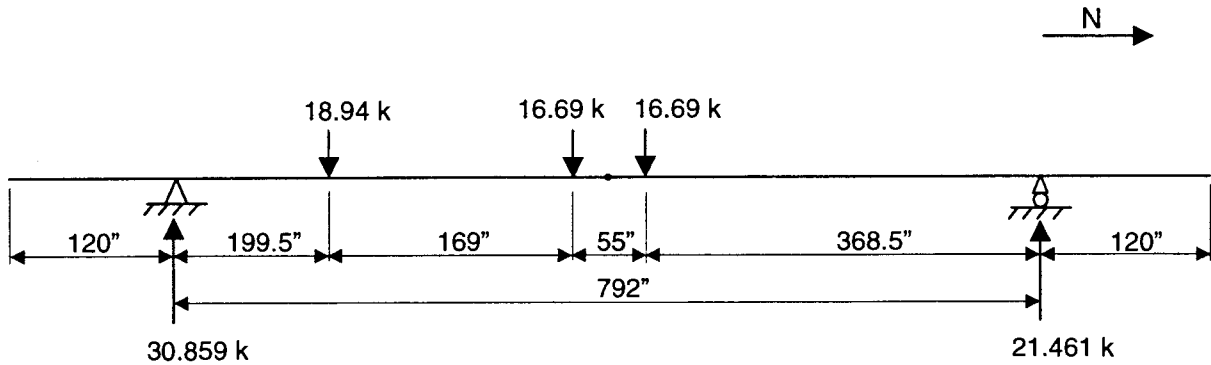
$$\epsilon_{\text{Theoretical}} = \frac{(M_{\text{LL}})(c)}{(E)(I)} = \frac{(697.1 \text{ in} \cdot \text{k})(12.0 \text{ in.})}{(29,000 \text{ ksi})(1,964 \text{ in}^4)} (10^6) = 147 \text{ MII}$$

$$\epsilon_{\text{Experimental,LT2}} = 129.6 \text{ MII}$$

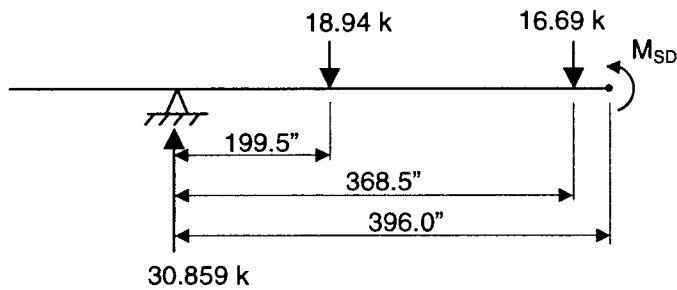
Thus, the live load moment is conservative.

## E.2 WCB Girder Design Moment Calculations

Once again, position the LT2 axle loads given in Figure 4.14 on the WCB with the tandem axles centered on the main span. For a statically determinate structure, the WCB can either be simply supported at its abutments or piers. For the WCB simply supported at its abutments, the analysis will produce an overly conservative value for  $M_{\text{SD}}$ . Therefore, determine  $M_{\text{SD}}$  from the WCB simply supported at its piers.



Again, determine the largest live load moment,  $M_{SD}$ , at midspan of the main span in the statically determinate WCB.



$$M_{SD} = (30.859 \text{ k})(396.0 \text{ in.}) - (18.94 \text{ k})(396 - 199.5 \text{ in.}) - (16.69 \text{ k})(396.0 - 368.5 \text{ in.}) = \underline{8,039.5 \text{ in} \cdot \text{k}}$$

Determine section properties for the longitudinal girders in the WCB RRFC (Previously listed in Table 5.2):

$$I_{Int} = 8,999 \text{ in}^4$$

$$I_{Ext} = 346 \text{ in}^4$$

$$\frac{I_{Int}}{I_{Ext}} = \frac{8,999}{346} = 26 \leq 26 \quad \therefore \text{OK} \quad (\text{Limitation check})$$

Determine the maximum live load moment in the interior girder at midspan of the main span:

$$\sum I_{RRFC} = (2)(346) + 8,999 = \underline{9,691 \text{ in}^4} \quad (7.3)$$

$$\omega = \frac{I_{Int}}{\sum I_{RRFC}} = \frac{8,999}{9,691} = \underline{0.929} \quad (7.2)$$

$$\psi = -(1.7)(0.929)^3 + (4.8)(0.929)^2 - (4.1)(0.929) + 1.9 = \underline{0.871} \quad (7.6)$$

$$M_{LL} = \frac{2}{3} (0.871)(0.929)(8039.5 \text{ in} \cdot \text{k}) = \underline{4332.5 \text{ in} \cdot \text{k}} \quad (7.1)$$

$$\sigma_{LL, \text{Midspan}} = \frac{(M_{LL})(c)}{I_D} = \frac{(4332.5 \text{ in} \cdot \text{k})(18.1 \text{ in.})}{(8,999 \text{ in}^4)} = \underline{8.71 \text{ ksi}}$$

Compare the interior girder's theoretical strain with its LT2 experimental strain:

$$\epsilon_{\text{Theoretical}} = \frac{(M_{LL})(c)}{(E)(I)} = \frac{(4332.5 \text{ in} \cdot \text{k})(18.1 \text{ in.})}{(29,000 \text{ ksi})(8,999 \text{ in}^4)} (10^6) = 300 \text{ MII}$$

$$\epsilon_{\text{Experimental, LT2}} = 219 \text{ MII}$$

Thus, the live load moment is conservative.

Determine the maximum live load moment in the exterior girder at midspan of the main span:

$$\omega = \frac{I_{\text{Ext}}}{\sum I_{\text{RRFC}}} = \frac{346}{9,691} = \underline{0.036} \quad (7.2)$$

$$\psi = (1800)(0.036)^3 - (270)(0.036)^2 + (20.1)(0.036) + 0.4 = \underline{0.855} \quad (7.7)$$

$$M_{LL} = \frac{2}{3} (0.855)(0.036)(8039.5 \text{ in} \cdot \text{k}) = \underline{163.7 \text{ in} \cdot \text{k}} \quad (7.1)$$

$$\sigma_{LL, \text{Midspan}} = \frac{(M_{LL})(c)}{I_D} = \frac{(163.7 \text{ in} \cdot \text{k})(7.5 \text{ in.})}{(346 \text{ in}^4)} = \underline{3.55 \text{ ksi}}$$

Compare the exterior girder's theoretical strain with its LT2 experimental strain:

$$\epsilon_{\text{Theoretical}} = \frac{(M_{LL})(c)}{(E)(I)} = \frac{(163.7 \text{ in} \cdot \text{k})(7.5 \text{ in.})}{(29,000 \text{ ksi})(346 \text{ in}^4)} (10^6) = 122 \text{ MII}$$

$$\epsilon_{\text{Experimental, LT2}} = 42 \text{ MII}$$

Thus, the live load moment is conservative.

## REFERENCES

1. Wipf, T. J., F. W. Klaiber, and T. L. Threadgold. *Use of Railroad Flat Cars for Low-Volume Road Bridges*. Iowa DOT Project TR-421. Iowa Department of Transportation. August, 1999. 141 pp.
2. Iowa Department of Transportation, Office of Transportation. *City, County, and City Maps Online*. [http://www.msp.dot.state.ia.us/trans\\_data/pdf/BUCHANAN.pdf?fmt=raw](http://www.msp.dot.state.ia.us/trans_data/pdf/BUCHANAN.pdf?fmt=raw). Accessed September 1, 2002.
3. Iowa Department of Transportation, Office of Transportation. *City, County, and City Maps Online*. [http://www.msp.dot.state.ia.us/trans\\_data/pdf/WINNEBAGO.pdf?fmt=raw](http://www.msp.dot.state.ia.us/trans_data/pdf/WINNEBAGO.pdf?fmt=raw). Accessed September 1, 2002.
4. American Association of State Highway and Transportation Officials (AASHTO). *AASHTO LRFD Bridge Design Specifications, First Edition, SI Units*. Washington, D.C. 1994.
5. American Association of State Highway and Transportation Officials (AASHTO). *Standard Specifications for Highway Bridges, Sixteenth Edition*. Washington, D.C. 1996.
6. Iowa Department of Transportation, Highway Division. Standard Designs. *Abutment Details 0° Skew – Steel Piling*, Standard No. J30C-17-87. June, 1987.
7. Swanson Analysis Systems, Inc. *ANSYS User's Manual for Revision 5.3*. Houston, PA. 1996.
8. Western Wood Products Association. *Western Woods Use Book, Structural Data and Design Tables*. Second Edition. Western Wood Products Association. Portland, OR. 1979.
9. American Society for Testing and Materials (ASTM). *2000 Annual Book of ASTM Standards*. ASTM A 370 – Standard Test Methods and Definitions for Mechanical Testing of Steel Products. Section 1, Volume 1.04. West Conshohocken, PA. 2000. pp. 165-168.
10. Bickford, William B. *Advanced Mechanics of Materials*. Menlo Park, California. 1998.

## **ACKNOWLEDGEMENTS**

The investigation presented in this thesis was conducted by the Bridge Engineering Center under the auspices of the Engineering Research Institute at Iowa State University. The research was sponsored by the Iowa Department of Transportation, Highway Division; and the Iowa Highway Research Board under Research Project TR-444.

I wish to thank Brian Keierleber, Buchanan County Engineer; and all of his personnel, plus the Winnebago County personnel for their cooperation and assistance with this project. I would also like to thank Terry J. Wipf and F. Wayne Klaiber for their guidance throughout the completion of this research. In addition, special thanks are extended to Doug Wood, ISU Research Laboratory Manager, for his help with the laboratory and field tests. Finally, thanks are given to the following ISU graduate and undergraduate students for their help with the construction, instrumentation, and field testing of the demonstration bridges: Emily Allison, Ben Dreier, Elizabeth Kash, Travis Konda, Meredith Nelson, and Bryan Williams.